UNIVERSITY OF SOUTHAMPTON

FACULTY OF ENGINEERING, SCIENCE AND MATHEMATICS

Optoelectronics Research Centre

Chirality and Metamaterials

Eric Plum

Thesis for the degree of Doctor of Philosophy

February 2010

UNIVERSITY OF SOUTHAMPTON

ABSTRACT

FACULTY OF ENGINEERING, SCIENCE AND MATHEMATICS

OPTOELECTRONICS RESEARCH CENTRE

Doctor of Philosophy

CHIRALITY AND METAMATERIALS

by Eric Plum

Electromagnetic metamaterials are artificial media that derive novel properties from periodic structuring on the sub-wavelength scale. Here, the consequences of two-dimensional (2D) and three-dimensional (3D) chirality for the electromagnetic properties of metamaterials are investigated. The focus of this work is on new ways of achieving circular conversion dichroism, optical activity and negative refraction in highly symmetric structures.

In the theoretical part of this work, fundamental constraints on polarization effects in planar metamaterials are established based on symmetry and energy conservation considerations.

Through the experimental study of 2D chirality, I have first observed circular conversion dichroism (i) in non-chiral structures and (ii) due to 2D-chiral arrangement of non-chiral elements. (iii) I have first seen enantiomerically sensitive reflection, yielding the experimental demonstration that circular conversion dichroism results in simultaneous directional asymmetries in transmission, reflection and absorption. In particular, a tunable transmission asymmetry of up to 21 % has been observed when extrinsic 2D chirality was associated with oblique incidence onto a non-chiral meandering wire pattern. At normal incidence circular conversion dichroism was seen for non-chiral split ring elements assembled into a 2D-chiral double-periodic array. Simultaneous directional and enantiomeric asymmetries in transmission (16 %), reflection (16 %) and absorption (32 %) were observed for normal incidence onto a double-periodic array of 2D-chiral split rings.

Regarding 3D chirality, I have (i) realized the first material with a negative refractive index due to chirality and (ii) observed optical activity in the first stereometamaterial. (iii) I have discovered that optical activity can be observed in non-chiral metamaterials and (iv) I have demonstrated that optical activity in such structures is tunable and occurs in transmission and reflection. In particular polarization rotation reaching 81° and circular dichroism of up to 26 dB have been observed for non-chiral arrays of split rings, when an extrinsically 3D-chiral experimental arrangement was formed by metamaterial and direction of incidence. Based on a previously-studied meta-molecule consisting of mutually twisted metal patterns in parallel planes, microwave and photonic stereometamaterials with optical activity have been realized in this thesis and such a structure has been shown to have a negative refractive index of -1.7 for right-handed circularly polarized microwaves.

Contents

List of Figures

List of Tables

DECLARATION OF AUTHORSHIP

I, Eric Plum, declare that the thesis entitled "Chirality and Metamaterials" and the work presented in the thesis are both my own, and have been generated by me as the result of my own original research. I confirm that:

- this work was done wholly or mainly while in candidature for a research degree at this University;
- where any part of this thesis has previously been submitted for a degree or any other qualification at this University or any other institution, this has been clearly stated;
- where I have consulted the published work of others, this is always clearly attributed;
- where I have quoted from the work of others, the source is always given. With the exception of such quotations, this thesis is entirely my own work;
- I have acknowledged all main sources of help;
- where the thesis is based on work done by myself jointly with others, I have made clear exactly what was done by others and what I have contributed myself;
- parts of this work have been published as the journal papers and conference contributions listed in Appendix D.

Signed: Eric Plum

Date: 18 February 2010

Acknowledgements

A PhD cannot be completed without help and support from various sources. Here I would like to thank those people who have helped me to get to this stage, in particular:

- Nikolay Zheludev and Vassili Fedotov, my supervisors, for providing sufficient guidance for successful research, while allowing me enough freedom to pursue my own ideas.
- My collaborators, without whom some of my work would not have been possible. Especially Xing-Xiang Liu for patiently completing tedious microscope experiments, Ranjan Singh for optimizing his terahertz spectroscopy experiment until the results were convincing and Jiangfeng Zhou for determining the refractive index of my twisted rosettes metamaterial.
- Simon Butler and the physics department workshop staff for assisting me in making various gadgets for my microwave and optical experiments.
- Walter Stein, my secondary school physics teacher who inspired me to study physics in the first place.
- My family, for their continuing support during my PhD and the years leading up to it.
- And finally my wife, Nadia, for her support, for keeping me well-fed and for her patience when I would come home at ridiculous hours.

Chapter 1

Introduction

1.1 Motivation

Control and manipulation of electromagnetic waves is at the heart of many industries from wireless communication, Internet and optical data storage to imaging and displays. Progress in these technologies places challenging demands on material properties and therefore structured electromagnetic materials rather than natural media are often used: Optical fibres, diffraction gratings, dielectric mirrors, Fresnel plates and photonic crystals are elementary optical components today. These established devices have revolutionized photonics by exploiting refraction, diffraction and interference resulting from artificial structuring on a scale larger than the wavelength.

Metamaterials are a special class of structured materials. Patterning on the subwavelength scale allows precise engineering of their electromagnetic properties over a range going far beyond natural media. Unlocking novel applications such as superlenses, invisibility cloaks, lasing interfaces and ultra-thin polarization optics, metamaterials are expected to lead to the next photonic revolution in science, industry and applications.

1.2 Structured Electromagnetic Materials

Special optical properties arising from structured materials are quite common in nature. The simplest example might be the opal, which consists of silica spheres a few 100 nm in diameter self-assembled into a regular lattice, see Fig. 1.1. It is sought after for its iridescent color that results from interference and diffraction. Evolution has led to

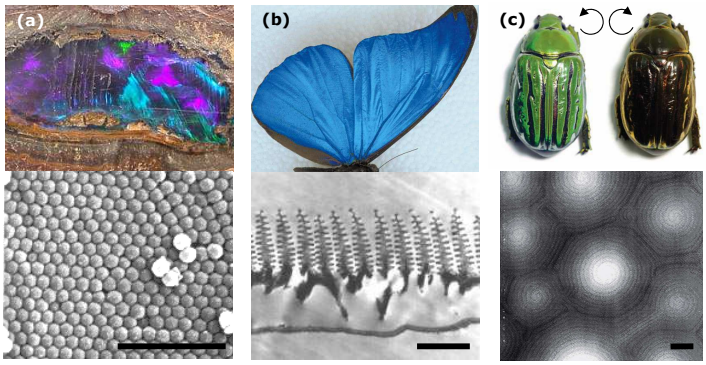

Figure 1.1: ***Structured electromagnetic materials in nature.*** *(a) Opals consist of silica nanospheres [5]. (b) The scales of the iridescent wings of the butterfly Morpho rhetenor are covered with tree-like nanostructures [2]. (c) The beetle Chrysina gloriosa has different colors under left and right circular polarizers due to the chiral structure of its exoskeleton [4]. All scale bars are 2 µm in length.*

much more complex structured materials in many butterflies, moths, beetles, birds, fish and plants [1]. A well-known example are butterfly wings that are iridescent due to interference in, e.g. tree-like, nanostructures [2]. Moth eyes have anti-reflective microstructures, reducing eye glare and making them less visible to predators [3]. And intriguingly the exoskeleton of some beetles has a chiral structure, making them appear differently under left and right circular polarizers [4].

Mankind has made use of structured electromagnetic materials long before any of the underlying mechanisms were understood. Already the Romans used metal nanoparticles to color glass. A particularly impressive example is the Lycurgus Cup, which appears green when illuminated from outside and red for illumination from inside [6], see Fig. 1.2. This unusual property is caused by gold and silver nanoparticles contained in the glass. Also some stained glass windows from the middle ages derive the color red from the plasmonic response of gold nanoparticles.

Understanding of the connection between structuring and optical properties became possible through Joseph von Fraunhofer's invention of the diffraction grating which transformed spectroscopy [9] and the theoretical foundations of electromagnetism laid by James C. Maxwell [10], followed by pioneering works of Lord Rayleigh and Jagadis C. Bose. Through the theoretical study of stacks of dielectric layers - today known as Bragg mirrors - Rayleigh understood how periodic structuring can cause total reflection of a particular wavelength [11]. This work led him to the realization, that also the iridescence found in existing materials results from interference due to periodic struc-

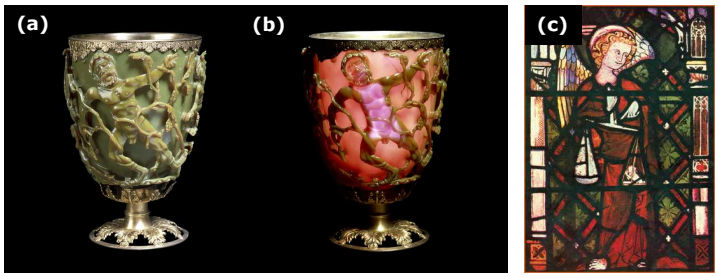

Figure 1.2: ***Historic use of structural color.*** *The Lycurgus Cup (Roman, 4th century AD) contains gold and silver nanoparticles, making it appear (a) green in reflection and (b) red in transmission [7]. (c) The color red in some medieval stained glass windows results from the surface plasmon resonance of gold nanoparticles [8]*

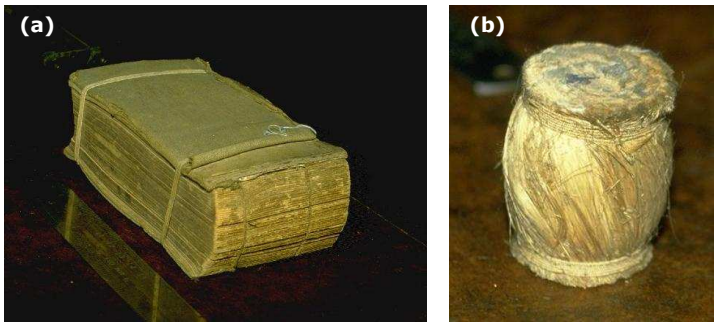

Figure 1.3: ***Polarization control using composite media: Examples from J. C. Bose's work on mm-waves.*** *(a) Linear polarizer consisting of metal foil in between the pages of a book (a railway timetable). (b) Bundle of twisted jute which rotates the polarization state [15].*

turing [12]. Bose used mm-waves to systematically study the link between structure and electromagnetic properties in composite media, e.g. he found that even a simple book has linearly polarizing properties, which are much enhanced by placing metal foil in between the pages [13], see Fig. 1.3. Through experiments with twisted bundles of jute, he observed that artificial 3D-chiral twisted structures - much like some natural materials - have the power to rotate the polarization state of electromagnetic waves [14].

Structured electromagnetic materials gained much more practical importance with the development of wireless communication and radar technology. The resulting - initially military - need for filters in the microwave band led to the development of frequency selective surfaces, these are arrays of resonators engineered to transmit or reject particular frequency bands [16–19], see Fig. 1.4 (a). Nowadays, frequency selective surfaces are used in radomes, dichroic reflectors, antennas [20], broadband communications, stealth applications and terahertz technology [21–23].

It had been known since Lord Rayleigh's work in 1887 [11], that periodic stacks of

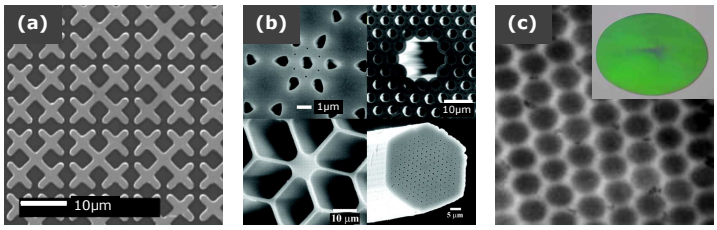

Figure 1.4: ***Frequency selective surfaces and photonic crystals.*** *(a) Multi-band frequency selective surface for the terahertz spectral range [23]. (b) Examples of photonic crystal fibres [24]. (c) Self-assembled opal-like photonic crystal based on polymer nanospheres [25].*

dielectric layers can show spectral ranges of almost total reflectivity, however, the true potential of photonic crystals - structures periodic on a scale larger than the wavelength - only became apparent through the work of Eli Yablonovitch and Sajeev John on three-dimensional photonic crystals in 1987. They showed that photonic crystals, which have stop bands resembling the band gap of semiconductors, can inhibit spontaneous emission [26] and localize photons [27]. This was the beginning of intense research on the topic, leading to first applications including LEDs with enhanced efficiency [28] and photonic crystal fibres [24], see Fig. 1.4 (b)-(c).

Structured electromagnetic materials are a rapidly growing area of research mainly driven by two factors. Firstly, reliable nanostructuring techniques like electron beam lithography and focussed ion beam milling have made nanoscale patterning feasible, which is required for novel functionalities in the important optical part of the spectrum. Secondly, the young field of metamaterials has opened up a huge range of novel functionalities.

1.3 Metamaterials

Metamaterials is a rapidly evolving field of research that covers a vast range of artificial structures and electromagnetic properties. Resulting from this, there is no universally accepted definition of what is meant by a metamaterial [29]. It is generally agreed that metamaterials are artificial media with unusual properties not found in their constituent materials, however, here we need something more specific and thus we will use the following definition:

Metamaterials are periodic arrays of artificial structures with a pitch smaller than

the wavelength of excitation.

Due to their sub-wavelength periodicity, metamaterials do not diffract. Therefore they appear homogeneous to an incident wave and can be described in terms of effective or averaged parameters that are controlled by the geometry of the metamaterial unit cell and its constituent materials. In analogy to natural materials, the elementary building block of a metamaterial, i.e. the metamaterial unit cell, is often referred to as a meta-molecule.

In a broader sense, Bose's twisted bundles of jute [14] which date back to the 19th century are often referred to as the first metamaterials. In 1920, Karl Lindman pioneered isotropic artificial chiral media by studying collections of randomly oriented metal helices of subwavelength size [30]. Amongst the first structures that strictly satisfy the above definition were two and three-dimensional arrays of metallic rods behaving like plasmas or dielectrics with a refractive index less than unity [31,32] (and a negative permittivity below the plasma frequency). These were soon followed by frequency selective surfaces, most of which may be regarded as planar metamaterials.

However, the diverse and rapidly growing field of metamaterials research that exists today was only born in 1999, when John Pendry et al. [33] suggested the use of split ring resonators (introduced earlier by Hardy and Whitehead [34]) to create artificial media with a - possibly negative - magnetic response. Just half a year later David Smith et al. [35] had demonstrated a split ring and wire metamaterial with simultaneously negative permittivity (wires) and negative permeability (split rings), see Fig. 1.5 (a). The huge importance of this becomes clear when considering two other works. Firstly, Veselago [36] predicted in 1968 that media with simultaneously negative permittivity and permeability would have a negative index of refraction. Secondly, in 2000 Pendry [37] came to the conclusion that a slab with a refractive index of -1 would act as a perfect lens, not limited by diffraction and therefore able to focus to an arbitrarily small spot. The huge potential of superlenses for imaging, data storage and lithography has been a main driver of metamaterials research ever since. After negative refraction [38] and superlensing [39] of microwaves had been demonstrated, attention shifted towards achieving a negative index for visible light. However, the high losses of metals at optical frequencies degrade the magnetic response of split rings [40] and different structures are required. Negative index metamaterial design evolved via layered wire pairs [41]

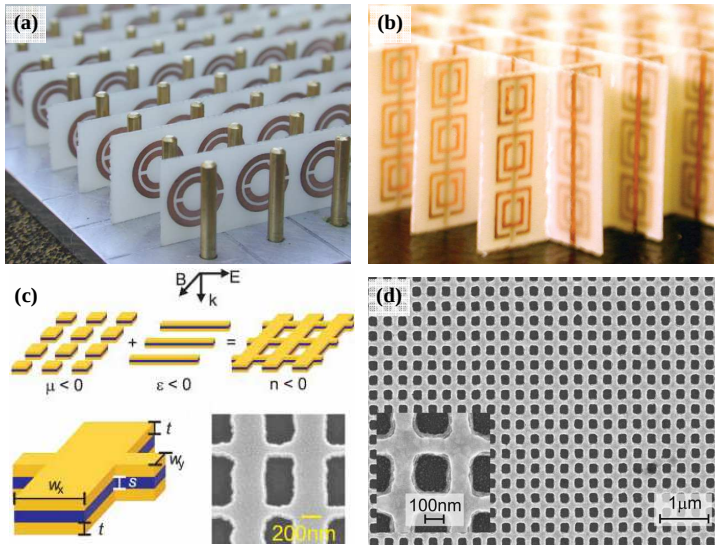

Figure 1.5: ***Negative index metamaterials****: (a) First metamaterial with simultaneously negative permittivity and permeability [35]. (b) The metamaterial used for the first demonstration of negative refraction [38]. Image taken from [44]. (c) Negative refraction in the optical part of the spectrum has been demonstrated for layered fishnet structures [42]. (d) SEM image of a fishnet structure with a negative refractive index at* 780 *nm [43].*

to fishnet structures [42, 43] which can show a negative index for visible light, see Fig. 1.5. However, so far all realizations of negative index materials suffer from substantial losses that are too high for most practical applications, therefore there is still a need to explore new avenues to negative refraction.

After the initial groundbreaking work on negative index metamaterials, it was soon realized that the potential of metamaterials is much broader. Resulting from the opportunity to precisely control electric and magnetic material properties the new research area of transformation optics emerged [45–47]. Its most notable application is the design of invisibility cloaks, which guide electromagnetic waves around a hidden object and have already been demonstrated in the microwave [48] and optical [49] parts of the spectrum. On the other hand, the study of 3D-chiral metamaterials has led to the observation of giant optical activity [50] and the discovery of a new class of negative index metamaterials [51, 52].

Various intriguing phenomena have been observed in planar metamaterials, which are particularly appealing for applications as they can be easily mass-produced by established planar technologies. For example wave plates of essentially zero thickness have been demonstrated [53, 54]. It may surprise that non-chiral planar metamaterials

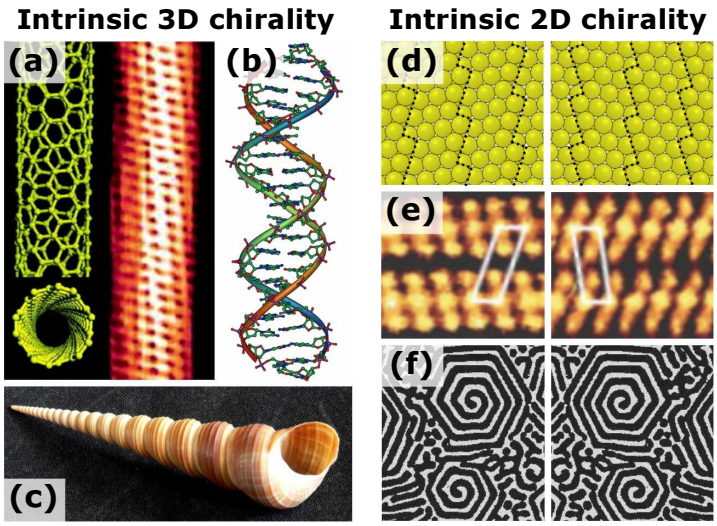

Figure 1.6: ***Examples of intrinsically chiral artificial and natural objects.*** *3D chirality: (a) single wall carbon nanotube (structure and tunneling electron microscope image) [66], (b) DNA double helix [67] and (c) seashell from the Turritellidae family [68]. 2D chirality: (d) chiral surface (643) of a gold monocrystal, (e) monolayer of (S, S)-tartaric acid (left) and (R, R)-tartaric acid (right) self-assembled on a copper surface [69] and (f) surface of a metal-metal eutectic [70].*

have been shown to act as tunable polarization rotators and circular polarizers [55,56]. High quality factor resonances trapping energy on the metamaterial surface were found to result from slightly asymmetric structuring [57]. Such resonances are linked to antisymmetric current oscillations, which can also cause a transparent metamaterial state resembling electromagnetically induced transparency [57–61]. Furthermore, the possibility of a lasing spaser - a planar metamaterial laser - is being investigated [62,63]. And remarkably, in 2006 a new fundamental electromagnetic effect causing directionally asymmetric transmission through 2D-chiral metamaterials has been discovered [64].

1.4 Chirality

> "I call any geometrical figure, or group of points, chiral, and say it has chirality, if its image in a plane mirror, ideally realized, cannot be brought to coincide with itself." Lord Kelvin (1904) [65].

1.4.1 3D Chirality

This famous definition of enantiomorphism by Lord Kelvin is usually applied in three dimensions (3D), where it defines objects like helices, proteins and the crystal lattice of quartz as *3D-chiral*, other examples are shown in Fig. 1.6 (a)-(c). It is widely accepted that materials of 3D-chiral symmetry show two important electromagnetic phenomena: circular birefringence and circular dichroism, jointly referred to as *optical activity*. These effects can be defined phenomenologically as follows:

Circular birefringence is the ability to rotate the plane of polarization of electromagnetic waves. The effect does not depend on the polarization state of the incident wave and is the same for opposite directions of wave propagation, see Fig. 1.7 (a).

Circular dichroism corresponds to different direct transmission (or reflection) levels for left-handed and right-handed circularly polarized waves. The effect is identical for opposite directions of wave propagation, see Fig. 1.7 (b).

In bulk media optical activity corresponds to different refractive indices for left-handed and right-handed circularly polarized waves. Circular birefringence arises from different real parts of these refractive indices, which result in different phase delays for left-handed and right-handed components of an electromagnetic wave and thus polarization rotation. Circular dichroism corresponds to different imaginary parts of these indices, which cause different absorption losses for circularly polarized waves of opposite handedness. However, here we will use the more general phenomenological definitions shown above, as no meaningful refractive index can be defined for the case of planar metamaterials of essentially zero thickness. Like the perceived twist of 3D-chiral objects (e.g. helices) is the same for opposite directions of observation, optical activity is the same for opposite directions of wave propagation.

Today, optical activity is used as a diagnostic tool in spectroscopy, analytical chemistry, crystallography and molecular biology for identifying the spacial arrangement of atoms. Due to the 3D-chiral nature of the biochemistry of life (DNA, proteins, ...), optical activity is even used as a signature effect for the detection of life in space missions. Furthermore optically active media used as polarization rotators or circular

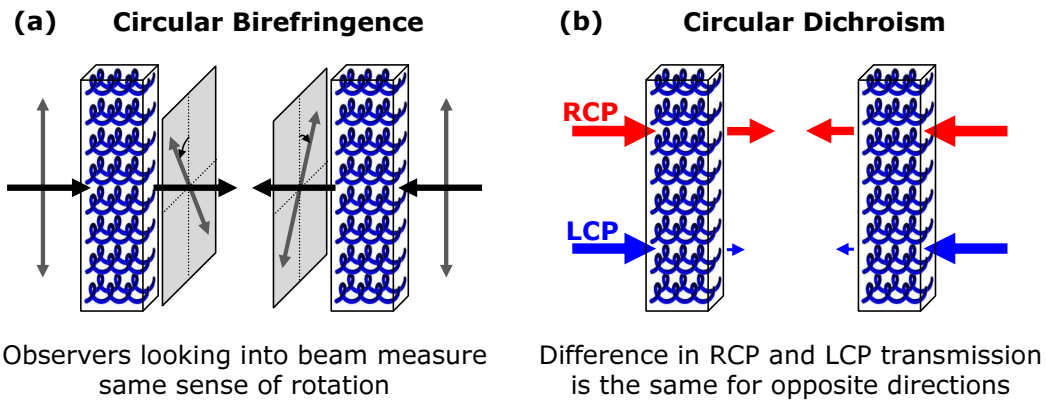

Figure 1.7: ***Polarization effects arising from 3D chirality.*** *(a) Circular birefringence rotates the polarization state of an electromagnetic wave. (b) Circular dichroism corresponds to different transmission levels for left-handed (LCP) and right-handed (RCP) circularly polarized waves. Both phenomena are the same for opposite directions of wave propagation.*

polarizers are important for optics, life science microscopy, photography and display applications [71].

Optical activity was discovered in 1811, when François J. D. Arago [72] observed that quartz has the ability to rotate the plane of polarization of linearly polarized light. Four decades later Louis Pasteur [73] observed that tartaric acid forms two types of chiral crystals that are mirror images of each other. He found that solutions from opposite crystals show circular birefringence of opposite sign while their equal mixture shows no circular birefringence at all. From this he deduced that molecules of tartaric acid must exist in two mirror forms associated with opposite crystals and polarization rotation of opposite sign. That 3D-chiral material symmetry leads to optical activity was first demonstrated directly in 1898 by J. C. Bose's mm-wave experiments, see Fig. 1.3 (b). Bose wrote: "In order to imitate the [polarization plane] rotation by liquids like sugar solutions, I made elements of 'molecules' of twisted jute, of two varieties, one kind being twisted to the right (positive) and the other twisted to the left (negative)..." and he found that the "twisted structure [of jute] produces an optical twist of the plane of polarization" [14]. More recently, artificial media consisting of oriented and random metal helices were studied by [30, 74] and [75] respectively and were found to exhibit high levels of polarization rotation in the presence of large circular dichroism.

There have been several different approaches to manufacturing artificial optically active structures for the optical part of the spectrum. Circularly birefringent sculptured

thin films consisting of helical pillars have been manufactured using physical vapor deposition [76]. Recent developments in fabrication via direct laser writing have lead high quality helical nanostructures. In particular, large circular dichroism has been demonstrated for helical structures in form of uniaxial [77] [see Fig. 1.8 (a)] and isotropic dielectric photonic crystals [78] and uniaxial gold metamaterials [79]. Optical activity has also been detected in structures based on planar elements. M. Kuwata-Gonokami et al. found that 2D arrays of thick 2D-chiral planar metal patterns that form a 3D-chiral object with the supporting dielectric substrate can show circular birefringence [80]. Similarly, circular dichroism was observed for a metamaterial based on pairs of aligned metal gammadions of different size in parallel planes [81].

The possibility of negative refraction in optically active media was first identified in 1981 by B. Bokut' et al. [82]. Two decades later 3D-chiral media started to attract substantial interest when J. Pendry [83] and S. Tretyakov et al. [84, 85] independently found that optically active media were promising candidates for negative refraction, with potential application as superlenses for circularly polarized waves [86]. While "traditional" negative index media require overlapping electric and magnetic resonances to achieve negative permittivity and permeability in the same frequency range, a single - sufficiently strong - resonance of circular birefringence was predicted to lead to negative refraction of one circular polarization [84]. Since no natural materials with sufficiently large circular birefringence are known, research focused on artificial structures.

A breakthrough was achieved through stereometamaterials, which derive their properties from the spacial arrangement of the "meta-atoms" forming their meta-molecules. Such structures, consisting of pairs of mutually twisted metal patterns in parallel planes, were first suggested by Svirko et al. [87] and an experimental study of a single 3D-chiral meta-molecule of this type found giant optical activity and a signature of circularly polarized backward waves [71], see Fig. 1.8 (b). Photonic stereometamaterials based on this concept show exceptionally large optical activity [50, 88] and corresponding microwave metamaterials can act as ultra-thin circular polarizer, polarization rotator and negative index medium for circularly polarized waves [51, 89], this will be discussed in detail in chapter 5. It should be noted that a negative refractive index due to circular birefringence has also been demonstrated for a more complex 3D-chiral terahertz metamaterial [52].

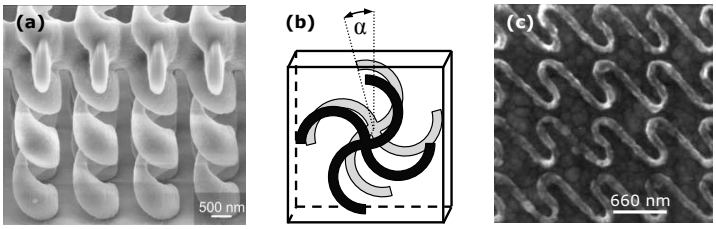

Figure 1.8: ***Chiral structured materials.*** *(a) Helical photonic crystal exhibiting a stop band for only one circular polarization [77]. (b) Meta-molecule with giant optical activity consisting of mutually twisted metal elements in parallel planes [71]. (c) Planar chiral metamaterial showing circular conversion dichroism in the near infrared [90].*

Even though optical activity is usually associated with intrinsically 3D-chiral materials, it was recently discovered that exceptionally large circular birefringence and circular dichroism can be observed for non-chiral planar metamaterials, if the mutual orientation of incident wave and metamaterial pattern forms a 3D-chiral experimental arrangement [55, 56]. Theoretical and experimental investigations of this intriguing phenomenon are presented in chapters 2 and 4 respectively.

1.4.2 2D Chirality

Lord Kelvin's definition of chirality can also be applied in two dimensions, where it describes the twisted nature of planar patterns like spirals or S-elements, other examples are shown in Fig. 1.6 (d)-(f). In contrast to 3D-chiral objects, two-dimensionally chiral (2D-chiral, planar chiral) patterns have the peculiar property that their sense of twist is reversed for observation from opposite directions [91, 92]. Thus waves interacting with front and back of a planar chiral interface see "different" structures, which could have different properties. As twisted planar patterns are rare in nature, their importance in optics has only started to emerge over the last decade.

Polarization rotation and ellipticity changes in beams diffracted from 2D-chiral gratings were discovered in 2003 [93, 94], indicating that 2D chirality is relevant to electromagnetism.

In 2006, the study of planar chiral metamaterials revealed a new fundamental electromagnetic effect: *Circular conversion dichroism* (which is known to lead to *asymmetric transmission*).

Circular conversion dichroism corresponds to left-to-right and right-to-left circular polarization conversion efficiencies, that are different from each other and

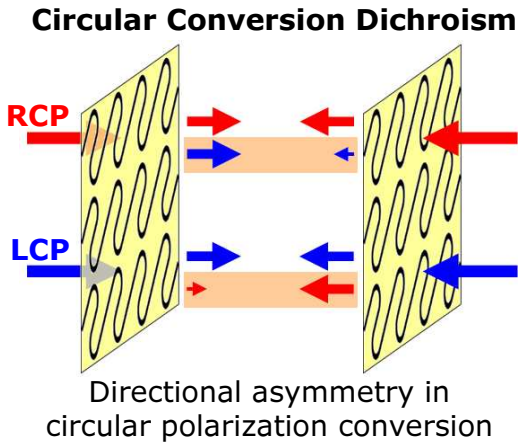

Figure 1.9: ***Circular conversion dichroism due to 2D chirality*** *corresponds to different levels of circular polarization conversion for right-handed (RCP) and left-handed (LCP) circularly polarized waves. The conversion efficiencies are reversed for opposite directions of wave propagation, resulting in asymmetric total transmission for counter-propagating waves of the same handedness.*

reversed for opposite propagation directions of the incident wave. The effect results in directionally asymmetric total transmission, reflection and absorption of circularly polarized waves, see Fig. 1.9.

Directionally asymmetric total transmission of circularly polarized waves was first reported for anisotropic, lossy, planar chiral metamaterials at microwave [64], terahertz [95] and optical [90] frequencies, see Fig. 1.8 (c). Recently, the effect was also reported for transmission through single plasmonic nanostructures [96]. Through numerical simulations [97] and microwave experiments [98] it was shown that asymmetric transmission is accompanied by corresponding behavior in reflection and absorption, and that these phenomena are linked to the excitation of enantiomerically sensitive current modes. Subsequently, it was demonstrated that circular conversion dichroism does not require intrinsically 2D-chiral structures, but that the effect can also be observed, if 2D chirality is associated with the mutual orientation of metamaterial and incident wave [99].

Circular conversion dichroism is characterized theoretically and experimentally in chapters 2 and 3 respectively.

1.5 Thesis Overview

Metamaterials offer a unique opportunity to study chirality and the associated electromagnetic phenomena systematically. This thesis represents such a study for linear periodic structures, which has led to several new topics and intriguing observations, including "asymmetric transmission at any lossy periodic interface", "optical activity of non-chiral metamaterials" and "negative refractive index due to circular birefringence".

Chapter 2 provides a theoretical analysis of polarization effects at planar metamaterials. The findings include that both 2D-chiral circular conversion dichroism (asymmetric transmission) and 3D-chiral optical activity (circular birefringence and dichroism) should be expected at non-chiral structured interfaces, if extrinsic chirality of the relevant type is associated with the direction of incidence onto the metamaterial. Fundamental limits are identified for directionally asymmetric transmission, reflection and absorption phenomena and the potential performance of planar metamaterial devices such as polarization rotators, circular polarizers and wave plates for transmission and reflection is assessed.

In chapter 3 circular conversion dichroism is investigated experimentally. It includes the first experimental demonstration that asymmetric transmission of circularly polarized waves is accompanied by corresponding asymmetries in reflection and absorption. Experimental evidence is presented indicating that the asymmetric phenomena should be possible for oblique incidence onto any lossy periodically structured interface. Furthermore, the microscopic origin of the effect is revealed through numerical simulations, building on theoretical considerations from the previous chapter.

Chapter 4 studies circular birefringence and circular dichroism in planar metamaterials experimentally. Planar structures cannot be intrinsically 3D-chiral, however, extrinsic 3D chirality can be associated with the propagation direction of the incident wave and the orientation of the metamaterial. Experiments show, that extrinsic 3D chirality leads to exceptionally large optical activity in transmission and reflection, suitable for the realization of tunable transmission and reflection polarization rotators and circular polarizers.

In chapter 5 the conventional symmetry of intrinsic 3D chirality is investigated for photonic and microwave stereometamaterials based on mutually twisted metal patterns

in parallel planes. Results include, that such structures can show giant optical activity, as well as negative electric and magnetic responses. Importantly, the first experimental demonstration of a negative refractive index due to circular birefringence is presented.

Finally, the work covered in this thesis is summarized in chapter 6. This is followed an appendix describing the experimental techniques that were used to study metamaterials in the microwave spectral range.

Chapter 2

Theory of Planar Metamaterials

Here the properties that linear planar metamaterials can exhibit for monochromatic electromagnetic plane waves are investigated starting from symmetry and energy conservation considerations. While this chapter aims to cover polarization effects in planar metamaterials and their potential applications in general, special attention is given to chiral polarization effects. The theory of planar metamaterials developed here forms the theoretical foundation for the experimental demonstrations of 2D-chiral and 3D-chiral phenomena reported in chapters 3 and 4.

2.1 Introduction

In recent years it has emerged that planar metamaterials offer a vast range of custom-designed electromagnetic functionalities. The most well-known example are wire grid polarizers, which are established standard components for microwaves, terahertz waves and the far-infrared. They are expected to be of increasing importance also for the near-infrared [100] and visible light [101]. Equally well-developed are frequency selective surfaces [16–19] which are used as filters in radar systems, antenna technology [20], broadband communications and terahertz technology [21,22]. However, the range of optical effects observable in planar metamaterials and the variety of potential applications have only become clear since metamaterials research took off in 2000 [35, 37]. Wave plate [53,54] as well as polarization rotator and circular polarizer [55,56] functionalities have been demonstrated in metamaterials of essentially zero thickness. Traditionally, such components are large as they rely on integrating weak effects over thick functional

materials. Also electromagnetically induced transparency (EIT) [57, 59–61, 102] and high quality factor resonances [57] have been observed at planar structured interfaces. And finally, a new fundamental electromagnetic effect, the directionally asymmetric transmission of circularly polarized waves (circular conversion dichroism), has been discovered in planar chiral metamaterials [64, 90, 98, 99].

Like metamaterials in general, planar metamaterials derive their properties from artificial structuring rather than atomic or molecular resonances and therefore appropriately scaled versions of such structures will show similar properties for radio waves, microwaves, terahertz waves and to some extent in the infrared and optical spectral regions, where losses are becoming more important. Planar metamaterials are compatible with well-established fabrication technologies like lithography and nanoimprint, allowing for high-throughput manufacturing and making them suitable for highly integrated applications and miniaturization.

The effects underlying the functionalities of planar metamaterials can be divided into two categories: dispersion phenomena including narrow resonances, stop bands and EIT-like behavior on one hand, and polarization phenomena such as optical activity, linear birefringence and circular conversion dichroism on the other hand. This chapter is devoted to the analysis of polarization phenomena in planar metamaterials.

Given the huge range of potential applications of planar metamaterials, it is time to ask what the fundamental limits are for the polarization functionalities of planar metamaterials. Here fundamental limitations for the performance of planar metamaterials are identified based on energy conservation and symmetry considerations.

Before we start, we need to clarify what we mean by a planar metamaterial. Idealized, a planar metamaterial is a flat two-dimensional surface of zero thickness that is periodically structured on the sub-wavelength scale. This ideal is best approximated by a single periodically patterned metal layer with a thickness that is comparable to the skin depth[1]. An ideal planar metamaterial is still well-approximated by a single periodically pattered metal or dielectric layer that is very thin compared to the wavelength. In practice such structures are often supported by a transparent substrate. Due to their

[1] The skin depth is the characteristic thickness of the current carrying layer at a conductor's surface. For metals at microwave frequencies it is around 1 μm. The skin depth δ_s can be calculated as $\delta_s = \sqrt{\frac{\rho}{\pi f \mu_0 \mu}}$, where ρ is the bulk resistivity, f is the frequency, μ_0 is the permeability of vacuum and μ is the relative permeability.

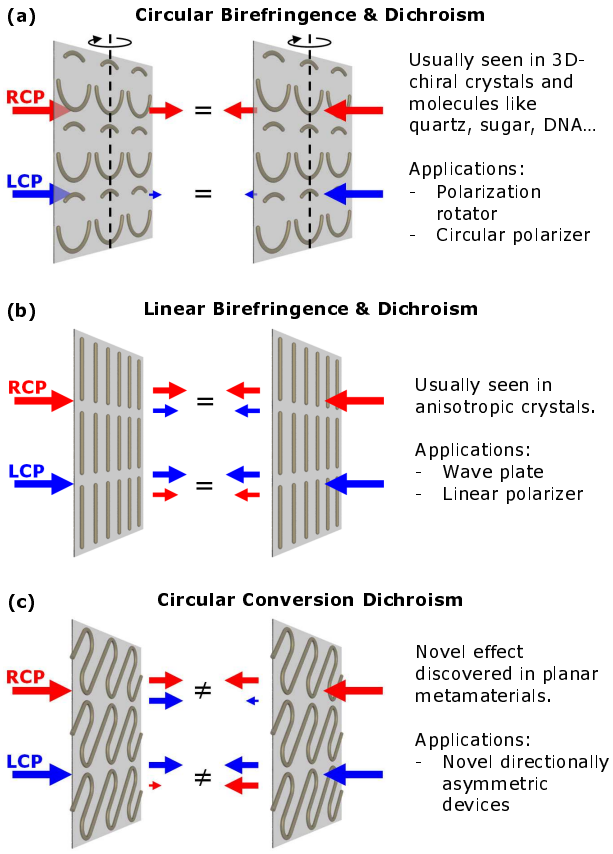

Figure 2.1: ***Polarization effects in planar metamaterials.*** *(a) Optical activity in the form of polarization rotation (circular birefringence) and differential direct transmission of right-handed (RCP) and left-handed (LCP) circularly polarized waves (circular dichroism) can occur at oblique incidence onto planar metamaterials. (b) Linear birefringence and dichroism lead to identical levels of circular polarization conversion for incident waves of either handedness or propagation direction. (c) Circular conversion dichroism corresponds to circular polarization conversion that depends on both direction and handedness of the incident wave. The effect leads to directionally asymmetric total transmission of circularly polarized waves.*

sub-wavelength periodicity planar metamaterials do not diffract electromagnetic waves at normal incidence. For oblique incidence at an angle θ from the normal, a planar structure of period p does not diffract the wavelength λ if $p(1+\sin|\theta|) < \lambda$ is satisfied. Here we consider only non-diffracting angles of incidence.

In section 2.2, oblique incidence onto a general planar metamaterial is considered and then the consequences of different symmetries of the metamaterial structure and the experimental arrangement are examined. It is shown that in general planar metamaterials can exhibit circular birefringence and dichroism (optical activity), linear and birefringence and dichroism, as well as circular conversion dichroism, see Fig. 2.1. Fol-

lowing general definitions in section 2.3, these phenomena are discussed further in section 2.4. In section 2.5, an analysis of polarization eigenstates for planar metamaterials is presented. In section 2.6 the role of energy conservation will be studied and a limit on losses in planar metamaterials will be derived. Also limits will be identified for the transmission, reflection and absorption asymmetries associated with circular conversion dichroism. The potential performance of planar metamaterials as linear polarizers, circular polarizers, wave plates or polarization rotators operating in transmission and/or reflection will be examined in section 2.7. The final section 2.8 is devoted to the special case of normal incidence onto planar metamaterials. In particular, scattering matrices will be presented for various types of planar metamaterials and it will be examined how the electromagnetic properties of planar metamaterials are linked to the current modes excited by incident electromagnetic waves.

In summary, this chapter provides a theoretical analysis of polarization effects for linear planar metamaterials in the absence of diffraction. It shall be noted that the theoretical analysis presented here is complemented by a substantial body of literature on bianisotropic media [103, 104].

2.2 General Planar Metamaterials

The transmission and reflection properties of a linear planar metamaterial can be written in terms of the transmission[2] and reflection matrices, t and r, which relate the transmitted and reflected electric fields, $\mathbf{E^t}$ and $\mathbf{E^r}$, to the incident field $\mathbf{E^0}$. Where the propagation direction of the incident wave, forwards or backwards, is important, it is indicated by an arrow over the matrix, vector or other quantity. For example for a forward propagating incident wave:

$$\overrightarrow{\mathbf{E}}^{\mathbf{t}} = \overrightarrow{t}\,\overrightarrow{\mathbf{E}}^{\mathbf{0}} \tag{2.1}$$

$$\overrightarrow{\mathbf{E}}^{\mathbf{r}} = \overrightarrow{r}\,\overrightarrow{\mathbf{E}}^{\mathbf{0}} \tag{2.2}$$

It is convenient to express transmission and reflection in terms of the scattering matrix s. As a planar metamaterial is just a non-diffracting array of scatterers, the transmitted field is simply the superposition of the scattered field and the incident

[2] Also known as Jones matrix.

wave, i.e.

$$\overrightarrow{t} = \overrightarrow{s} + 1, \tag{2.3}$$

where 1 is the unit matrix.

As illustrated by Fig. 2.2 (a), we will define the polarization state of any electromagnetic wave in its own right-handed Cartesian coordinate system **xyz**, where **x** is perpendicular to the plane of incidence[3], **y** is parallel to the plane of incidence and **z** is the wave's propagation direction. **y** is chosen consistently so that its projection onto the metamaterial is parallel for all waves within the same plane of incidence.

For example, incident and transmitted waves, as well as scattered fields (measured in the transmission direction), all have the same propagation direction and therefore the same coordinates **xyz**. The coordinates for an incident wave **xyz** and the reflected wave $\mathbf{x_r y_r z_r}$ have anti-parallel x-axes $\mathbf{x_r} = -\mathbf{x}$. The coordinates **xyz** and $\mathbf{x'y'z'}$ for waves with opposite propagation directions are related by $\mathbf{x'} = -\mathbf{x}$, $\mathbf{y'} = \mathbf{y}$ and $\mathbf{z'} = -\mathbf{z}$.

Planar structures can only couple to tangential electric fields and normal magnetic fields [4]. Therefore two electromagnetic waves with identical tangential electric fields and identical normal magnetic fields cannot be distinguished by a planar metamaterial. In terms of the electric field - which fully defines an electromagnetic plane wave - these waves correspond to mirror images with respect to the plane of the metamaterial.

In particular, this implies that the electric field radiated by a planar metamaterial (or planar current configuration) must be symmetric with respect to the metamaterial. However, the polarization states [see Fig. 2.2 (b)] of waves scattered in the transmission and reflection directions are defined in different coordinate systems [see Fig. 2.2 (a)], in which they have the opposite handedness. This is why the reflection matrix (describing scattering in the reflection direction) differs from the scattering matrix (describing scattering in the transmission direction) by a coordinate transformation. Choosing right-handed (RCP, +) and left-handed (LCP, -) circularly polarized waves as our

[3] The plane of incidence contains the propagation direction and the metamaterial's surface normal.

[4] Coupling to normal electric fields and tangential magnetic fields is not possible, as the electric charges cannot leave the plane of the structure.

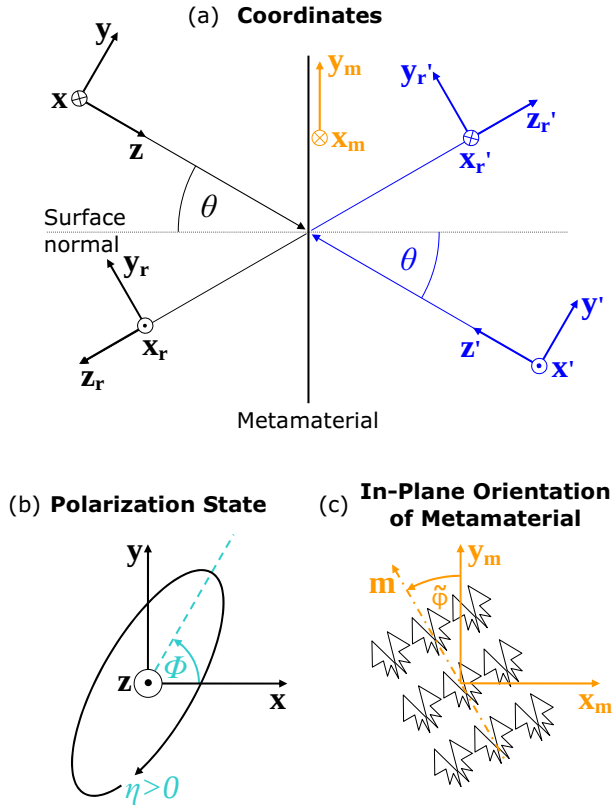

Figure 2.2: ***Coordinate systems, polarization state and metamaterial orientation.*** *(a) Each wave's polarization state is defined in its own right-handed Cartesian coordinate system defined by its propagation direction and the plane of incidence, see text. Here the coordinates are shown for a wave incident on the metamaterial's front* $\mathbf{xyz}$ *(back* $\mathbf{x'y'z'}$*) and for the corresponding reflected wave* $\mathbf{x_r y_r z_r}$ *(*$\mathbf{x'_r y'_r z'_r}$*). (b) Polarization state. Looking along the negative* $\mathbf{z}$*-axis, i.e. into the beam, positive ellipticity* η *corresponds to a right-handed path of the electric field vector at a fixed position in space. The azimuth* Φ *is measured from the positive* $\mathbf{x}$*-axis and increases towards the positive* $\mathbf{y}$*-axis. (c) The metamaterial's orientation* $\tilde{\varphi}$ *corresponds to a preferred direction, e.g. a line of (glide) mirror symmetry* $\mathbf{m}$ *or direction of anisotropy, which is measured from the positive* $\mathbf{y_m}$*-axis, increasing towards the negative* $\mathbf{x_m}$*-axis.* $\mathbf{x_m y_m}$ *correspond to the coordinates of a forward-propagating wave* $\mathbf{xy}$ *projected onto the metamaterial.*

basis, the reflection matrix for forward propagating incident waves is

$$\overrightarrow{r} = \sigma \overrightarrow{s}, \tag{2.4}$$

where σ_{ij}, which is 0 for $i = j$ and 1 otherwise, switches between the coordinate systems for the incident and reflected waves. Transmission and reflection matrices are linked by (2.3) and (2.4) and this relationship is illustrated by Fig. 2.3 for a real planar metamaterial.

As discussed above, planar metamaterials can only couple to tangential electric

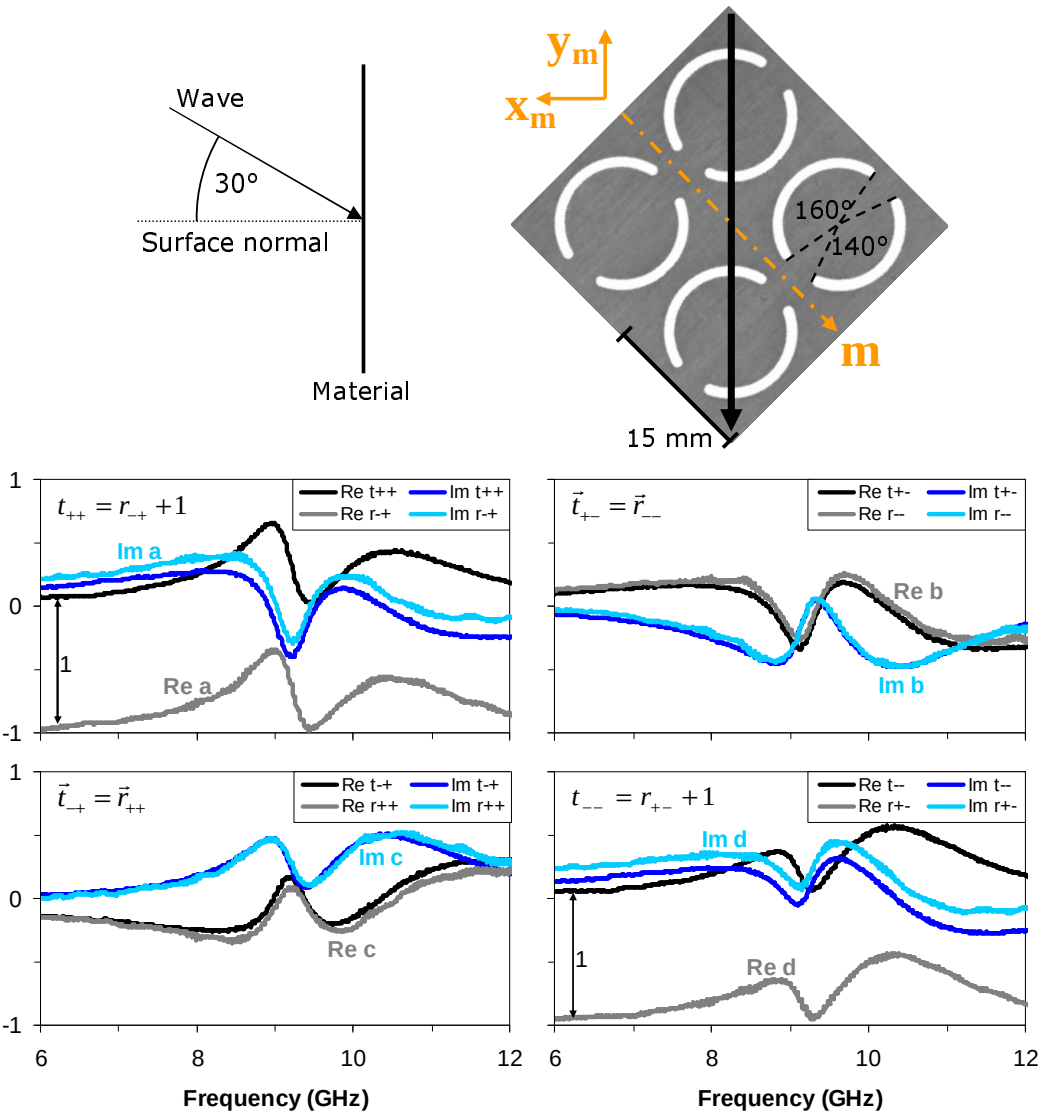

Figure 2.3: ***Experimentally measured transmission and reflection matrices for a planar metamaterial.*** *The structure is a 1 mm thick aluminum film perforated with an array of asymmetrically split ring apertures and was studied under oblique incidence conditions $\theta = 30°, \tilde{\varphi} = 135°$, as illustrated by the inset showing the incident wave projected onto the metamaterial (wallpaper symmetry group pm). Within experimental accuracy, these results confirm the relationship defined by (2.3) and (2.4) between transmission and reflection matrices, which is written out explicitly in the upper left corners of the graphs. This metamaterial will be discussed in detail in section 4.4 and simulations showing the current modes this structure can support are presented in appendix C.*

fields and normal magnetic fields. Therefore two electromagnetic waves that do not differ in these field components must excite the metamaterial in the same way. In particular this is the case for circularly polarized waves of opposite handedness that are incident in the same plane at angles θ and $-\theta$ from the normal on the front and back of the metamaterial, see Fig. 2.4 (a). These waves must cause the same scattered

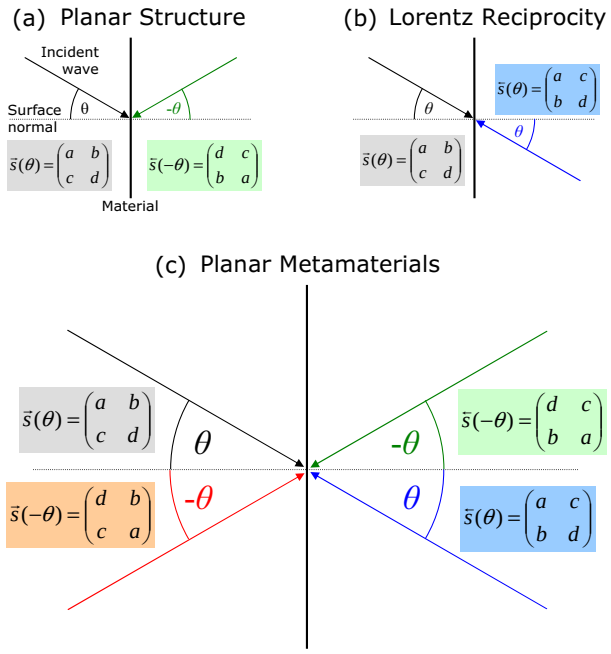

Figure 2.4: ***Scattering matrices for opposite angles and/or opposite directions of incidence*** *in the same plane. (a) Form of the scattering matrices for waves incident at opposite angles $\pm\theta$ on opposite sides of a planar metamaterial according to conditions (2.5) and (2.6). (b) Form of the scattering matrices for opposite directions of incidence as required by Lorentz reciprocity, see equations (2.7) and (2.8). (c) For non-magnetized planar metamaterials both (a) and (b) must apply, thus the scattering coefficients b, c are reversed for opposite propagation directions, while the coefficients a, d are reversed for opposite angles of incidence $\pm\theta$.*

field. Taking into account that the scattering matrix describes the scattered field in the respective transmission direction (opposite handedness for the considered cases), we can identify pairs of identical scattering coefficients for opposite angles of incidence on opposite sides of the metamaterial.

$$\overrightarrow{s_{++}}(\theta) = \overleftarrow{s_{--}}(-\theta) \quad \text{and} \quad \overrightarrow{s_{--}}(\theta) = \overleftarrow{s_{++}}(-\theta), \tag{2.5}$$

$$\overrightarrow{s_{+-}}(\theta) = \overleftarrow{s_{-+}}(-\theta) \quad \text{and} \quad \overrightarrow{s_{-+}}(\theta) = \overleftarrow{s_{+-}}(-\theta). \tag{2.6}$$

If no static static magnetic field is present, and thus no Faraday effect, the Lorentz reciprocity lemma [105] must hold. Lorentz reciprocity requires for opposite propagation directions that $\overrightarrow{t_{ij}} = \overleftarrow{t_{ji}}$, which due to (2.3) is equivalent to $\overrightarrow{s_{ij}} = \overleftarrow{s_{ji}}$. This gives

us [see also Fig. 2.4 (b)]

$$\overrightarrow{s_{++}}(\theta) = \overleftarrow{s_{++}}(\theta) \quad \text{and} \quad \overrightarrow{s_{--}}(\theta) = \overleftarrow{s_{--}}(\theta), \tag{2.7}$$

$$\overrightarrow{s_{+-}}(\theta) = \overleftarrow{s_{-+}}(\theta) \quad \text{and} \quad \overrightarrow{s_{-+}}(\theta) = \overleftarrow{s_{+-}}(\theta). \tag{2.8}$$

By combining (2.5)-(2.8), we arrive at four complex coefficients describing the scattering properties of a planar metamaterial for one plane of incidence

$$a(\theta) := \overrightarrow{s_{++}}(\theta) = \overleftarrow{s_{++}}(\theta) = \overrightarrow{s_{--}}(-\theta) = \overleftarrow{s_{--}}(-\theta), \tag{2.9}$$

$$b(\theta) := \overrightarrow{s_{+-}}(\theta) = \overleftarrow{s_{-+}}(\theta) = \overrightarrow{s_{+-}}(-\theta) = \overleftarrow{s_{-+}}(-\theta), \tag{2.10}$$

$$c(\theta) := \overrightarrow{s_{-+}}(\theta) = \overleftarrow{s_{+-}}(\theta) = \overrightarrow{s_{-+}}(-\theta) = \overleftarrow{s_{+-}}(-\theta), \tag{2.11}$$

$$d(\theta) := \overrightarrow{s_{--}}(\theta) = \overleftarrow{s_{--}}(\theta) = \overrightarrow{s_{++}}(-\theta) = \overleftarrow{s_{++}}(-\theta). \tag{2.12}$$

The corresponding scattering matrices are written out explicitly in Fig. 2.4 (c), where

$$a(\theta) = d(-\theta), \qquad d(\theta) = a(-\theta), \tag{2.13}$$

$$b(\theta) = b(-\theta), \qquad c(\theta) = c(-\theta). \tag{2.14}$$

A planar metamaterial's response depends not only on the angle of incidence θ, but also on the orientation $\tilde{\varphi} \in [0, 2\pi)$ of the metamaterial structure in its plane. With reference to Fig. 2.4 (c), reversal of the angle of incidence, $\theta \to -\theta$, is equivalent to an in-plane rotation of the metamaterial by π, i.e. $\tilde{\varphi} \to \tilde{\varphi} + \pi$. Therefore $\overrightarrow{s}(\theta, \tilde{\varphi}) = \overrightarrow{s}(-\theta, \tilde{\varphi} + \pi)$ and

$$a(\theta, \tilde{\varphi}) = d(\theta, \tilde{\varphi} + \pi), \qquad d(\theta, \tilde{\varphi}) = a(\theta, \tilde{\varphi} + \pi), \tag{2.15}$$

$$b(\theta, \tilde{\varphi}) = b(\theta, \tilde{\varphi} + \pi), \qquad c(\theta, \tilde{\varphi}) = c(\theta, \tilde{\varphi} + \pi). \tag{2.16}$$

For reference the scattering, transmission and reflection matrices for opposite di-

rections of incidence (same θ, φ) onto a planar metamaterial are given explicitly:

$$\overrightarrow{s} = \begin{pmatrix} a & b \\ c & d \end{pmatrix} \quad \text{and} \quad \overleftarrow{s} = \begin{pmatrix} a & c \\ b & d \end{pmatrix}, \tag{2.17}$$

$$\overrightarrow{t} = \begin{pmatrix} a+1 & b \\ c & d+1 \end{pmatrix} \quad \text{and} \quad \overleftarrow{t} = \begin{pmatrix} a+1 & c \\ b & d+1 \end{pmatrix}, \tag{2.18}$$

$$\overrightarrow{r} = \begin{pmatrix} c & d \\ a & b \end{pmatrix} \quad \text{and} \quad \overleftarrow{r} = \begin{pmatrix} b & d \\ a & c \end{pmatrix}. \tag{2.19}$$

2.2.1 Lossless Complementary Planar Metamaterials

According to Babinet's principle, complementary waves ($\mathbf{E^{cpl,0}} = c\mathbf{B^0}, \mathbf{B^{cpl,0}} = -\mathbf{E^0}/c$) incident on complementary perfectly conducting plane thin screens cause transmitted fields $\mathbf{E^t}, \mathbf{B^t}$ and $\mathbf{E^{cpl,t}}, \mathbf{B^{cpl,t}}$, which are related by $\mathbf{E^t} - c\mathbf{B^{cpl,t}} = \mathbf{E^0}$ and $\mathbf{B^t} + \mathbf{E^{cpl,t}}/c = \mathbf{B^0}$ [106, 107].

This requires the transmission matrices of complementary planar metamaterials to be related as follows

$$\overrightarrow{t} = \begin{pmatrix} a+1 & b \\ c & d+1 \end{pmatrix} \quad \text{and} \quad \overrightarrow{t^{cpl}} = \begin{pmatrix} -a & b \\ c & -d \end{pmatrix}. \tag{2.20}$$

The corresponding scattering matrices are

$$\overrightarrow{s} = \begin{pmatrix} a & b \\ c & d \end{pmatrix} \quad \text{and} \quad \overrightarrow{s^{cpl}} = \begin{pmatrix} -(a+1) & b \\ c & -(d+1) \end{pmatrix}. \tag{2.21}$$

Thus, apart from a phase shift by π, complementary lossless planar metamaterials have interchanged direct transmission and scattering properties for circularly polarized waves, e.g. $t^{cpl}_{++} = -s_{++}$. On the other hand the circular polarization conversion coefficients (off-diagonal elements) are the same for such complementary structures, e.g. $\overrightarrow{t^{cpl}_{-+}} = \overrightarrow{s^{cpl}_{-+}} = \overrightarrow{t_{-+}} = \overrightarrow{s_{-+}}$.

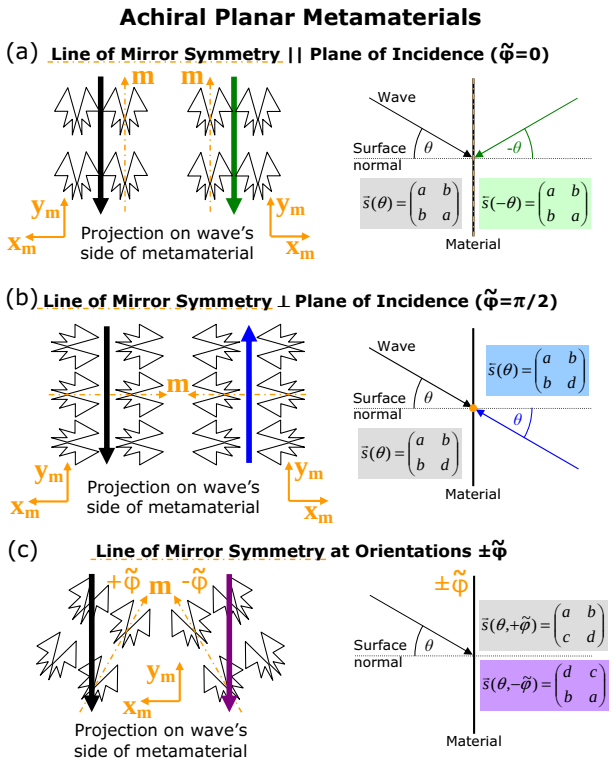

Figure 2.5: ***Achiral planar metamaterials****: Special orientations $\tilde{\varphi}$ of the metamaterial's line of (glide) mirror symmetry* $\mathbf{m}$ *relative to the plane of incidence [*$\mathbf{y_m}$*-axis, see Fig. 2.2 (c)], illustrated for a pattern belonging to the pm wallpaper symmetry group. (a) For $\tilde{\varphi} = 0$ or π opposite angles of incidence on opposite sides of the metamaterial correspond to identical experiments with identical scattering matrices and therefore $a = d$ and $b = c$. (b) For $\tilde{\varphi} = \frac{\pi}{2}$ or $\frac{3\pi}{2}$ opposite directions of incidence correspond to identical experiments with identical scattering matrices and therefore $b = c$. (c) For the same direction of incidence, opposite metamaterial orientations $\pm\tilde{\varphi}$ result in mirrored experiments with the same properties for opposite circular polarizations.*

2.2.2 Achiral Planar Metamaterials

As introduced in section 1.4, a structure that cannot be superimposed with its mirror image is called 3D-chiral. Infinitely thin planar objects cannot be 3D-chiral, as they can always be superimposed with their mirror image through rotation by π around the line of reflection that was used to create the mirror image. However, the notion of chirality also exists in two dimensions: any planar object that cannot be superimposed with its mirror image without being lifted off the plane is called 2D-chiral.

Like all planar periodic structures, planar metamaterials can be classified according to their wallpaper symmetry group [93,108,109]. For the examples of planar metamaterials presented here, we specify the wallpaper symmetry group using the crystallographic notation [110]. For an overview over all seventeen wallpaper symmetry groups refer to

appendix B.

Planar metamaterials with a line of (glide) mirror symmetry **m** are achiral and will be considered further in this section. The orientation of a 2D-achiral metamaterial pattern with respect to the plane of incidence is of special significance. This orientation is most conveniently defined by an angle $\tilde{\varphi}$ between the pattern's line of (glide) mirror symmetry **m** and the $\mathbf{y_m}$-axis along which the plane of incidence crosses the metamaterial plane.

For planar metamaterials with only one line of (glide) mirror symmetry[5], an in-plane rotation by π results in a different metamaterial orientation with the same line of mirror symmetry. In order to resolve this a direction needs to be assigned to the line of mirror symmetry **m** in this case[6]. For metamaterials with multiple lines of mirror symmetry[7], a particular mirror line needs to be chosen. Here we measure $\tilde{\varphi}$ from the $\mathbf{y_m}$-axis to the line of mirror symmetry **m**, increasing towards the *negative* $\mathbf{x_m}$-axis [compare Fig. 2.2 (c)].

Before considering general values of $\tilde{\varphi}$, we will consider special cases corresponding to the metamaterial's (glide) mirror line being either parallel ($\tilde{\varphi} = 0, \pi$) or perpendicular ($\tilde{\varphi} = \frac{\pi}{2}, \frac{3\pi}{2}$) to the plane of incidence.

As illustrated by Fig. 2.5 (a), if the metamaterial has a line of (glide) reflection symmetry **m** parallel to the plane of incidence, identical experiments result from waves incident at angles θ and $-\theta$ on opposite sides of the metamaterial. These experiments can be superimposed by rotating one of them by π around **m**. Identical experiments must have identical scattering matrices, $\overrightarrow{s}(\theta) = \overleftarrow{s}(-\theta)$, and therefore $a = d$ **and** $b = c$ **must hold for planar metamaterials with a (glide) mirror line parallel to the plane of incidence (**$\tilde{\varphi} = 0$ **or** π**)**, compare Fig. 2.4 (c).

Fig. 2.5 (b) illustrates the case when the metamaterial has a line of (glide) reflection symmetry **m** perpendicular to the plane of incidence. In this case, opposite directions of incidence result in identical experiments, which can be superimposed by rotating one experiment by π around **m**. The corresponding scattering matrices must be identical, $\overrightarrow{s}(\theta) = \overleftarrow{s}(\theta)$, and therefore $b = c$ **must hold for planar metamaterials with a**

[5] Wallpaper symmetry groups with a single line of (glide) reflection: *pm*, *pg*, *cm*.

[6] For example, narrow end to wide end of the pattern.

[7] Wallpaper symmetry groups with multiple lines of (glide) reflection: *pmm*, *pmg*, *pgg*, *cmm*, *p*4*m*, *p*4*g*, *p*3*m*1, *p*31*m*, *p*6*m*.

(glide) mirror line perpendicular to the plane of incidence ($\tilde{\varphi} = \frac{\pi}{2}$ or $\frac{3\pi}{2}$), compare Fig. 2.4 (c).

Thus the following conditions apply to achiral planar metamaterials:

$$a(\theta, n\pi) = d(\theta, n\pi), \tag{2.22}$$

$$b(\theta, n\tfrac{\pi}{2}) = c(\theta, n\tfrac{\pi}{2}) \quad \text{for} \quad n \in \mathbb{Z}. \tag{2.23}$$

Fig. 2.5 (c) illustrates the case of a fixed direction of incidence onto an achiral planar metamaterial for opposite metamaterial orientations $\pm\tilde{\varphi}$. These experiments are mirror images of each other and therefore they must show the same behavior for opposite circular polarizations,

$$a(\theta, +\tilde{\varphi}) = d(\theta, -\tilde{\varphi}), \tag{2.24}$$

$$b(\theta, +\tilde{\varphi}) = c(\theta, -\tilde{\varphi}). \tag{2.25}$$

2.2.3 Normal Incidence onto Achiral Planar Metamaterials

The special cases when the metamaterial's line of (glide) mirror symmetry is either parallel or perpendicular to the plane of incidence have particular relevance to the limit of normal incidence onto achiral planar metamaterials. At normal incidence any plane containing the metamaterial's surface normal can be considered the plane of incidence, including those parallel and perpendicular to the metamaterial's line of (glide) mirror symmetry **m**. Therefore the *physical* restrictions for both of these cases must apply to normal incidence.

However, while at oblique incidence these special cases correspond to **m** being perpendicular or parallel to the **x**-axis of the incident wave's coordinates, at normal incidence the plane of incidence and therefore the orientations of **xy** are not defined by the experimental geometry. No new physics should appear if we rotate the coordinate system around the **z**-axis. Later we will find that for normal incidence a rotation of the coordinate system by some angle $-\Delta_\varphi$ (or the metamaterial by $+\Delta_\varphi$) around the **z**-axis simply corresponds to a change in the phases of b and c, which is given explicitly by (2.74). The remaining restrictions that must hold for **normal incidence onto**

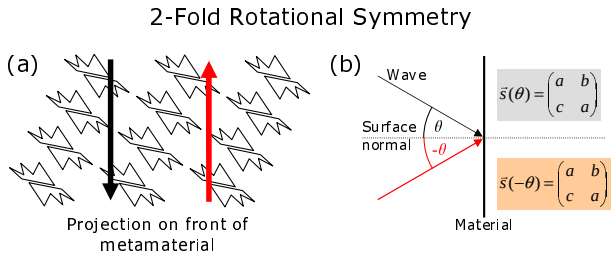

Figure 2.6: ***2-fold rotational symmetry****, illustrated for a pattern in the p2 wallpaper symmetry group. (a) Opposite angles of incidence ±θ onto a planar metamaterial with 2-fold rotational symmetry result in identical experiments. (b) The corresponding scattering matrices must also be identical, therefore a = d.*

achiral planar metamaterials are

$$a = d \quad \text{and} \quad |b| = |c|. \tag{2.26}$$

Note that $b = c$ must hold in the special coordinate systems in which the **x**-axis is either perpendicular or parallel to the metamaterial's line of (glide) mirror symmetry.

2.2.4 2-Fold Rotational Symmetry or Normal Incidence

Here we will consider two common cases, 2-fold rotational symmetry[8] (for any angle of incidence) and normal incidence (for any planar metamaterial).

As illustrated by Fig. 2.6, opposite angles of incidence onto the same side of a planar metamaterial with 2-fold rotational symmetry result in the same experiment. One experiment can be superimposed with the other through a rotation by π around the metamaterial's normal. The corresponding scattering matrices must be identical, $\overrightarrow{s}(+\theta) = \overrightarrow{s}(-\theta)$, and therefore $a = d$.

On the other hand, for any planar metamaterial $\overrightarrow{s}(\theta) = \overrightarrow{s}(-\theta)$ must hold for the limiting case $\theta = 0$, and therefore $a = d$ is required at normal incidence.

Thus for (i) **planar metamaterials at normal incidence** and (ii) **2-fold rotationally symmetric planar metamaterials at any given angle of incidence** $\pm\theta$, the most general form the scattering matrices can take is

$$\overrightarrow{s} = \begin{pmatrix} a & b \\ c & a \end{pmatrix} \quad \text{and} \quad \overleftarrow{s} = \begin{pmatrix} a & c \\ b & a \end{pmatrix}. \tag{2.27}$$

[8] Wallpaper symmetry groups with 2-fold rotational symmetry: *p2*, *pmm*, *pmg*, *pgg*, *cmm*, *p4*, *p4m*, *p4g*, *p6*, *p6m*.

For the corresponding transmission and reflection matrices, see (2.18) and (2.19), with $a = d$.

2.3 Definitions

2.3.1 Alternative Description of the Scattering Coefficients

It turns out to be convenient to make the following definitions for the diagonal elements of the scattering matrix

$$a = Ae^{i(\xi-2\delta)} - \tfrac{1}{2} \quad \text{and} \quad d = De^{i(\xi+2\delta)} - \tfrac{1}{2}. \tag{2.28}$$

These definitions allow us to specify a, d in terms of the real parameters A, D, ξ, δ, which we define as

$$A := |a + \tfrac{1}{2}| \quad \text{and} \quad D := |d + \tfrac{1}{2}| \tag{2.29}$$

$$\xi := \tfrac{\arg(a+\frac{1}{2})+\arg(d+\frac{1}{2})}{2}, \xi \in (-\pi, \pi] \tag{2.30}$$

$$\delta := \tfrac{\arg(d+\frac{1}{2})-\arg(a+\frac{1}{2})}{4}, \delta \in (-\tfrac{\pi}{2}, \tfrac{\pi}{2}). \tag{2.31}$$

Importantly, some later arguments regarding the meaning of δ, require us to choose a phase convention. We choose ξ, δ, so that $\xi \pm 2\delta \in (-\pi, \pi]$. This convention is automatically satisfied if we choose $\arg(a + \frac{1}{2}), \arg(d + \frac{1}{2}) \in (-\pi, \pi]$ and follow the above definitions.

Similarly it is convenient to define alternative parameters κ, φ for the phases of the off-diagonal elements of the scattering matrix b and c.

$$b = |b|e^{i(\kappa-2\varphi)} \quad \text{and} \quad c = |c|e^{i(\kappa+2\varphi)}, \tag{2.32}$$

where κ and φ are defined as

$$\kappa := \frac{\arg(b) + \arg(c)}{2}, \kappa \in [0, 2\pi) \tag{2.33}$$

$$\varphi := \frac{\arg(c) - \arg(b)}{4}, \varphi \in [0, \tfrac{\pi}{2}). \tag{2.34}$$

It will be shown that in the case of normal incidence or of 2-fold rotationally sym-

metric planar metamaterials φ is the azimuth of one eigenstate for forward propagation, and that in these cases the eigenpolarizations are independent of κ. We will also find that for lossless metamaterials without linear birefringence / dichroism, δ specifies the polarization azimuth rotation of the transmitted field.

2.3.2 Polarization States

In a circular basis, the azimuth Φ of a polarization state $\mathbf{E} = (E_+, E_-)$ is defined as

$$\Phi = -\frac{1}{2}[\arg(E_+) - \arg(E_-)], \tag{2.35}$$

and its ellipticity angle η is

$$\eta = \frac{1}{2}\arcsin\left(\frac{|E_+|^2 - |E_-|^2}{|E_+|^2 + |E_-|^2}\right). \tag{2.36}$$

Clearly, any polarization can be represented as a vector $\mathbf{E} = (E_+, E_-)$, where any collinear vectors $\mathbf{E'} = \tau\mathbf{E}, \tau \in \mathbb{C}$ represent the same polarization state. The squared magnitude $|\mathbf{E}|^2$ represents the power of the electromagnetic wave. As we only consider linear materials, none of the phenomena discussed here depend on the power of the incident wave, and therefore it is sufficient to consider incident waves of normalized amplitude $\hat{\mathbf{u}} = \frac{\mathbf{E}}{|\mathbf{E}|}$. All normalized polarization states can be written as

$$\hat{\mathbf{u}} = \begin{pmatrix} \sin(\beta)e^{i(\gamma-\alpha)} \\ \cos(\beta)e^{i(\gamma+\alpha)} \end{pmatrix}, \tag{2.37}$$
$$\alpha \in (-\tfrac{\pi}{2}, \tfrac{\pi}{2}], \qquad \beta \in [0, \tfrac{\pi}{2}], \qquad \gamma \in [0, 2\pi).$$

From (2.35) and (2.36) follows that the azimuth and ellipticity of $\hat{\mathbf{u}}$ are

$$\begin{aligned} \Phi(\hat{\mathbf{u}}) &= \alpha, \\ \eta(\hat{\mathbf{u}}) &= \beta - \tfrac{\pi}{4}. \end{aligned}$$

Thus $\hat{\mathbf{u}}$ represents a polarization state of azimuth α and ellipticity angle $\beta - \frac{\pi}{4}$. Different values of γ correspond to the same polarization state at different times.

2.4 Polarization Effects

The following two subsections discuss the electromagnetic effects corresponding to $a \neq d$ (optical activity) and $|b| \neq |c|$ (circular conversion dichroism). Note that for a general lossy (see below) planar metamaterial without 2-fold rotational symmetry at oblique incidence both effects should be expected to occur, if the structure does not have a line of (glide) mirror symmetry either parallel or perpendicular to the plane of incidence. In these cases the scattering matrix takes its most general form, which allows the magnitudes and phases of the scattering coefficients a, b, c, d to be all different.

It will be demonstrated in the third subsection, that $b = c = 0$ corresponds to transmission and reflection properties that are independent of the incident wave's polarization azimuth, while linear birefringence / dichroism is present in all other cases.

2.4.1 Optical Activity at Oblique Incidence ($a \neq d$)

For oblique incidence onto a planar metamaterial that does not have 2-fold rotational symmetry[9], we found that generally $\overrightarrow{t_{++}} \neq \overrightarrow{t_{--}}$, or $a \neq d$ should be expected, if the metamaterial does not have a line of (glide) mirror symmetry in the plane of incidence. We will find that $a \neq d$ corresponds to optical activity, i.e. circular birefringence and circular dichroism. These effects are normally associated with 3D chirality.

In order to see how $a \neq d$ leads to circular birefringence, consider the scattered field for an incident wave $\hat{\mathbf{u}}$ with azimuth α as defined in (2.37). The scattered field is (for forward-propagation)

$$\begin{aligned} \overrightarrow{\mathbf{E}^{\mathbf{s}}} &= \overrightarrow{s}\,\hat{\mathbf{u}}(\alpha) \\ &= \begin{pmatrix} a & b \\ c & d \end{pmatrix} \begin{pmatrix} \sin(\beta)e^{i(\gamma-\alpha)} \\ \cos(\beta)e^{i(\gamma+\alpha)} \end{pmatrix} \\ &= \begin{pmatrix} a\sin(\beta)e^{i(\gamma-\alpha)} + b\cos(\beta)e^{i(\gamma+\alpha)} \\ c\sin(\beta)e^{i(\gamma-\alpha)} + d\cos(\beta)e^{i(\gamma+\alpha)} \end{pmatrix}. \end{aligned} \tag{2.38}$$

Now we will calculate the azimuth rotation, i.e. the difference between the azimuth of scattered and incident waves. As the azimuth of a polarization state $\mathbf{E}$ is $\Phi =$

[9] Wallpaper symmetry groups without 2-fold rotational symmetry: $p1$, pm, pg, cm, $p3$, $p3m1$, $p31m$.

$-\frac{1}{2}[\arg(E_+) - \arg(E_-)]$, see (2.35), the azimuth rotation can be written as

$$\begin{aligned}
\Delta\Phi^s &= \Phi(\overrightarrow{\mathbf{E}}^{\mathbf{s}}) - \Phi(\hat{\mathbf{u}}) \\
&= -\tfrac{1}{2}\Big[\arg(a\sin(\beta)e^{i(\gamma-\alpha)} + b\cos(\beta)e^{i(\gamma+\alpha)}) \\
&\quad - \arg(c\sin(\beta)e^{i(\gamma-\alpha)} + d\cos(\beta)e^{i(\gamma+\alpha)})\Big] \\
&\quad + \tfrac{1}{2}\Big[\arg(\sin(\beta)e^{i(\gamma-\alpha)}) - \arg(\cos(\beta)e^{i(\gamma+\alpha)})\Big] \\
&= -\tfrac{1}{2}\left[\arg(a + b\cot(\beta)e^{+i2\alpha})\right. \\
&\quad \left. - \arg(c\tan(\beta)e^{-i2\alpha} + d))\right] \\
&= -\tfrac{1}{2}\left[\arg(a) - \arg(d)\right. \\
&\quad + \arg(1 + \tfrac{b}{a}\cot(\beta)e^{+i2\alpha}) \\
&\quad \left. - \arg(1 + \tfrac{c}{d}\tan(\beta)e^{-i2\alpha}))\right]. \qquad (2.39)
\end{aligned}$$

We can clearly see, that for $b = c = 0$ the azimuth rotation does not depend on the azimuth of the incident wave, as we would expect for an ideal circularly birefringent medium. The eigenstates corresponding to this case of pure optical activity will be derived in section 2.5.1. In the general case, however, the planar metamaterial may also show linear birefringence or linear dichroism and the rotation can depend on the azimuth α of the incident wave. Therefore it is more meaningful to consider the average rotation experienced by all waves with the same ellipticity. Clearly, when averaging over all $\alpha \in (-\frac{\pi}{2}, \frac{\pi}{2}]$, the last two terms must vanish, giving us the **average azimuth rotation for the scattered field**

$$< \Delta\Phi^s >= -\tfrac{1}{2}\left[\arg(a) - \arg(d)\right]. \qquad (2.40)$$

Similarly, it can be shown that the azimuth of the transmitted field is rotated by

$$\begin{aligned}
\Delta\Phi^t &= -\tfrac{1}{2}\left[\arg(a+1) - \arg(d+1)\right. \\
&\quad + \arg(1 + \tfrac{b}{a+1}\cot(\beta)e^{+i2\alpha}) \\
&\quad \left. - \arg(1 + \tfrac{c}{d+1}\tan(\beta)e^{-i2\alpha}))\right] \qquad (2.41)
\end{aligned}$$

and the **average azimuth rotation for the transmitted field** is

$$< \Delta\Phi^t >= -\tfrac{1}{2}\left[\arg(a+1) - \arg(d+1)\right]. \tag{2.42}$$

Note that the azimuth rotation for scattered and reflected fields has opposite signs, $\Delta\Phi^r = -\Delta\Phi^s$, as scattering rotation is measured looking into the incident beam while reflection rotation is measured looking into the reflected beam.

It can be easily seen, that generally $a \neq d$ leads not only to circular birefringence, but also to circular dichroism. Transmission circular dichroism corresponds to different direct transmission levels for opposite circular polarizations

$$\Delta T := |t_{++}|^2 - |t_{--}|^2 = |a+1|^2 - |d+1|^2 \tag{2.43}$$

and for planar metamaterials it is accompanied by analogous phenomena in scattering and reflection

$$\Delta S := |s_{++}|^2 - |s_{--}|^2 = |a|^2 - |d|^2, \tag{2.44}$$

$$\Delta R := |r_{-+}|^2 - |r_{+-}|^2 = |a|^2 - |d|^2. \tag{2.45}$$

Note that polarization states are always measured looking into the beam, thus the reflected beam must be measured in a different coordinate system, which gives rise to different indices in (2.45).

Circular dichroism must not be confused with the directionally asymmetric effect introduced in the next section, for which different transmission (reflection) levels for opposite circular polarizations arise from circular polarization conversion. Circular dichroism has nothing to do with circular polarization conversion. The following relation, which is equivalent to (2.43), allows separating of the asymmetric transmission effect from transmission circular dichroism in measurements with a polarization insensitive detector.

$$\Delta T = \frac{(\overrightarrow{T_+} + \overleftarrow{T_+}) - (\overrightarrow{T_-} + \overleftarrow{T_-})}{2}, \tag{2.46}$$

where $T_\pm = |t_{\pm\pm}|^2 + |t_{\mp\pm}|^2$ corresponds to the total transmission, including circular

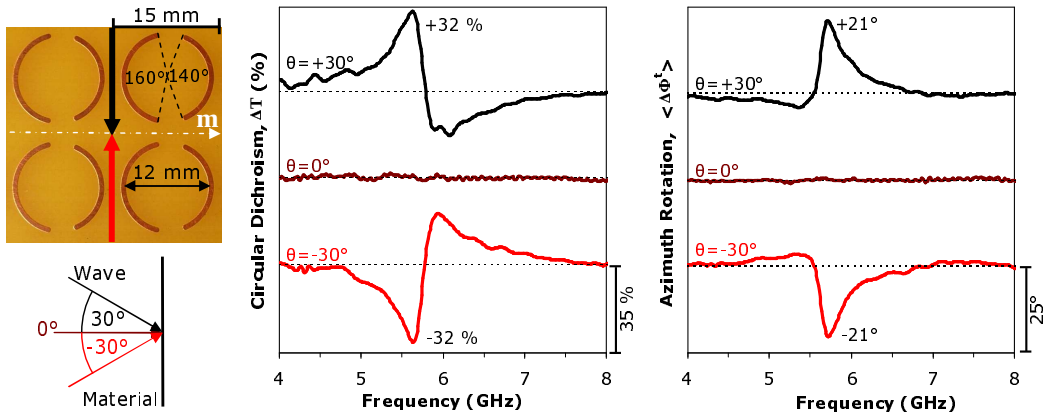

Figure 2.7: ***Experimental demonstration of optical activity due to extrinsic 3D chirality.*** *Spectra of transmission circular dichroism, ΔT, and polarization rotation, $< \Delta\Phi^t >$, measured for a planar metamaterial based on achiral asymmetrically split wire rings (wallpaper symmetry group pm). The respective zero level is indicated by a dashed line. The 3D-chiral phenomena have reversed signs for opposite angles of incidence $\theta = \pm 30°$ and vanish at normal incidence. The structure's line of mirror symmetry* $\mathbf{m}$ *is oriented perpendicular to the plane of incidence ($\tilde{\varphi} = \frac{\pi}{2}$), which ensures the absence of the asymmetric effects discussed in subsection 2.4.2. How extrinsic 3D chirality controls the properties of this metamaterial is discussed in detail in chapter 4 and reference [55].*

polarization conversion, in the indicated direction.

As the diagonal elements of the scattering and transmission matrices do not depend on reversal of the propagation direction, (2.40)-(2.45) apply to forward and backward propagation. For the opposite angle of incidence $-\theta$ and in-plane rotations of the metamaterial by π, however, the roles of a and d are reversed, see (2.13) and (2.15), and these equations change sign. In other words **circular birefringence and circular dichroism are the same for opposite propagation directions, but the effects change sign for opposite angles of incidence and in-plane rotations of the metamaterial by** π. It follows that polarization rotation and circular dichroism in planar metamaterials without 2-fold rotational symmetry are tunable via the angle of incidence. The effects are "switched off" at normal incidence and can be "switched on" with one sign for angles of incidence $\theta > 0$ and the other sign for $\theta < 0$.

It was derived in section 2.2.1 that lossless complementary planar metamaterials have interchanged direct scattering and transmission coefficients for circularly polarized waves (apart from an overall phase shift). Therefore **transmission and scattering optical activity are interchanged for lossless complementary planar metamaterials**.

For achiral planar metamaterials[10], it follows from (2.22) that optical activity is absent, if the metamaterial has a line of (glide) mirror symmetry in the plane of incidence. Thus for the orientations $\tilde{\varphi} = 0, \pi$, circular birefringence and circular dichroism are absent independent of θ. Equation (2.24) implies that for achiral planar metamaterials the signs of circular birefringence and circular dichroism will be reversed for in-plane metamaterial orientations $\pm\tilde{\varphi}$. (Of course, as we found for the general case, the signs will also be reversed for orientations $\tilde{\varphi}, \tilde{\varphi}+\pi$ or alternatively tilt angles $\pm\theta$.) Importantly, if the achiral planar metamaterial has a line of (glide) mirror symmetry perpendicular to the plane of incidence, i.e. $\tilde{\varphi} = \frac{\pi}{2}, \frac{3\pi}{2}$, the asymmetric phenomena for $|b| \neq |c|$ that will be discussed in the section 2.4.2 are absent, while circular birefringence and circular dichroism are still permitted. Thus achiral planar metamaterials allow optical activity without asymmetric phenomena. Experimental results illustrating this case are shown in Fig. 2.7 and chapter 4.

Optical activity is generally associated with 3D chirality. One might correctly argue that a planar structure, which can always be superimposed with its mirror image via an out-of-the-plane rotation by π, cannot be 3D-chiral. However, it turns out that for oblique incidence onto a structure without 2-fold rotational symmetry, the metamaterial and the incident beam form a 3D-chiral experimental arrangement, if the metamaterial does not have a line of (glide) mirror symmetry in the plane of incidence, see Figs. 2.8 (c) and (e). Chirality arising from the mutual orientation of metamaterial and incident beam has been called *extrinsic chirality* [55], in order to distinguish it from *intrinsic chirality* which refers to the symmetry of a material, see Fig. 2.8 (a).

Optical activity due to extrinsic 3D chirality was first predicted by Bunn [111] and later detected in liquid crystals [112, 113]. However, the topic attracted hardly any attention until the observation of large circular birefringence and circular dichroism due to extrinsic 3D chirality in planar metamaterials [55, 56], see chapter 4.

Inherently tunable optical activity in planar metamaterials allows the realization of tunable planar metamaterial polarization rotators and circular polarizers. The potential performance of such devices will be discussed in sections 2.7.4 and 2.7.5.

For any planar metamaterial at normal incidence, and for planar metamaterials

[10] Achiral wallpaper symmetry groups without 2-fold rotational symmetry: pm, pg, cm, $p3m1$, $p31m$.

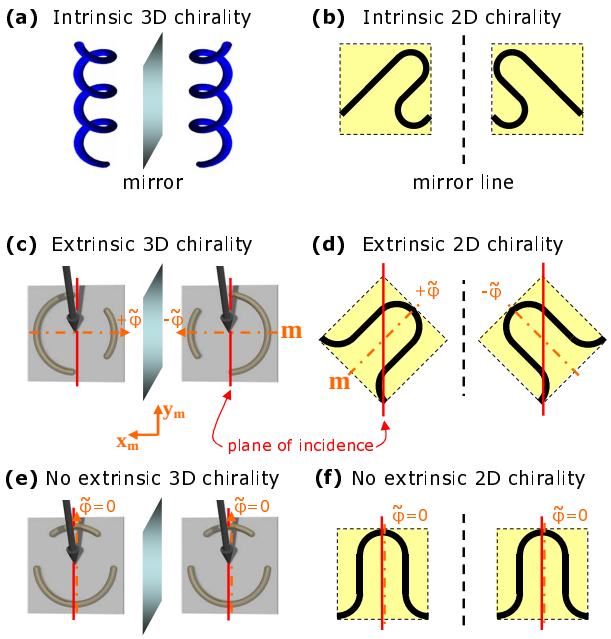

Figure 2.8: ***Intrinsic and extrinsic chirality.*** *Panels (a) and (b) show examples of intrinsically 3D-chiral and 2D-chiral elements respectively. (c) Extrinsic 3D chirality: the arrangement of structure and incident wave cannot be superimposed with its mirror image. (d) Extrinsic 2D chirality: the structure combined with the direction introduced by the plane of incidence cannot be superimposed with its mirror image without being lifted off the plane. Panels (e) and (f) show configurations where extrinsic chirality is absent.*

with 2-fold rotational symmetry[11] in general, equality of the diagonal elements of the transmission matrix is required, i.e. $\overrightarrow{t_{++}} = \overrightarrow{t_{--}}$, and thus optical activity is prohibited. This should also be expected, as the metamaterial and the incident beam cannot form an extrinsically 3D-chiral experimental arrangement in these cases.

2.4.2 Circular Conversion Dichroism ($|b| \neq |c|$)

Intriguing behavior may also arise from the in general non-equal off-diagonal terms of the transmission matrix. Consider right-handed circularly polarized $\mathbf{E^0} = (1, 0)^{tr}$ waves with opposite propagation directions incident on front and back of a planar

[11] Wallpaper symmetry groups with 2-fold rotational symmetry: *p*2, *pmm*, *pmg*, *pgg*, *cmm*, *p*4, *p*4*m*, *p*4*g*, *p*6, *p*6*m*.

metamaterial.

$$\overrightarrow{\mathbf{E}}^{\mathbf{t}} = \overrightarrow{t}(\theta,\tilde{\varphi})\overrightarrow{\mathbf{E}}^{\mathbf{0}} = \begin{pmatrix} a+1 \\ c \end{pmatrix} \tag{2.47}$$

$$\overleftarrow{\mathbf{E}}^{\mathbf{t}} = \overleftarrow{t}(\theta,\tilde{\varphi})\overleftarrow{\mathbf{E}}^{\mathbf{0}} = \begin{pmatrix} a+1 \\ b \end{pmatrix}$$

Assuming the case of $|b(\theta,\tilde{\varphi})| > |c(\theta,\tilde{\varphi})|$, this implies that the considered planar structure would be less transparent for right-handed circularly polarized waves that are incident on its front than its back. One can easily see that the transmission asymmetry has to be reversed for left-handed waves. The asymmetry arises from different circular polarization conversion efficiencies $\overleftarrow{t_{-+}} = b$ and $\overrightarrow{t_{-+}} = c$ for opposite propagation directions of the same circular polarization (circular conversion dichroism).

If we calculate the reflectivity for right-handed circularly polarized waves, we find

$$\begin{aligned} \overrightarrow{\mathbf{E}}^{\mathbf{r}} &= \overrightarrow{r}(\theta,\tilde{\varphi})\overrightarrow{\mathbf{E}}^{\mathbf{0}} = \begin{pmatrix} c \\ a \end{pmatrix} \\ \overleftarrow{\mathbf{E}}^{\mathbf{r}} &= \overleftarrow{r}(\theta,\tilde{\varphi})\overleftarrow{\mathbf{E}}^{\mathbf{0}} = \begin{pmatrix} b \\ a \end{pmatrix}. \end{aligned} \tag{2.48}$$

Assuming again that $|b(\theta,\tilde{\varphi})| > |c(\theta,\tilde{\varphi})|$, this implies that the considered planar structure would be simultaneously less transparent and less reflective for right-handed waves that are incident on its front than its back. The asymmetry is reversed for left-handed waves. As a fraction of incident power, the transmission asymmetry and reflection asymmetry are

$$\overrightarrow{T_{\pm}} - \overleftarrow{T_{\pm}} = \overrightarrow{R_{\pm}} - \overleftarrow{R_{\pm}} = \pm(|c|^2 - |b|^2), \tag{2.49}$$

where $\overrightarrow{T_{\pm}}, \overrightarrow{R_{\pm}}, \overleftarrow{T_{\pm}}, \overleftarrow{R_{\pm}}$ correspond to the transmitted (T) and reflected (R) power fractions for circularly polarized (right, + or left, -) incident waves with opposite propagation directions (arrows). For example the transmitted power fraction for a forward-propagating right-handed circularly polarized incident wave is $\overrightarrow{T_{+}} = |t_{++}|^2 + |\overrightarrow{t_{-+}}|^2$.

This corresponds to an asymmetry of losses, L, of

$$\overrightarrow{L_\pm} - \overleftarrow{L_\pm} = \mp 2(|c|^2 - |b|^2), \tag{2.50}$$

where $\overrightarrow{L_\pm}, \overleftarrow{L_\pm}$ correspond to the "lost" power fractions for circularly polarized (right, + or left, -) incident waves with opposite propagation directions (arrows). Thus, a planar metamaterial for which $|b| \neq |c|$ will have larger losses for one circular polarization for forward propagation and for the other circular polarization for backward propagation. Limits on the magnitude of the asymmetries in transmission, reflection and losses will be derived from energy conservation in section 2.6.2, while the eigenstates associated with circular conversion dichroism are discussed in section 2.5.2.

In particular the asymmetric phenomena, which occur when $|b| \neq |c|$, imply that at least one circular polarization experiences losses. For metamaterials, which do not diffract, the only loss-mechanism is absorption. Thus **for lossless planar metamaterials circular conversion dichroism cannot occur and $|b| = |c|$ must hold**. However, note that in principle diffraction losses could play the same role as absorption losses and thus the asymmetric phenomena may be possible in non-absorbing planar diffraction gratings, i.e. structures that would be lossless planar metamaterials at longer wavelengths.

For any planar metamaterial the angular dependence of the parameters b and c must obey equations (2.14) and (2.16), which imply that the difference $|c|^2 - |b|^2$ takes the same value for opposite angles of incidence $\pm\theta$ and for in-plane rotations of the metamaterial by π.

$$\begin{aligned}(|c|^2 - |b|^2)(\theta, \tilde{\varphi}) &= (|c|^2 - |b|^2)(-\theta, \tilde{\varphi}) \\ &= (|c|^2 - |b|^2)(\theta, \tilde{\varphi} + \pi)\end{aligned} \tag{2.51}$$

This indicates that circular conversion dichroism is the same for opposite angles of incidence $\pm\theta$. For in-plane rotation of the metamaterial, the asymmetric behavior is periodic with period π, i.e. the metamaterial must show the same circular conversion dichroism for orientations $\tilde{\varphi}$ and $\tilde{\varphi} + \pi$.

For achiral planar metamaterials[12] the scattering coefficients b and c must also obey

[12] Achiral wallpaper symmetry groups: *pm*, *pg*, *cm*, *pmm*, *pmg*, *pgg*, *cmm*, *p4m*, *p4g*, *p3m1*, *p31m*,

(2.23) and (2.25), from which we can conclude that the difference $|c|^2 - |b|^2$ is an odd function of the metamaterial orientation $\tilde{\varphi}$ that is zero for multiples of $\frac{\pi}{2}$.

$$\begin{aligned} (|c|^2 - |b|^2)(\theta, +\tilde{\varphi}) &= -(|c|^2 - |b|^2)(\theta, -\tilde{\varphi}) \quad \text{and} \\ (|c|^2 - |b|^2)(\theta, n\tfrac{\pi}{2}) &= 0 \quad \text{for} \quad n \in \mathbb{Z} \end{aligned} \tag{2.52}$$

This means that for achiral planar metamaterials the directional asymmetries are reversed for in-plane orientations $\pm\tilde{\varphi}$ of the metamaterial, and that circular conversion dichroism is absent if the metamaterial has a line of (glide) mirror symmetry either parallel ($\tilde{\varphi} = 0, \pi$) or perpendicular ($\tilde{\varphi} = \frac{\pi}{2}, \frac{3\pi}{2}$) to the plane of incidence, see Fig. 2.10 and chapter 3.3. In particular it follows that achiral planar metamaterials do not allow the directionally asymmetric effects for the special case of normal incidence.

Importantly, cases that allow circular conversion dichroism, while optical activity ($a \neq d$), which has been discussed in the preceding section, cannot occur, are (i) lossy planar metamaterials with 2-fold rotational symmetry[13] and (ii) normal incidence onto lossy 2D-chiral planar metamaterials[14] (that are anisotropic, as explained in section 2.4.3).

The asymmetric transmission, reflection and absorption phenomena arise from reversed right-to-left and left-to-right circular polarization conversion efficiencies for opposite directions of wave propagation. Such properties resemble the perceived handedness of 2D-chiral patterns (e.g., flat spirals), which is reversed for opposite directions of observation. In fact, the above mentioned symmetry requirements are equivalent to stating that circular conversion dichroism requires 2D chirality. This can be either intrinsic 2D chirality of the planar metamaterial itself, see Fig. 2.8 (b), or it can be extrinsic 2D chirality of the experimental arrangement. Extrinsic 2D chirality is present if the metamaterial pattern combined with the direction introduced by the plane of incidence is 2D-chiral, i.e. if they cannot be superimposed with their mirror image without being lifted off the plane, see Figs. 2.8 (d) and (f). In other words, starting from normal incidence, extrinsic 2D chirality results from tilting a planar metamaterial around any axis that does not coincide with a line of mirror symmetry (or glide reflection).

Asymmetric transmission was discovered in 2006 for normal incidence of microwaves

p6m.

[13] Wallpaper symmetry groups with 2-fold rotational symmetry: *p2*, *pmm*, *pmg*, *pgg*, *cmm*, *p4*, *p4m*,

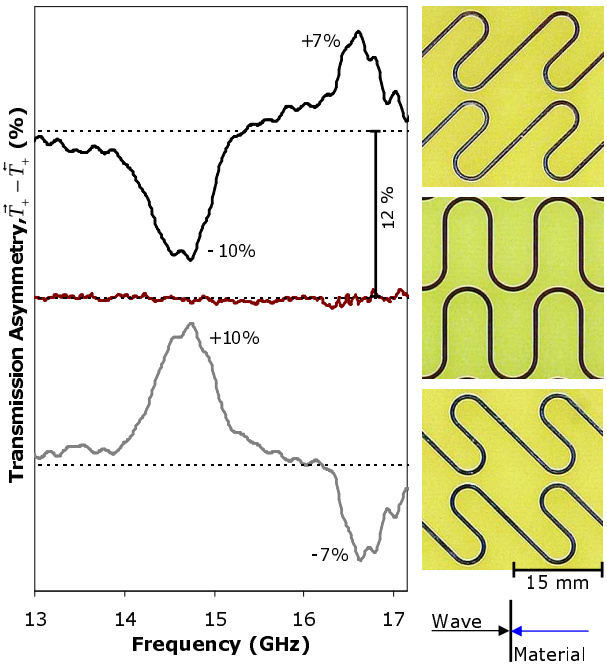

Figure 2.9: ***Experimental demonstration of asymmetric transmission at normal incidence due to intrinsic 2D chirality.*** *The spectral dependence of the directional transmission asymmetry, $\overrightarrow{T_+} - \overleftarrow{T_+}$, for right-handed circularly polarized waves is shown for right-handed, achiral and left-handed forms of the metamaterial (wallpaper symmetry groups p2, pmg, p2). The respective zero level is indicated by a dashed line. The insets show the front side of the structures. See reference [64] for a detailed discussion of the experimental work.*

onto an intrinsically 2D-chiral metamaterial [64], which is shown in Fig. 2.9. Soon thereafter the effect was also seen for planar metamaterials in optics [90] and for terahertz waves [95], as well as for single plasmonic nanostructures [96]. Corresponding asymmetries were first numerically predicted [97] and then measured [98] for reflection and absorption, see chapter 3.2.1. Asymmetric transmission due to extrinsic 2D chirality has been discovered in 2009 for oblique incidence onto an achiral metamaterial [99], see Fig. 2.10 and chapter 3.3.

2.4.3 Linear Birefringence and Linear Dichroism ($b \neq 0$ and/or $c \neq 0$)

Whenever a structure's electromagnetic properties depend on the azimuth of the incident wave, linear birefringence and/or dichroism are present. In their pure form, these phenomena are associated with orthogonal linearly polarized eigenpolarizations (see

p4g, *p6*, *p6m*.

[14] Anisotropic 2D-chiral wallpaper symmetry groups: *p1*, *p2*.

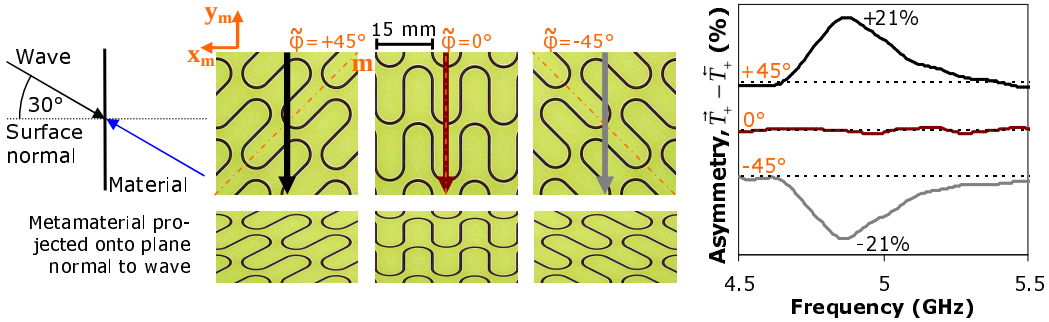

Figure 2.10: ***Experimental demonstration of asymmetric transmission due to extrinsic 2D chirality.*** *The spectral dependence of the directional transmission asymmetry, $\overrightarrow{T_+} - \overleftarrow{T_+}$, for right-handed circularly polarized waves is shown for orientations $\tilde{\varphi} = 0, \pm\frac{\pi}{4}$ of the achiral metamaterial (wallpaper group pmg). The respective zero level is indicated by a dashed line. The angle of incidence is $\theta = 30°$ in all cases. Note that the metamaterial's projection onto the plane normal to the direction of incidence is 2D-chiral when extrinsic 2D chirality is present. Refer to chapter 3.3 and reference [99] for detailed discussions of this experimental work.*

section 2.5.2), which experience different phase delays (linear birefringence) or different transmission/reflection/absorption levels (linear dichroism).

At normal incidence, linear birefringence and dichroism can only be observed for anisotropic planar metamaterials, where for achiral anisotropic structures[15] the preferred directions (i.e. eigenpolarizations) are parallel and perpendicular to the line of (glide) mirror symmetry. For 2D-chiral anisotropic planar metamaterials[16] the preferred directions are not well-defined by the geometry and therefore they can be frequency-dependent.

At oblique incidence, the situation is more complex, as new preferred directions parallel and perpendicular to the plane of incidence are introduced by the experimental arrangement. Thus isotropic planar metamaterials[17] can show anisotropic polarization effects at oblique incidence. For achiral anisotropic planar metamaterials the preferred directions become frequency-dependent at oblique incidence if the line of (glide) mirror symmetry is not parallel or perpendicular to the plane of incidence, as the structural anisotropy competes with the preferred directions introduced by oblique incidence. For 2D-chiral anisotropic planar metamaterials the preferred directions are obviously frequency-dependent at oblique incidence.

We note that at oblique incidence isotropic structures can exhibit linear birefrin-

[15] Achiral anisotropic wallpaper symmetry groups: *pm*, *pg*, *cm*, *pmm*, *pmg*, *pgg*, *cmm*.
[16] 2D-chiral anisotropic wallpaper symmetry groups: *p*1, *p*2.
[17] Isotropic wallpaper symmetry groups: *p*3, *p*3*m*1, *p*31*m*, *p*4, *p*4*m*, *p*4*g*, *p*6, *p*6*m*.

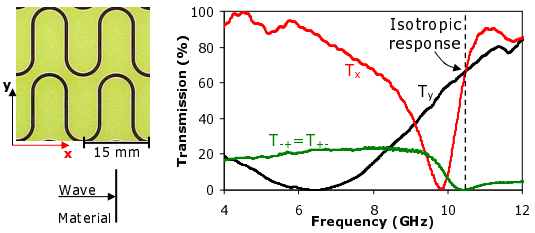

Figure 2.11: ***Experimental example of a metamaterial exhibiting linear dichroism.*** *Normal incidence transmission spectra for waves polarized perpendicular (***x***) and parallel (***y***) to the metamaterial's line of mirror symmetry. Consistently with its highly anisotropic structure, the planar metamaterial (wallpaper group pmg) generally shows substantial linear dichroism, $T_x - T_y$. This is reflected by non-zero circular polarization conversion T_{-+}. However, at 10.5 GHz linear dichroism vanishes: transmission levels for* **x** *and* **y** *polarizations are identical and circular polarization conversion is absent. Refer to reference [53] for more details on this experimental work.*

gence / dichroism. Also, at specific frequencies linear birefringence / dichroism may be absent for anisotropic planar metamaterials, as is illustrated by Fig. 2.11.

In order to see what scattering properties correspond to linear birefringence / dichroism, let's consider the azimuth rotation and ellipticity angle of the scattered field for some incident wave $\hat{\mathbf{u}}$ of azimuth α. Any polarization state with azimuth α can be written as (2.37)

$$\hat{\mathbf{u}} = \begin{pmatrix} \sin(\beta)e^{i(\gamma-\alpha)} \\ \cos(\beta)e^{i(\gamma+\alpha)} \end{pmatrix},$$
$$\alpha \in (-\tfrac{\pi}{2}, \tfrac{\pi}{2}], \qquad \beta \in [0, \tfrac{\pi}{2}], \qquad \gamma \in [0, 2\pi).$$

The azimuth rotation of the scattered field is given by (2.39)

$$\begin{aligned} \Delta\Phi^s \;=\; & -\tfrac{1}{2}\left[\arg(a) - \arg(d)\right. \\ & + \arg(1 + \tfrac{b}{a}\cot(\beta)e^{+i2\alpha}) \\ & \left. - \arg(1 + \tfrac{c}{d}\tan(\beta)e^{-i2\alpha}))\right]. \end{aligned}$$

Thus $\Delta\Phi^s$ depends on the azimuth α of the incident wave if and only if at least one of the scattering coefficients b, c is non-zero. It follows that all scattering matrices with $b \neq 0$ or $c \neq 0$ correspond to the presence of linear birefringence / dichroism.

To see whether all diagonal scattering matrices correspond to the absence of linear birefringence / dichroism, we must check whether the ellipticity angle of the scattered

field is also independent of the incident wave's azimuth α when $b = c = 0$.

The scattered field for $b = c = 0$ is (for forward- and backward-propagation since $b = c$)

$$\begin{aligned}\mathbf{E^s} &= s\,\hat{\mathbf{u}} \\ &= \begin{pmatrix} a & 0 \\ 0 & d \end{pmatrix} \begin{pmatrix} \sin(\beta)e^{i(\gamma-\alpha)} \\ \cos(\beta)e^{i(\gamma+\alpha)} \end{pmatrix} \\ &= \begin{pmatrix} a\sin(\beta)e^{i(\gamma-\alpha)} \\ d\cos(\beta)e^{i(\gamma+\alpha)} \end{pmatrix}.\end{aligned}$$

Using (2.36) we get the ellipticity angle of the scattered field

$$\begin{aligned}\eta^s &= \frac{1}{2}\arcsin\left(\frac{|E_+^s|^2 - |E_-^s|^2}{|E_+^s|^2 + |E_-^s|^2}\right) \\ &= \frac{1}{2}\arcsin\left(\frac{|a\sin(\beta)|^2 - |d\cos(\beta)|^2}{|a\sin(\beta)|^2 + |d\cos(\beta)|^2}\right).\end{aligned}$$

Clearly also the ellipticity angle of the scattered field does not depend on the azimuth α of the incident field, if $b = c = 0$. By replacing a, d with $a+1, d+1$ we could write the same proof for the transmitted field. **Thus all scattering matrices with $b = c = 0$ correspond to the absence of linear birefringence / dichroism, while all other scattering matrices correspond to the presence of linear birefringence and/or linear dichroism.**

Importantly, it follows that circular conversion dichroism ($|b| \neq |c|$), which has been discussed in section 2.4.2, can only occur if linear birefringence and/or linear dichroism is present.

We will speak of pure linear birefringence / dichroism, if no other polarization effects are present. This requires simultaneous absence of circular conversion dichroism ($|b| = |c| \neq 0$) and optical activity ($a = d$). Linear dichroism in planar metamaterials can be exploited for the realization of linear polarizers, and linear birefringence allows planar metamaterial wave plates to be developed. The potential performance of such devices will be discussed in sections 2.7.2 and 2.7.3.

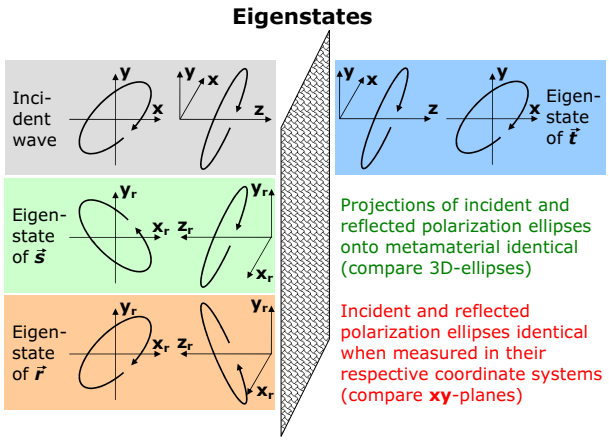

Figure 2.12: ***Eigenstates*** *of the transmission (blue), scattering (green) and reflection (red) matrices. For scattering eigenstates the projections of the polarization ellipses of the incident and reflected waves onto the metamaterial are the same, whereas for eigenstates of the reflection matrix, the incident and reflected waves have the same parameters in their mutually rotated coordinate systems.*

2.5 Eigenstates

To gain a better understanding of polarization effects in planar metamaterials, here we study the associated eigenstates. The transmission eigenstates simply correspond to those polarization states that are transmitted without any change in azimuth and ellipticity, see Fig. 2.12 (blue). For reflection the situation is more complex. As polarization states must be measured looking into the beam, the reflection matrix relates incident and reflected waves that are measured in mutually rotated coordinate systems, compare Fig. 2.12 (gray) with (red). Thus the eigenstates of the reflection matrix are polarization states for which the azimuth and ellipticity of the incident and reflected waves are the same in their respective coordinate systems. This, however, is not physically meaningful, as it depends on the choice of coordinates (orientation of $\mathbf{x}$ and $\mathbf{x_r}$ in the plane normal to the propagation direction). **For reflection the eigenstates of the scattering matrix**, which describes reflection in the coordinates of the incident wave, **are physically meaningful eigenstates**. For eigenstates of the scattering matrix the projection of the polarization ellipses of the incident and reflected waves onto the metamaterial are the same.

For the scattering eigenstates, the eigenvalues $\lambda^s_{1,2}$ are given by the eigenvalue equa-

tion

$$\begin{aligned} \det\left[\overrightarrow{s}-\lambda^s\right] &= \det\begin{pmatrix} a-\lambda^s & b \\ c & d-\lambda^s \end{pmatrix} \\ &= (a-\lambda^s)(d-\lambda^s)-bc=0 \end{aligned} \tag{2.53}$$

which, for both forward and backward propagation, has the solutions

$$\begin{aligned} \lambda^s_{1,2} &= \frac{a+d}{2} \pm \sqrt{\left(\frac{a-d}{2}\right)^2+bc} \\ &= \frac{a+d}{2} \pm \sqrt{\left(\frac{a-d}{2}\right)^2+|bc|e^{i2\kappa}}. \end{aligned} \tag{2.54}$$

Similarly, the eigenvalues of the transmission matrix are

$$\lambda^t_{1,2} = 1+\frac{a+d}{2} \pm \sqrt{\left(\frac{a-d}{2}\right)^2+|bc|e^{i2\kappa}} \tag{2.55}$$

for both forward and backward propagation. Thus the simple relation

$$\lambda^t_{1,2} = 1+\lambda^s_{1,2} \tag{2.56}$$

applies for transmission and scattering eigenvalues in planar metamaterials. Note that the eigenvalues do not depend on φ.

The scattering eigenstates (or eigenvectors) for the general case can be calculated from the eigenvector equation, for forward propagation

$$\begin{aligned} \overrightarrow{s}\,\overrightarrow{\mathbf{v}} &= \lambda\overrightarrow{\mathbf{v}} \\ \begin{pmatrix} a & b \\ c & d \end{pmatrix}\begin{pmatrix} \overrightarrow{v}_+ \\ \overrightarrow{v}_- \end{pmatrix} &= \lambda\begin{pmatrix} \overrightarrow{v}_+ \\ \overrightarrow{v}_- \end{pmatrix} \\ \begin{pmatrix} a\overrightarrow{v}_+ + b\overrightarrow{v}_- \\ c\overrightarrow{v}_+ + d\overrightarrow{v}_- \end{pmatrix} &= \lambda\begin{pmatrix} \overrightarrow{v}_+ \\ \overrightarrow{v}_- \end{pmatrix}, \end{aligned} \tag{2.57}$$

where $\overrightarrow{\mathbf{v}}$ is an eigenstate. By eliminating λ from the two conditions contained in the

last line, we arrive at the eigenstate condition

$$a + b\frac{\overrightarrow{v}_-}{\overrightarrow{v}_+} = c\frac{\overrightarrow{v}_+}{\overrightarrow{v}_-} + d. \tag{2.58}$$

Note that by replacing a and d with $a+1$ and $d+1$, we get the corresponding condition for the transmission eigenstates. Clearly (2.58) remains unchanged by this substitution, and thus the eigenstate conditions for both forward transmission and forward scattering are identical. It follows that **planar metamaterials have identical transmission and scattering eigenstates**. This becomes obvious when considering that for transmission eigenstates the superposition of scattered field and incident wave must have the same polarization state as the incident wave on its own. This can only be achieved if transmission eigenstates are simultaneously scattering eigenstates. Note however, that we have to **distinguish between eigenstates for forward-propagating and backward-propagating incident waves**. The eigenstate condition for backward-propagation corresponds to (2.58) with reversed values of b and c,

$$a + c\frac{\overleftarrow{v}_-}{\overleftarrow{v}_+} = b\frac{\overleftarrow{v}_+}{\overleftarrow{v}_-} + d. \tag{2.59}$$

In the general case, when the polarization effects of optical activity, circular conversion dichroism, linear birefringence and linear dichroism may occur simultaneously, any pair of polarization states is the pair of eigenstates of some scattering matrix. Thus it is more instructive to derive the eigenstates associated with specific polarization effects. Here we do this for the cases of pure optical activity ($b = c = 0$) and the absence of optical activity ($a = d$). Note that the latter case corresponds to the general eigenstates for (i) normal incidence onto planar metamaterials and (ii) any angle of incidence onto 2-fold rotationally symmetric planar metamaterials, as in these cases $a = d$ always applies.

2.5.1 Eigenstates for Pure Optical Activity ($b = c = 0$)

Optical activity, i.e. circular birefringence and circular dichroism, has been introduced in section 2.4.1. Pure optical activity corresponds to the special situation when no other polarization effects are present. In this case $b = c = 0$ is required, which results in diagonal scattering and transmission matrices and simple solutions for eigenvalues

and eigenstates. The eigenvalues given by (2.54) and (2.55) simplify to the diagonal elements of the corresponding matrices

$$\lambda_1^s = \quad a, \qquad \lambda_2^s = b, \tag{2.60}$$

$$\lambda_1^t = \quad a+1, \qquad \lambda_2^t = b+1, \tag{2.61}$$

while the eigenstates $\mathbf{v_{1,2}}$ simply correspond to the polarization states that form our basis, i.e. right-handed and left-handed circular polarizations

$$\mathbf{v_1} = \begin{pmatrix} 1 \\ 0 \end{pmatrix}, \qquad \mathbf{v_2} = \begin{pmatrix} 0 \\ 1 \end{pmatrix}. \tag{2.62}$$

Note that eigenvalues and eigenstates with the same indices correspond to each other, and that in this case eigenvalues and eigenstates are the same for opposite propagation directions. For the opposite angle of incidence $-\theta$ the roles of a and b are reversed, which means in this case that the same eigenstates correspond to the opposite eigenvalues.

So in the case of pure optical activity, i.e. $b = c = 0$, the eigenstates are counter-rotating circular polarizations.

2.5.2 Eigenstates in the Absence of Optical Activity ($a = d$)

Here we derive the eigenstates for planar metamaterials not showing optical activity. Such structures can show the directionally asymmetric transmission, reflection and absorption effects identified in section 2.4.2 as well as linear birefringence and dichroism in their purest forms. Note that $a = d$ is automatically satisfied in two important cases for which optically active behavior cannot occur. These are (i) normal incidence onto any planar metamaterial and (ii) any angle of incidence onto 2-fold rotationally symmetric planar metamaterials[18]. Therefore the eigenvalues and eigenstates derived here are the complete set for cases (i) and (ii).

For $a = d$ the scattering and transmission eigenvalues given by (2.54) and (2.55)

[18] Wallpaper symmetry groups with 2-fold rotational symmetry: $p2$, pmm, pmg, pgg, cmm, $p4$, $p4m$, $p4g$, $p6$, $p6m$.

respectively simplify to

$$\lambda^s_{1,2} = \quad a \pm \sqrt{bc} \quad = a \pm \sqrt{|bc|}e^{i\kappa}, \tag{2.63}$$

$$\lambda^t_{1,2} = \quad a + 1 \pm \sqrt{bc} \quad = a + 1 \pm \sqrt{|bc|}e^{i\kappa}, \tag{2.64}$$

which apply to both forward and backward propagation. Solutions λ_1 and λ_2 correspond to "+" and "-" respectively. Note that the eigenvalues do not depend on φ.

The transmission and scattering eigenstates for forward-propagation are given by (2.58), which simplifies for $a = d$ to

$$\frac{(\overrightarrow{v}_+)^2}{(\overrightarrow{v}_-)^2} = \frac{b}{c}. \tag{2.65}$$

Note that the equivalent expression for the backward-propagation eigenstates has reversed values of b and c. From the magnitude of the terms in (2.65) we can follow the ellipticity angle η of the eigenstates, while the azimuth follows from their phases. Thus the eigenstates are fully defined by condition (2.65).

Generally the ellipticity angle of a polarization state is given by (2.36)

$$\eta = \frac{1}{2}\arcsin\left(\frac{|E_+|^2 - |E_-|^2}{|E_+|^2 + |E_-|^2}\right).$$

By considering the magnitudes of all terms in (2.65) we can easily see that for the forward-propagation eigenstates, $\mathbf{E} = \overrightarrow{\mathbf{v}}_{\mathbf{1,2}}$, the ellipticity angle must be

$$\overrightarrow{\eta} = \frac{1}{2}\arcsin\left(\frac{|b| - |c|}{|b| + |c|}\right). \tag{2.66}$$

This indicates that both eigenstates must have the same ellipticity angle. In particular, if they are not linear polarizations, they must be co-rotating. For backward propagation the roles of b and c are reversed and therefore

$$\overleftarrow{\eta} = -\overrightarrow{\eta}, \tag{2.67}$$

which indicates that also the eigenstates for backward propagation are co-rotating if they are not linear; however, they have the opposite handedness compared to the eigenstates for forward propagation.

The azimuth Φ of a polarization state is generally given by (2.35)

$$\Phi = -\tfrac{1}{2}\left(\arg(E_+) - \arg(E_-)\right).$$

By considering the phases of all terms in (2.65) it can easily be seen that for the forward-propagation eigenstates $\mathbf{E^0} = \overrightarrow{\mathbf{v}}_{\mathbf{1,2}}$ the following phase condition must be satisfied

$$\arg(\overrightarrow{v}_+) - \arg(\overrightarrow{v}_-) = \begin{cases} \frac{\arg(b)-\arg(c)}{2} \\ \frac{\arg(b)-\arg(c)}{2} - \pi. \end{cases} \tag{2.68}$$

With (2.35) the azimuths $\Phi_{1,2}$ of the forward-propagation eigenstates are found to be

$$\overrightarrow{\Phi_1} = \frac{\arg(c) - \arg(b)}{4} = \varphi, \tag{2.69}$$

$$\overrightarrow{\Phi_2} = \varphi + \tfrac{\pi}{2}. \tag{2.70}$$

For backward propagation the azimuths of the eigenstates are

$$\begin{aligned} \overleftarrow{\Phi_1} &= -\varphi, \\ \overleftarrow{\Phi_2} &= -\varphi + \tfrac{\pi}{2}, \end{aligned} \tag{2.71}$$

as in this case the roles of b and c are switched.

Thus for normal incidence or 2-fold rotational symmetry, planar metamaterials have eigenstates with orthogonal azimuths $\Phi_{1,2}$. The parameter φ, defined in (2.34), simply corresponds to the azimuth of one of the eigenstates for forward propagation in these cases. Note that, in their respective coordinate systems, the eigenstates for backward propagation are rotated relative to those for forward propagation by -2φ.

By combining the magnitudes of the terms in (2.65) with the phase conditions (2.68) and normalizing we can write the **eigenstates for forward-propagation for normal incidence or 2-fold rotational symmetry**

$$\begin{aligned} \overrightarrow{\mathbf{v}}_{\mathbf{1}} &= \frac{e^{i\gamma}}{\sqrt{|b|+|c|}} \begin{pmatrix} \sqrt{|b|}e^{-i\varphi} \\ \sqrt{|c|}e^{i\varphi} \end{pmatrix}, \\ \overrightarrow{\mathbf{v}}_{\mathbf{2}} &= \frac{e^{i\gamma}}{\sqrt{|b|+|c|}} \begin{pmatrix} \sqrt{|b|}e^{-i(\varphi+\pi/2)} \\ \sqrt{|c|}e^{i(\varphi+\pi/2)} \end{pmatrix}, \end{aligned} \tag{2.72}$$

where the eigenstate azimuth φ is defined by (2.34). Different values of $\gamma \in [0, 2\pi)$, which has been included for completeness, correspond to the same polarization state at different times. The **eigenstates for backward propagation**, where b and c are switched, are

$$\begin{aligned} \overleftarrow{\mathbf{v}}_{\mathbf{1}} &= \frac{e^{i\gamma}}{\sqrt{|b|+|c|}} \begin{pmatrix} \sqrt{|c|}e^{-i(-\varphi)} \\ \sqrt{|b|}e^{i(-\varphi)} \end{pmatrix}, \\ \overleftarrow{\mathbf{v}}_{\mathbf{2}} &= \frac{e^{i\gamma}}{\sqrt{|b|+|c|}} \begin{pmatrix} \sqrt{|c|}e^{-i(-\varphi+\pi/2)} \\ \sqrt{|b|}e^{i(-\varphi+\pi/2)} \end{pmatrix}. \end{aligned} \tag{2.73}$$

The eigenpolarizations do not depend on the scattering coefficients $a = d$ and the phase κ. Note that the eigenvalues λ_i and the eigenvectors $\mathbf{v_i}$ with the same indices do correspond to each other.

Importantly, we found that planar metamaterials not showing optical activity ($a = d$) have eigenstates with orthogonal azimuths. In the general case, when $|b| \neq |c|$, the directionally asymmetric transmission, reflection and absorption effects discussed in section 2.4.2 are present, and the eigenstates are co-rotating with the same ellipticity angle. In the special case of $|b| = |c| \neq 0$, which corresponds to linear birefringence and dichroism without the presence of other polarization effects, the eigenstates are simply orthogonal linear polarizations.

Note that, for *normal incidence*, the azimuths of the eigenstates, if well-defined, must correspond to preferred directions of the metamaterial. For 2D-chiral anisotropic metamaterials[19] these preferred directions may be frequency-dependent, while for non-chiral anisotropic planar metamaterials[20] they must be oriented parallel and perpendicular to the pattern's line(s) of mirror symmetry. The orientation of a line of mirror symmetry is given by $\tilde{\varphi}$ which is measured in the coordinates for forward propagation at normal incidence. Thus the azimuth of one normal incidence forward-propagation eigenstate, φ or $\varphi + \frac{\pi}{2}$ (measured from the $\mathbf{x}$-axis) must correspond to $\tilde{\varphi}$ (measured from the $\mathbf{y_m}$-axis). So for normal incidence onto metamaterials with a single line of (glide) mirror symmetry, $\varphi = \tilde{\varphi} + n\frac{\pi}{2}$ must hold for some $n \in \mathbb{Z}$.

Obviously, at normal incidence, if φ is well-defined, rotation of the metamaterial by

[19] 2D-chiral anisotropic wallpaper symmetry groups: $p1$, $p2$.
[20] Achiral anisotropic wallpaper symmetry groups: pm, pg, cm, pmm, pmg, pgg, cmm.

some angle $+\Delta_\varphi$ must result in the same rotation of the eigenstates, without affecting the eigenvalues or the ellipticity of the eigenstates. Thus at normal incidence the rotation $\tilde{\varphi} \to \tilde{\varphi}+\Delta_\varphi$ must simply translate into a change of the parameter $\varphi \to \varphi+\Delta_\varphi$. From (2.32) it follows that an **in-plane rotation of a planar metamaterial at normal incidence by $+\Delta_\varphi$ corresponds to**

$$b \to be^{-i2\Delta_\varphi} \quad \text{and} \quad c \to ce^{+i2\Delta_\varphi}. \tag{2.74}$$

2.6 Energy Conservation

Energy conservation implies that the combined power of the transmitted and reflected waves plus losses, $L \geq 0$, must equal the power of the incident wave. Here we consider the case of forward-propagation; the opposite propagation direction corresponds to reversed values of b and c.

$$\begin{aligned} |\mathbf{E^0}|^2 &= |\mathbf{E^t}|^2 + |\mathbf{E^r}|^2 + L|\mathbf{E^0}|^2 \\ &= |\overrightarrow{t}\,\mathbf{E^0}|^2 + |\overrightarrow{r}\,\mathbf{E^0}|^2 + L|\mathbf{E^0}|^2 \end{aligned} \tag{2.75}$$

Division by $|\mathbf{E^0}|^2$ allows us to introduce the unit vector $\hat{\mathbf{u}} = \mathbf{E^0}/|\mathbf{E^0}|$.

$$1 - L = |\overrightarrow{t}\,\hat{\mathbf{u}}|^2 + |\overrightarrow{r}\,\hat{\mathbf{u}}|^2 \tag{2.76}$$

This condition must be satisfied for any incident polarization, i.e. for any complex unit vector $\hat{\mathbf{u}}$. All possible unit vectors or polarization states can be written as (2.37)

$$\hat{\mathbf{u}} = \begin{pmatrix} \sin(\beta)e^{i(\gamma-\alpha)} \\ \cos(\beta)e^{i(\gamma+\alpha)} \end{pmatrix},$$
$$\alpha \in (-\tfrac{\pi}{2}, \tfrac{\pi}{2}], \qquad \beta \in [0, \tfrac{\pi}{2}], \qquad \gamma \in [0, 2\pi).$$

Thus energy conservation for forward-propagation written out explicitly is

$$\begin{aligned} 1-L &= \left| \begin{pmatrix} a+1 & b \\ c & d+1 \end{pmatrix} \begin{pmatrix} \sin(\beta)e^{i(\gamma-\alpha)} \\ \cos(\beta)e^{i(\gamma+\alpha)} \end{pmatrix} \right|^2 \\ &+ \left| \begin{pmatrix} c & d \\ a & b \end{pmatrix} \begin{pmatrix} \sin(\beta)e^{i(\gamma-\alpha)} \\ \cos(\beta)e^{i(\gamma+\alpha)} \end{pmatrix} \right|^2 \\ &\forall \quad \alpha, \beta, \gamma. \end{aligned} \tag{2.77}$$

This simplifies to

$$\begin{aligned} 0 \geq -L &= p_1 \sin^2\beta + p_2 \cos^2\beta \\ &+ \sin 2\beta[p_4 \cos(2\alpha) - p_5 \sin(2\alpha)] \\ &\forall \quad \alpha \in (-\tfrac{\pi}{2}, \tfrac{\pi}{2}], \beta \in [0, \tfrac{\pi}{2}] \end{aligned} \tag{2.78}$$

with the parameters

$$\tfrac{1}{2}p_1 := |a|^2 + |c|^2 + Re(a) \tag{2.79}$$

$$\tfrac{1}{2}p_2 := |d|^2 + |b|^2 + Re(b) \tag{2.80}$$

$$\begin{aligned} \tfrac{1}{2}p_4 &:= Re(a+\tfrac{1}{2})Re(b) + Im(a+\tfrac{1}{2})Im(b) \\ &+ Re(d+\tfrac{1}{2})Re(c) + Im(d+\tfrac{1}{2})Im(c) \end{aligned} \tag{2.81}$$

$$\begin{aligned} \tfrac{1}{2}p_5 &:= Re(a+\tfrac{1}{2})Im(b) - Im(a+\tfrac{1}{2})Re(b) \\ &- Re(d+\tfrac{1}{2})Im(c) + Im(d+\tfrac{1}{2})Re(c). \end{aligned} \tag{2.82}$$

Expression (2.78) is equivalent to

$$\begin{gathered} 0 \geq p_1 \sin^2\beta + p_2 \cos^2\beta + p_3 \sin 2\beta \\ \forall\, \beta \in [0, \tfrac{\pi}{2}], \end{gathered} \tag{2.83}$$

where the parameter p_3 corresponds to

$$\begin{aligned} p_3 &:= \sqrt{(p_4)^2 + (p_5)^2} \\ &= 2\left\{|a+\tfrac{1}{2}|^2|b|^2 + |d+\tfrac{1}{2}|^2|c|^2\right. \\ &+ 2|a+\tfrac{1}{2}||d+\tfrac{1}{2}||b||c| \\ &\cdot \left.\cos[\arg((a+\tfrac{1}{2})(d+\tfrac{1}{2})) - \arg(bc)]\right\}^{\frac{1}{2}} \\ &= 2\left\{A^2|b|^2 + D^2|c|^2 + 2AD|b||c|\cos[2\xi - 2\kappa]\right\}^{\frac{1}{2}}. \end{aligned} \tag{2.84}$$

The parameters A, D, ξ, κ used in the last line are defined by (2.29), (2.30) and (2.33).

The right hand side of (2.83) reaches its largest value for β_0 given by

$$\beta_0 = \begin{cases} \frac{1}{2}\arctan\left(2\frac{p_3}{p_2-p_1}\right) & \text{for } p_1 < p_2 \\ \frac{\pi}{4} & \text{for } p_1 = p_2 \\ \frac{1}{2}\arctan\left(2\frac{p_3}{p_2-p_1}\right) + \frac{\pi}{2} & \text{for } p_1 > p_2. \end{cases} \tag{2.85}$$

Therefore energy conservation is satisfied, if equation (2.83) is satisfied for β_0 both in the cases of forward and backward propagation, where backward-propagation corresponds to reversed roles of b and c in all formulas. (If this is satisfied, energy conservation for the opposite angle of incidence $-\theta$ is also satisfied.)

While this does define the scattering coefficients that satisfy energy conservation, it is not very intuitive. One can easily see that the energy conservation equation (2.83) requires $p_{1,2} \leq 0$. As we will find for the lossless case, $p_3 = 0$ corresponds to a constraint on the possible values of the phase κ. We will derive that for lossless planar metamaterials κ has two solutions for each allowed pair of values of a, d (except for trivial cases). The constraint on κ is less tight for lossy planar metamaterials.

$p_{1,2} \leq 0$ can be written as

$$\left|a+\tfrac{1}{2}\right|^2 + |c|^2 \leq \left(\tfrac{1}{2}\right)^2, \tag{2.86}$$

$$\left|d+\tfrac{1}{2}\right|^2 + |b|^2 \leq \left(\tfrac{1}{2}\right)^2, \tag{2.87}$$

which must also hold for reversed values of b and c, due to energy conservation for the opposite propagation direction.

From this we can obtain for a, b and the magnitudes of $|b|$ and $|c|$ that

$$\left|a+\tfrac{1}{2}\right|, \left|d+\tfrac{1}{2}\right| \leq \tfrac{1}{2}, \tag{2.88}$$

$$|b|, |c| \leq \sqrt{\tfrac{1}{4} - \max\left(\left|a+\tfrac{1}{2}\right|^2, \left|d+\tfrac{1}{2}\right|^2\right)} \leq \tfrac{1}{2}. \tag{2.89}$$

Note that by using (2.29) these conditions can rewritten in terms of the alternative parameters A, D resulting in the simplified forms

$$A, D \leq \tfrac{1}{2},$$

$$|b|, |c| \leq \sqrt{\tfrac{1}{4} - \max\left(A^2, D^2\right)} \leq \tfrac{1}{2}.$$

From (2.88) and (2.89) it follows that, in the complex plane, the solutions for a, b, c, d must always fall in the regions indicated in Fig. 2.14 (a).

For the lossless case the conditions $|a+\frac{1}{2}| = |d+\frac{1}{2}|$ and the left equality of (2.89) are required. Compared to any chosen lossless solution, $|a+\frac{1}{2}|, |d+\frac{1}{2}|, |b|, |c|$ may take smaller values for a lossy planar metamaterial, see Fig. 2.14 (b).

2.6.1 Maximum Losses

Note that losses in planar metamaterials cannot be arbitrarily large. For largest losses transmission and reflection must be simultaneously minimized, i.e. in transmission the scattered field must destructively interfere with the incident wave, while the scattered field must not be too large to keep reflection low. It is clear that maximum destructive interference between scattered field and incident wave will occur if the scattered field and the incident wave are of the same polarization state, however, with a phase difference of π. Thus maximum losses will occur for an eigenstate $\mathbf{E^0}$ with a negative real scattering eigenvalue λ^s. Due to energy conservation the magnitude of an eigenvalue cannot be greater than 1 and therefore $\lambda^s \in [-1, 0)$. As maximum losses occur for an eigenstate, the scattered field can be written as $\mathbf{E^s} = \lambda^s \mathbf{E^0}$ and the absorbed power

fraction, L, corresponds to

$$\begin{aligned} L|\mathbf{E^0}|^2 &= |\mathbf{E^0}|^2 - |\mathbf{E^t}|^2 - |\mathbf{E^r}|^2 \\ &= |\mathbf{E^0}|^2 - |\mathbf{E^0} + \mathbf{E^s}|^2 - |\mathbf{E^s}|^2 \\ &= |\mathbf{E^0}|^2 - (1+\lambda^s)^2|\mathbf{E^0}|^2 - (\lambda^s)^2|\mathbf{E^0}|^2 \\ &= -2(\lambda^s + (\lambda^s)^2)|\mathbf{E^0}|^2, \end{aligned} \tag{2.90}$$

or $L = -2(\lambda^s + (\lambda^s)^2)$, which reaches its largest value of $L = \frac{1}{2}$ for $\lambda^s = -\frac{1}{2}$. So **absorption losses L in planar metamaterials are limited to**

$$L \leq 50\% \tag{2.91}$$

of the incident power. Note that this derivation does not make any assumptions about the particular structure of the scattering matrix and therefore the limit for losses (2.91) applies to any planar metamaterial for any polarization and any angle of incidence.

The lossiest metamaterial must absorb 50% for any polarization state, therefore any polarization state must be an eigenstate with eigenvalue $\lambda^s = -\frac{1}{2}$. Thus the **lossiest scattering matrix** is

$$\overrightarrow{s} = \overleftarrow{s} = \begin{pmatrix} -\frac{1}{2} & 0 \\ 0 & -\frac{1}{2} \end{pmatrix}. \tag{2.92}$$

The same result can be found by minimizing the right hand side of (2.78) for all polarization states α, β, which is equivalent to requiring $p_1 = p_2 =$ minimum.

2.6.2 Maximum Circular Conversion Dichroism

As derived in the previous section, losses in planar metamaterials cannot exceed 50%. In section 2.4.2 we derived equations (2.49) and (2.50) describing transmission, reflection and absorption asymmetries in planar metamaterials for the general case

$$\begin{aligned} \overrightarrow{T_\pm} - \overleftarrow{T_\pm} = \overrightarrow{R_\pm} - \overleftarrow{R_\pm} &= \pm(|c|^2 - |b|^2), \\ \overrightarrow{L_\pm} - \overleftarrow{L_\pm} &= \mp 2(|c|^2 - |b|^2). \end{aligned}$$

As losses cannot exceed 50% in any case, the maximum asymmetry would be achieved for losses of 0% for one propagation direction and losses of 50% for the other. This corresponds to a maximum transmission asymmetry and reflection asymmetry for circular polarization of 25% each. Thus **in general for planar metamaterials**

$$|\overrightarrow{T_\pm} - \overleftarrow{T_\pm}| = |\overrightarrow{R_\pm} - \overleftarrow{R_\pm}| = |(|c|^2 - |b|^2)| \leq 25\% \tag{2.93}$$

$$|\overrightarrow{L_\pm} - \overleftarrow{L_\pm}| = 2|(|c|^2 - |b|^2)| \leq 50\%. \tag{2.94}$$

As illustrated by Fig. 2.13 and discussed in chapter 3.2.1, transmission, reflection and absorption asymmetries reaching about $\frac{2}{3}$ of these theoretical limits have been observed experimentally. Does energy conservation allow circular conversion dichroism to actually reach the above limits? From (2.89) follows that the magnitudes of $|b|$ and $|c|$ cannot exceed $\frac{1}{2}$, thus the limits for the asymmetry given by (2.93) and (2.94) can only be achieved if $b = 0$ and $|c| = \frac{1}{2}$ or vice versa. So one of the scattering coefficients $|b|, |c|$ must have the maximum allowed magnitude of $\frac{1}{2}$ and therefore $a = b = -\frac{1}{2}$ is required to satisfy (2.89).

In summary the largest possible circular conversion dichroism, reaching the limits specified in (2.93) and (2.94), can only be achieved for the scattering coefficients

$$a = d = -\frac{1}{2}, \qquad b = 0, \qquad c = \frac{1}{2}e^{i\nu}, \tag{2.95}$$

with $\nu \in [-\pi, \pi)$ or reversed values of b and c. Note that all of these sets of scattering coefficients satisfy energy conservation (2.83) with (p_1, p_2, p_3) taking the values $(0, -\frac{1}{2}, 0)$ or $(-\frac{1}{2}, 0, 0)$.

The fact that solution (2.95) and its counterpart with b, c switched are the only maximum asymmetry solutions implies that maximum circular conversion dichroism can only be achieved when the planar metamaterial does not simultaneously show optical activity, which would require $a \neq d$. Also it follows that the maximum asymmetry for circularly polarized waves propagating in opposite directions can only be achieved

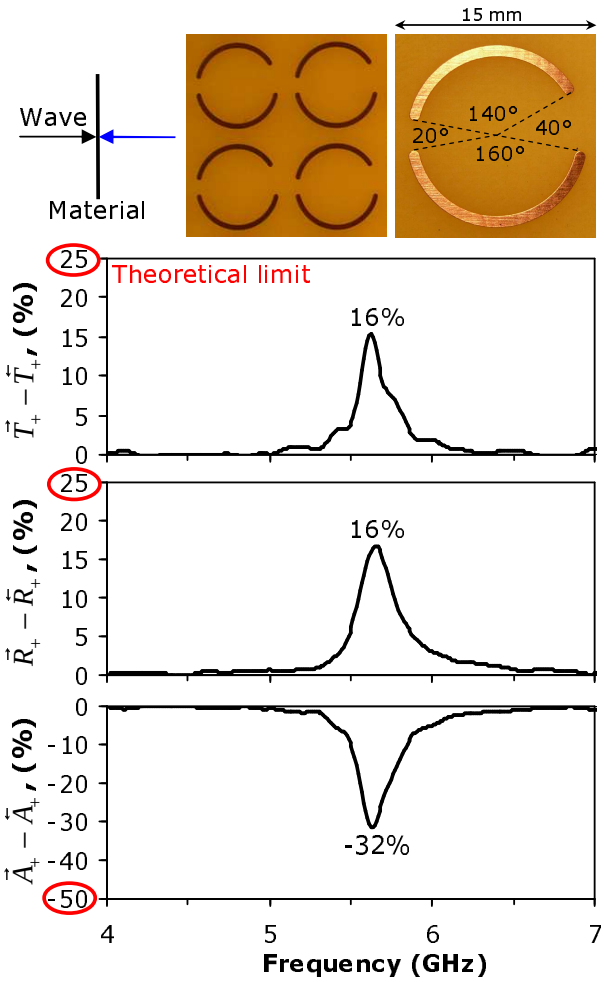

Figure 2.13: ***Experimental demonstration of circular conversion dichroism near the theoretical limit.*** *Directional asymmetries in transmission, reflection and absorption of circularly polarized waves measured at normal incidence onto a 2D-chiral split ring metamaterial (wallpaper group p1). The asymmetries reach $\frac{2}{3}$ of the theoretical limits given in (2.93) and (2.94). Refer to chapter 3.2.1 and reference [98] for details.*

for

$$\begin{aligned} \overrightarrow{T_+} = \overleftarrow{T_-} = 50\% \quad &\text{and} \quad \overrightarrow{T_-} = \overleftarrow{T_+} = 25\% \\ \overrightarrow{R_+} = \overleftarrow{R_-} = 50\% \quad &\text{and} \quad \overrightarrow{R_-} = \overleftarrow{R_+} = 25\% \\ \overrightarrow{L_+} = \overleftarrow{L_-} = 0\% \quad &\text{and} \quad \overrightarrow{L_-} = \overleftarrow{L_+} = 50\% \end{aligned} \tag{2.96}$$

and for the same set of equations with the left and right columns of percentages swapped.

It follows from (2.72) and (2.73) that the eigenstates for the largest circular con-

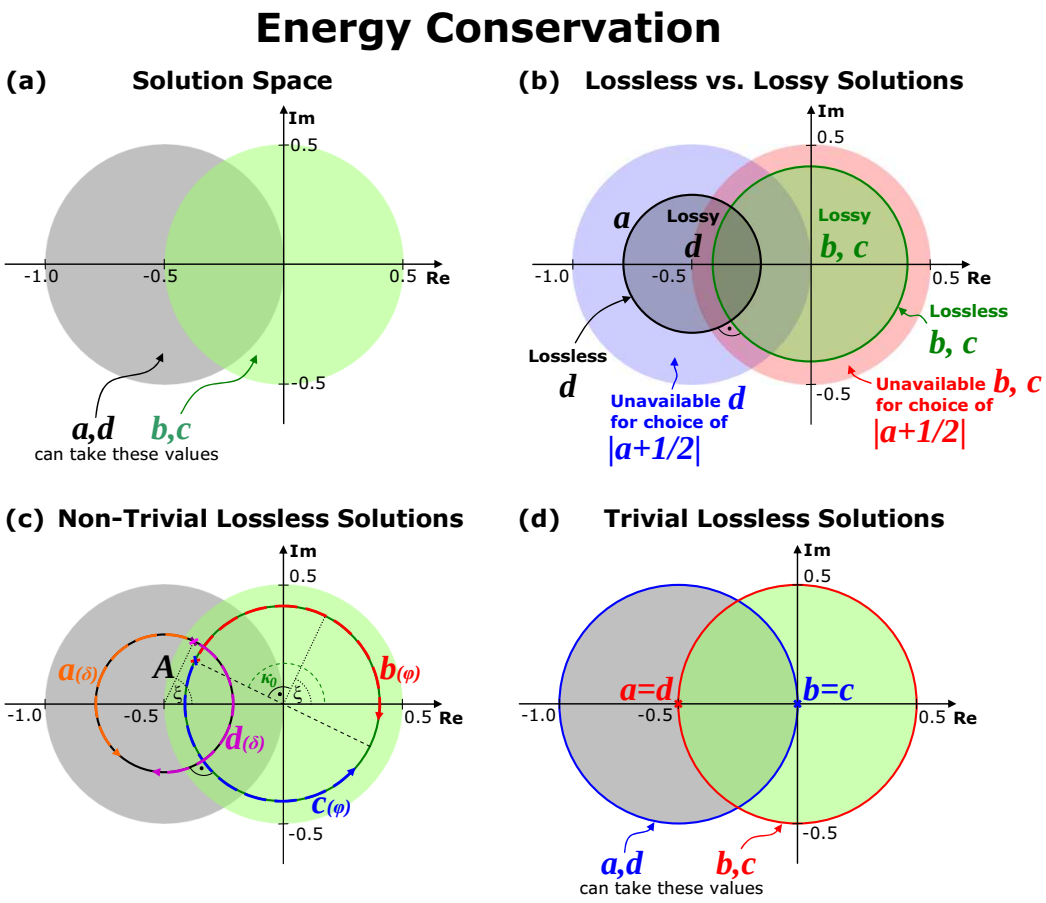

Figure 2.14: ***Constraints on the scattering coefficients*** a, b, c, d ***from energy conservation.*** *(a) The solution space for* a, b, c, d*. (b) Lossy vs. lossless solutions for* b, c, d *for a particular choice of* $|a + \frac{1}{2}| = const$ *(here* $1/\sqrt{3}$*). Roles of* a, d *can be switched. (c) The non-trivial solutions (2.105) for the lossless case illustrated for an arbitrary choice of* A, ξ*. Solutions for* a, b *are corresponding points on the dashed arrows indicating* a *and* b *as functions of* δ*. Solutions* b, c *are corresponding points on the dashed arrows indicating* b *and* c *as functions of the parameter* φ*. (d) Trivial solutions for the lossless case:* $a = -\frac{1}{2}$ *is shown in red (2.106) and* $b = c = 0$ *is plotted in blue (2.107).*

version dichroism correspond to one degenerate circularly polarized eigenstate. As previously derived for structures exhibiting circular conversion dichroism but not optical activity, the eigenstates for opposite propagation directions have the opposite handedness.

Importantly, directionally asymmetric transmission, reflection and absorption can only occur for planar metamaterials that are lossy.

2.6.3 Lossless Planar Metamaterials

For lossless planar metamaterials, the equality in equation (2.83) must hold for all β. Thus the expressions p_1, p_2, p_3 must all be zero. The conditions $p_{1,2} = 0$ are equivalent to the equality in expressions (2.86) and (2.87), which must also hold for reversed values of b, c due to lossless behavior for the opposite propagation direction. From this it follows that the following relations must hold for lossless planar metamaterials

$$|a + \tfrac{1}{2}| = |d + \tfrac{1}{2}| \quad \leq \tfrac{1}{2}, \tag{2.97}$$

$$|b| = |c| \quad \leq \tfrac{1}{2}, \tag{2.98}$$

$$\left|a + \tfrac{1}{2}\right|^2 + |b|^2 \quad = \left(\tfrac{1}{2}\right)^2. \tag{2.99}$$

Rewritten in terms of the alternative parameters A, D defined by (2.29) these conditions simplify to

$$\begin{aligned} A = D \quad &\leq \tfrac{1}{2}, \\ |b| = |c| \quad &\leq \tfrac{1}{2}, \\ A^2 + |b|^2 \quad &= (\tfrac{1}{2})^2. \end{aligned}$$

Note that condition (2.98) implies that lossless planar metamaterials cannot show the asymmetric transmission, reflection and absorption effects identified in section 2.4.2. Expression (2.99) describes two circles in the complex plane that intersect orthogonally [see Fig. 2.14 (b)]. In the lossless case a and d lie on a circle of radius $A = D$ centered at $-\frac{1}{2}$, while b and c lie on a circle of radius $|b| = |c|$ centered at the origin. The sum of the squared radii of both circles is $\frac{1}{4}$. In particular this implies that the maximum radius of either circle is $\frac{1}{2}$.

For lossless planar metamaterials p_3, defined by (2.84), must also be zero. Using (2.97) and (2.98), $p_3 = 0$ simplifies to

$$\begin{aligned} & |a + \tfrac{1}{2}||b| \left\{1 + \cos[\arg((a + \tfrac{1}{2})(d + \tfrac{1}{2})) - 2\kappa]\right\} \\ = \;& A|b| \left\{1 + \cos[2\xi - 2\kappa]\right\} \\ = \;& 0, \end{aligned} \tag{2.100}$$

where a, ξ and κ are defined by (2.29), (2.30) and (2.33). Thus the non-trivial solutions of $p_3 = 0$ correspond to $\cos[2\xi - 2\kappa] = -1$, which requires κ to take one of the values

$$\kappa_0 := \xi \pm \tfrac{\pi}{2}. \tag{2.101}$$

Condition (2.100) also has two trivial solutions corresponding to the cases [see Fig. 2.14 (d)]

$$a = d \;=\; -\frac{1}{2} \tag{2.102}$$

$$\text{or} \quad b = c \;=\; 0. \tag{2.103}$$

Note that we defined κ_0 as the allowed values for κ in the lossless non-trivial case.

So any lossless planar metamaterial must satisfy conditions (2.97), (2.98) and (2.99), and additionally one of (2.101), (2.102) and (2.103). The latter three are the non-trivial and trivial solutions of $p_3 = 0$.

Note that for the lossless case (2.99) allows us to write the values $|b| = |c|$ as functions of A

$$|b| = |c| = \sqrt{\tfrac{1}{4} - |a + \tfrac{1}{2}|^2} = \sqrt{\tfrac{1}{4} - A^2} \leq \tfrac{1}{2}. \tag{2.104}$$

Using expressions (2.28) and (2.32) to express a, b, c, d in terms of the alternative parameters, we can easily write down the lossless non-trivial scattering matrices [see Fig. 2.14 (c)]

$$\overrightarrow{s} = \begin{pmatrix} a & b \\ c & d \end{pmatrix} = \begin{pmatrix} Ae^{i(\xi - 2\delta)} - \frac{1}{2} & |b|e^{i(\kappa_0 - 2\varphi)} \\ |b|e^{i(\kappa_0 + 2\varphi)} & Ae^{i(\xi + 2\delta)} - \frac{1}{2} \end{pmatrix}, \tag{2.105}$$

$$A \in (0, \tfrac{1}{2}), \quad \xi \in (-\pi, \pi], \quad \delta \in (-\tfrac{\pi}{2}, \tfrac{\pi}{2}), \quad \varphi \in [0, \tfrac{\pi}{2}),$$

where κ_0 and $|b|$ are given by (2.101) and (2.104) respectively. Note that there are four independent parameters for the lossless non-trivial solutions, compared to eight free parameters for general planar metamaterials.

For the trivial cases (2.102), (2.103) we get the trivial solutions [see Fig. 2.14 (d)]

$$\overrightarrow{s} = \frac{1}{2}\begin{pmatrix} -1 & e^{i(\kappa-2\varphi)} \\ e^{i(\kappa+2\varphi)} & -1 \end{pmatrix}, \qquad \begin{matrix} \kappa \in [0, 2\pi), & \varphi \in [0, \frac{\pi}{2}), \end{matrix} \tag{2.106}$$

$$\overrightarrow{s} = \tfrac{1}{2}\begin{pmatrix} e^{i(\xi-2\delta)} - 1 & 0 \\ 0 & e^{i(\xi+2\delta)} - 1 \end{pmatrix}, \qquad \begin{matrix} \xi \in (-\pi, \pi], & \delta \in (-\frac{\pi}{2}, \frac{\pi}{2}) \end{matrix} \tag{2.107}$$

All scattering matrices allowed for lossless planar metamaterials are given by (2.105), (2.106) and (2.107).

How can we interpret these solutions? Clearly, $|b| = |c|$ must be satisfied for all lossless planar metamaterials and thus the directional asymmetries in transmission, reflection and absorption, which were discussed in section 2.4.2, cannot be observed for lossless planar metamaterials.

For (2.105) and (2.107) the diagonal elements of the scattering matrix, a and d are allowed to take different values, which corresponds to the effects of circular dichroism and circular birefringence, see section 2.4.1. It follows that these phenomena may occur in lossless planar metamaterials. Note that circular birefringence without circular dichroism corresponds to the special case of $\xi = 0$. Due to $A = D$, circular dichroism without circular birefringence cannot be achieved in lossless planar metamaterials, except for the case of a perfect circular polarizer, where circular birefringence cannot be defined, see section 2.7.5. (2.106) is a special case that does not allow circular dichroism or circular birefringence.

Solutions (2.105) and (2.106) correspond to responses with linear birefringence / dichroism, as they have $|b| = |c| \neq 0$, see section 2.4.3. In the absence of optical activity, $a = d$, the eigenstates are linearly polarized with azimuths φ and $\varphi + \frac{\pi}{2}$ for forward-propagation, see section 2.5.2. Special cases of these linearly birefringent / dichroic lossless solutions without optical activity correspond to lossless linear polarizers and lossless wave plates. These important cases will be identified and discussed in sections 2.7.2 and 2.7.3.

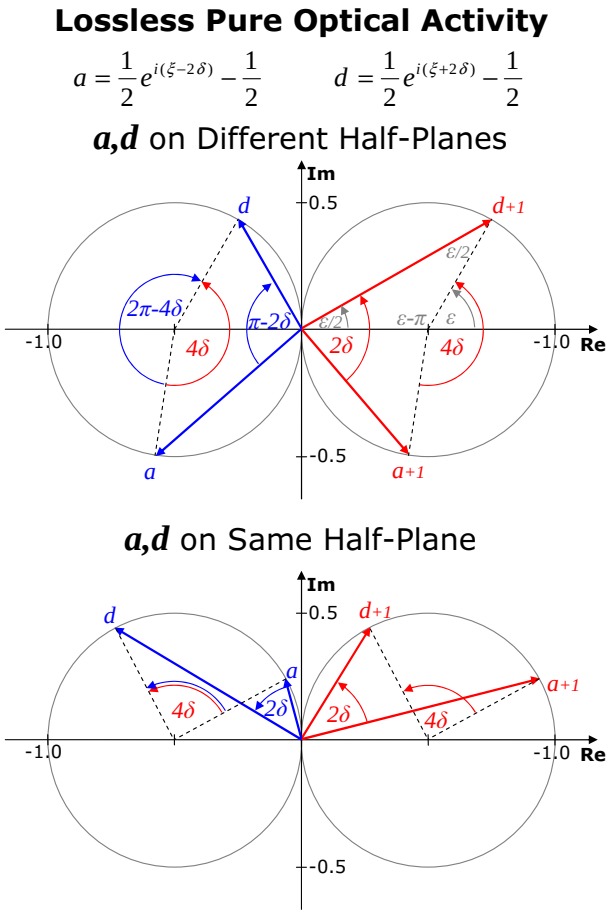

Figure 2.15: *(red) For* ***lossless metamaterials without linear birefringence / dichroism****,* $a+1$ *and* $d+1$ *lie on a circle through the origin centered at* $+\frac{1}{2}$*. The angle from* $a+1$ *to* $d+1$ *around the circle's center that faces away from the origin is* $\arg(d+\frac{1}{2}) - \arg(a+\frac{1}{2}) = 4\delta$*, see (2.31). The angle* $\arg(d+1) - \arg(a+1)$ *that the same points form with the origin is just half as large. (Basic geometry, proof sketched in gray on top panel, same idea in all cases.) (blue) For the angle* $\arg(d) - \arg(a)$ *from* a *to* d *we must distinguish two cases. The top panel shows that if* a *and* d *fall in different half-planes (lower/upper),* $\arg(d) - \arg(a)$ *is just half as large as* $2\pi - 4\delta$*. The bottom panel shows that* $\arg(d) - \arg(a) = \arg(d+1) - \arg(a+1) = 2\delta$ *if* a *and* d *fall in the same half-plane (upper/lower).*

Lossless solution (2.107), which has $b = c = 0$, corresponds to a response that does not depend on the azimuth of the incident wave, see section 2.4.3. It must be stressed that this family of solutions corresponds to lossless planar metamaterials without linear birefringence / dichroism that may exhibit circular birefringence and circular dichroism. Thus energy conservation allows pure optical activity (circular birefringence and circular dichroism) in lossless planar metamaterials. The next section studies lossless pure optical activity in more detail, while sections 2.7.4 and 2.7.5 will discuss the special cases of lossless polarization rotators and circular polarizers respectively.

2.6.4 Lossless Planar Metamaterials Without Linear Birefringence / Dichroism ($L = 0, b = c = 0$)

Here we study optical activity for lossless planar metamaterials without linear birefringence / dichroism. The complete set of scattering matrices for this case is given by (2.107), and the corresponding eigenstates are derived in section 2.5.1. Note that in general optically active behavior can only occur at oblique incidence onto planar metamaterials without 2-fold rotational symmetry. Quantitatively the properties discussed here can only be realized for planar metamaterials that are also lossless. Importantly, absence of linear birefringence / dichroism at some particular frequency does not require the metamaterial itself to be isotropic. First we will derive polarization rotation and circular dichroism for lossless planar metamaterials without linear birefringence / dichroism in general, and then in sections 2.7.4 and 2.7.5 the special cases of an ideal lossless rotator and circular polarizer will be discussed, respectively.

Since in our case the metamaterial properties do not depend on the azimuth of the incident wave, it follows from (2.40) and (2.42) that the polarization azimuths of the scattered and transmitted waves will be rotated by

$$\begin{aligned} \Delta\Phi^s &= \tfrac{1}{2} \quad (\arg(d) - \arg(a)) \,, \\ \Delta\Phi^t &= \tfrac{1}{2} \quad (\arg(d+1) - \arg(a+1)) \,. \end{aligned} \tag{2.108}$$

Note that for lossless planar metamaterials without linear birefringence / dichroism both a and d are of the form $\frac{1}{2}e^{i(\xi \mp 2\delta)} - \frac{1}{2}$, where ξ, δ are chosen to satisfy the phase convention $\xi \pm 2\delta \in (-\pi, \pi]$. As illustrated by Fig. 2.15, $\arg(d+1) - \arg(a+1) = 2\delta$ follows for this case. The phase difference $\arg(d) - \arg(a)$ is 2δ if a, d lie in the same half-plane (upper or lower) and $\pi - 2\delta$ otherwise. From these results we obtain the **polarization azimuth rotations for lossless planar metamaterials without linear birefringence / dichroism** for the scattered and transmitted fields

$$\begin{aligned} \Delta\Phi^s &= \begin{cases} \delta & \\ \frac{\pi}{2} - \delta & \end{cases} \text{for} \begin{array}{l} Im(a)Im(d) \geq 0 \\ Im(a)Im(d) < 0 \end{array} , \\ \Delta\Phi^t &= \delta. \end{aligned} \tag{2.109}$$

Circular dichroism for transmission and scattering are generally given by (2.43) and (2.44), which in our lossless case without linear birefringence / dichroism take the form

$$\begin{aligned}\Delta S &= |a|^2 - |d|^2 \\ &= |\frac{1}{2}e^{i(\xi-2\delta)} - \tfrac{1}{2}|^2 - |\tfrac{1}{2}e^{i(\xi+2\delta)} - \frac{1}{2}|^2, \\ \Delta T &= |a+1|^2 - |d+1|^2 \\ &= |\frac{1}{2}e^{i(\xi-2\delta)} + \tfrac{1}{2}|^2 - |\tfrac{1}{2}e^{i(\xi+2\delta)} + \frac{1}{2}|^2.\end{aligned}$$

After simplifying we find that **for lossless planar metamaterials without linear birefringence / dichroism, circular dichroism for scattering and transmission is given by**

$$\Delta S = -\sin(\xi)\sin(2\delta), \tag{2.110}$$

$$\Delta T = +\sin(\xi)\sin(2\delta). \tag{2.111}$$

2.7 Applications and Limitations

We are used to a variety of optical components, some of which are polarization insensitive, like ideal mirrors, beam splitters and attenuators, while others, like wave plates, linear and circular polarizers and polarization rotators are used to manipulate polarization states. In this section, we explore the potential of planar metamaterial realizations of these components.

Planar metamaterials acting as mirrors, beam splitters or reflective attenuators should not be surprising, as the usual realizations of these components can be understood as trivial cases of planar metamaterials. The same applies to wire grid linear polarizers commonly used in the microwave, terahertz and mid-infrared parts of the spectrum.

Here we show that planar metamaterials can also be used as wave plates, which can be very efficient for small phase delays. Large phase delays, however, come at the cost of large insertion losses, and $\lambda/2$-plates cannot be realized.

We find that at oblique incidence, planar metamaterials can act as polarization rotators or circular polarizers. Polarization rotators can be very efficient for small

rotation angles, but large rotation angles come at the cost of large insertion losses, and rotation angles of $\pm\frac{\pi}{2}$ cannot be realized. Circular polarizers are not limited in efficiency.

Importantly, planar metamaterials allow the realization of wave plates, linear and circular polarizers and polarization rotators that operate in transmission and/or reflection. Thus planar metamaterials provide an opportunity to develop novel components like reflection wave plates, reflection circular polarizers and reflection polarization rotators and to miniaturize of the corresponding existing transmission components.

Note that for all functionalities listed here, apart from attenuators, the best performance can be achieved with lossless planar metamaterials.

2.7.1 Attenuators, Beam Splitters, Mirrors and Empty Space

Attenuators, beam splitters, mirrors and empty space exhibit neither linear birefringence / dichroism ($b = c = 0$) nor optical activity ($a = d$). Thus they correspond to scattering matrices

$$\overrightarrow{s} = \begin{pmatrix} a & 0 \\ 0 & a \end{pmatrix}, \qquad |a + \tfrac{1}{2}| \leq \tfrac{1}{2}. \tag{2.112}$$

The corresponding scattered (reflected) and transmitted power fractions S and T are

$$\begin{aligned} S &= |a|^2, \\ T &= |a+1|^2. \end{aligned} \tag{2.113}$$

The equality $|a + \frac{1}{2}| = \frac{1}{2}$ corresponds to all lossless planar metamaterials without linear birefringence / dichroism and optical activity. Using (2.28), all lossless a can be written as $a = \frac{1}{2}(e^{i\xi} - 1)$, which allows us to rewrite the scattered and transmitted

power fractions for the **lossless case** as

$$\begin{aligned} S &= \sin^2\left(\tfrac{\xi}{2}\right), \\ T &= \cos^2\left(\tfrac{\xi}{2}\right). \end{aligned} \tag{2.114}$$

Lossless planar metamaterials showing neither linear birefringence / dichroism nor optical activity are beam splitters. The transmitted and scattered power fractions are given by (2.114). A simple $50-50$ beam splitter corresponds to $\xi = \pm\frac{\pi}{2}$, while the two limiting cases are a perfect mirror for $\xi = \pi$ ($a = -1$) and empty space with $\xi = 0$ ($a = 0$).

All lossy planar metamaterials without linear birefringence / dichroism and without optical activity, i.e. $|a + \frac{1}{2}| < \frac{1}{2}$, correspond to attenuating beam splitters. Note that absorption losses in planar metamaterials cannot exceed 50%. Absorption losses of 50% for any polarization state correspond to $a = -\frac{1}{2}$.

2.7.2 Linear Polarizer

A transmission linear polarizer transmits one specific linearly polarized component of the incident wave without changing its polarization state, while it is opaque for the orthogonal linearly polarized component. A reflection linear polarizer shows corresponding behavior for the scattered field.

Thus linear polarizers must have orthogonal linearly polarized eigenstates, where for reflection linear polarizers one scattering eigenvalue is zero and for transmission linear polarizers one transmission eigenvalue is zero. Orthogonal, linearly polarized eigenstates correspond to linearly dichroic (and/or birefringent) behavior without optical activity or circular conversion dichroism, i.e. $a = d$ and $|b| = |c|$. The additional requirement that one eigenvalue must be zero allows us to write linear polarizer conditions based on the eigenvalue equations (2.63) and (2.64). A reflection linear polarizer must satisfy

$$a = \pm|b|e^{i\kappa} \tag{2.115}$$

for one sign and a transmission linear polarizer must satisfy

$$a = \pm|b|e^{i\kappa} - 1 \tag{2.116}$$

for one sign.

Linear polarizers that operate in transmission and reflection are of particular interest. It can be easily seen that (2.115) and (2.116) can only be simultaneously satisfied for $|b| = \frac{1}{2}$, $\kappa \in \{0, \pi\}$ and $a = -\frac{1}{2}$.

Thus all **simultaneous transmission and reflection linear polarizers** are given by

$$\overrightarrow{s} = \frac{1}{2}\begin{pmatrix} -1 & \pm e^{-i2\varphi} \\ \pm e^{i2\varphi} & -1 \end{pmatrix}, \quad \varphi \in [0, \tfrac{\pi}{2}). \tag{2.117}$$

These scattering matrices correspond to the lossless planar metamaterial solution (2.106) with $\kappa \in \{0, \pi\}$. It follows that energy conservation is satisfied and that **simultaneous reflection and transmission planar metamaterial linear polarizers**, like good wire grid polarizers [100, 101], **must be lossless**. They completely transmit one linear polarization and completely reflect the orthogonal linear polarization. Note that the parameter φ specifies the azimuth of either the transmitted or the reflected polarization state. At normal incidence φ simply corresponds to the orientation of the linear polarizer.

Importantly, all lossy (and many lossless) planar metamaterial linear polarizers only work for either reflection or transmission, as they do not reflect/transmit the wanted polarization completely. To see this, consider a reflection linear polarizer that reflects the wanted linear polarization completely. It must have scattering eigenvalues $|\lambda^s_{1,2}| = 1, 0$. Due to $\lambda^t_{1,2} = \lambda^s_{1,2} + 1$ [see (2.56)] and energy conservation $|\lambda^s_i|^2 + |\lambda^t_i|^2 \leq 1$ the scattering eigenvalues must be $\lambda^s_{1,2} = -1, 0$ and the corresponding transmission eigenvalues are $\lambda^t_{1,2} = 0, 1$. Thus a planar metamaterial reflection linear polarizer that reflects the wanted polarization completely must also work for transmission (and vice versa). As discussed in the preceding paragraph, this is only possible if no absorption losses are present.

It follows that **all planar metamaterial linear polarizers with** 100% **efficiency are lossless, work simultaneously for both reflection and transmission** and are given by (2.117). Here efficiency is the reflected or transmitted power fraction for the desired polarization state.

2.7.3 Wave Plates

A wave plate introduces some phase delay ρ between two orthogonal, linearly polarized components of an electromagnetic wave. For any wave plate, the polarization state of these orthogonal, linearly polarized components will not be affected by the wave plate and therefore these components must be eigenstates. As wave plates have identical transmission levels for both eigenstates, the corresponding eigenvalues must have the same magnitude, i.e. they only differ by the desired phase difference ρ.

Wave plates do not show optical activity or circular conversion dichroism and thus $a = d$ and $|b| = |c|$. The behavior of wave plates is simply linearly birefringent.

It follows from section 2.5.1 that orthogonal linearly polarized eigenstates result automatically from $a = d$ and $|b| = |c|$. Thus all scattering matrices that additionally have eigenvalues of the same magnitude correspond to wave plates.

Here we generalize the concept of wave plates also to the scattered field. Thus, we consider scattering wave plates and transmission wave plates. Scattering wave plates act as wave plates for the reflected wave. In order to simplify this derivation we introduce a parameter $\tilde{a}$, which is defined differently for scattering and transmission wave plates.

$$\begin{aligned} \text{scattering:} \qquad & \tilde{a} := a, \\ \text{transmission:} \qquad & \tilde{a} := a + 1 \end{aligned} \tag{2.118}$$

In the absence of optical activity, the eigenvalues are given by (2.63) and (2.64) for scattering and transmission, respectively. Here, with $|b| = |c|$ and the definition of $\tilde{a}$, these equations simplify to

$$\lambda_{1,2} = \tilde{a} \pm |b| e^{i\kappa},$$

for both scattering and transmission eigenstates. Clearly, $|\lambda_1| = |\lambda_2|$ is only satisfied

when the vectors represented by $\tilde{a}$ and $e^{i\kappa}$ in the complex plane are perpendicular to each other, i.e.

$$\kappa = \arg(\tilde{a}) \pm \tfrac{\pi}{2}. \tag{2.119}$$

The angle formed by the sum and difference of two perpendicular vectors is twice the arc tangent of the ratio of their magnitudes. Therefore the phase difference $\rho \in [0, \pi]$ between the eigenvalues corresponds to

$$\rho = |\arg\lambda_2 - \arg\lambda_1| = 2\arctan\left|\frac{b}{\tilde{a}}\right|. \tag{2.120}$$

All scattering matrices with $a = d$ and $|b| = |c|$, which additionally satisfy condition (2.119) and energy conservation correspond to wave plates. For scattering wave plates $\tilde{a} = a$, while for transmission wave plates $\tilde{a} = a + 1$.

The phase difference induced by a scattering wave plate is

$$\rho^s \quad = 2\arctan\left|\tfrac{b}{a}\right| \quad \leq 2\arctan\sqrt{\frac{Re(a)+1}{-Re(a)}}, \tag{2.121}$$

where we used inequality (2.89) to write the largest possible $|b|$ in terms of a. Similarly the phase difference induced by a transmission wave plate is

$$\rho^t \quad = 2\arctan\left|\tfrac{b}{a+1}\right| \quad \leq 2\arctan\sqrt{\frac{-Re(a)}{Re(a)+1}}. \tag{2.122}$$

Planar metamaterials have identical scattering and transmission eigenstates. As wave plates have orthogonal linearly polarized eigenstates, the corresponding scattering and transmission matrices can always be written in the orthogonal eigenstate basis. Written in the eigenbasis both scattering and transmission matrices become diagonal with the corresponding eigenvalues as entries. For a scattering wave plate both scattering eigenvalues have the same magnitude, and therefore the scattered power fraction S for any incident polarization is simply given by the squared magnitude of its scattering

eigenvalues

$$\begin{aligned} S = |\lambda^s|^2 &= |a|^2 + |b|^2 \\ &\leq |a|^2 + \tfrac{1}{4} - |a + \tfrac{1}{2}|^2 = -Re(a). \end{aligned} \tag{2.123}$$

Similarly the transmission level of a transmission wave plate is given by the squared magnitude of its transmission eigenvalues

$$\begin{aligned} T = |\lambda^t|^2 &= |a + 1|^2 + |b|^2 \\ &\leq |a + 1|^2 + \tfrac{1}{4} - |a + \tfrac{1}{2}|^2 = Re(a) + 1. \end{aligned} \tag{2.124}$$

Importantly, **a planar metamaterial $\lambda/2$-plate cannot be realized**. A phase delay of π in transmission requires $a = -1$ [see (2.122)], but for $a = -1$ the wave plate must be opaque. Similarly, for a scattering $\lambda/2$-plate $a = 0$ would be required, but for $a = 0$ the wave plate cannot reflect.

Lossy planar metamaterial wave plates [53, 54] typically work for either transmission or scattering. However, there is one important exception: if $a \in \mathbb{R}$ and thus also $\tilde{a} \in \mathbb{R}$ the wave plate condition (2.119) will be satisfied for both scattering and transmission by $\kappa = \pm\frac{\pi}{2}$. It follows that all **wave plates** that simultaneously work **for transmission and scattering** are given by

$$\begin{aligned} \overrightarrow{s} &= \begin{pmatrix} a & b \\ c & d \end{pmatrix} = \begin{pmatrix} a & |b|e^{i(\pm\frac{\pi}{2} - 2\varphi)} \\ |b|e^{i(\pm\frac{\pi}{2} + 2\varphi)} & a \end{pmatrix}, \\ -1 < a < 0, &\quad |b| \leq \sqrt{\tfrac{1}{4} - (a + \tfrac{1}{2})^2}, \quad \varphi \in [0, \tfrac{\pi}{2}), \end{aligned} \tag{2.125}$$

where one preferred direction is given by φ. All solutions (2.125) satisfy energy conservation (2.83) as $p_3 = 0$ for $A = D$, $|b| = |c|$ and $\kappa - \xi = \pm\frac{\pi}{2}$, and as the conditions (2.88) and (2.89), which arise from $p_{1,2}$, are obviously satisfied. The limiting cases $a \in \{-1, 0\}$, which lead to $|b| = 0$, correspond to a phase delay of $\rho = 0$ and the absence of linear birefringence (and linear dichroism). As a and $|b|$ are both free parameters, the possible choices for phase delays for transmitted and reflected waves are largely independent in lossy planar metamaterial wave plates that work simultaneously in transmission and reflection.

Lossless Wave Plates

All scattering matrices allowed by energy conservation for lossless planar metamaterials are given by (2.105), (2.106) and (2.107). As shown in the previous section, wave plates must satisfy $a = d$ (i.e. $\delta = 0$).

In the non-trivial case (2.105) lossless planar metamaterials must meet condition $\kappa = \arg(a + \frac{1}{2}) \pm \frac{\pi}{2}$ (2.101), while wave plates must satisfy $\kappa = \arg(\tilde{a}) \pm \frac{\pi}{2}$ (2.119). Clearly these conditions can only be simultaneously satisfied if $a \in \mathbb{R}$ and thus $\arg(a + \frac{1}{2}), \arg(\tilde{a}) \in \{0, \pi\}$. The trivial lossless solution (2.106) satisfies $a \in \mathbb{R}$ automatically. Note that the other lossless trivial solution (2.107) is not relevant to wave plates as it leads to $|b| = 0$, i.e. a phase delay of $\rho = 0$ (absence of linear birefringence).

Thus **all lossless planar metamaterial wave plates are given by**

$$\overrightarrow{s} = \begin{pmatrix} a & |b|e^{i(\pm\frac{\pi}{2}-2\varphi)} \\ |b|e^{i(\pm\frac{\pi}{2}+2\varphi)} & a \end{pmatrix}, \tag{2.126}$$
$$-1 < a < 0, \qquad |b| = \sqrt{\tfrac{1}{4} - (a + \tfrac{1}{2})^2}, \qquad \varphi \in [0, \tfrac{\pi}{2}),$$

where φ specifies one preferred direction. All lossless wave plates are simultaneously wave plates for scattered and transmitted waves. Importantly, in the lossless case there is only one free parameter a, apart from the orientation of the anisotropic direction φ. Therefore the phase delays ρ^s and ρ^t for scattering and transmission are not independent in lossless planar metamaterial wave plates, and (2.121) and (2.122) become equalities

$$\rho^s \quad = 2\arctan\left|\tfrac{b}{a}\right| \quad = 2\arctan\sqrt{\frac{a+1}{-a}}, \tag{2.127}$$

$$\rho^t \quad = 2\arctan\left|\tfrac{b}{a+1}\right| \quad = 2\arctan\sqrt{\frac{-a}{a+1}}. \tag{2.128}$$

It follows that

$$\rho^s + \rho^t = \pi. \tag{2.129}$$

Also equations (2.123) and (2.124) for the scattered power fraction S and the transmitted power fraction T for any incident polarization become equalities, and can be

written in terms of the phase delay using (2.127) and (2.128)

$$S = \quad -a \quad = cos^2\left(\frac{\rho^s}{2}\right), \tag{2.130}$$

$$T = \quad a+1 \quad = cos^2\left(\frac{\rho^t}{2}\right). \tag{2.131}$$

It follows that a large phase delay comes at the cost of a large insertion loss. For example a transmission phase delay of $\frac{3\pi}{4}$ can only be achieved with 15% transmission, while the corresponding $\frac{\pi}{4}$ scattering phase delay is achieved with 85% reflection. The special case of $\rho^s = \rho^t = \frac{\pi}{2}$, i.e. the lossless $\lambda/4$-plate, has transmission and reflection levels of 50% each.

From (2.121)-(2.124) and (2.127)-(2.131) it follows that lossless planar metamaterial wave plates introduce larger phase delays combined with higher transmission and scattering levels than lossy planar metamaterial wave plates. Simply put, lossless wave plates perform better.

2.7.4 Polarization Rotators

Here we examine the special case of polarization rotators. Note that rotators require oblique incidence onto planar metamaterials without 2-fold rotational symmetry. Polarization rotators rotate the azimuth of any polarization state by some fixed angle $\Delta\Phi$ without affecting the ellipticity of the polarization state.

As shown in section 2.4.3, the same azimuth rotation for any polarization state requires the absence of linear birefringence / dichroism, which is equivalent to $b = c = 0$. For this case energy conservation (2.83) reduces to the simple condition $|a+\frac{1}{2}|, |d+\frac{1}{2}| \leq \frac{1}{2}$, where the equalities correspond to the lossless case, see the gray circles in Fig. 2.16.

From (2.40) and (2.42) it follows that for the absence of linear birefringence / dichroism the azimuth rotations $\Delta\Phi^s$ and $\Delta\Phi^t$ are given by

$$\Delta\Phi^s = -\tfrac{1}{2}\left[\arg(a) - \arg(d)\right], \tag{2.132}$$

$$\Delta\Phi^t = -\tfrac{1}{2}\left[\arg(a+1) - \arg(d+1)\right]. \tag{2.133}$$

Thus, for scattering the rotation is half as large as the angle formed by a and d with the origin, and for transmission the rotation is half as large as the angle formed by $a+1$

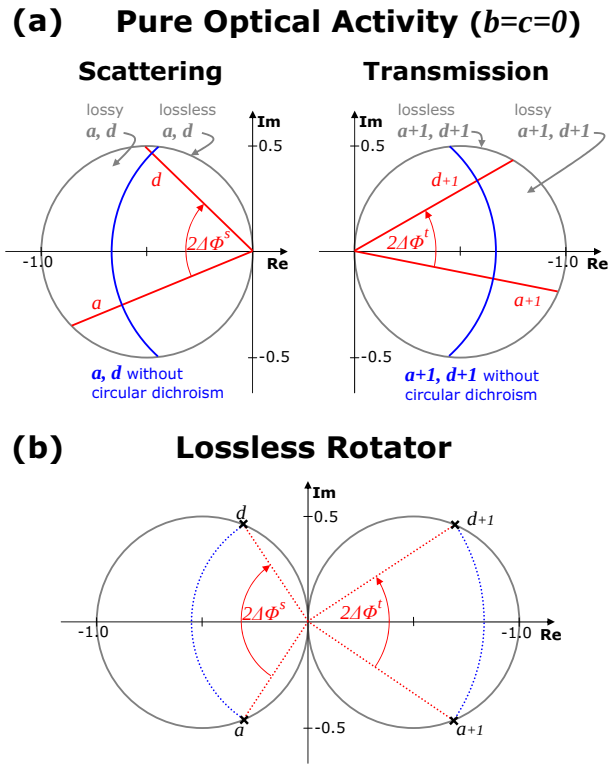

Figure 2.16: ***Pure optical activity and lossless rotators.*** *As shown in section 2.4.3, absence of linear birefringence / dichroism requires $b = c = 0$. For this case energy conservation (2.83) allows all a, d that satisfy $|a + \frac{1}{2}|, |d + \frac{1}{2}| \leq \frac{1}{2}$. The equalities, corresponding to the lossless case, are indicated by gray circles. The relevant coefficients for scattering are a, d, while the relevant transmission coefficients are $a+1, d+1$. (a) For lossless planar metamaterials the scattering and transmission coefficients must fall on the gray circles, while for lossy planar metamaterials all values within the gray circles are allowed. Circular dichroism is only absent if the relevant coefficients have the same magnitude, i.e. fall on the same (blue) circle around the origin. The angle that both coefficients form with the origin is twice as large as the polarization azimuth rotation $\Delta\Phi$ experienced by incident waves. (b) The lossless rotator is the special case where circular dichroism and losses are absent.*

and $d + 1$ with the origin, see the red lines in Fig. 2.16.

Rotators do not change the ellipticity of any polarization state, thus a scattering rotator must not have scattering circular dichroism (2.44), and a transmission rotator must not have transmission circular dichroism (2.43). For scattering rotators this requires $|a| = |d|$, while for transmission rotators $|a + 1| = |d + 1|$ is needed, see the blue arcs in Fig. 2.16.

Due to the absence of circular dichroism, the scattering matrix of a scattering rotator is diagonal with entries a, d (= eigenvalues) of equal magnitude. Therefore the

scattered power fraction S of a scattering rotator is

$$S = |a|^2$$

independent of the incident polarization state. Similarly the transmitted power fraction of a transmission rotator is

$$T = |a + 1|^2.$$

It can easily be seen from Fig. 2.16 (a), that the largest reflectivity S for any choice of $\Delta\Phi^s$ (angle between red lines, left panel) without scattering circular dichroism (a and d on same blue circle) corresponds to the lossless case (gray line). Similarly, the largest transmission T for any choice of $\Delta\Phi^t$ without transmission circular dichroism corresponds to the lossless case, see right panel. **Thus for any azimuth rotation, the most transparent transmission rotator and the most reflective scattering rotator are lossless.** We will find in the following section that for lossless scattering/transmission rotators the reflected/transmitted power fraction is $\cos^2(\Delta\Phi)$. Therefore the scattered power fraction of a scattering rotator is

$$S = |a|^2 \leq \cos^2(\Delta\Phi^s), \tag{2.134}$$

and similarly the transmitted power fraction of a transmission rotator is

$$T = |a + 1|^2 \leq \cos^2(\Delta\Phi^t). \tag{2.135}$$

Typically lossy planar metamaterial rotators [55] will only work for scattered or transmitted fields. However, there are rotator solutions ($a \neq d$) that satisfy $|a| = |d|$ and $|a + 1| = |d + 1|$ simultaneously. All of these **scattering and transmission rotators** are given by $d = \bar{a}$, where $\bar{a}$ is the complex conjugate of a. The corresponding scattering matrices are

$$\overrightarrow{s} = \begin{pmatrix} a & 0 \\ 0 & \bar{a} \end{pmatrix}, \tag{2.136}$$
$$|a + \tfrac{1}{2}| \leq \tfrac{1}{2}.$$

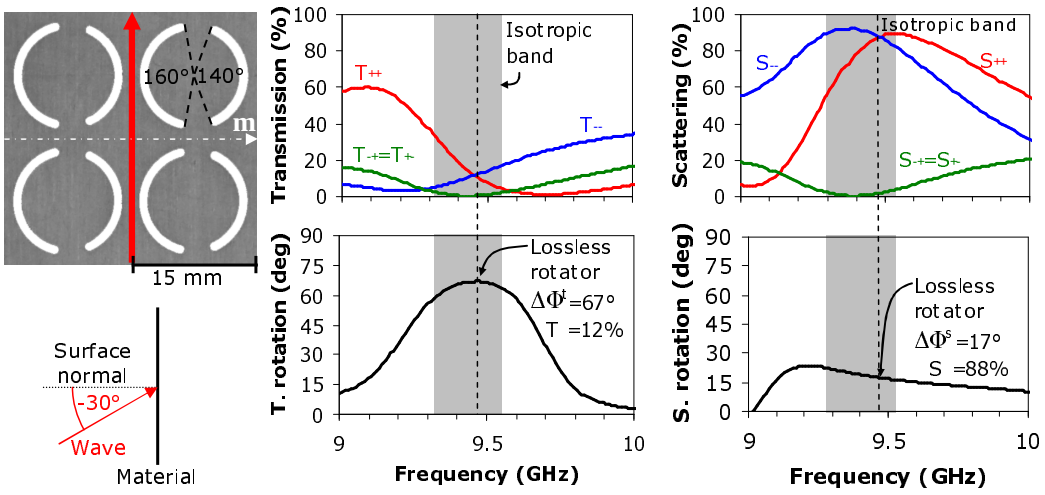

Figure 2.17: ***Experimental demonstration of an almost ideal lossless rotator*** *response for a 1 mm thick aluminum film perforated with asymmetrically split ring apertures (wallpaper group pm). At 9.46 GHz linear birefringence / dichroism ($T_{-+} = T_{+-} = 0$ and $S_{-+} = S_{+-} = 0$) and circular dichroism ($T_{++} = T_{--}$ and $S_{++} = S_{--}$) are absent both in transmission and scattering. Here transmission rotation of* $67°$ *is achieved at 12% transmission (limit* $\cos^2 67° = 15\%$*), and scattered field rotation of* $17°$ *is achieved at 88% scattering (limit* $\cos^2 17° = 91\%$*). Transmission and scattering rotation add up to* $84°$ *(ideal case* $90°$*). All data shown correspond to oblique incidence at* $\theta = -30°$ *with the metamaterial's line of mirror symmetry* $\mathbf{m}$ *perpendicular to the plane of incidence. The structure's optically active properties are discussed in detail in section 4.4 and its transmission characteristics are also presented in reference [56]. Furthermore the resonant current modes that can be excited in this metamaterial are shown in appendix C.*

The Lossless Rotator

Here we examine the special case of lossless rotators. Note that lossless rotators require oblique incidence onto lossless planar metamaterials without 2-fold rotational symmetry.

Lossless rotators must correspond to lossless scattering matrices without any linear birefringence / dichroism ($b = c = 0$) or circular dichroism for scattering ($|a| = |d|$) or transmission ($|a + 1| = |d + 1|$). All lossless scattering matrices without linear birefringence / dichroism are given by (2.107). From (2.110) and (2.111) it follows that circular dichroism is generally absent simultaneously for scattered and transmitted fields. For our phase convention, $\xi \pm 2\delta \in (-\pi, \pi]$, all circularly birefringent solutions without circular dichroism correspond to $\xi = 0$.

Thus the scattering matrices of all lossless rotators are given by (2.107) with $\xi = 0$:

$$\overrightarrow{s} = \frac{1}{2}\begin{pmatrix} e^{-i2\delta} - 1 & 0 \\ 0 & e^{+i2\delta} - 1 \end{pmatrix}, \qquad \delta \in (-\tfrac{\pi}{2}, \tfrac{\pi}{2}). \tag{2.137}$$

Note that this just corresponds to (2.136) with $|a + \frac{1}{2}| = \frac{1}{2}$.

Above we found that for any given azimuth rotation the most transparent transmission rotator and the most reflective scattering rotator are lossless. In order to assess the potential of planar metamaterials as rotators we will calculate transmission, reflection and the associated polarization rotation for the lossless case. As the diagonal elements have the same magnitude, both in case of the scattering matrix and the transmission matrix, the scattered power fraction S and transmitted power fraction T are given by

$$\begin{aligned} S = \quad |d|^2 \quad &= \frac{1}{4}|e^{i2\delta} - 1|^2, \\ T = \quad |d+1|^2 \quad &= \frac{1}{4}|e^{i2\delta} + 1|^2, \end{aligned}$$

which simplifies to

$$\begin{aligned} S &= \sin^2\delta \quad , \\ T &= \cos^2\delta \quad . \end{aligned} \tag{2.138}$$

In the lossless, case without linear birefringence / dichroism or circular dichroism the polarization rotation for scattered and transmitted fields is given by (2.109), where $Im(a)Im(d) \leq 0$. It follows that lossless rotators rotate the scattered and transmitted waves by

$$\begin{aligned} \Delta\Phi^s &= \tfrac{\pi}{2} - \delta, \\ \Delta\Phi^t &= \delta. \end{aligned} \tag{2.139}$$

Thus the scattering matrices of all **lossless rotators** are given by (2.137). Their transmission and reflection levels are described by (2.138) and their rotary power is given by (2.139). As illustrated by Fig. 2.17 and discussed in chapter 4, real planar

metamaterials can come very close to ideal lossless rotators [56]. Importantly, a **large polarization rotation of the transmitted wave comes at the expense of reduced transmission, while a large rotation of the scattered field comes at the expense of reduced reflection**. Thus planar metamaterial rotators can be efficient only for small rotation angles. For example a transmission rotator that rotates up to 6° can be $\geq 99\%$ transparent, while one rotating by 45° can only transmit up to 50%. **In general lossless planar metamaterial rotators have the lowest insertion losses that can be achieved with planar metamaterial rotators.** Due to being measured in different coordinate systems, the rotation for scattering and reflection has opposite signs.

2.7.5 Circular Polarizers

The behavior discussed here can only occur at oblique incidence onto planar metamaterials without 2-fold rotational symmetry.

A transmission circular polarizer transmits one circular polarization without changing its polarization state, while it is opaque for the other circular polarization. A reflection circular polarizer shows analogous behavior for the scattered field.

Thus circular polarizers must have counter-rotating circularly polarized eigenstates, where for reflection polarizers one scattering eigenvalue and for transmission polarizers one transmission eigenvalue is zero. Counter-rotating circularly polarized eigenstates correspond to optical activity without linear birefringence / dichroism, i.e. $b = c = 0$ (see section 2.5.1). This leaves us with diagonal scattering matrices which have scattering eigenvalues as their entries. For reflection circular polarizers exactly one scattering eigenvalue is zero, thus all reflection circular polarizers are given by

$$\overrightarrow{s}(\theta) = \begin{pmatrix} 0 & 0 \\ 0 & \lambda \end{pmatrix} \quad \text{and} \quad \overrightarrow{s}(-\theta) = \begin{pmatrix} \lambda & 0 \\ 0 & 0 \end{pmatrix}, \qquad (2.140)$$
$$|\lambda + \tfrac{1}{2}| \leq \tfrac{1}{2}, \lambda \neq 0,$$

which correspond to reflection of left-handed and right-handed incident circular components, respectively. The reflected power fraction of the desired circular component is $|\lambda|^2$.

Similarly for transmission circular polarizers exactly one transmission eigenvalue must be zero. From $\lambda^t_{1,2} = \lambda^s_{1,2} + 1$ [see (2.56)] it follows that exactly one diagonal entry of the scattering matrix must be -1 and thus all transmission circular polarizers are given by

$$\overrightarrow{s}(\theta) = \begin{pmatrix} \lambda & 0 \\ 0 & -1 \end{pmatrix} \quad \text{and} \quad \overrightarrow{s}(-\theta) = \begin{pmatrix} -1 & 0 \\ 0 & \lambda \end{pmatrix}, \qquad |\lambda + \tfrac{1}{2}| \leq \tfrac{1}{2}, \lambda \neq -1, \tag{2.141}$$

which correspond to transmission of right-handed and left-handed incident circular components, respectively. The transmitted power fraction of the desired circular component is $|\lambda + 1|^2$.

As circular polarizers rely on optical activity, which is reversed for opposite angles of incidence $\pm\theta$, **a planar metamaterial circular polarizer for one circular polarization $\overrightarrow{s}(\theta)$ can always be turned into a circular polarizer for the other circular polarization $\overrightarrow{s}(-\theta)$ by reversing the angle of incidence**.

Obviously, circular polarizers that work simultaneously for transmission and reflection are of particular interest. It can easily be seen that the only matrices that satisfy (2.140) and (2.141) are

$$\overrightarrow{s}(\theta) = \begin{pmatrix} 0 & 0 \\ 0 & -1 \end{pmatrix} \quad \text{and} \quad \overrightarrow{s}(-\theta) = \begin{pmatrix} -1 & 0 \\ 0 & 0 \end{pmatrix}. \tag{2.142}$$

The corresponding eigenvalues have magnitudes $0, 1$, both in case of scattering and transmission, and thus one circular polarization is completely transmitted, while the other is completely reflected. In fact (2.142) corresponds to lossless solution (2.107) with $\xi = \frac{\pi}{2}$ and $\delta = \pm\frac{\pi}{4}$. It follows that **simultaneous transmission and reflection planar metamaterial circular polarizers must be lossless**.

All lossy planar metamaterial circular polarizers can only work for either reflection or transmission. Note that there are also lossless circular polarizers that only work either in reflection or transmission.

It can be easily seen that scattering circular polarizers (2.140) and transmission circular polarizers (2.141), which reflect or transmit 100% of the desired circular com-

ponent, must correspond to the special case (2.142), which is lossless and works simultaneously for reflection and transmission. Therefore **all planar metamaterial circular polarizers with** 100% **efficiency are lossless, work simultaneously for reflection and transmission** and are given by (2.142).

In this case $\overrightarrow{s}(\theta)$ corresponds to 100% transmission of right-handed circular polarization and 100% reflection of left-handed circular polarization, while the properties for $\overrightarrow{s}(-\theta)$ are reversed. Interestingly, as the reflected wave changes handedness, $\overrightarrow{s}(\theta)$ splits any beam into two right-handed circularly polarized beams, while $\overrightarrow{s}(-\theta)$ splits any wave into two left-handed circularly polarized beams.

Note that (2.142) can also by found by maximizing circular dichroism in lossless planar metamaterials without linear birefringence / dichroism, see (2.110) and (2.111).

2.8 Normal Incidence

Here we explore the properties of planar metamaterials under normal incidence conditions. We found in section 2.2.4 that for normal incidence $a = d$ must hold, and that therefore optical activity cannot be observed in this case. We also found that circular conversion dichroism, i.e. directionally asymmetric transmission, reflection and absorption for $|b| \neq |c|$, can occur at normal incidence onto planar metamaterials only if they are 2D-chiral, lossy and anisotropic. The arguments for this were presented in sections 2.2.3, 2.4.2, and 2.4.3, respectively.

The following three sections examine normal incidence for the cases of achiral, isotropic and lossless planar metamaterials. For each of these cases the scattering matrices allowed by symmetry and energy conservation will be derived. Furthermore, it will be shown that for normal incidence onto lossless or isotropic planar metamaterials, 2D chirality does not lead to any polarization effect: For normal incidence the scattering matrices of all lossless ($a = d$, $|b| = |c|$) or isotropic ($a = d$, $b = c = 0$) planar 2D-chiral metamaterials could also correspond to achiral planar metamaterials ($a = d$, $|b| = |c|$).

The fourth section will look into properties of the current modes that can be excited in planar metamaterials at normal incidence. In particular the current mode that leads to the maximum circular conversion dichroism will be derived.

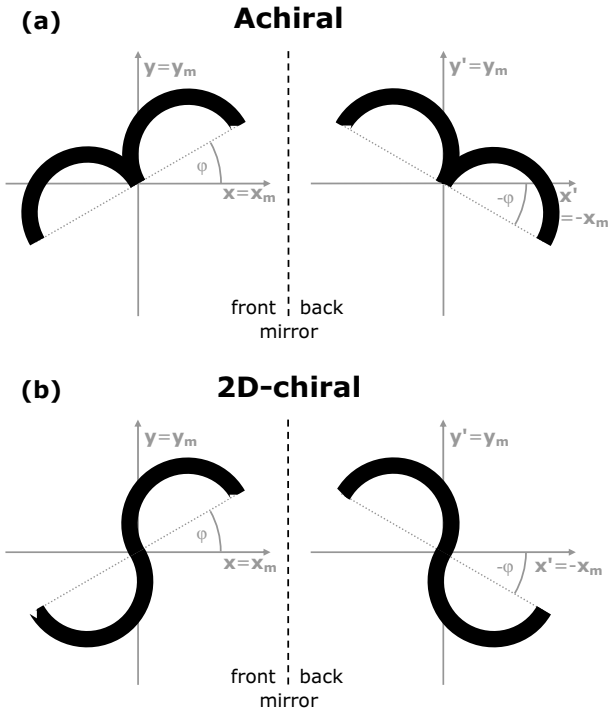

Figure 2.18: ***Achiral and planar chiral patterns*** *and their mirror images, which correspond to the pattern seen from the other side. (a) Achiral patterns and their mirror image are not different from each other as they can be superimposed by an in-plane rotation of the mirror image by* 2φ*. (b) 2D-chiral patterns are different from their mirror image, as the pattern and its mirror image cannot be superimposed by an in-plane rotation. In the 2D-chiral case the pattern and its mirror image have opposite senses of twist.*

2.8.1 Achiral Planar Metamaterials at Normal Incidence

For planar metamaterials, waves normally incident on the front and back see mirror images of the structure, see Fig. 2.18. If the structure and its mirror image, i.e. the patterns seen by forward and backward propagating waves, cannot be superimposed without being lifted off the plane, the metamaterial is 2D-chiral. In case of normal incidence on achiral structures[21] forward and backward propagating waves see the same pattern. However, the reflected pattern will be rotated by an angle -2φ, see Fig. 2.18 and section 2.5.2 (at normal incidence eigenstate azimuth = metamaterial orientation seen by the wave). Thus in the achiral case we must be able to overlap the mirror-image structure with the original by a $+2\varphi$ in-plane rotation. According to (2.74) this rotation corresponds to multiplying the components b and c with phase factors $e^{-i(4\varphi)}$ and $e^{i(4\varphi)}$ correspondingly. After this rotation the rotated scattering matrix $\overleftarrow{s}^{rot}$ must

[21] Achiral wallpaper symmetry groups: *pm*, *pg*, *cm*, *pmm*, *pmg*, *pgg*, *cmm*, *p4m*, *p4g*, *p3m1*, *p31m*, *p6m*.

be equal to the original scattering matrix $\overrightarrow{s}$.

$$\overrightarrow{s} = \begin{pmatrix} a & b \\ c & a \end{pmatrix} \tag{2.143}$$

$$\overleftarrow{s}^{rot} = \begin{pmatrix} a & c\ e^{-i(4\varphi)} \\ b\ e^{i(4\varphi)} & a \end{pmatrix} \tag{2.144}$$

For the achiral case at normal incidence $\overrightarrow{s} = \overleftarrow{s}^{rot}$ must hold, and therefore

$$c = b\ e^{i(4\varphi)}. \tag{2.145}$$

By using $b = |b|e^{i(\kappa-2\varphi)}$ (2.32) this gives us $c = |b|e^{i(\kappa+2\varphi)}$. Written in this form the **scattering matrices for normal incidence on achiral planar metamaterials** are

$$\overrightarrow{s} = \begin{pmatrix} a & |b|e^{i(\kappa-2\varphi)} \\ |b|e^{i(\kappa+2\varphi)} & a \end{pmatrix}, \tag{2.146}$$

$$\overleftarrow{s} = \begin{pmatrix} a & |b|e^{i(\kappa+2\varphi)} \\ |b|e^{i(\kappa-2\varphi)} & a \end{pmatrix},$$

$$\varphi \in [0, \tfrac{\pi}{2}), \qquad |a + \tfrac{1}{2}| \leq \tfrac{1}{2},$$

where the allowed values for κ are derived below (2.151) and $|b|$ must satisfy (2.89), which simplifies in this case to

$$|b| \leq \sqrt{\tfrac{1}{4} - |a + \tfrac{1}{2}|^2} \quad \leq \quad \tfrac{1}{2}. \tag{2.147}$$

This set of scattering matrices implies that achiral planar metamaterials can serve as normal incidence linear polarizers or wave plates operating in transmission and/or reflection. Obviously normal incidence attenuators, beam splitters and mirrors can also be realized using achiral planar metamaterials, see section 2.7.

It follows from the results obtained in section 2.5.2 that achiral planar metamaterials at normal incidence have linear, orthogonal eigenstates, where one eigenstate for forward (backward) propagation has azimuth $+\varphi$ $(-\varphi)$. Note that for anisotropic achiral metamaterials the orientation $\tilde{\varphi}$ of the structure's line of (glide) mirror symmetry must correspond to the orientation of a polarization eigenstate. As $\tilde{\varphi}$ is measured

in the coordinates of a normally incident forward-propagating wave, the relationship $\tilde{\varphi} = \varphi + n\frac{\pi}{2}$ must be satisfied for some $n \in \mathbb{Z}$.

Since $|b| = |c|$, **for the achiral case, the asymmetric transmission, reflection and loss phenomena for opposite propagation directions of the same circular polarization cannot occur at normal incidence. Thus at normal incidence circular conversion dichroism requires intrinsically 2D-chiral metamaterials.**

Note that these considerations do not exclude circular conversion dichroism, i.e. $|b| \neq |c|$, in lossy achiral planar metamaterials at oblique incidence. These considerations also do not exclude optical activity, i.e. $a \neq d$, in achiral planar metamaterials at oblique incidence.

In order to find the allowed values for the parameter κ, we must examine the general energy conservation condition (2.83). For normal incidence onto achiral planar metamaterials we found $a = d$ and $|b| = |c|$, and therefore $p_1 = p_2$ [see definitions (2.79) and (2.80)] must hold, which simplifies the energy conservation condition to

$$p_3 \leq -p_1. \tag{2.148}$$

Note that (2.79) is equivalent to $\frac{1}{2}p_1 = |a + \frac{1}{2}|^2 + |c|^2 - \frac{1}{4}$, and that p_3 is defined by (2.84). Using this and $a = d$, $|b| = |c|$ and the alternative parameters A, ξ, κ defined in (2.29), (2.30) and (2.33), equation (2.148) can be written as

$$\sqrt{2}A|b|\sqrt{1 + \cos[2(\xi - \kappa)]} \leq \tfrac{1}{4} - A^2 + |b|^2. \tag{2.149}$$

Due to $(1 + \cos 2\alpha) = 2\cos^2\alpha$ this is equivalent to

$$|\cos[\xi - \kappa]| \leq \frac{\frac{1}{4} - A^2 + |b|^2}{2A|b|}. \tag{2.150}$$

This expression describes how much the parameter κ can deviate from $\kappa_0 = \xi \pm \frac{\pi}{2}$, the values allowed in the lossless case, see (2.101). Because of $a = d$, in our case the simplified expression $\xi = \arg(a + \frac{1}{2})$ holds, so that

$$|\kappa - \kappa_0| \leq \left|\arcsin\left(\frac{\frac{1}{4} - A^2 - |b|^2}{2|b|A}\right)\right|$$

or, in terms of the scattering coefficient a,

$$|\kappa - \kappa_0| \leq \left| \arcsin \left(\frac{\frac{1}{4} - \left|a + \frac{1}{2}\right|^2 - |b|^2}{2|b|\left|a + \frac{1}{2}\right|} \right) \right| \tag{2.151}$$

applies for the non-trivial solutions of (2.148). For the trivial solutions, which have either $a = -\frac{1}{2}$ or $b = 0$, all values of $\kappa \in [0, 2\pi)$ are allowed.

2.8.2 Isotropic Planar Metamaterials at Normal Incidence

At normal incidence, isotropic planar metamaterials do not have a preferred direction and therefore their response cannot depend on the azimuth of the incident wave. In section 2.4.3, we have shown that such an absence of linear birefringence / dichroism is equivalent to $b = c = 0$. Taking the energy conservation condition (2.88) into account, this gives us the set of scattering matrices allowed for normal incidence onto isotropic planar metamaterials

$$\overrightarrow{s} = \overleftarrow{s} = \begin{pmatrix} a & 0 \\ 0 & a \end{pmatrix}, \quad |a + \tfrac{1}{2}| \leq \tfrac{1}{2}. \tag{2.152}$$

This set of scattering matrices implies that isotropic planar metamaterials can serve as normal incidence attenuators, beam splitters and mirrors, see section 2.7.1. Note, that these scattering matrices are a subset of those allowed for normal incidence onto achiral planar metamaterials (2.146). Thus for normal incidence onto isotropic planar metamaterials, 2D-chiral symmetry cannot lead to any polarization effect.

Importantly, any planar metamaterial with 3-fold or higher rotational symmetry[22] is isotropic. This can be seen from the fact that for any chosen direction in a pattern with 3-fold or higher rotational symmetry there is at least one different direction that is absolutely equivalent. Therefore such structures do not have any preferred direction, and their transmission and reflection properties must be independent of the azimuth of normally incident waves.

[22] Isotropic wallpaper symmetry groups: $p3$, $p3m1$, $p31m$, $p4$, $p4m$, $p4g$, $p6$, $p6m$.

2.8.3 Lossless Planar Metamaterials: Normal Incidence or 2-Fold Rotational Symmetry

Here we determine the scattering matrices and associated properties for the cases of (i) any lossless planar metamaterials at normal incidence and (ii) 2-fold rotationally symmetric lossless planar metamaterials[23] at any angle of incidence.

All lossless planar metamaterials must satisfy energy conservation without losses. The complete set of scattering matrices meeting this requirement is given by (2.105), (2.106) and (2.107). In section 2.2.4 we found that $a = d$ holds for any planar metamaterial at normal incidence and that the same constraint applies to 2-fold rotationally symmetric planar metamaterials at any angle of incidence. Thus the scattering matrices for cases (i) and (ii) are the subset of (2.105), (2.106) and (2.107) for which $a = d$ is satisfied. This subset is

$$\overrightarrow{s} = \begin{pmatrix} a & |b|e^{i(\kappa_0 - 2\varphi)} \\ |b|e^{i(\kappa_0 + 2\varphi)} & a \end{pmatrix}, \qquad \begin{matrix} |a + \frac{1}{2}| \in (0, \frac{1}{2}), & \varphi \in [0, \frac{\pi}{2}), \end{matrix} \tag{2.153}$$

with $|b|$ and κ_0 given by (2.101) and (2.104), respectively, and

$$\overrightarrow{s} = \frac{1}{2}\begin{pmatrix} -1 & e^{i(\kappa - 2\varphi)} \\ e^{i(\kappa + 2\varphi)} & -1 \end{pmatrix}, \qquad \begin{matrix} \kappa \in [0, 2\pi), & \varphi \in [0, \frac{\pi}{2}), \end{matrix} \tag{2.154}$$

$$\overrightarrow{s} = \begin{pmatrix} a & 0 \\ 0 & a \end{pmatrix}, \qquad |a + \tfrac{1}{2}| = \tfrac{1}{2}. \tag{2.155}$$

For (i) normal incidence onto any lossless planar metamaterial and for (ii) any angle of incidence onto a 2-fold rotationally symmetric lossless planar metamaterial all allowed scattering matrices are given by (2.153), (2.154) and (2.155).

It follows from (2.66), (2.69) and (2.70) that the eigenstates are orthogonal linear

[23] Wallpaper symmetry groups with 2-fold rotational symmetry: $p2$, pmm, pmg, pgg, cmm, $p4$, $p4m$, $p4g$, $p6$, $p6m$.

polarizations, where the azimuth of one forward-propagation eigenstate is given by φ. Solutions (2.153) and (2.154) have $|b| = |c| \neq 0$ and thus φ is well-defined by (2.34). It follows that these solutions correspond to lossless planar metamaterials exhibiting linear birefringence and/or linear dichroism. Importantly, these scattering matrices include the special cases of lossless linear polarizers and wave plates, which are discussed in sections 2.7.2 and 2.7.3 respectively. Thus lossless planar metamaterials can serve as normal incidence linear polarizers and wave plates that operate in transmission and/or reflection.

In contrast to this (2.155) corresponds to lossless planar metamaterials without linear birefringence / dichroism, i.e. mirrors ($a = -1$), empty space ($a = 0$) and lossless beam splitters, see section 2.7.1.

Importantly, 2D-chiral circular conversion dichroism ($|b| \neq |c|$) or 3D-chiral optical activity ($a \neq d$) cannot occur in the considered cases (i) and (ii). We found in section 2.4.2 that directionally asymmetric transmission, reflection and absorption phenomena rely on absorption losses. Therefore, circular conversion dichroism cannot be observed for lossless planar metamaterials in general, not even if they have 2D-chiral symmetry. Such a generalization cannot be made for 3D-chiral optical activity, which can occur for oblique incidence onto a lossless planar metamaterial without 2-fold rotational symmetry.

Note that the scattering matrices (2.153), (2.154) and (2.155) are a subset of those allowed for normal incidence onto achiral planar metamaterials (2.146). Thus for normal incidence onto lossless planar metamaterials, 2D-chiral symmetry cannot lead to any polarization effect. The same holds for 2-fold rotationally symmetric lossless planar metamaterials at any angle of incidence.

2.8.4 Current Modes in Planar Metamaterials at Normal Incidence

The response of any planar metamaterial is controlled by the currents excited in the planar structure, which are the source of the scattered field. For planar metal patterns the current response can be very strong, especially in the mid-infrared and at lower frequencies where metals are good conductors. In dielectrics, which can only support displacement currents, the current response is weaker. Here we explore, for the case of normal incidence, how basic characteristics of the excited current mode translate into

electromagnetic properties of the material.

For linear planar metamaterials, the transmitted, reflected and absorbed power fractions cannot depend on the power of the incident wave. In other words the transmitted power $|\mathbf{E^t}|^2$ and the reflected power $|\mathbf{E^r}|^2$ must scale with the power of the incident wave $|\mathbf{E^0}|^2$ and the corresponding fields scale with each other in the same way. At the same time the currents $\mathbf{J}$ excited in the metamaterial scale with the magnitude of the incident field $\mathbf{E^0}$ (Ohm's law). It follows that currents scale with fields, while powers scale with squared currents.

In general a current mode $\mathbf{J}$, i.e. the current configuration excited by the incident wave in a metamaterial unit cell, can have radiating and non-radiating components. Here the non-radiating component corresponds to anti-symmetric currents, that cannot radiate as their radiated fields would destructively interfere in the far-field [57]. The radiating components correspond to the currents that are not compensated for within the unit cell. Their $\mathbf{x}$ and $\mathbf{y}$-components, which are the source of the $\mathbf{x}$ and $\mathbf{y}$-components of the scattered field, are given by

$$E_x^s \propto < J_x > \;=\; \frac{1}{A}\int J_x dA, \tag{2.156}$$

$$E_y^s \propto < J_y > \;=\; \frac{1}{A}\int J_y dA, \tag{2.157}$$

where the relevant area A corresponds to one metamaterial unit cell. Note that in this section, $< Q >$, will always correspond to the quantity Q averaged over the unit cell, i.e. $\frac{1}{A}\int Q dA$. While only $< J_x >$ and $< J_y >$ contribute to the scattered field, all currents contribute to absorption losses, L, which are locally proportional to the squared current.

$$L \propto < |\mathbf{J}|^2 > \;=\; \frac{1}{A}\int |\mathbf{J}|^2 dA \tag{2.158}$$

From the scattered $\mathbf{x}$ and $\mathbf{y}$-polarizations we can calculate the scattered circular polarizations

$$E_\pm^s = \frac{1}{\sqrt{2}}(E_x^s \pm i E_y^s), \tag{2.159}$$

where we assumed a $e^{+i\omega t}$-convention for the time dependence. (For the opposite

convention the "±" on the right-hand-side would turn into "∓".) In terms of current components this corresponds to

$$< J^s_{\pm} >= \frac{1}{\sqrt{2}}(< J^s_x > \pm i < J^s_y >), \tag{2.160}$$

which also holds locally, i.e. without $< ... >$.

Any current mode can be decomposed into three components, a right-handed scattering component $< J^s_+ >$, a left-handed scattering component $< J^s_- >$ and a non-radiating anti-symmetric component $\mathbf{J^{ns}}$. The non-scattering component has the special property $< \mathbf{J^{ns}} >= 0$ and can be written as

$$\mathbf{J^{ns}} \quad = \quad \mathbf{J} - < \mathbf{J} > . \tag{2.161}$$

Note that at normal incidence the entries of the scattering matrix quantify coupling to the scattering current components. i.e. s_{++} describes coupling from incident right-handed circular polarization E^0_+ to the right-handed circular scattering current component $< J_+ >$, while s_{-+} describes coupling from incident right-handed circular polarization E^0_+ to the left-handed circular scattering current component $< J_- >$. Throughout this chapter the entries of scattering matrices have been written in terms of the scattering coefficients a, b, c, d introduced by (2.9)-(2.12).

Let's consider circularly polarized waves normally incident onto a planar metamaterial. Instead of speaking about the right-handed or left-handed current components, it is more convenient to speak about the current-component with the same or the opposite handedness as the incident circularly polarized wave. Let's call the current component with the same handedness as the incident wave the co-rotating component and the current component with the opposite handedness the counter-rotating component, see Fig. 2.19.

Importantly, at normal incidence we found that $a = d$, or $\overrightarrow{s}_{++} = \overrightarrow{s}_{--} = \overleftarrow{s}_{++} = \overleftarrow{s}_{--}$. Thus coupling of circularly polarized waves to the co-rotating current component is always the same, independent of the wave's handedness or direction. It follows that also the scattered field arising from the co-rotating current component must always be the same for normally incident circularly polarized waves, apart from reversal of all handednesses for opposite incident circular polarizations. In particular interference

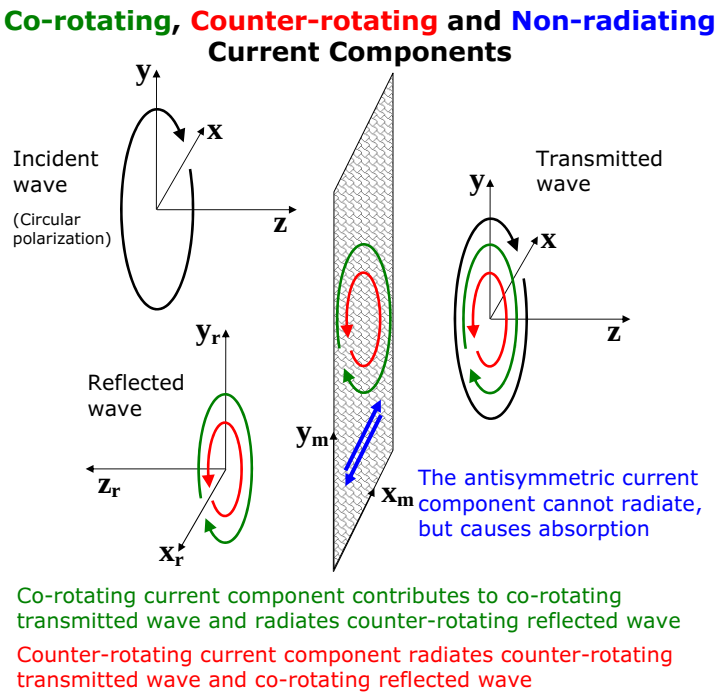

Figure 2.19: ***Current components at normal incidence.*** *Circular polarization normally incident onto a planar metamaterial excites a co-rotating (green), a counter-rotating (red) and a non-radiating (blue) current component. In transmission, the co-rotating current component radiates a co-rotating field which interferes with the incident wave forming the co-rotating transmitted field, while the counter-rotating current component radiates the counter-rotating component of the transmitted field. In reflection, due to a change in coordinates, each current component radiates the reflected field component that is opposite to its own handedness.*

between the scattered field and the incident wave, which determines the co-rotating transmitted field component, must always be the same. This means that for normally incident circularly polarized waves, losses, transmission and reflection arising from the co-rotating current component always take the same values.

From energy conservation follows, that the remaining power, which must be a constant for normally incident circularly polarized waves, must be split somehow between losses, transmission and reflection associated with the other current components. These are the counter-rotating current component, which radiates the counter-rotating transmitted field and the co-rotating reflected field and the non-scattering component. In lossy metamaterials, all current components do contribute to losses, however, the non-scattering current component is special in the sense that it leads to absorption of all power that is coupled to it. Note that for lossless metamaterials the non-scattering component cannot cause absorption and therefore it becomes irrelevant to the above

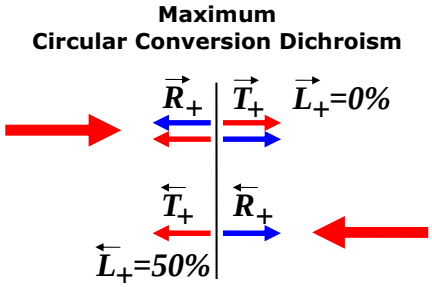

Power Coupling to Current Components

	Co-rotating	Counter-rotating	Non-scattering
Forward	***25%***	***50%***	***0%***
Backward	***25%***	***0%***	***50%***

Figure 2.20: ***Maximum circular conversion dichroism for planar metamaterials.*** *For counter-propagating circularly polarized waves of the same handedness, the largest possible directional asymmetry in transmission and reflection is* 25% *each, corresponding to an asymmetry of* 50% *for losses. This requires that the non-scattering current component is not excited for one propagation direction, while it receives* 50% *of the power for the opposite propagation direction.*

energy balance, i.e. for lossless planar metamaterials normally incident circularly polarized waves must couple equally well to the counter-rotating current component.

Interesting behavior occurs, when the coupling efficiency to the counter-rotating current component has a different magnitude $|b| \neq |c|$ for opposite circular polarizations (same direction) or opposite propagation directions (same circular polarization). Less efficient coupling to the counter-rotating component translates into more efficient coupling to the non-scattering component and thus increased absorption losses. This is how, microscopically, $|b| \neq |c|$ leads to the directionally asymmetric loss, transmission and reflection phenomena discussed in section 2.4.2.

The Current Modes for Maximum Circular Conversion Dichroism

The maximum directional asymmetry in losses, transmission and reflection, see section 2.4.2, that is allowed by energy conservation, corresponds to the scattering coefficients given by (2.95). They are either $a = -\frac{1}{2}, b = 0, |c| = \frac{1}{2}$, or the same with reversed values of b and c. Let's try to understand what this means, see also Fig. 2.20.

$a = -\frac{1}{2}$ describes coupling to the co-rotating current component, which radiates a counter-rotating reflected wave with $|a|^2 = 25\%$ of the incident power. In transmission,

the co-rotating scattered field entirely destructively interferes with the incident wave, limiting co-rotating transmission to $|a+1|^2 = 25\%$ of the incident power. Therefore, the co-rotating current component cannot lose energy in the transmission direction. In the limit of small losses, this means that 25% of the incident power couple to the co-rotating current component, which are entirely reflected.

$b = 0, |c| = \frac{1}{2}$ or vice versa means for opposite propagation directions of the same circular polarization that for one direction the remaining 50% of the incident power will be entirely dissipated in the non-scattering current component, while for the opposite direction the remaining 50% will be entirely coupled to the counter-rotating current component and thus equally split between counter-rotating transmission and co-rotating reflection.

So in the latter case only the two scattering current components are excited. As they radiate equally strongly in reflection, they must have the same magnitude and their superposition must simply correspond to an **electric dipole current mode**.

On the other hand the superposition of the co-rotating and non-scattering current components will be **dominated by** the **non-scattering currents** as these must dissipate energy at a much faster rate than the scattering currents. This is particularly true for the most extreme case which assumes that absorption is negligible for the scattering current components and thus the non-scattering component must have very large currents to dissipate 50% of the incident power.

The excitation of an electric dipole mode and a non-scattering mode has indeed been confirmed for a planar metamaterial exhibiting large asymmetries in transmission, reflection and absorption [98], see chapter 3.2.1.

2.9 Summary

In summary we found that planar metamaterials can show two distinctly different polarization effects of chiral nature. Importantly, neither one of these effects requires the metamaterial itself to be chiral.

The first effect corresponds to optical activity, i.e. circular birefringence and circular dichroism. In terms of the scattering or transmission matrices for circularly polarized waves, optical activity corresponds to non-equal diagonal elements. Conventionally,

optical activity has been associated with 3D-chiral structures. Just like 3D-chiral structures have the same sense of twist when observed from opposite sides, optical activity is the same for opposite propagation directions. Even though planar metamaterials cannot have 3D-chiral symmetry, we found that **circular birefringence and circular dichroism** can occur in planar metamaterials if the following conditions are met

- oblique incidence
- no 2-fold rotational symmetry[24]
- no (glide) mirror line parallel to the plane of incidence.

Note that under these conditions, the experimental arrangement consisting of the metamaterial combined with the direction of incidence has 3D-chiral symmetry (extrinsic 3D chirality). Due to its dependence on the angle of incidence, optical activity in planar metamaterials is inherently tunable. In this respect it is particularly useful that circular birefringence and circular dichroism each are absent at normal incidence and have opposite signs for opposite angles of incidence. Experimental results confirming this behavior are presented in chapter 4.

The second phenomenon of chiral nature is circular conversion dichroism, which leads to asymmetric transmission, reflection and absorption of circularly polarized waves of the same handedness for opposite directions of propagation. The asymmetric behavior arises from reversed right-to-left and left-to-right circular polarization conversion efficiencies for opposite propagation directions. Thus in terms of scattering or transmission matrices for circular polarization the phenomenon corresponds to different magnitudes of the off-diagonal terms. **At oblique incidence circular conversion dichroism requires** structures that have

- losses,
- no (glide) mirror line parallel or perpendicular to the plane of incidence,

while at **normal incidence** planar metamaterials with

- losses,

[24] Wallpaper symmetry groups without 2-fold rotational symmetry: $p1$, pm, pg, cm, $p3$, $p3m1$, $p31m$.

- 2D chirality,
- anisotropy,

are required[25]. Note that at normal incidence the reversed circular polarization conversion efficiencies for opposite propagation directions correspond to the reversed sense of twist of 2D-chiral structures for opposite directions of observation. At oblique incidence, the above criteria require that the metamaterial combined with the direction introduced by the plane of incidence is 2D-chiral (extrinsic 2D chirality). Thus, while optical activity is a 3D-chiral phenomenon, circular conversion dichroism is of 2D-chiral nature. We found that circular conversion dichroism relies on asymmetric absorption losses and that therefore the asymmetric phenomenon cannot occur in lossless planar metamaterials. In general the asymmetry of losses cannot exceed 50% of the incident power, while the asymmetries in transmission and reflection cannot exceed 25% each. These largest asymmetries correspond to the excitation of an electric dipole current mode and a very strong anti-symmetric current mode for opposite propagation directions of the same circularly polarized wave. Simulations supporting the excitation of such current modes in an intrinsically 2D-chiral planar metamaterial that shows large directional transmission, reflection and absorption asymmetries are presented in chapter 3.2.1. Experimental demonstrations of circular conversion dichroism due to extrinsic 2D chirality are presented in chapter 3.3.

Both pure optical activity and the largest possible circular conversion dichroism have circularly polarized eigenstates. However, while optical activity has the same counter-rotating eigenstates for opposite propagation directions, the strongest asymmetric effect has a single degenerate circularly polarized eigenstate, which is left-handed for one propagation direction and right-handed for the opposite direction.

Apart from chiral polarization effects planar metamaterials can also show linear birefringence and linear dichroism. In terms of scattering or transmission matrices for circularly polarized waves, these phenomena corresponds to at least one non-zero off-diagonal element. At normal incidence linear birefringence and linear dichroism can only be observed for anisotropic metamaterials[26]. Importantly, this is not true

[25] 2D-chiral anisotropic wallpaper symmetry groups: $p1$, $p2$.
[26] Anisotropic wallpaper symmetry groups: $p1$, $p2$, pm, pg, cm, pmm, pmg, pgg, cmm.

at oblique incidence, when the experimental arrangement introduces new preferred directions in and perpendicular to the plane of incidence. Therefore almost any planar metamaterial can have linear birefringence / dichroism at oblique incidence. Exceptions include the special cases of perfect mirrors and empty space. The eigenstates associated with pure linear birefringence and dichroism, i.e. without the presence of chiral polarization effects, are orthogonal linear polarization states.

In general we found that for truly planar metamaterials, absorption losses cannot exceed 50% of the incident power.

Importantly, planar metamaterials can act as linear or circular polarizers, wave plates or polarization rotators. Each of these functionalities can be realized for transmission and/or reflection. In particular this allows the realization of reflection circular polarizers, reflection wave plates and reflection rotators. The lowest possible insertion loss for planar metamaterial wave plates and rotators increases with their phase delay and rotation angle, respectively. Low phase delay wave plates and weak rotators can have very low insertion losses, while planar metamaterial $\lambda/2$-plates and $\pm\frac{\pi}{2}$-rotators cannot be realized. Planar metamaterial rotators and circular polarizers require oblique incidence and have the interesting property that their rotation and polarizing properties, respectively, are reversed for opposite angles of incidence.

Chapter 3

Circular Conversion Dichroism in Planar Metamaterials

3.1 Introduction

Circular conversion dichroism is a fundamental electromagnetic effect leading to directionally asymmetric total transmission, reflection and absorption of circularly polarized waves. The asymmetries arise from left-to-right and right-to-left circular polarization conversion efficiencies, that are different from each other and reversed for opposite propagation directions of the incident wave. A general introduction to circular conversion dichroism is presented in section 1.4.2 and for planar metamaterials the phenomenon is characterized theoretically in chapter 2. Here the most important findings are reiterated:

At normal incidence circular conversion dichroism can only occur for planar metamaterials that are lossy, anisotropic and intrinsically 2D-chiral. At oblique incidence the phenomenon should be observable for any lossy planar metamaterial, provided it has no line of (glide) mirror symmetry in or perpendicular to the plane of incidence. As derived in section 2.5.2, circular conversion dichroism is associated with co-rotating elliptical polarization eigenstates of orthogonal orientation. The handedness of the eigenstates is reversed for opposite propagation directions. Following section 2.6.2, the largest possible directional asymmetries in transmission and reflection each are 25% of the incident power, while the asymmetry in absorption can reach up to 50%. As shown

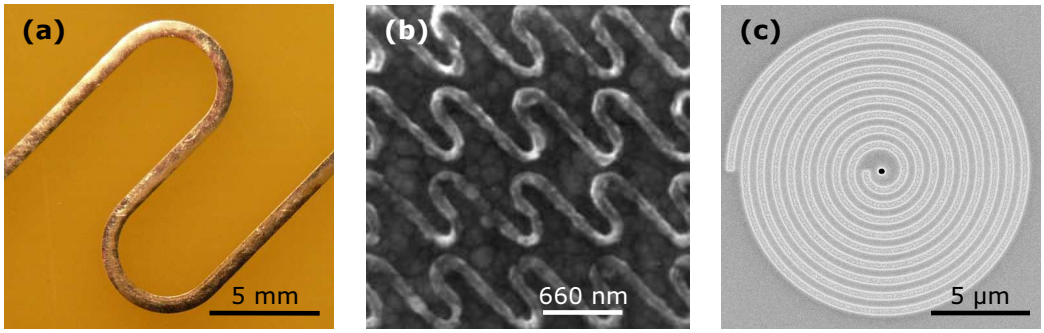

Figure 3.1: ***Intrinsically 2D-chiral structures known to exhibit circular conversion dichroism.*** *(a) 2D-chiral "fishscale" meta-molecule for microwaves [64]. (b) Photonic metamaterial based on the chiral "fishscale" pattern (wallpaper symmetry group p2) [90]. (c) Single plasmonic nanostructure with a small aperture at its center [96].*

in section 2.8.4, these largest asymmetries can only be achieved through excitation of two particular current modes for opposite propagation directions of the same circular polarization: (i) a dissipative mode dominated by non-scattering currents and (ii) an electric dipole current mode.

Prior to the work presented in this thesis, directional transmission asymmetries of up to 10% of the incident power had been observed for microwave [64] and photonic [90] planar metamaterials[1] and single plasmonic nanostructures [96] based on lossy, anisotropic, intrinsically 2D-chiral meta-molecules, see Fig. 3.1. It had been shown through numerical simulations that asymmetric transmission should be accompanied by similar effects in reflection and absorption [97]. Furthermore, it had been reported that circular conversion dichroism should be associated with co-rotating elliptical polarization eigenstates [64, 114]. It must be stressed, that all previous demonstrations of circular conversion dichroism can be attributed to intrinsic molecular 2D chirality.

In this chapter the different types of 2D chirality are studied experimentally. Section 3.2 looks at planar metamaterials with intrinsic 2D chirality, which can arise on either the molecular level [95,98] (2D-chiral meta-molecules) or the structural level [115] (2D-chiral array of non-chiral meta-molecules). In section 3.3 extrinsic 2D chirality is investigated. Extrinsic 2D chirality is a property of the experimental arrangement, which is present, when starting from normal incidence a planar metamaterial is tilted around any axis that is not parallel or perpendicular to a line of (glide) mirror sym-

[1] Wallpaper symmetry group $p2$.

metry. In this case, the metamaterial pattern combined with the direction introduced by the plane of incidence is 2D-chiral, see Fig. 2.8 (d). Also extrinsic 2D chirality can occur on the molecular [99] and/or structural [115] level. Circular conversion dichroism is detected for all four cases of intrinsic and extrinsic molecular and structural 2D chirality.

The results for intrinsic molecular 2D chirality, which are presented in section 3.2.1, include the first experimental demonstration of the directional reflection and absorption asymmetries associated with circular conversion dichroism. The asymmetries reach $\frac{2}{3}$ of the theoretical limits given above, and through numerical simulations they are shown to be linked to excitation of non-scattering and electric dipole currents for opposite propagation directions of the same circular polarization [98]. Also the first observation of circular conversion dichroism at terahertz frequencies will be shown [95]. For extrinsic 2D chirality, a tunable transmission asymmetry exceeding $\frac{4}{5}$ of the theoretical limit (twice as large as previous results) is demonstrated in section 3.3.1 [99]. Finally, the results presented in section 3.3.2 indicate that extrinsic structural 2D chirality should lead to circular polarization conversion at oblique incidence onto any lossy periodically structured interface.

3.2 Intrinsic 2D Chirality

Any planar pattern that cannot be superimposed with its mirror image without being lifted off its plane is intrinsically 2D-chiral. In periodic structures, intrinsic 2D chirality can arise either on the molecular or on the structural level. All previous detections of circular conversion dichroism took place for (arrays of) intrinsically 2D-chiral meta-molecules, see Fig. 3.1. This case of molecular chirality will be covered by section 3.2.1. However, intrinsic 2D chirality can also result from assembling non-chiral objects into an array, when the meta-molecules do not have a line of (glide) mirror symmetry that coincides with a mirror line of the array's lattice. Such structural chirality is discussed in section 3.2.2.

3.2.1 Molecular Intrinsic 2D Chirality

Pushing Circular Conversion Dichroism towards the Theoretical Limit

As illustrated by Fig. 2.9, previous demonstrations of circular conversion dichroism never lead to directional transmission asymmetries exceeding 10% of the incident power [64, 90, 96]. Following sections 2.6.2 and 2.8.4 transmission asymmetries of up to 25% should be possible, if e.g. right-handed circularly polarized waves could excite an electric dipole current when incident on the front of the metamaterial and a mode dominated by non-scattering currents when incident on the back of the metamaterial. For what type of metamaterial might we expect such a response?

It has been reported that arrays of split rings with non-chiral symmetry breaking allow the efficient excitation of non-scattering currents by linearly polarized waves [57], see Fig. 3.2 (a). Here scattering is inhibited through the excitation of opposite currents in the two wires making up each split ring. In the idealized case, the wires would radiate fields that exactly cancel each other in the far-field and therefore the energy coupled to this anti-symmetric mode is trapped at the metamaterial surface. This is why this non-scattering current configuration is also referred to as a "trapped mode".

It should be kept in mind, that there is no such thing as a perfectly non-scattering current mode, as such a mode could not be coupled to. Without any scattered fields, a planar metamaterial would necessarily be 100% transparent. Therefore a non-scattering current component can only be excited when some energy couples to a co-rotating radiative mode, see section 2.8.4. However, energy coupled to the radiative current component is efficiently reradiated, while energy in the non-scattering current component remains trapped until it is dissipated. Therefore the total current configuration can correspond to the non-scattering currents plus a minor perturbation.

Large circular conversion dichroism requires the excitation of such a trapped mode for only one of two opposite propagation directions of the same circularly polarized wave. This can only be possible for structures that (i) can support non-scattering currents and (ii) couple differently to identical circularly polarized waves incident on their front and back. The former requirement is satisfied by asymmetrically split rings [57], while the latter point requires 2D chirality. Therefore **split ring resonators with 2D-chiral symmetry breaking** are a promising candidate for large circular conver-

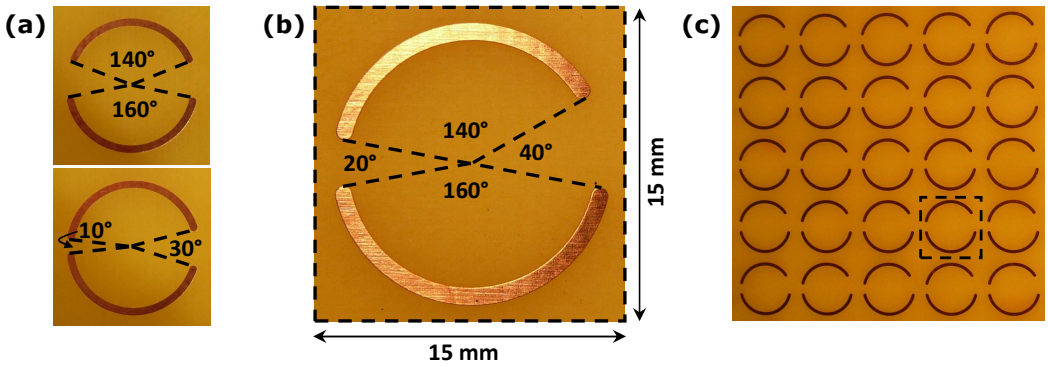

Figure 3.2: ***Split rings with achiral and 2D-chiral symmetry breaking.*** *(a) Split rings with achiral symmetry breaking are known for non-scattering "trapped" currents excited by linearly polarized waves [57]. (b) Split ring meta-molecule with 2D-chiral symmetry breaking. The radius of the split ring is 6 mm and the line width is 0.8 mm. The thickness of the copper layer is 35 µm and the thickness of the supporting FR4 PC board is 1.6 mm. (c) Photograph of a fragment of the 2D-chiral split ring metamaterial's front. The pattern belongs to wallpaper symmetry group p1. One meta-molecule is marked by a dashed box.*

sion dichroism. Here we investigate this idea for a planar microwave metamaterial. Most of the following results have also been published as [98].

As illustrated by Fig. 3.2 (b), a 2D-chiral split ring consists in our case of two wires of different lengths, separated by two gaps of different sizes. As this meta-molecule design has no line of mirror symmetry (or glide reflection), it is 2D-chiral. Its planar twist or handedness could be defined as "rotation from long wire via short gap to short wire". Due to absence of rotational symmetry, the meta-molecule is also anisotropic. A planar metamaterial, composed of a double-periodic array of these meta-molecules, was etched from copper on a lossy dielectric substrate (dielectric constant $\varepsilon \simeq 4.5 - 0.2i$), see Fig. 3.2 (c). The molecule is repeated every 15 mm, ensuring that the metamaterial does not diffract below 20 GHz. Being anisotropic, 2D-chiral and lossy the structure satisfies the general requirements for circular conversion dichroism at normal incidence, which were derived in chapter 2.

Both normal incidence transmission and reflection of microwaves were measured for this metamaterial using the experimental technique and data processing method described in appendix A.1. In order to approximate the structure's normal incidence reflection properties eight reflection measurements were averaged for which the incident beam deviated from the normal by 3.5° in eight different directions (top, top-right, etc.).

Transmission and reflection measurements show that the structure does indeed have a resonance exhibiting large circular conversion dichroism between 5.5 and 6 GHz, which

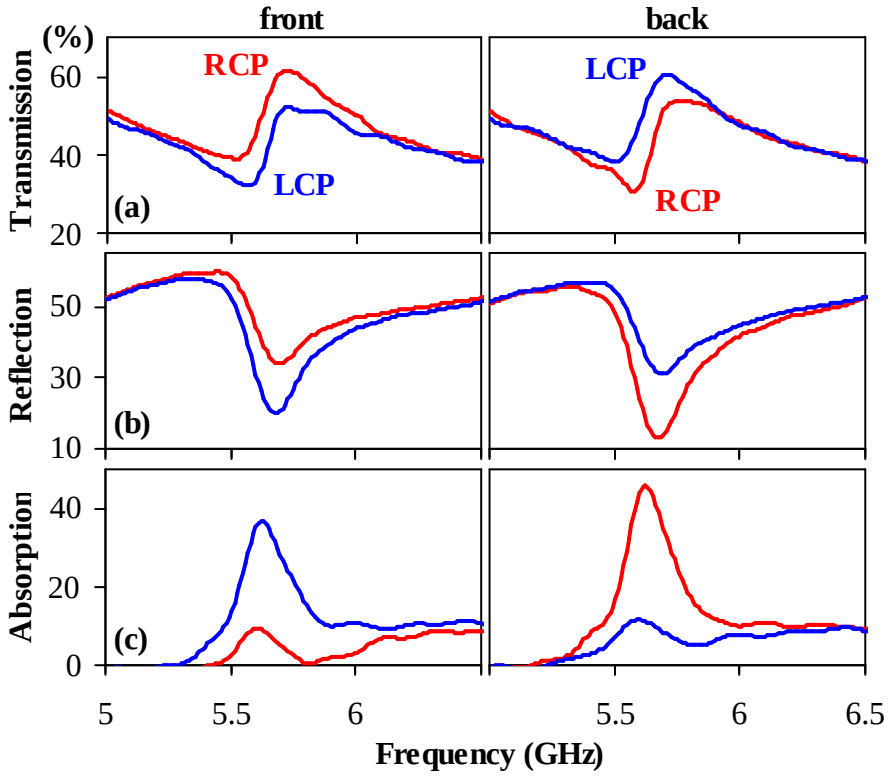

Figure 3.3: ***Spectra for the 2D-chiral split ring metamaterial*** *for LCP (red) and RCP (blue) microwaves normally incident on its front (left) and back (right). (a) Total transmission. (b) Total reflection. (c) Absorption.*

is where the non-chiral split rings shown in Fig. 3.2 (a) have their trapped mode resonances [57]. Fig. 3.3 shows total transmission, reflection and absorbtion levels for right/left (LCP/RCP) circularly polarized beams incident on the front/back of the metamaterial. At the resonance, the metamaterial's properties depend on both propagation direction and handedness of the incident wave. For example, the metamaterial is more transparent for RCP incident on its front than its back. Just as predicted by (2.49), we find exactly the same directional asymmetry for transmission and reflection: The metamaterial is simultaneously more transparent and more reflective for RCP incident on its front than its back. This shows that the directional asymmetries in transmission and reflection must be entirely accounted for by directionally asymmetric losses, $L_\pm = 1 - T_\pm - R_\pm$. As the structure does not diffract, these losses have to be due to absorption. Thus the metamaterial acts as an absorber for RCP waves incident on its back, here absorption is fairly close to the theoretical limit of 50% identified in (2.91). On the other hand RCP waves incident on the metamaterial's front experi-

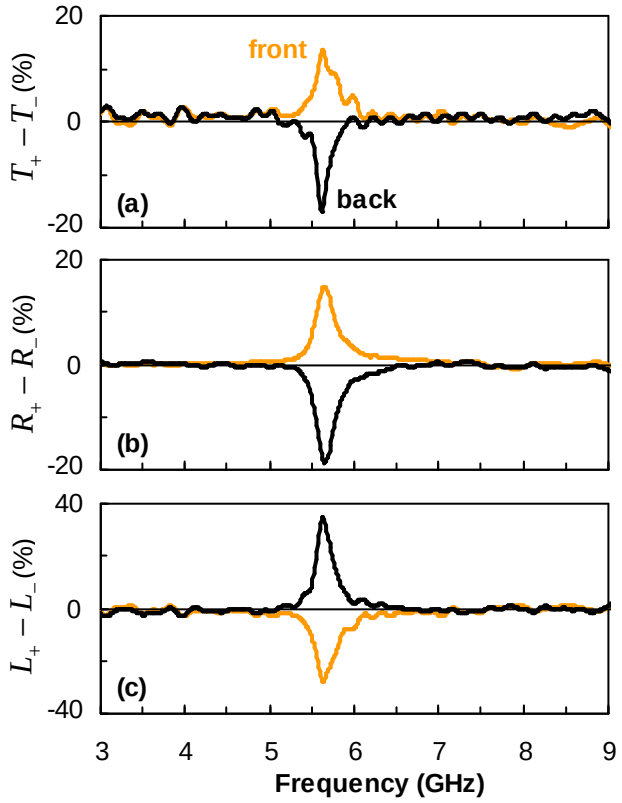

Figure 3.4: ***Asymmetries in transmission, reflection and absorption*** *measured for RCP and LCP microwaves normally incident on the 2D-chiral split ring metamaterial's front (orange) and back (black). (a) Transmission asymmetry. (b) Reflection asymmetry. (c) Absorption asymmetry.*

ence only small losses. For LCP, the directional transmission, reflection and absorption asymmetries are just reversed, as required by (2.49) and (2.50).

In general, the directional asymmetries for one circular polarization, i.e. $\overrightarrow{T_+} - \overleftarrow{T_+}$, are equivalent to circular polarization conversion asymmetries for one propagation direction, i.e. $\overrightarrow{T_{-+}} - \overrightarrow{T_{+-}}$. In absence of circular dichroism[2] (always absent at normal incidence), this is the same as the polarization asymmetries for RCP and LCP incident on the same side of the metamaterial, i.e. $\overrightarrow{T_+} - \overrightarrow{T_-}$. These polarization asymmetries for transmission, reflection and absorption are shown directly in Fig. 3.4. Near 5.7 GHz, the transmission and reflection asymmetries each reach about 16% of the incident power, while the asymmetry in absorption corresponds to 32%. The achieved asymmetries corresponds to $\frac{2}{3}$ of the theoretical limit (2.91) and they substantially exceed the largest transmission asymmetry (10%) observed in previous studies [64].

[2]Circular dichroism was absent within experimental accuracy: $t_{++} = t_{--}$, $r_{-+} = r_{+-}$.

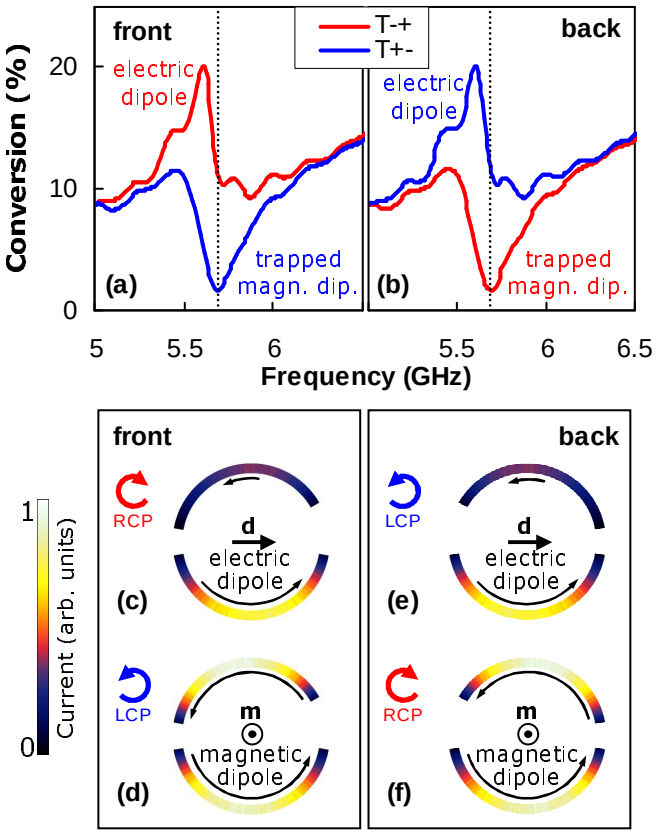

Figure 3.5: ***Resonant circular conversion dichroism.*** *Panels (a) and (b) show circular polarization conversion spectra measured in transmission for RCP (red) and LCP (blue) microwaves normally incident on the structure's front and back. Panels (c)-(f) present the magnitude of resonant currents along the ring at about 5.7 GHz. The instantaneous direction of the currents is indicated by arrows: (c) RCP incident on the structure's front excites a strongly scattering electric dipole-like current mode (strong polarization conversion). (d) LCP excites a weakly-scattering magnetic mode (conversion minimum). Panels (e) and (f) show current distributions for circularly polarized waves incident on the structure from the opposite side.*

The asymmetric metamaterial response is controlled by circular polarization conversion. This is illustrated by Fig. 3.5 (a), which shows the polarization conversion levels for LCP and RCP incident on the metamaterial's front. Within experimental accuracy the efficiencies of conversion in transmission and reflection are the same, i.e. $T_{-+} = R_{++}$ and $T_{+-} = R_{--}$. At around 5.7 GHz the polarization conversion for RCP reaches 20 %, while the conversion for LCP drops below 2 %, leading to a very large circular conversion dichroism within a narrow spectral range. The situation is similar for waves incident on the back of the metamaterial, however, with reversed roles of RCP and LCP.

To understand the nature of the large circular conversion dichroism I numerically

calculated the distribution of currents in the split rings excited by circularly polarized waves normally incident on the metamaterial using a full 3D Maxwell FEM solver in the frequency domain [see Fig. 3.5 (c)-(f)]. The pattern of the metamaterial was modeled as an array of ideally conducting metal split rings of zero thickness (which is a fair approximation at microwave frequencies), while all other parameters of the structure were chosen identical to those of the real sample. The modeling took advantage of the periodicity of the structure, which was represented by a single unit cell with periodic boundary conditions imposed on the computational domain in the lateral directions. Two distinct regimes of resonant excitation can be identified, which depend on handedness and propagation direction of the incident wave. The response to excitation with a right circularly polarized wave (RCP, +) incident on the front of the structure is essentially electric dipolar in nature with the dipole oriented along the split of the ring [Fig. 3.5 (c)]. Radiation of the induced oscillating linear dipole can be presented as a sum of left and right circular polarizations where the left-handed component of scattering gives rise to strong resonant polarization conversion [red curve, Fig. 3.5 (a)]. On the contrary, the response to excitation with a left circularly polarized wave (LCP, −) is essentially a magnetic dipolar non-scattering mode. Here the induced magnetic moment is perpendicular to the metamaterial plane and is created by anti-symmetric currents flowing in opposite sectors of the ring [see Fig. 3.5 (d)]. The anti-symmetric current mode is weakly coupled to free space, scattering is low [57] and polarization conversion is at its minimum [blue curve, Fig. 3.5 (a)]. Due to weak scattering, energy coupled to the magnetic mode is trapped in the anti-symmetric current oscillation and eventually dissipated in the lossy dielectric substrate, which results in large absorption losses [Fig. 3.3 (c)]. When the propagation direction is reversed, i.e. the wave enters the structure from the opposite side, the perceived sense of planar chirality of the design reverses: the larger split on the right now appears to be on the left of the ring. Now the roles of left and right circular polarizations are swapped around: the left circular polarization excites an electric response [Fig. 3.5 (e)] while the right circular polarization excites a predominantly magnetic response in the metamaterial [Fig. 3.5 (f)]. Indeed, polarization conversion is now at its maximum for left circular polarization and at a minimum for right circular polarization, as shown in Fig. 3.5 (b).

Thus circular conversion dichroism arises from excitation of (i) an electric dipole-

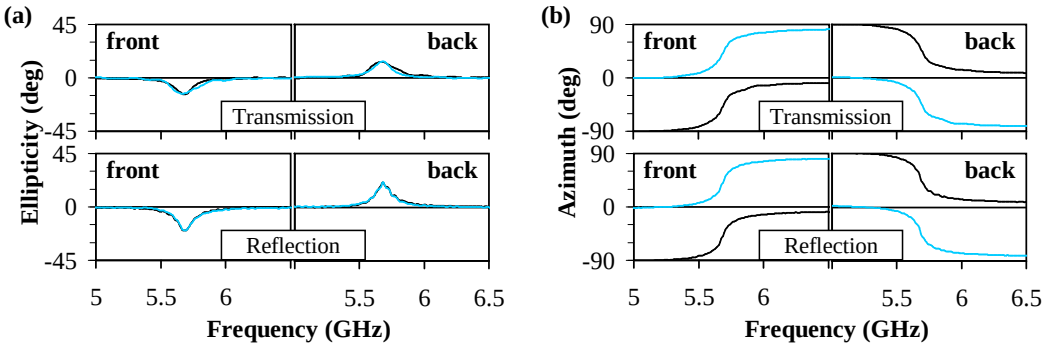

Figure 3.6: ***Transmission and reflection eigenstates of the 2D-chiral split ring metamaterial*** *for normal incidence. (a) Ellipticity. (b) Azimuth.*

like "conversion" mode and (ii) a weakly scattering anti-symmetric "absorption" mode by circularly polarized waves of either handedness or opposite propagation direction, just as predicted in section 2.8.4.

Although the structure shows strong resonant polarization conversion for circularly polarized electromagnetic waves, certain polarization states remain unchanged on transmission or scattering. Fig. 3.6 shows the ellipticity angle and azimuth of the metamaterial's transmission and scattering eigenstates. In non-resonant regions the eigenstates are a pair of orthogonal linear polarizations with the azimuth corresponding approximately to the directions along and perpendicular to the ring's split. At the resonance, however, the eigenstates become co-rotating orthogonal ellipses. The scattering eigenstates, which are the physically meaningful eigenstates for reflection (see section 2.5), are the same as the transmission eigenstates within experimental accuracy. For opposite propagation directions, the handedness of the eigenstates is reversed. This is in full agreement with the general properties of eigenstates derived in section 2.5.2 for planar metamaterials with circular conversion dichroism and without optical activity.

It is worth noting that the 2D-chiral split ring design is an ideal platform for engineering planar metamaterials with asymmetric properties. The spectral width of the metamaterial's asymmetric response is controlled by 2D-chiral symmetry breaking, where a larger asymmetry leads to broadening of the asymmetric band. Furthermore, transmission, reflection and absorption asymmetries even closer to the theoretical limit should be realizable through optimization of 2D-chiral symmetry breaking and substrate losses.

In summary, the study of the 2D-chiral split ring metamaterial has led to (i) the

first observation of asymmetric reflection and absorption due to circular conversion dichroism, (ii) the identification of the underlying microscopic mechanism (scattering electric dipole and non-scattering dissipative current modes) and (iii) enhanced circular conversion dichroism.

Circular Conversion Dichroism at Terahertz Frequencies

This work is the result of a collaboration. The experiments were carried out by Ranjan Singh from Oklahoma State University, who also manufactured the metamaterial. The simulations were performed by Christoph Menzel and Carsten Rockstuhl from Friedrich Schiller University Jena. I extracted the metamaterial properties for circularly polarized waves and the eigenstates from the linearly polarized experimental and numerical data. Furthermore, I was involved in planning the experiments and I interpreted the results. Most of the following work has been published as [95].

The terahertz spectral region has tremendous technological importance since many biological materials and substances have molecular vibration frequencies in this regime, making it highly attractive for sensing, material characterization, spectroscopy and biomedical imaging [116]. In spite of intense research activity in this domain over the past decade terahertz radiation has proved to be challenging to detect, measure, propagate and manipulate since electronic and magnetic responses of natural materials die out at these frequencies, thus earning the name of the so-called "terahertz gap". Recently, terahertz metamaterials [52, 117–124] have emerged as promising functional materials for use in the terahertz gap, but the region still suffers from a severe shortage of devices needed for fully exploiting the attractive potential applications of terahertz radiation.

The work presented here constitutes the first observation of circular conversion dichroism in the terahertz domain. By demonstrating directionally asymmetric transmission of circularly polarized waves through a terahertz metamaterial, it adds a tool for the manipulation of terahertz radiation. Through simulations, circular conversion dichroism is linked to the direction and polarization-dependent excitation of current modes in the metamaterial, which are compatible with the arguments presented in section 2.8.4. Furthermore, various bands of positive, negative and zero phase and group velocities are identified indicating the opportunity to develop polarization sensitive

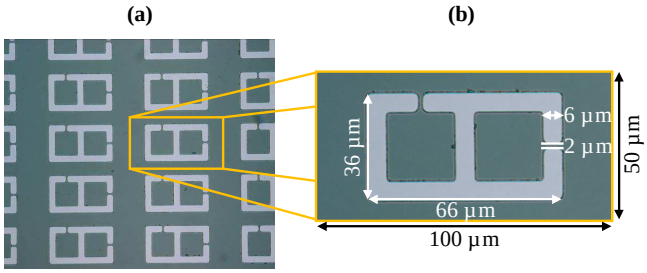

Figure 3.7: ***Planar chiral terahertz metamaterial*** *belonging to wallpaper symmetry group p1. (a) Front side of the metamaterial consisting of 200 nm thick aluminum wires on an n-type silicon substrate. (b) Metamaterial unit cell.*

negative index and slow light media based on such metamaterials.

The metamaterial structure[3], which is shown in Fig. 3.7(a), is based on pairs of split rings of orthogonal orientation that are joined together forming a 2D-chiral pattern. The planar twist of the structure can be defined as from "gap on long side" to "gap on short side", making the structure right-handed when observed from the structured front and left-handed when observed from the back. The planar chiral metamaterial sample was fabricated by conventional photolithography from a 200 nm thick aluminum layer deposited on a 640 μm thick silicon substrate with n-type resistivity 12 Ω cm and an absorption constant of 5/cm [125]. Fig. 3.7(b) shows detailed dimensions of the metamaterial's rectangular unit cell which is $100 \times 50 \mu m^2$ in size rendering the structure non-diffracting at normal incidence for frequencies up to 3 THz. The metamaterial's transmission characteristics were studied at normal incidence using terahertz time-domain spectroscopy (THz-TDS) [126,127]. The terahertz beam incident on the sample had a frequency independent diameter of 3.5 mm and thus illuminated about 2000 unit cells at the center of the 10×10 mm^2 metamaterial array. Using parallel or crossed linear polarizers placed before and after the sample, the amplitude and phase of all components of the metamaterial's transmission matrix was measured relative to a blank silicon substrate. In order to determine the metamaterial's properties for circularly polarized waves, the transmission matrix was transformed to the circular polarization basis using the method described in appendix A.1. The metamaterial's transmission characteristics, as well as the current configurations excited in the metamaterial unit cell, were also simulated using the Fourier Modal Method (FMM) [128].

[3]This metamaterial was originally designed to study coupling between bright and dark eigenmodes in pairs of split rings [125].

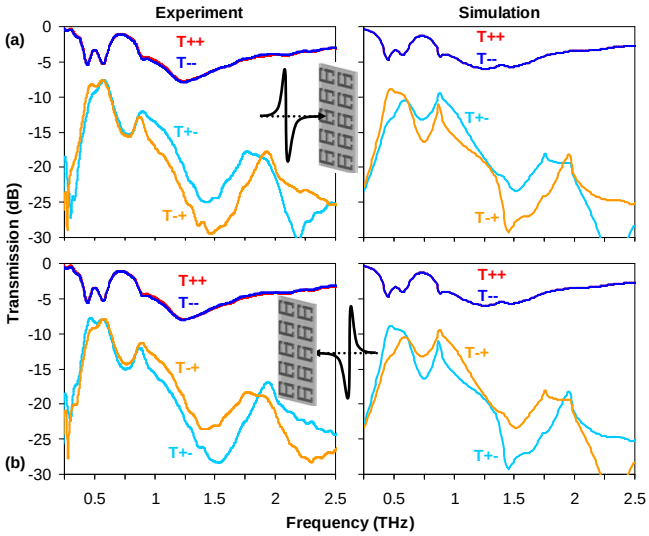

Figure 3.8: ***Transmission spectra for circularly polarized terahertz waves*** *incident on (a) front and (b) back of the metamaterial array. It can be clearly seen that the circular polarization conversion efficiencies T_{-+} and T_{+-} are reversed for opposite directions of propagation.*

As illustrated by Fig. 3.8, the numerical and experimental results show that the metamaterial's direct transmission for circular polarization is reciprocal as coefficients $t_{++} = t_{--}$ are both identical and independent of the direction of propagation. Thus circular birefringence $\arg(t_{++}) - \arg(t_{--})$ and circular dichroism $T_{++} - T_{--}$, which are associated with 3D chirality, are negligible indicating that the metamaterial - which is formally 3D-chiral due to the substrate on only one side of the metal pattern - behaves like a truly planar structure.

In contrast to direct transmission, the right-to-left T_{-+} and left-to-right T_{+-} circular polarization conversion levels depend on both the direction of wave propagation and the handedness of the incident wave, indicating the presence of circular conversion dichroism. The observed effect is fully consistent with the derivations in chapter 2 for circular conversion dichroism at normal incidence onto a planar metamaterial. In particular, counter-propagating circularly polarized waves of the same handedness experience different levels of circular polarization conversion, while their direct transmission levels are identical, for example $\overrightarrow{T}_{-+} \neq \overleftarrow{T}_{-+}$ and $\overrightarrow{T}_{++} = \overleftarrow{T}_{++}$ in case of RCP. It follows that the metamaterial's total transmission for RCP, $T_+ = T_{++} + T_{-+}$, is asymmetric with respect to opposite directions of wave propagation. Furthermore the conversion efficiencies for RCP and LCP are simply interchanged for opposite di-

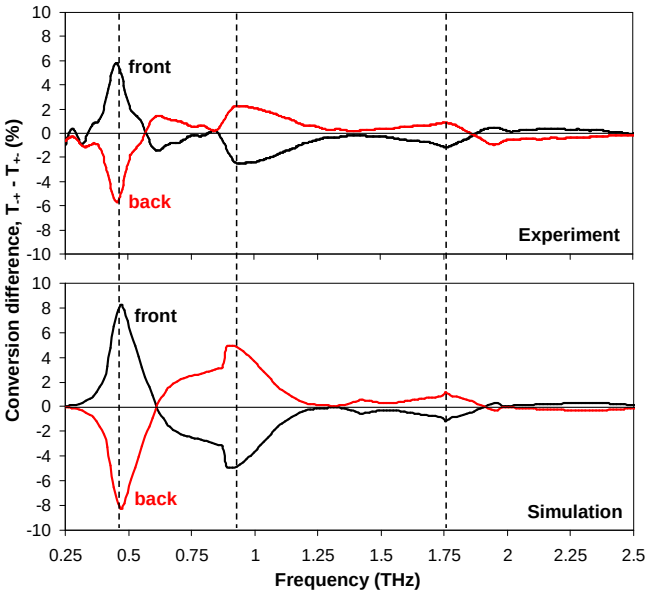

Figure 3.9: ***Transmission asymmetry*** $T_+ - T_- = T_{-+} - T_{+-}$ *for right-handed and left-handed circularly polarized waves incident on either front (black curves) or back (red curves) of the metamaterial sample.*

rections of wave propagation, i.e. $\overrightarrow{T}_{+-} = \overleftarrow{T}_{-+}$. This has two significant consequences: Firstly, the directional transmission asymmetry $\overrightarrow{T}_+ - \overleftarrow{T}_+ = \overrightarrow{T}_{-+} - \overleftarrow{T}_{-+}$ is identical to the total transmission difference for opposite circular polarizations propagating in the same direction, $\overrightarrow{T}_+ - \overrightarrow{T}_- = \overrightarrow{T}_{-+} - \overrightarrow{T}_{+-}$. Secondly, the metamaterial has the same transmission properties for circularly polarized waves of opposite handedness propagating in opposite directions, i.e. $\overrightarrow{T}_+ = \overleftarrow{T}_-$ and $\overrightarrow{T}_- = \overleftarrow{T}_+$.

Fig. 3.9 shows the total transmission asymmetry for circularly polarized terahertz waves incident on the structure's front and back directly. Experimental and numerical results are generally in good agreement and show that asymmetric transmission takes place over the entire studied spectral range from 0.25 to 2.5 THz. The largest asymmetry of total transmission occurs around 0.47 THz, where the structure is measured to be 6% (simulation: 8%) more transparent for RCP than LCP terahertz waves incident on its front. For waves incident on the metamaterial's back the situation is reversed with larger total transmission for LCP than RCP by the same amount.

Similarly to the microwave metamaterial discussed in the previous section, numerical simulations confirm that circular conversion dichroism in the terahertz metamaterial is linked to the excitation of "enantiomerically sensitive" current modes, these are induced charge oscillations that depend on the mutual handedness of the wave and the

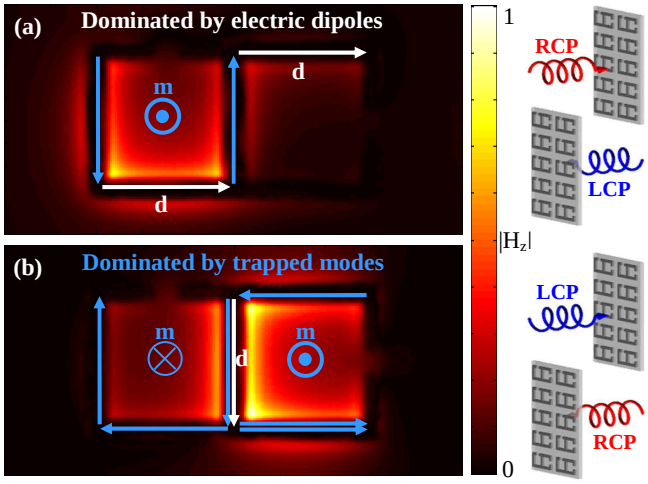

Figure 3.10: ***Current modes linked to the resonant transmission asymmetry*** *at 0.47 THz. The current oscillations in the wires of the structure are represented by arrows, while the color-scale indicates the magnitude of the magnetic field the currents induce normal to the metamaterial's plane. The current configurations can be decomposed in scattering electric dipole components* **d** *and non-scattering (trapped) magnetic dipole components* **m**, *marked in white and blue respectively. Note the radical difference in the excitation patterns caused by circular polarizations of either opposite handedness or opposite propagation direction.*

metamaterial pattern [97, 98]. This is particularly evident at at 0.47 THz, where the metamaterial shows a resonant transmission asymmetry. Here, numerical simulations show radically different patterns of currents when the metamaterial structure is excited by left or right circularly polarized waves: a RCP wave entering the metamaterial from the front side induces a strongly anisotropic electric dipole current oscillation **d** along the long side of the unit cell that is responsible for the efficient circular polarization conversion, see Fig. 3.10(a). On the contrary, the current mode excited by a LCP wave propagating in the same direction is dominated by anti-symmetric current oscillations, which correspond to magnetic moments **m** oscillating normal to the metamaterial plane, see Fig. 3.10(b). As the magnetic components cannot interact with the incident and scattered fields (which propagate parallel to **m**), this current configuration is weakly coupled to free space. These weakly scattering currents, known as trapped modes [57,98], trap energy at the metamaterial surface resulting in increased absorption losses, reduced circular polarization conversion and lower total transmission. Consistently with the smaller transmission asymmetry, for the terahertz metamaterial the non-scattering and electric dipole currents are not as pronounced as for the microwave metamaterial discussed in the previous section. Nevertheless, they can be clearly iden-

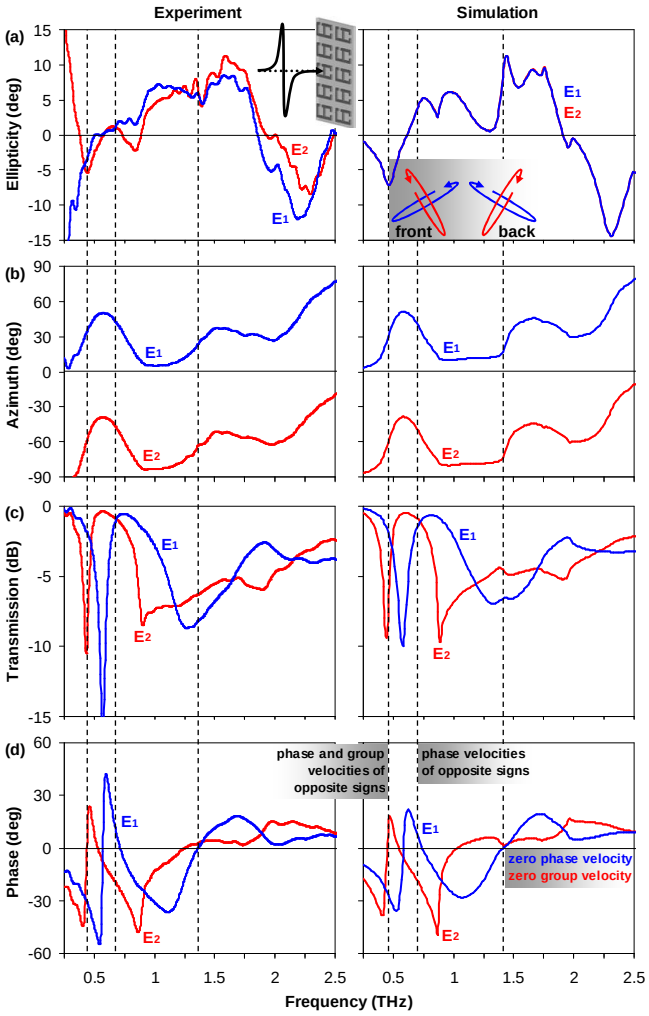

Figure 3.11: ***Transmission eigenstates*** $\mathbf{E_1}$ *and* $\mathbf{E_2}$ *for forward propagation in terms of (a) ellipticity angle and (b) azimuth. (c) Transmission level and (d) phase delay for these eigenpolarizations.*

tified, confirming the general microscopic mechanism of circular conversion dichroism introduced in section 2.8.4.

Although the metamaterial shows strong circular polarization conversion, certain polarization states remain unchanged on transmission. Ellipticity and azimuth of the transmission eigenstates for waves incident on the structure's front are shown in Figs. 3.11 (a) and (b) respectively. Similarly to the microwave metamaterial discussed in the previous section and as derived in section 2.5.2, the structure has co-rotating elliptical eigenstates. This fact underlines how different circular conversion dichroism is from optical activity or the Faraday effect (which have counter-rotating circular eigenstates). The eigenpolarizations have orthogonal orientations and their handedness is

reversed for the opposite propagation direction, see inset to Fig. 3.11 (a). Fig. 3.11 (c) and (d) illustrate the metamaterial's transmission properties for its eigenpolarizations in terms of transmission levels and phase delay. Intriguingly, the metamaterial pattern can introduce positive as well as negative phase delays, indicating that positive and negative phase velocities should be expected in a bulk material based on the structure. The group velocity, whose sign is determined by the slope of the phase as a function of frequency, can only be discussed for stable eigenstates. However, eigenstate stability in a finite medium may be achieved for any frequency by limiting the pulse spectrum. Therefore, in principle, also the group velocity may be defined even if the eigenstates depend on frequency. Various bands of positive and negative phase dispersion indicate that in 2D-chiral bulk metamaterials group velocities of either sign may be possible. For example at 0.45 THz the eigenstates appear to have both opposite phase velocities and opposite group velocities, while at 0.95 THz their group velocities are almost identical, but their phase velocities have opposite signs. Finally at 1.41 THz the phase velocity of eigenstate $\mathbf{E_1}$ and the group velocity of $\mathbf{E_2}$ are zero. These results indicate an opportunity to develop polarization sensitive negative index and slow light media for elliptically polarized waves on the basis of bulk 2D-chiral anisotropic metamaterials.

In summary, the study of the intrinsically 2D-chiral terahertz metamaterial has led to the first observation of circular conversion dichroism at terahertz frequencies, providing a novel directionally asymmetric way of manipulating terahertz radiation.

3.2.2 Structural Intrinsic 2D Chirality

All previous demonstrations of circular conversion dichroism [64,90,96], as well as those presented in the previous section, took place for (arrays of) intrinsically 2D-chiral meta-molecules. However, also non-chiral particles can be arranged in structurally 2D-chiral arrays [129]. As illustrated by Fig. 3.12, an array has intrinsic structural 2D chirality, if its meta-molecules have no line of (glide) mirror symmetry that coincides with a mirror line associated with the array's lattice[4]. In this case, mirror-forms of the array cannot be superimposed by translations and rotations in the plane, which makes the entire structure 2D-chiral. Intrinsic structural 2D chirality has previously attracted

[4]Structural chirality also plays a role for arrays of intrinsically 2D-chiral meta-molecules, as such meta-molecules do not have any line of (glide) mirror symmetry.

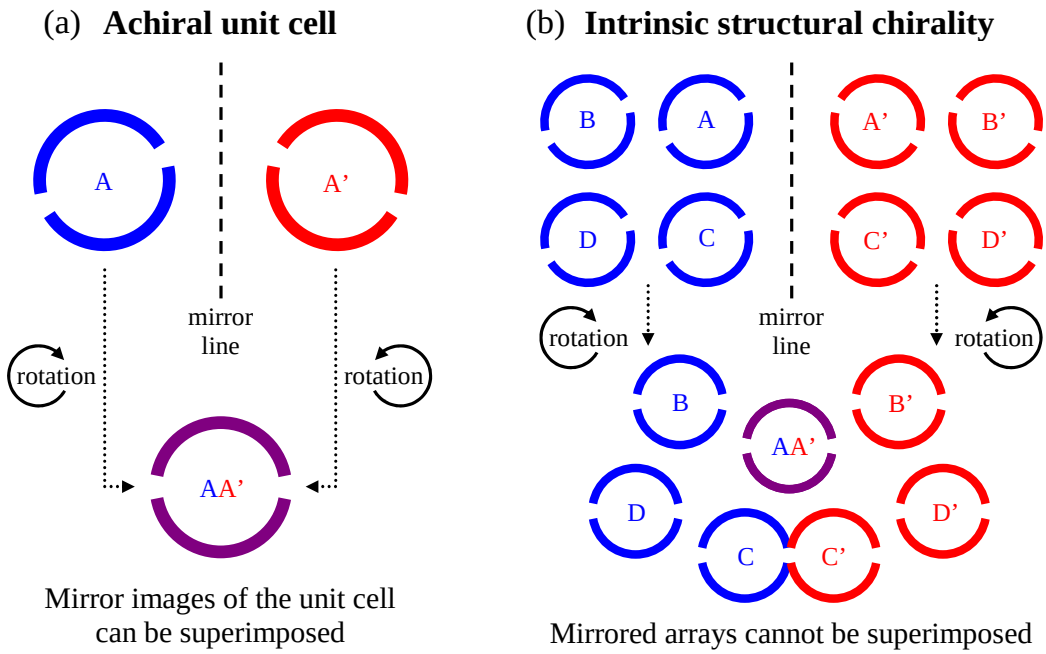

Figure 3.12: ***Intrinsic structural 2D chirality.*** *Anisotropic achiral meta-molecules (a) can form a structurally planar chiral array (b). While a single meta-molecule (blue) and its mirror image (red) can be superimposed by translation and rotation (purple), certain arrays of such meta-molecules show planar enantiomorphism: congruency can only be achieved for one meta-molecule in the array (purple) while the rest of the mirrored arrays does not coincide.*

attention as a source of chiral effects in diffraction gratings, where it was shown to lead to polarization azimuth rotation in diffracted beams [93, 94].

The results presented here demonstrate that intrinsic structural 2D chirality leads to circular conversion dichroism in periodic arrays of non-chiral particles, provided that losses and anisotropy are present as derived in chapter 2. Most of these findings have also been reported in [115].

Here the role of intrinsic structural 2D chirality is studied for planar metamaterials based on non-chiral split rings, with the dimensions specified in Fig. 3.13. The metamaterial structures were formed by a square array of about 200 meta-molecules separated by 15 mm, which rendered the structures non-diffracting at normal incidence below 20 GHz. The patterns were etched from a 35 μm copper layer covering 1.6 mm thick lossy FR4 printed circuit boards (Im $\varepsilon \sim 0.1$) using standard photolithography. The normal incidence transmission properties of the metamaterials were measured using the experimental and data processing techniques described in appendix A.1. Eight different versions of the split ring array were studied, where the orientation of the split

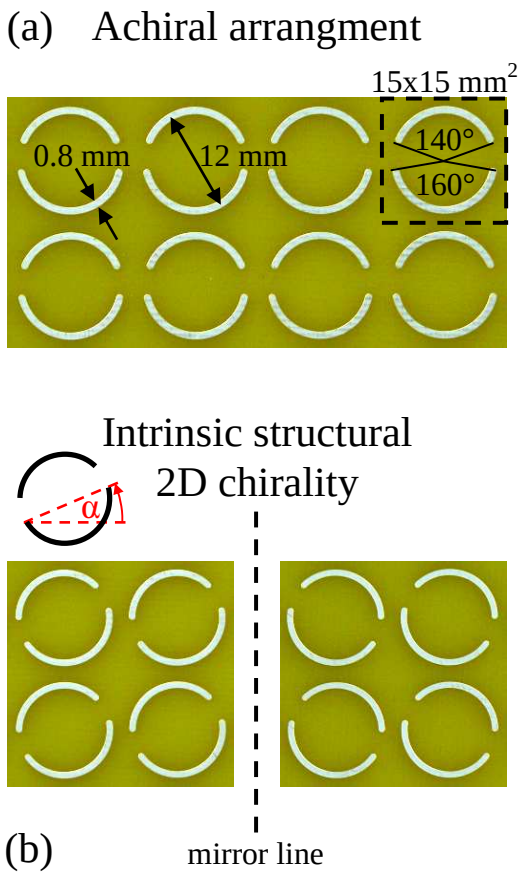

Figure 3.13: ***Metamaterial samples without and with intrinsic structural 2D chirality.*** *(a) Achiral arrangement of asymmetrically split rings belonging to wallpaper symmetry group pm. (b) Rotation of the split rings by an angle $\alpha \neq n \cdot 45°$, $n \in \mathbb{Z}$ leads to intrinsic structural 2D chirality of the array, which becomes different from its mirror image and belongs to wallpaper symmetry group p1.*

α was varied in steps of $11.25° = \pi/16$ rad relative to the achiral arrangement shown in Fig. 3.13 (a). As illustrated in Fig. 3.13 (b), split orientations $\pm\alpha$ correspond to structural planar chirality of opposite handedness, while split orientations α and $\alpha + 90°$ lead to identical metamaterial arrays.

Fig. 3.14 presents typical spectra of direct transmission T_{++}, T_{--} and circular polarization conversion T_{-+}, T_{+-} for achiral and chiral arrangements of split rings. For all versions of the split ring array, the direct transmission intensities (as well as field transmission coefficients t_{++} and t_{--}) do not depend on the handedness or propagation direction of incident circularly polarized waves. In particular this shows that in our case any 3D chirality introduced by presence of the substrate [80] is too small to lead to significant circular birefringence, $\arg(t_{++}) - \arg(t_{--})$, or circular dichroism,

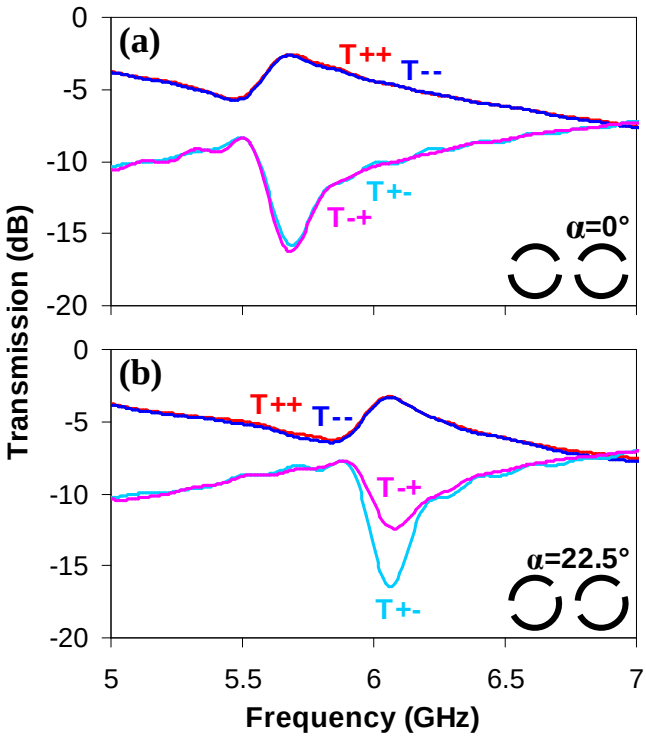

Figure 3.14: ***Transmission spectra for metamaterial samples without and with intrinsic structural 2D chirality.*** *Direct transmission T_{++}, T_{--} and circular polarization conversion T_{-+}, T_{+-} spectra for normal incidence onto (a) an achiral array of asymmetrically split rings ($\alpha = 0°$) and (b) an array of asymmetrically split rings which has intrinsic structural 2D chirality ($\alpha = 22.5°$). Insets show the metamaterial pattern as seen by the incident wave.*

$T_{++} - T_{--}$. Non-zero circular polarization conversion indicates the presence of linear birefringence / dichroism for all split ring arrays. Fig. 3.14 (a) shows that for an achiral array of split rings the intensities of circular polarization conversion are identical and independent of the propagation direction, indicating the complete absence of circular conversion dichroism. When, however, the split rings are rotated by an angle α to form a structurally 2D-chiral array, normal incidence transmission through the metamaterial shows a resonant region around 6 GHz where the right-to-left and left-to-right conversion efficiencies are different from each other, $T_{-+} \neq T_{+-}$, as illustrated by Fig. 3.14 (b) for $\alpha = 22.5°$. Furthermore, the conversion efficiencies are simply interchanged for opposite directions of propagation, $\overrightarrow{T}_{ij} = \overleftarrow{T}_{ji}$, and thus for example RCP waves incident on front and back of the metamaterial will experience different levels of circular polarization conversion, $\overrightarrow{T}_{-+} \neq \overleftarrow{T}_{-+}$. Given that the direct transmission terms are independent of the propagation direction, the total transmission

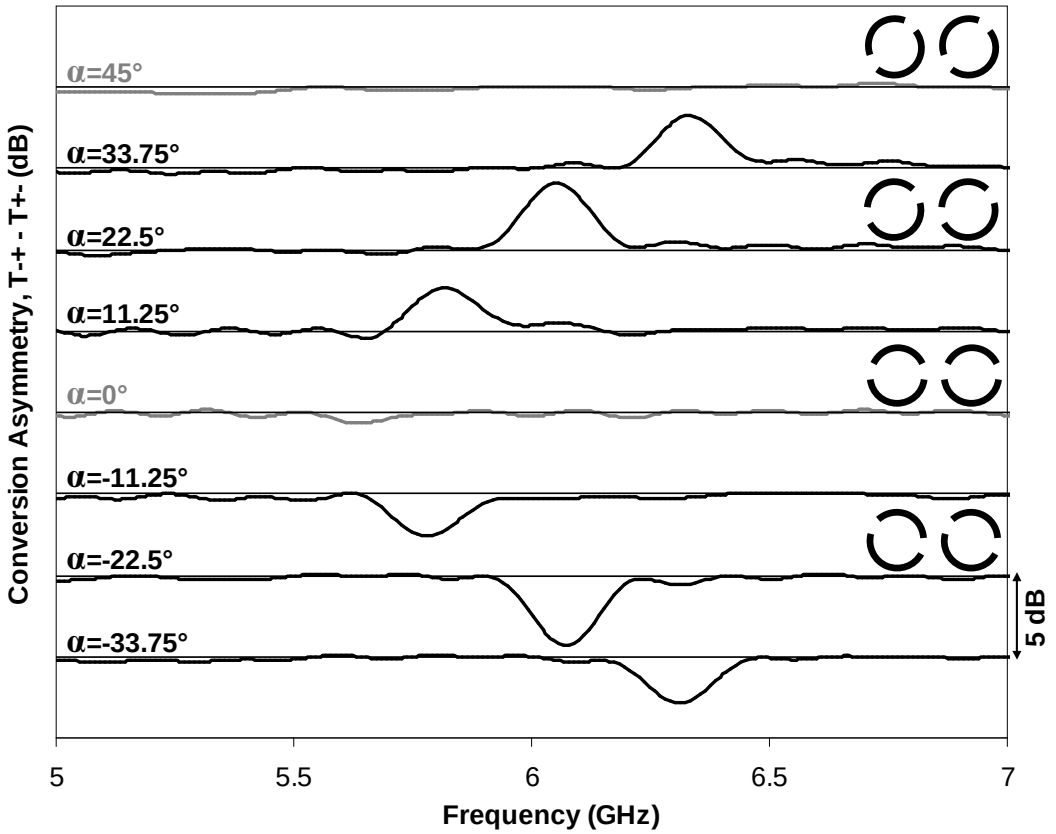

Figure 3.15: ***Circular conversion dichroism as a function of intrinsic structural chirality.*** *The conversion asymmetry, $T_{-+} - T_{+-}$, is shown for normal incidence onto arrays of asymmetrically split rings as a function of the split's orientation α. The respective zero level is indicated by a horizontal line. Insets show the metamaterial pattern as seen by the incident wave.*

(i.e. transmission measured with a polarization insensitive detector), $T_+ = T_{++} + T_{-+}$, is different for identical circularly polarized waves incident on front and back of the metamaterial array.

Fig. 3.15 illustrates the dependence of circular conversion dichroism on the orientation of the meta-molecules. When the split rings are rotated by a multiple of 45°, structural 2D chirality of the array is absent and circular conversion dichroism cannot be detected. The other orientations of the split rings studied here lead to a 0.2 GHz wide band of circular conversion dichroism observed between 5.5 and 6.5 GHz, whose exact spectral position and magnitude are controlled by the split's orientation α. The largest asymmetry was observed for $\alpha = \pm 22.5° = \pm\pi/8$ rad, where the difference in circular polarization conversion, $T_{-+} - T_{+-}$, is about 4 dB. As should be expected, mirror-forms $\pm\alpha$ of the split ring array show circular conversion dichroism of opposite

sign.

Importantly, circular conversion dichroism due to structural planar chirality is a direct consequence of electromagnetic interactions between meta-molecules, as there can be no first-order contribution from individual achiral meta-molecules. The split ring array studied here represents the limiting case of strong inter-molecular coupling, while an example of weak inter-molecular coupling will be discussed in section 3.3.2. Regular arrays of asymmetrically split rings are known to exhibit a strong resonant response of collective nature established through strong interactions between split rings [130]. When excited by a circularly polarized wave this interaction appears to be resonantly perturbed by the 2D-chiral arrangement of the array in a way that depends on the incident wave's handedness and propagation direction. Such polarization sensitive excitation previously observed in planar chiral meta-molecules has been called enantiomerically sensitive current mode (or plasmon) [97] and has been linked to circular conversion dichroism, see sections 2.8.4 and 3.2.1. The sensitivity of this enantiomerically sensitive resonance to changes in the inter-molecular coupling conditions is particularly evident in the substantial frequency-shift of the resonance with changing orientation α of the split, as presented in Fig. 3.15.

In summary, the experiments presented here confirm the existence of circular conversion dichroism due to intrinsic structural chirality in arrays of achiral meta-molecules.

3.3 Extrinsic 2D Chirality

Usually, chirality is considered an intrinsic property of a material's geometry. However, as introduced in chapter 2, see Fig. 2.8, chirality can also be imposed extrinsically by the experimental arrangement. Here we focus on extrinsic 2D chirality. Starting from normal incidence, extrinsic 2D chirality results from tilting any periodically structured interface around any axis that is neither parallel nor perpendicular to a line of (glide) mirror symmetry. In this case the structure combined with the direction introduced by the tilt axis (or plane of incidence)[5] is 2D-chiral, i.e. they cannot be superimposed with their mirror image without being lifted out of their plane. Like intrinsic 2D chirality, also extrinsic 2D chirality can apply to the individual meta-molecules [see Fig. 3.16 (b)]

[5]Tilt axis and plane of incidence are perpendicular to each other and it does not matter which one of these directions is chosen.

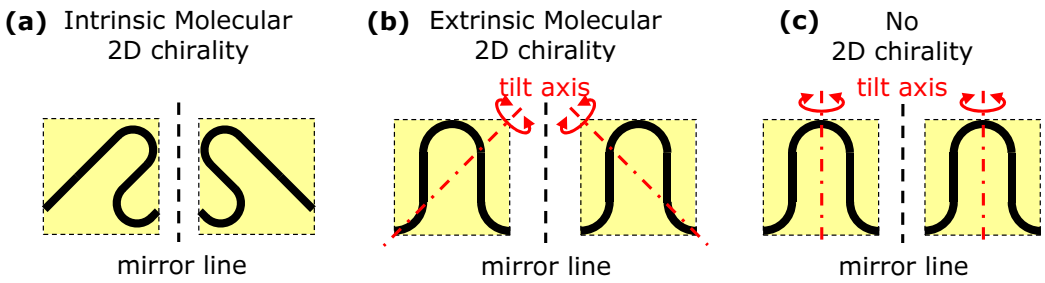

Figure 3.16: ***Intrinsic and extrinsic molecular 2D chirality****: (a) Intrinsically 2D-chiral meta-molecules cannot be superimposed with their mirror image without being lifted off the plane. (b) An intrinsically achiral planar meta-molecule forms an extrinsically 2D-chiral experimental arrangement with the incident wave if it is tilted around an axis that is neither parallel or perpendicular to a line of (glide) mirror symmetry. In this case the meta-molecule combined with the tilt axis is 2D-chiral. (c) If, however, the tilt axis is parallel (or perpendicular) to a molecular axis of (glide) mirror symmetry extrinsic 2D chirality vanishes.*

or to the structure of the metamaterial array as a whole [see Fig. 3.21 (b)]. These cases of molecular and structural extrinsic 2D chirality are investigated experimentally in sections 3.3.1 and 3.3.2, respectively.

3.3.1 Molecular Extrinsic 2D Chirality

The experimental work presented here showed for the first time that circular conversion dichroism can occur in structures that are not intrinsically 2D-chiral. It is demonstrated that extrinsic molecular 2D chirality leads to circular conversion dichroism in a non-chiral lossy planar metamaterial. Most of the following results have also been published in [99].

As illustrated by Fig. 3.16, any planar meta-molecule, that is not perfectly rotationally symmetric, can become extrinsically 2D-chiral at oblique incidence. Starting from normal incidence, molecular extrinsic 2D-chirality is achieved by tilting the meta-molecule around any axis that is neither parallel or perpendicular to a line of (glide) mirror symmetry. In the resulting experimental arrangement, the meta-molecule combined with the direction introduced by the tilt axis (or plane of incidence) is 2D-chiral. Configurations of opposite handedness correspond to rotation around tilt axes that are mirror images of each other, see Fig. 3.16 (b).

Circular conversion dichroism was observed in a planar metamaterial structure based on a continuous anisotropic fish-scale pattern, which has a line of mirror symmetry and therefore does not posses intrinsic 2D chirality. It was previously studied

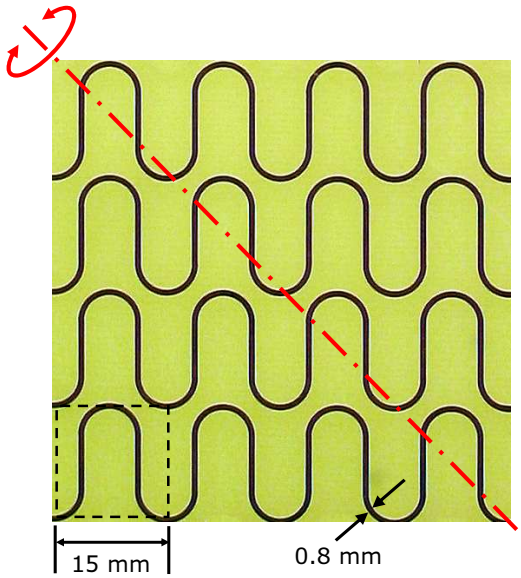

Figure 3.17: ***Metamaterial sample showing circular conversion dichroism due to extrinsic 2D chirality****: "fish-scale" array of wires belonging to wallpaper symmetry group pmg. A meta-molecule is indicated by a dashed box.*

for its resonant properties at normal incidence[6] [53]. The pattern, which is shown in Fig. 3.17, is formed by a double-periodic array of meandering 0.8 mm wide metal strips sandwiched between two 1.6 mm thick lossy dielectric substrates (dielectric constant $\varepsilon = 4.5 - i0.2$). The metamaterial sample has a lateral dimension of about 220×220 mm^2 and a unit cell 15×15 mm^2 in size, which renders the periodic structure non-diffracting below 13 GHz for any angle of incidence of up to 30°. The transmission characteristics of the structure were studied at normal and oblique incidence using the experimental and data processing techniques described in appendix A.1. In all experiments presented here, the metamaterial's in-plane orientation was $\tilde{\varphi} = -45°$, as defined in Fig. 2.2. Thus, when looking along the incident beam, the metamaterial's line of mirror symmetry was rotated by 45° counter-clockwise relative to the plane of incidence.

Fig. 3.18 presents measurements of the direct transmission levels T_{++}, T_{--} and circular polarization conversion levels T_{-+}, T_{+-} of the planar metamaterial in terms of power. The structure's direct transmission levels are identical for circularly polarized waves of either handedness, $T_{++} = T_{--}$, indicating the complete absence of 3D-chiral circular dichroism. This observation is supported by section 2.4.1, where we found

[6]The metamaterial was designed by Sergey Prosvirnin from the National Academy of Sciences of Ukraine for this earlier project [53].

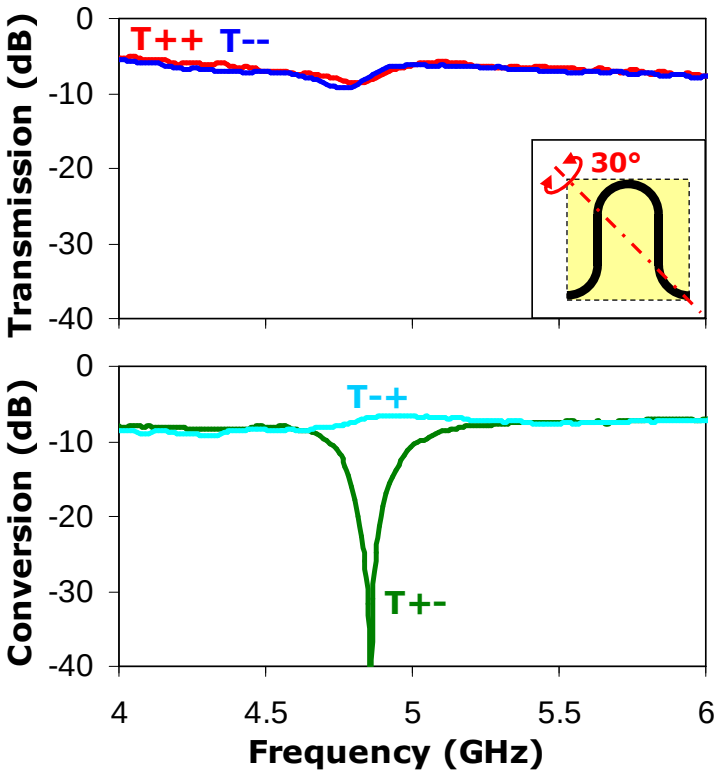

Figure 3.18: ***Transmission and circular polarization conversion spectra of the extrinsically 2D-chiral metamaterial*** *($\theta = 30°$), showing presence of 2D-chiral circular conversion dichroism and absence of 3D-chiral optical activity.*

that 3D-chiral optical activity cannot occur for any planar metamaterial with 2-fold rotational symmetry, see Fig. 3.17. On the other hand, clear evidence of resonant circular conversion dichroism is seen, $T_{+-} \neq T_{-+}$. Exactly like the intrinsically 2D-chiral structures discussed in the previous sections, the extrinsically 2D-chiral metamaterial shows directionally asymmetric total transmission of circularly polarized waves.

Extrinsic 2D chirality is illustrated further by Fig. 3.19 which shows the total transmission asymmetry measured for different angles of incidence θ. As should be expected no chiral polarization response is seen at normal incidence, when extrinsic 2D chirality vanishes. Circular conversion dichroism gradually increases with increasing tilt angle: for $\theta = 10°$ the total transmission difference (which peaks at around 4.8 GHz) is 7%, reaching 15% and 21% for respectively $\theta = 20°$ and $\theta = 30°$. Here opposite angles of tilt/incidence result in the same sign of the asymmetry, while a reversal was observed for opposite in-plane orientations $\pm\tilde{\varphi}$ of the metamaterial as derived in section 2.4.2. In this particular case these enantiomeric configurations correspond to mutually or-

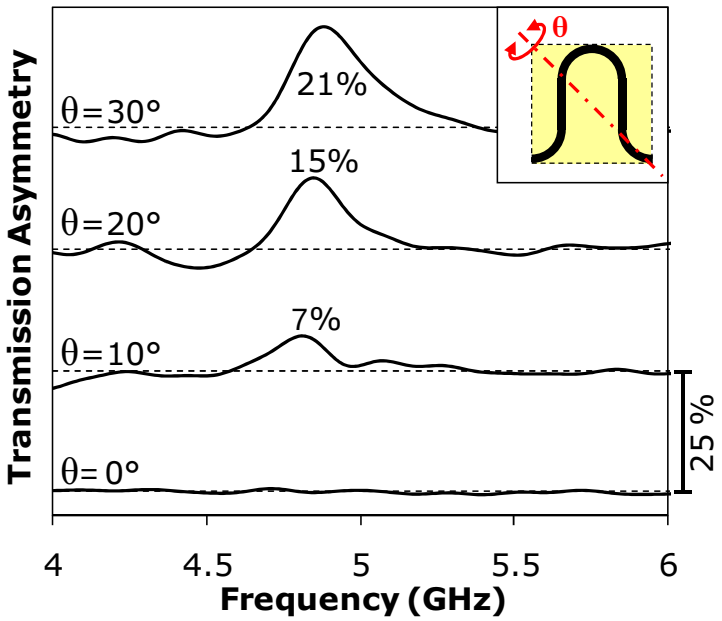

Figure 3.19: ***Circular conversion dichroism as a function of extrinsic 2D chirality.*** *The directional transmission asymmetry depends on the angle of incidence θ and vanishes at normal incidence. The respective zero level is indicated by a dashed line.*

thogonal planes of incidence, as illustrated by Fig. 3.16 (b). It should be noted that a transmission asymmetry of 21% of the incident power is remarkably large. It corresponds to more than $\frac{4}{5}$ of the theoretical limit derived in section 2.6.2 and implies that the metamaterial must show an absorption asymmetry of 42% for opposite directions of incidence of the same circularly polarized wave.

While the formal definition of extrinsic 2D chirality is given at the beginning of this section, more intuitive understanding of its meaning can be derived from Fig. 3.20, which shows the meta-molecule as it is perceived by the incident wave. More technically, it shows the meta-molecule's projection onto to the plane normal to the direction of incidence. If extrinsic (without intrinsic)[7] 2D chirality is present, then this projection will become 2D-chiral. In our case, it is interesting to note that the projection of the extrinsically 2D-chiral meta-molecule resembles the structure in which circular conversion dichroism was first discovered [64], see Fig. 2.9.

In summary, this work has demonstrated that extrinsic 2D chirality leads to circular

[7] If an intrinsically 2D-chiral structure corresponds to the projection of a tilted non-chiral pattern, then tilting it by the same angle around the perpendicular axis will result in a *non-chiral projection*, which is a smaller version of the original non-chiral pattern. Nevertheless intrinsic and extrinsic 2D chirality are simultaneously present in this case. Consider tilting the distorted pattern of Fig. 3.20 (b) around the perpendicular axis.

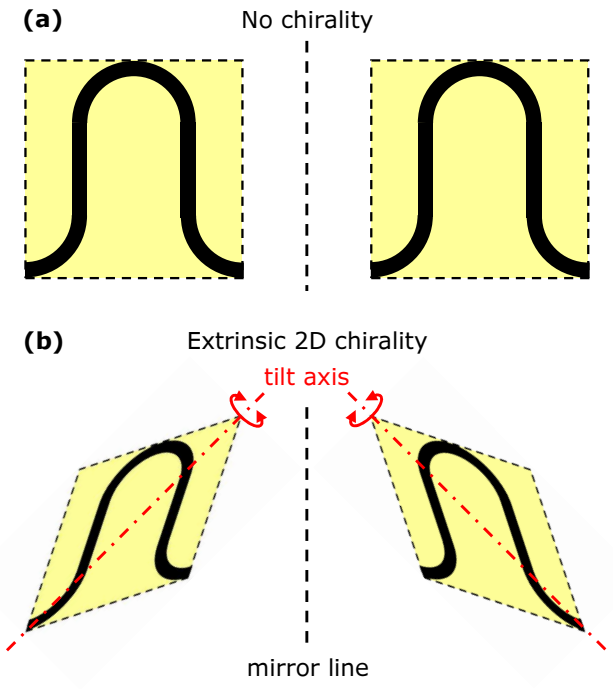

Figure 3.20: ***Intuitive interpretation of extrinsic 2D chirality.*** *Non-chiral structure seen by an observer looking along the direction of light propagation at normal (a) and oblique (b) incidence. If the non-chiral structure is tilted around an axis neither parallel nor perpendicular to a line of (glide) mirror symmetry, the pattern's projection onto the plane normal to the incident wave's propagation direction becomes 2D-chiral with two enantiomeric forms.*

conversion dichroism at oblique incidence on lossy non-chiral structures. It has been shown that circular conversion dichroism achieved in this way is inherently tunable via the angle of incidence and that the effect can be exceptionally large. Here the large circular conversion dichroism can be attributed to extrinsic molecular 2D chirality, even though a contribution from extrinsic structural 2D chirality cannot be excluded[8], see next section.

3.3.2 Structural Extrinsic 2D Chirality

Not only molecular 2D chirality, but also structural 2D chirality can arise extrinsically from the mutual orientation of metamaterial and incident wave. Here it will be shown that extrinsic structural 2D chirality should lead to **circular conversion dichroism at any lossy periodically structured interface**. The experimental results suggest,

[8]Similarly, intrinsic molecular 2D chirality is always accompanied by intrinsic structural 2D chirality, as the meta-molecules do not have a line of (glide) mirror symmetry that could coincide with a mirror line of the array's lattice.

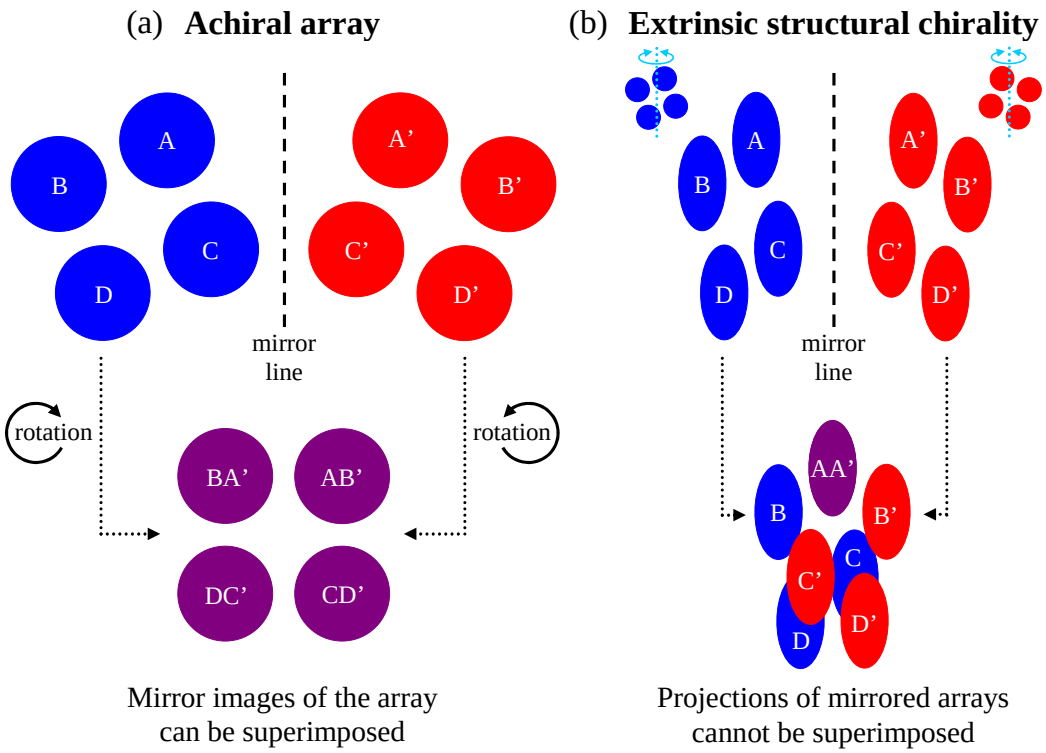

Figure 3.21: ***Extrinsic structural 2D chirality.*** *(a) A regular array of highly symmetric meta-molecules (blue) is congruent with its mirror image (red) and therefore does not have intrinsic chirality. (b) However, when it is tilted around an axis that does not coincide with a mirror line of the array's lattice, its projection onto the plane normal to the observation direction becomes structurally 2D-chiral.*

that circular conversion dichroism may be a common phenomenon, rather than a curiosity of planar chiral metamaterials. Most of the following findings have also been reported in [115].

As illustrated by Fig. 3.21, extrinsic structural 2D chirality arises for any periodically structured interface if starting from normal incidence it is tilted around any axis that does not coincide with a mirror line of the array's lattice[9]. It is apparent from Fig. 3.21 (b), that a 2D-chiral distortion of the array's lattice[10] will be seen by an observer looking along the direction of incidence in this case. Remarkably, extrinsic structural 2D chirality does not depend on the internal geometry of the meta-molecules, therefore even a regular array of particles with the highest symmetry, i.e. disks or spheres, can become extrinsically 2D-chiral at oblique incidence. This implies that

[9] As periodic lattices of points (marking meta-molecule positions) always have perpendicular mirror lines, this is equivalent to saying that the *plane of incidence* should not coincide with a mirror line of the array's lattice.

[10] The perceived 2D-chiral lattice distortion only applies if the lattice of meta-molecule positions is not intrinsically 2D-chiral, i.e. it must have a line of (glide) mirror symmetry.

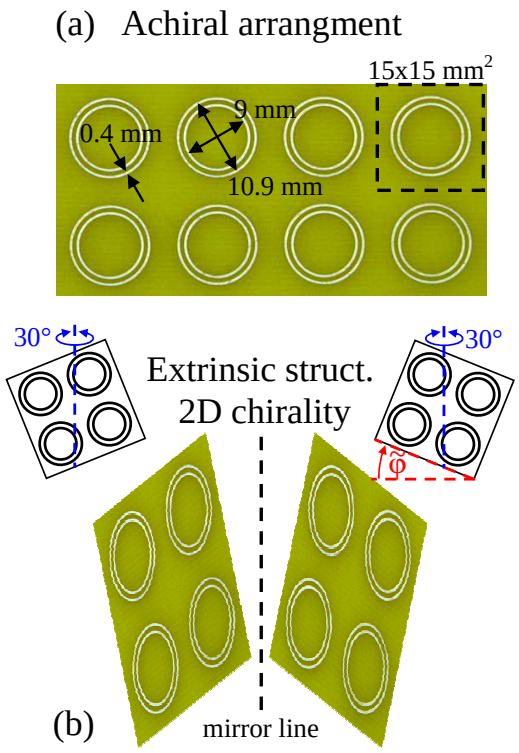

Figure 3.22: ***Metamaterial orientations without and with extrinsic structural 2D chirality.*** *(a) Achiral orientation of the double ring array belonging to wallpaper symmetry group p4m. (b) At oblique incidence, even a regular array of rings can become extrinsically 2D-chiral: For orientations $\tilde{\varphi} \neq n \cdot 45°$, $n \in \mathbb{Z}$ the projection of the double ring array onto the plane normal to the direction of incidence is 2D-chiral.*

various 2D-chiral phenomena may be expected at any planar regular array containing identical particles of any symmetry.

Here extrinsic structural chirality is investigated for the double ring array[11] shown in Fig. 3.22. The metamaterial structure consists of a square array of about 200 meta-molecules, which are 15×15 mm^2 in size rendering the metamaterial non-diffracting below 13 GHz for angles of incidence of up to 30°. The pattern was etched from a 35 μm thick copper layer covering a 1.6 mm thick lossy FR4 printed circuit board (Im $\varepsilon \sim 0.1$) using standard photolithography. The transmission properties of the metamaterial were measured using the experimental and data processing methods described in appendix A.1. The double ring array was characterized at $\theta = 30°$ oblique incidence for different orientations $\tilde{\varphi}$ of the array relative to the plane of incidence. For $\tilde{\varphi} \neq n \cdot 45°$ ($n \in \mathbb{Z}$) the projection of the entire pattern onto the plane normal to the propagation direction

[11] The metamaterial was designed by Sergey Prosvirnin from the National Academy of Sciences of Ukraine for its isotropic resonant response, which is insensitive to positional disorder of the meta-molecules [130] and mimics electromagnetically induced transparency [131].

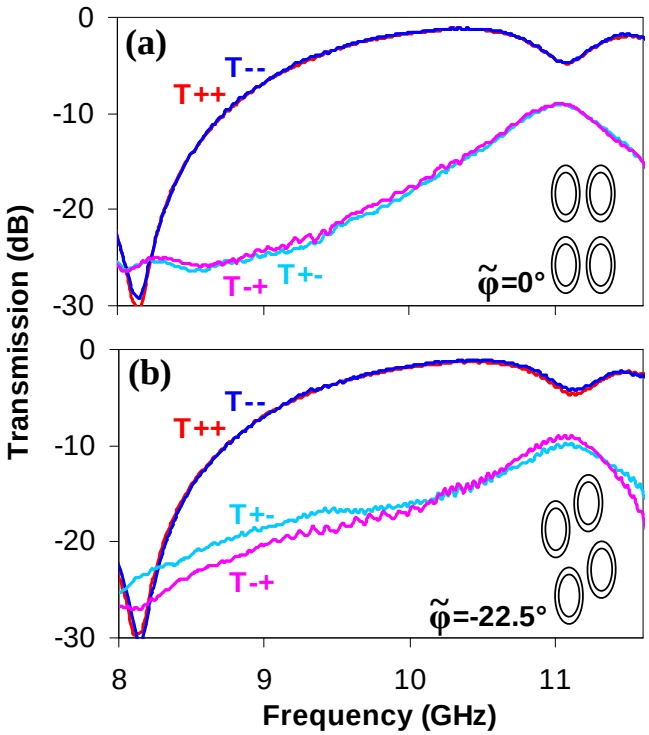

Figure 3.23: ***Transmission spectra for metamaterial orientations without and with extrinsic structural 2D chirality.*** *Direct transmission T_{++}, T_{--} and circular polarization conversion T_{-+}, T_{+-} are shown for $\theta = 30°$ oblique incidence onto the double ring array. (a) Orientation without 2D chirality ($\tilde{\varphi} = 0°$). (b) Orientation with extrinsic structural 2D chirality ($\tilde{\varphi} = -22.5°$). The insets show the metamaterial pattern projected onto the plane normal to the incident beam.*

becomes 2D-chiral. Orientations $\pm\tilde{\varphi}$ correspond to extrinsically 2D-chiral arrangements of opposite handedness, while an in-plane rotation of the metamaterial by 90° results in an identical experimental configuration.

Fig. 3.23 presents typical spectra of the direct transmission intensities T_{++}, T_{--} and the circular polarization conversion levels T_{-+}, T_{+-} for achiral and chiral orientations of the double ring metamaterial. In all studied cases, the direct transmission intensities (as well as field transmission coefficients t_{++} and t_{--}) did not depend on handedness or propagation direction of incident circularly polarized waves. In particular this shows that in our case any 3D chirality introduced by presence of the substrate [80] is too small to lead to significant circular birefringence $\arg(t_{++}) - \arg(t_{--})$ or circular dichroism $T_{++} - T_{--}$. The presence of circular polarization conversion indicates a linearly birefringent / dichroic metamaterial response in all cases. As the metamaterial pattern itself is isotropic, the this must be due to the preferred directions introduced by oblique inci-

dence, as discussed in section 2.4.3. Here this is particularly evident in the anisotropic distortion of the metamaterial pattern's projection onto the plane perpendicular to the direction of incidence. As illustrated by Fig. 3.23 (a), when extrinsic structural 2D chirality is absent, the circular polarization conversion efficiencies are identical and independent of the propagation direction, indicating the complete absence of circular conversion dichroism. When, however, the double ring array is rotated in its plane by an angle $\tilde{\varphi}$, so that for oblique incidence its projection onto the plane normal to the wave propagation direction becomes 2D-chiral, a broad band of asymmetric circular polarization conversion appears [as shown in Fig. 3.23 (b) for $\theta = 30°$ and $\tilde{\varphi} = -22.5°$]. Furthermore, the experimental data indicate that the conversion efficiencies are simply interchanged for opposite directions of propagation, $\overrightarrow{T}_{ij} = \overleftarrow{T}_{ji}$ and thus, for example, RCP waves incident on front and back of the metamaterial experience different levels of circular polarization conversion, $\overrightarrow{T}_{-+} \neq \overleftarrow{T}_{-+}$. As the direct transmission terms are independent of the propagation direction, the total transmission $T_+ = T_{++} + T_{-+}$ is different for opposite propagation directions of the same circularly polarized wave.

Fig. 3.24 illustrates the dependance of circular conversion dichroism on the metamaterial's in-plane orientation. The double ring array is extrinsically 2D-chiral at oblique incidence for in-plane orientations $\tilde{\varphi}$ excluding multiples of 45° and exhibits relatively wide bands of circular conversion dichroism. As derived in section 2.4.2 the sign of the effect is reversed for orientations $\pm\tilde{\varphi}$, which correspond to enantiomeric forms of the array's projection.

Thus, the measurements presented here confirm the existence of circular conversion dichroism due to extrinsic structural 2D chirality in arrays of meta-molecules of the highest symmetry. While asymmetric transmission was initially only known for normal incidence onto lossy arrays of anisotropic and intrinsically 2D-chiral meta-molecules [64, 90, 96], we are now able to identify a much larger class of structures exhibiting the effect: **circular conversion dichroism can occur for any lossy array of particles, when its projection onto the plane normal to the direction of incidence is 2D-chiral and anisotropic**[12]. At oblique incidence any regular array of even perfectly symmetric particles can become planar chiral and anisotropic in projection, while at

[12] Additionally circular conversion dichroism can also occur in those special cases, where intrinsic 2D chirality and/or anisotropy vanishes in projection.

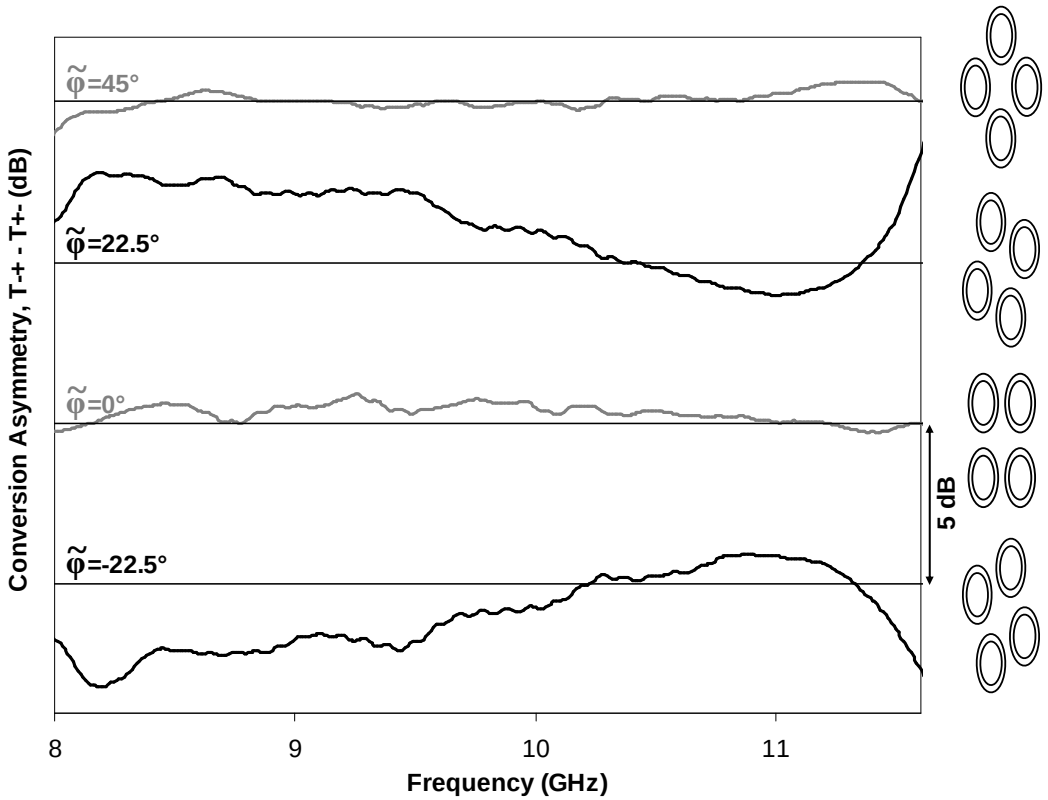

Figure 3.24: ***Circular conversion dichroism as a function of extrinsic structural 2D chirality.*** *The conversion asymmetry, $T_{-+} - T_{+-}$, is shown for $\theta = 30°$ oblique incidence onto the double ring metamaterial as a function of its in-plane orientation $\tilde{\varphi}$. The respective zero level is indicated by a horizontal line. Insets show the metamaterial pattern as seen by an observer looking along the incident beam.*

normal incidence - when the structure and its projection coincide - planar chirality and anisotropy must be properties of the array itself.

However, the findings of this study have much more far-reaching implications: The observation of a signature 2D-chiral phenomenon (circular conversion dichroism) implies that also other effects connected to 2D chirality should be observable in arrays of simple achiral building blocks. For example 2D-chiral patterns show polarization rotation in diffracted beams [93, 94]. The results presented here imply that this 2D-chiral diffraction effect may be possible at any regularly patterned interface. Furthermore, circular birefringence [80, 132, 133] and circular dichroism [81] have been observed at non-diffracting planar chiral patterns on dielectric substrates making 3D-chiral objects. Similarly patterns with extrinsic 2D chirality will become extrinsically 3D-chiral (see chapter 4) if they are placed on a substrate or at the interface between two different media. Therefore we may expect that even a simple square array of spherical particles

on a substrate could exhibit circular birefringence and circular dichroism at oblique incidence. Finally, as extrinsic 2D chirality can arise from interaction of any directed quantity with a regular pattern, chiral effects could even be envisaged for, e.g., a beam of chiral molecules interacting with a regularly structured achiral surface.

Importantly, circular conversion dichroism due to structural planar chirality is a direct consequence of electromagnetic interactions between meta-molecules, as there can be no first-order contribution from individual achiral meta-molecules. An example of strong inter-molecular coupling is studied in section 3.2.2. The double ring array discussed here is an example of a metamaterial system with weak inter-molecular coupling [130]. The source of structural 2D chirality in this case has a non-resonant, broadband nature leading to a relatively small asymmetry in circular polarization conversion [see Fig. 3.23 (b)].

In summary, it has been experimentally demonstrated that circular conversion dichroism can occur at oblique incidence onto any lossy periodically structured plane. These results greatly expand the range of natural and artificial materials in which circular conversion dichroism may be expected, making it a mainstream electromagnetic effect rather than a curiosity of planar chiral metamaterials. Indeed, while only few natural examples of intrinsically 2D-chiral interfaces are known, regular arrays of simple particles are much more common and much easier to manufacture. This indicates that directional asymmetries in transmission, reflection and absorption of circularly polarized waves should be observable in natural and self-assembled structures. Prime candidates for circular conversion dichroism at oblique incidence are planar metamaterial structures, square arrays of plasmonic spheres or semiconductor quantum dots and lossy double-periodic gratings, which have the same symmetry, as the double ring array studied here.

3.4 Summary

In this chapter, it has been demonstrated that not only **intrinsically 2D-chiral meta-molecules**, but also 2D chirality associated with various arrangements of non-chiral objects can lead to circular conversion dichroism, i.e. directionally asymmetric transmission, reflection and absorption of circularly polarized waves. Here three cases can

be distinguished:

- **Intrinsic structural 2D chirality** is present in periodic arrays, when the meta-molecules do not have any line of (glide) mirror symmetry that coincides with a mirror line of the array's lattice.
- Starting from normal incidence, **extrinsic molecular 2D chirality** results from tilting a meta-molecule around an axis that is neither parallel nor perpendicular to a molecular line of (glide) mirror symmetry.
- Beginning with normal incidence, **extrinsic structural 2D chirality** is introduced by tilting a periodic array of particles around any axis that does not coincide with a mirror line of the array's lattice.

Apart from 2D chirality, circular conversion dichroism also requires the presence of absorption losses and anisotropy. At normal incidence anisotropy must be an intrinsic property of the material, while at oblique incidence preferred directions are imposed by the experimental arrangement. Importantly, extrinsic structural 2D chirality and a linearly birefringent / dichroic material response can result from oblique incidence onto any periodic pattern and therefore circular conversion dichroism is possible at any lossy periodically structured interface. Because of its dependence on the mutual orientation of metamaterial and incident wave, circular conversion dichroism due to extrinsic 2D chirality is inherently tunable and vanishes at normal incidence.

Furthermore, it has been shown that large circular conversion dichroism is associated with the excitation of electric dipole and non-scattering currents for opposite propagation directions of the same circularly polarized wave. Directional transmission asymmetries of up to 21% have been achieved, which corresponds to more than $\frac{4}{5}$ of the theoretical limit and exceeds previous results by a factor of two. It has been shown for the first time experimentally that circular conversion dichroism is associated with enantiomerically sensitive and directionally asymmetric reflection and absorption of circularly polarized waves and the phenomenon has been demonstrated for the first time at terahertz frequencies.

Chapter 4

Optical Activity in Non-Chiral Planar Metamaterials

4.1 Introduction

Optical activity, which manifests itself as circular birefringence and circular dichroism (see Fig. 1.7), is a fundamental electromagnetic effect corresponding to different direct transmission (and/or reflection) properties for right-handed (RCP, +) and left-handed (LCP, -) circularly polarized waves. Its tremendous technological importance has been outlined in section 1.4.1. Circular birefringence is the ability to rotate the polarization state of electromagnetic waves. As derived in section 2.4.1, the average polarization rotation in transmission and reflection (scattering)[1] corresponds to a phase difference between the direct transmission (reflection) coefficients for RCP and LCP,

$$< \Delta\Phi^t > \;=\; -\tfrac{1}{2}\left[\arg(t_{++}) - \arg(t_{--})\right], \tag{4.1}$$

$$< \Delta\Phi^s > = - < \Delta\Phi^r > \;=\; -\tfrac{1}{2}\left[\arg(r_{-+}) - \arg(r_{+-})\right], \tag{4.2}$$

[1] Scattering rotation is measured looking into the incident beam, while reflection rotation is measured looking into the reflected beam, therefore $\Delta\Phi^s = -\Delta\Phi^r$.

while circular dichroism corresponds to different direct transmission (reflection/scattering) levels for RCP and LCP,

$$\Delta T = T_{++} - T_{--}, \tag{4.3}$$

$$\Delta S = \Delta R = R_{-+} - R_{+-}, \tag{4.4}$$

where $T_{ij} = |t_{ij}|^2$ and $R_{ij} = |r_{ij}|^2$. In contrast to 2D-chiral circular conversion dichroism, see chapter 3, optical activity is the same for opposite directions of wave propagation and the phenomenon is not connected to circular polarization conversion.

As detailed in section 1.4.1, optical activity has been linked to **intrinsically 3D-chiral[2] materials** through the pioneering works of François J. D. Arago [72], Louis Pasteur [73], and Jagadis C. Bose [14] over the course of the 19$^{\text{th}}$ century. Since then optical activity has been associated with structures of intrinsically 3D-chiral symmetry, like proteins, the crystal lattice of quartz and helices, see Figs. 4.1 (a) and 1.6 (a)-(c). Intrinsically 3D-chiral twist is only possible for structures of non-zero thickness, therefore any electromagnetic manifestations of intrinsic 3D chirality require interaction of wave and material over some distance. In natural media significant polarization rotation only accumulates over interaction lengths that are large compared to the wavelength, while we will see in chapter 5 that smaller (but non-zero) interaction lengths are sufficient in highly resonant intrinsically 3D-chiral metamaterial structures. Owing to the small interaction length[3] associated with reflection, reflection optical activity has been found to be tiny and of little practical importance. This is why circular birefringence and circular dichroism are usually considered transmission phenomena. Nevertheless, reflection polarization rotation [135,136] (cinnabar [137], GaAs [138], chiral liquids [134]) and reflection circular dichroism (solutions of camphorquinone [139] and proteins [140], chiral polyfluorene films [141]) have been detected for intrinsically 3D-chiral media.

In spite of optical activity being commonly associated with 3D-chiral structures, we found in chapter 2 that circular birefringence and circular dichroism should also occur at oblique incidence onto **planar structures**, which **cannot have intrinsic 3D chirality**. Following section 2.4.1, **planar metamaterials should show optical**

[2] Any object that cannot be superimposed with its mirror image is intrinsically 3D-chiral.

[3] The interaction length and magnitude of reflection optical activity can be enhanced through multiple reflection/scattering approaches [134].

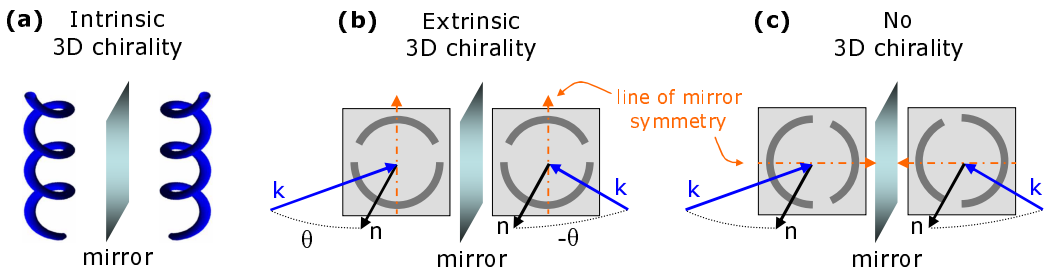

Figure 4.1: ***Intrinsic and extrinsic 3D chirality:*** *(a) Mirror forms of an intrinsically 3D-chiral object cannot be superimposed. (b) An extrinsically 3D-chiral experiment cannot be superimposed with its mirror image. In this example the structure has a mirror line perpendicular to the plane of incidence ($\tilde{\varphi} = 90°$) and therefore extrinsic 2D chirality is absent. The direction of incidence is indicated by the wave vector* $\mathbf{k}$*, which forms an angle* θ *with the surface normal* $\mathbf{n}$*. (c) If the structure has a line of (glide) mirror symmetry in the plane of incidence ($\tilde{\varphi} = 0°, 180°$), the experiment and its mirror image can be superimposed by rotation around* $\mathbf{n}$ *and therefore extrinsic 3D (and 2D) chirality is absent.*

activity in transmission and reflection, if **extrinsic 3D chirality** is associated with the mutual orientation of incident beam and metamaterial pattern. Extrinsic 3D chirality is present when the experiment (metamaterial and direction of incidence) is different from its mirror image and therefore 3D-chiral, see Fig. 4.1 (b). This is the case when the following conditions are met:

- oblique incidence,
- no 2-fold rotational symmetry[4],
- no (glide) mirror line in the plane of incidence.

In contrast to intrinsic 3D chirality, extrinsic 3D chirality is inherently tunable. Opposite angles of incidence should lead to circular birefringence and circular dichroism of opposite sign, while these chiral phenomena must be absent at normal incidence. The potential performance of tunable planar metamaterial polarization rotators and circular polarizers has been assessed in sections 2.7.4 and 2.7.5 respectively. It should be noted that extrinsic 3D chirality will be accompanied by extrinsic 2D chirality, unless the metamaterial has a line of (glide) mirror symmetry perpendicular to the plane of incidence. For lossy planar metamaterials, presence of extrinsic 2D chirality will lead to circular conversion dichroism, as shown in section 3.3.

In this chapter it will be demonstrated experimentally for planar metamaterials, that extrinsic 3D chirality leads to exceptionally large and tunable circular birefrin-

[4]Wallpaper symmetry groups without 2-fold rotational symmetry: $p1$, pm, pg, cm, $p3$, $p3m1$, $p31m$.

gence and circular dichroism in transmission [55,56,99] and reflection [142]. The results prove that structured planar interfaces are suitable as tunable ultra-thin polarization rotators and circular polarizers operating in transmission and reflection. Optical activity due to extrinsic 3D chirality is demonstrated both in the microwave and optical [56] parts of the spectrum, indicating that planar metamaterials have potential as polarization controllers in miniaturized photonic circuits. In contrast to artificial 3D-chiral structures, such planar devices are inherently tunable and can be easily mass-produced using existing planar technologies.

It should be noted that the possibility of optical activity due to extrinsic chirality has been known for a long time [111] and that the effect has been detected for transmission through liquid crystals about 40 years ago [112, 113]. However, it has only been recognized through the work presented here, that extrinsic 3D chirality can lead to large optical activity of practical importance.

4.2 Tunable Optical Activity at Microwave Frequencies

The results presented here demonstrated for the first time that extrinsic 3D chirality leads to transmission circular birefringence and circular dichroism in planar metamaterials. These phenomena are shown to be inherently tunable via the angle of incidence. Most of the following work has also been published in [55].

Following chapter 2, polarization rotation and circular dichroism should be expected for oblique incidence onto any planar metamaterial that does not have an axis of 2-fold rotational symmetry. For a first study of these 3D-chiral phenomena in planar structures - and for most practical applications - it is desirable to avoid the simultaneous presence of 2D-chiral circular conversion dichroism. The 2D-chiral effect can be excluded for special orientations of non-chiral planar patterns and it is prohibited in lossless planar metamaterials. One of the simplest meta-molecules, which has a line of mirror symmetry, but no axis of 2-fold rotation is the asymmetrically split ring resonator [57].

Here transmission optical activity is studied for a planar metamaterial consisting of a regular two-dimensional array of such metal split rings supported by 1.6 mm thick

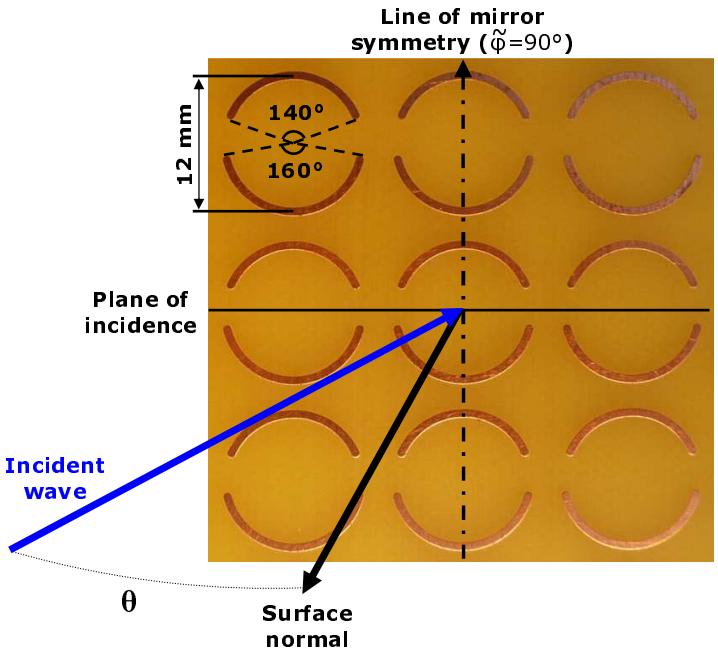

Figure 4.2: ***Planar metamaterial showing optical activity due to extrinsic 3D chirality.*** *The structure has a line of mirror symmetry, but no axis of 2-fold rotational symmetry and consists of asymmetrically split wire rings on a dielectric substrate (wallpaper symmetry group pm). In the experiments reported here, starting from normal incidence, extrinsic 3D chirality was introduced by tilting the metamaterial around its line of mirror symmetry. Thus the structure's line of symmetry is always normal to the plane of incidence ($\tilde{\varphi} = 90°$), ensuring absence of extrinsic 2D chirality.*

(lossy) dielectric substrate[5], see Fig. 4.2. The copper rings were split asymmetrically into pairs of arcs of different length separated by equal gaps. The planar metamaterial sample was approximately 220 × 220 mm^2 large and had a square unit cell of 15 × 15 mm^2, which ensured no diffraction at normal or oblique incidence up to 30° for frequencies below 13 GHz.

Using the method described in appendix A.1, transmission through the metamaterial was measured at various angles of incidence in the range from $\theta = -30°$ to $+30°$ achieved by tilting the sample around its symmetry axis. Thus in all experiments the metamaterial's line of mirror symmetry was normal to the plane of incidence (i.e. $\tilde{\varphi} = 90°$) and therefore extrinsic 2D chirality was not present. This is supported by the absence of circular conversion dichroism in the experimental data, which shows identical levels of circular polarization conversion for right-handed (RCP, +) and left-handed (LCP, -) circularly polarized waves, i.e. $T_{-+} = T_{+-}$, see Fig. 4.3. However, circu-

[5]The metamaterial was designed by Sergey Prosvirnin from the National Academy of Sciences of Ukraine for the study of narrow resonances associated with anti-symmetric trapped current modes [57].

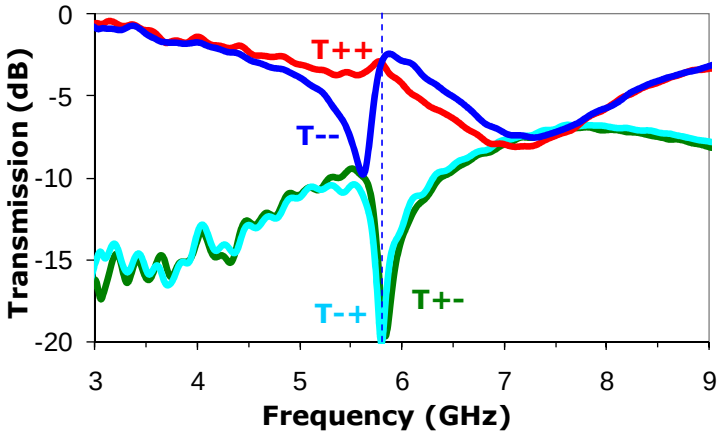

Figure 4.3: ***Extrinsically 3D-chiral transmission through a planar metamaterial.*** *Direct transmission T_{++}, T_{--} and circular polarization conversion levels T_{-+}, T_{+-} measured for an angle of incidence of $\theta = 30°$ and an in-plane metamaterial orientation of $\tilde{\varphi} = 90°$ (see Fig. 4.2). The blue dashed line marks a frequency of pure circular birefringence, here circular dichroism and linear birefringence / dichroism are virtually absent.*

lar polarization conversion was generally non-zero, indicating the expected presence linear birefringence / dichroism. Importantly, in extrinsically 3D-chiral experimental configurations, the metamaterial's direct transmission coefficients were generally not equal, $t_{++} \neq t_{--}$, revealing the presence of optical activity. It should be noted that polarization rotation $< \Delta\Phi^t >$ and circular dichroism ΔT cannot be explained by just linear birefringence / dichroism, as these phenomena do not contribute to either ΔT or $< \Delta\Phi^t >$, see (4.1) and (4.3). Particularly, while linear anisotropy causes a polarization state dependent modulation of azimuth rotation, it has no effect on the material's average polarization rotary power $< \Delta\Phi^t >$, see section 2.4.1. In all cases experiments performed in opposite directions of wave propagation yielded identical results.

Transmission spectra obtained for $\theta = +30°$ incidence are presented in Fig. 4.3. A resonant region showing circular dichroism, $T_{++} \neq T_{--}$, can be seen between 5 and 7 GHz. Due to linear anisotropy the metamaterial also shows weak polarization conversion $T_{+-} = T_{-+}$. At 5.8 GHz, however, linear birefringence / dichroism vanish, resulting in circular polarization eigenstates and, as circular dichroism is also absent, the material behaves like a pure circularly birefringent medium in the direction of wave propagation. As shown in Fig. 4.4, it rotates the polarization azimuth by about 20° without changing the polarization state's ellipticity, while transmission losses represented by T_{++} and T_{--} are less than 3 dB. Considering the metamaterial's thickness of only 1/32 of the wavelength, the rotary power of this non-optimized structure is

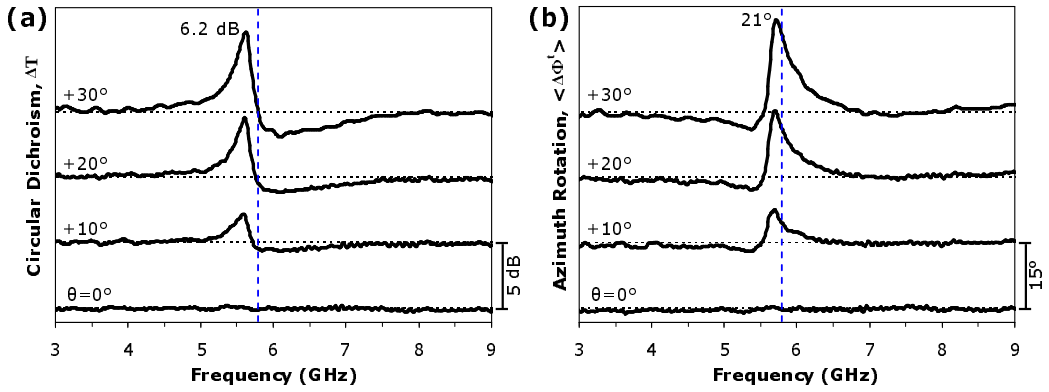

Figure 4.4: ***Tunable optical activity due to extrinsic 3D chirality.*** *(a) Transmission circular dichroism and (b) polarization rotation for angles of incidence from $\theta = 0°$ to $+30°$ ($\tilde{\varphi} = 90°$). Angles of incidence $-\theta$ result in reversed signs of these manifestations of optical activity. A frequency at which pure polarization rotation on a background of vanishing linear birefringence / dichroism can be seen is marked by a vertical dashed line. The respective zero level is indicated by a horizontal dashed line.*

remarkable. The non-chiral structure also shows substantial circular dichroism, which reaches more than 6 dB at 5.6 GHz.

Importantly, the strength (as well as sign) of the metamaterial's optically active response depends on the angle of incidence θ, as illustrated by Fig. 4.4. At normal incidence both circular dichroism and polarization azimuth rotation are absent. When the structure is tilted relative to the beam, as shown in Fig. 4.2, a continuous increase in the strength of its optically active response is observed. For example, at 5.6 GHz circular dichroism increases from 0 to 2.3, 4.6 and 6.2 dB, when the angle of incidence is increased from 0 to 30° in steps of 10°. Simultaneously, the polarization azimuth rotation - at 5.8 GHz - increases almost linearly from 0 to 7, 15 and 21°. The shape and position of the corresponding resonance appears to depend weakly on the tilt angle. Furthermore, it was observed that tilting the metamaterial in the opposite direction (i.e. $\theta < 0$) simply reverses the signs of rotation and circular dichroism.

Consistently with the predictions of section 2.4.1, the following key features of the optically active response of planar non-chiral metamaterials have been identified: (i) no effect can be observed at normal incidence, $\theta = 0$; (ii) the magnitude of polarization rotation and circular dichroism is controlled by the tilt angle (angle of incidence); (iii) equal tilt in opposite directions, $\pm\theta$, yields circular dichroism and polarization rotation of opposite signs. A microscopic model explaining these characteristics in terms of electric and magnetic dipole moments excited in the structure is presented in section

4.5.

In summary, it has been demonstrated that extrinsic 3D chirality leads to large and tunable circular birefringence and circular dichroism in planar metamaterials. Even though the effect occurs only for anisotropic patterns, a spectral band where linear birefringence and linear dichroism are practically absent has been observed. Like isotropic optically active media, the structure has counter-rotating circularly polarized eigenstates in this band, and as circular dichroism is also absent it acts as a polarization rotator. The simplicity of the planar structure allows it to be easily scaled to the optical part of the spectrum, making it a promising candidate for polarization control also at optical frequencies, see section 4.3.

4.3 Tunable Optical Activity in Optics

The work presented in this section is the result of a collaboration. The metamaterial was manufactured by Yifang Chen from Rutherford Appleton Laboratory and the experiments were conducted by Xing-Xiang Liu at University of Southampton. I planned the experiments and processed the data. Additionally I upgraded[6] the polarization capabilities of the microspectrophotometer used in the experiments to make this work possible.Most of the following results have also been published in [56].

Here it is demonstrated that optical activity due to extrinsic 3D chirality also occurs in the optical part of the spectrum. Circular birefringence and circular dichroism are observed for oblique incidence transmission through a planar photonic nanostructure[7], which essentially corresponds to a nanoscale version of the metamaterial studied in the previous section, see Fig. 4.5 (a). The photonic metamaterial consists of asymmetrically split aluminum nanorings manufactured by electron beam lithography on a glass substrate and has a size of $500 \times 500\ \mu\text{m}^2$. The period of the nanostructure is 500 nm, which ensures the absence of diffraction in the near infrared.

The structure's transmission properties for the incidence conditions indicated in Fig. 4.5 (a) were studied in the 800 - 2000 nm spectral range using a microspectropho-

[6] I designed and manufactured a holder for polarizing optics and a rotation mount for an analyzer. For the upgrade, I used the following optics: two linear polarizers (Thorlabs LPNIR100, 650-2000 nm), one superachromatic quarter wave plate (Bernhard Halle Nachfl. GmbH RSU 2.4.10, 600-2700 nm).

[7] This metamaterial was originally designed by Sergey Prosvirnin and Vyacheslav V. Khardikov from National Academy of Sciences of Ukraine for the study of narrow resonances associated with trapped current modes [57] in the near infrared.

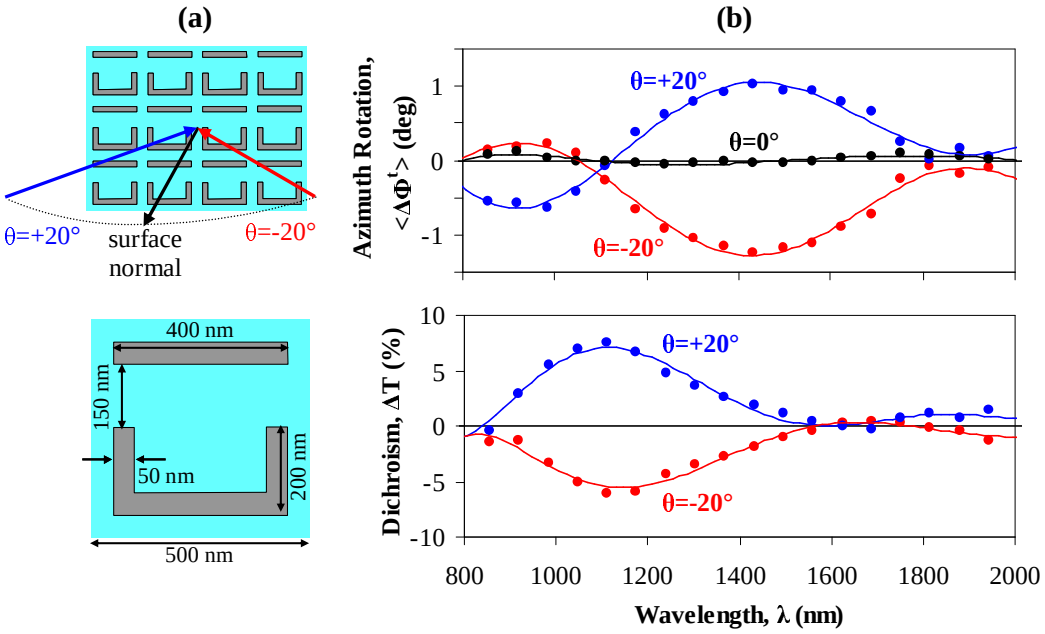

Figure 4.5: ***Circular birefringence and circular dichroism in a planar photonic nanostructure.*** *(a) The metamaterial belonging to wallpaper symmetry group pm consists of an array of 50 nm thick asymmetrically split aluminum nanorings which are supported by a 500 μm thick silica substrate. (b) Measurements of polarization rotation and circular dichroism in transmission for angles of incidence of* $\theta = \pm 20°$ *(*$\tilde{\varphi} = 90°$*).*

tometer with an incoherent light source. Transmission circular dichroism ΔT was measured as the total transmission difference for incident RCP and LCP averaged for opposite directions of propagation. However, it should be noted that within experimental accuracy the transmission difference for RCP and LCP did not depend on the propagation direction, indicating the expected absence of 2D-chiral circular conversion dichroism. Circularly polarized waves were created using a broadband linear polarizer and a superachromatic wave plate. The average polarization azimuth rotation $< \Delta\Phi^t >$ was measured using a broadband polarizer and a broadband analyzer, see footnote[8] for details. Importantly, the metamaterial's optically active properties cannot be explained by linear birefringence / dichroism, which does not contribute to ΔT and $< \Delta\Phi^t >$. In particular, linear anisotropy, which leads to a polarization state dependent modulation

[8]The *polarization azimuth* of the transmitted wave was measured by mapping the polarization ellipse with an analyzer in steps of 15° (24 analyzer positions), recording transmission spectra for each orientation. The *change in polarization azimuth* was determined by comparing such azimuth measurements on the metamaterial with reference measurements taken on the glass substrate. Finally, in order to isolate circular birefringence from linear birefringence / dichroism, the *change in polarization azimuth was averaged* for different incident linearly polarized waves in azimuthal steps of 15° (24 polarizations). Thus for each spectrum of average polarization rotation Xing-Xiang Liu recorded $24 \cdot 2 \cdot 24 = 1152$ transmission spectra. This help is gratefully acknowledged.

of azimuth rotation, has no effect on the material's average polarization rotary power $< \Delta\Phi^t >$, see section 2.4.1.

As illustrated by Fig. 4.5 (b), the photonic metamaterial shows no optical activity at normal incidence, $\theta = 0$. However, when it is tilted around its line of symmetry, bands of circular birefringence and circular dichroism appear, where enantiomeric experimental arrangements, $\theta = \pm 20°$, $\tilde{\varphi} = 90°$, lead to reversed signs of these manifestations of optical activity. Circular dichroism and circular birefringence were found to be absent in non-chiral control experiments, where the metamaterial's line of mirror symmetry was contained in the plane of incidence, $\theta = \pm 20°$, $\tilde{\varphi} = 0°$. These characteristics of the observed optical activity are in agreement with the predictions made in section 2.4.1 based on theoretical considerations and their microscopic origin is discussed in section 4.5.

On the absolute scale, the effects observed in the non-optimized planar metamaterial are comparable to more complex and thicker intrinsically 3D-chiral layered nanostructures, which have attracted attention for their strong optically active response. For example, the observed transmission circular dichroism of 7% is as large as for metamaterials based on pairs of aligned gold gammadions of different sizes [81]. The observed polarization rotation, which exceeds 1°, is about three times larger than that detected for photonic nanostructures based on mutually twisted metal patterns in parallel planes [50], see section 5.3. In contrast to these intrinsically 3D-chiral structures, the optical activity observed here is inherently tunable, as it arises from extrinsic 3D chirality.

It may be expected that extrinsic 3D chirality can lead to much larger circular birefringence and circular dichroism in optimized photonic planar metamaterials. For example, improvements may be anticipated for (i) an optimized split ring geometry, (ii) an array of slits instead of wires, see section 4.4, (iii) the use of a lower loss metal like gold instead of aluminum, and (iv) better overall quality of the nanostructure (i.e. periodicity, defects, surface roughness, ...). However, as all metals are lossy at optical frequencies, the theoretical performance limits for planar metamaterial polarization rotators and circular polarizers, discussed in sections 2.7.4 and 2.7.5, will not be achievable in the optical part of the spectrum. Nevertheless, planar metamaterials, being tunable and generally much easier to fabricate than intrinsically 3D-chiral

structures, could supersede the latter as ultra-thin circular polarizers and polarization rotators.

In summary strong circular birefringence and circular dichroism due to extrinsic 3D chirality has been demonstrated in a non-chiral planar photonic metamaterial.

4.4 Giant Optical Activity in Transmission and Reflection

Here transmission and reflection optical activity due to extrinsic 3D chirality is studied for a lossless planar metamaterial. The observed circular birefringence is exceptionally large, approaching the theoretical limits identified in section 2.7.4. Most of the following findings have also been reported in [99, 142].

As derived in sections 2.7.4 and 2.7.5, the magnitude of circular birefringence and circular dichroism in planar metamaterials can only approach the theoretical limits in lossless structures. Losses were certainly the main limiting factor for the optically active response of the photonic wire split ring metamaterial (section 4.3) and absorption in the lossy substrate may also have limited the circular birefringence and circular dichroism of the corresponding microwave metamaterial (section 4.2). Therefore it is desirable to study extrinsic 3D chirality for a lossless structure. As metals are essentially perfect conductors at microwave frequencies, a lossless microwave metamaterial can be realized by eliminating the dielectric substrate.

In case of the wire split ring arrays discussed in the previous sections, the substrate is required to hold the wire structures in place. However, the complementary structure, an array of split ring apertures, can be realized without a substrate. The metamaterial studied here[9] is such an array of asymmetric split ring apertures, which is essentially complementary to the wire structure discussed in section 4.2, apart from the substrate and minor differences regarding line width and metal thickness. As illustrated by Fig. 4.6, the apertures, which were cut into a 1 mm thick aluminum sheet, consist of two slits corresponding to 140° and 160° arcs respectively. These apertures are repeated every 15 mm, making the array non-diffracting at frequencies below 13 GHz for angles of incidence up to 30°. For simulations revealing the current modes that this aperture array can support, refer to appendix C.

[9] This metamaterial was designed by Nikitas Papasimakis for the study of narrow resonances associated with trapping energy on a planar metamaterial [57].

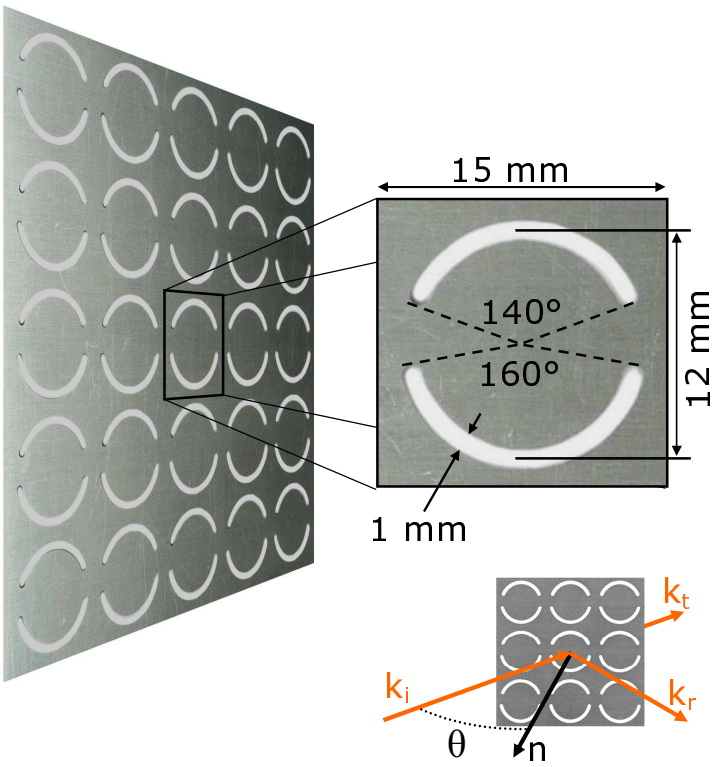

Figure 4.6: ***Lossless metamaterial exhibiting strong transmission and reflection optical activity at oblique incidence.*** *The structure belongs to wallpaper symmetry group pm and consists of a 1 mm thick aluminum sheet perforated with a regular array of asymmetrically split ring apertures.*

Transmission and reflection of the metamaterial were measured at various angles of incidence θ and in-plane metamaterial orientations $\tilde{\varphi}$ using the experimental and data processing techniques discussed in appendix A.1. Following section 2.4.1, extrinsic 3D chirality without extrinsic 2D chirality results when starting from normal incidence the structure is tilted around its line of mirror symmetry, so that this mirror line is normal to the plane of incidence ($\tilde{\varphi} = \pm 90°$). Chirality of either type is absent when the metamaterial's line of mirror symmetry coincides with the plane of incidence ($\tilde{\varphi} = 0, 180°$). For intermediate in-plane orientations of the structure, extrinsic chirality of either type is present, however, as the metamaterial is lossless the presence of 2D chirality should not lead to circular conversion dichroism, see section 2.4.2.

Typical transmission and reflection spectra for extrinsically 3D-chiral orientations of the metamaterial are shown in Fig. 4.7 for $\theta = +30°$, $\tilde{\varphi} = +90°$. The structure's fundamental resonance can be clearly seen between 9 and 10 GHz, where the wavelength corresponds to approximately twice the slit length. When extrinsic 3D chirality is

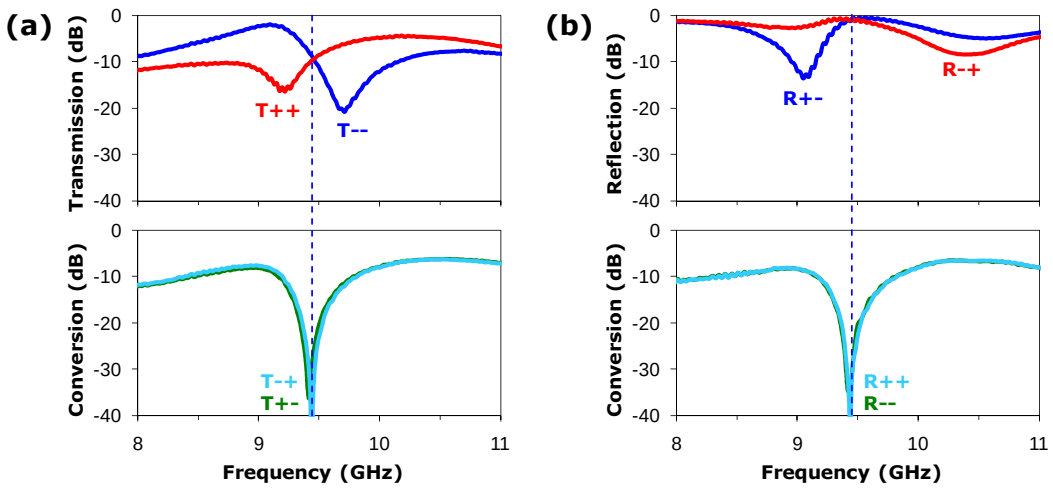

Figure 4.7: ***(a) Transmission and (b) reflection spectra of a lossless optically active planar metamaterial,*** *measured at $\theta = 30°$ incidence ($\tilde{\varphi} = 90°$). The vertical dashed line indicates a frequency where linear birefringence / dichroism vanish.*

present, the direct transmission levels $T_{++} \neq T_{--}$ as well as the direct reflection[10] levels $R_{-+} \neq R_{+-}$ are generally different from each other, indicating the presence of circular dichroism in transmission and reflection. On the other hand, the circular polarization conversion levels are identical and generally non-zero for both circular polarizations as well as for transmission and reflection $T_{-+} = T_{+-} = R_{++} = R_{--}$, indicating the presence of linear birefringence / dichroism and the absence of circular conversion dichroism associated with 2D chirality (see chapter 3). As predicted for lossless structures, circular conversion dichroism was also absent for extrinsically 2D-chiral experimental configurations. Remarkably, there is a narrow frequency band around 9.4 GHz where linear birefringence / dichroism vanish and the metamaterial behaves like an ideal 3D-chiral medium.

Fig. 4.8 illustrates how the metamaterial's circular dichroism and circular birefringence depend on the angle of incidence θ for a fixed metamaterial orientation of $\tilde{\varphi} = 90°$. To avoid confusion, here the average scattering rotation $< \Delta\Phi^{s} >= - < \Delta\Phi^{r} >$, rather than the average reflection rotation is presented. This defines polarization rotation for both transmission and reflection (scattering) as they would be measured by an observer looking into the incident beam, where counter-clockwise rotation has a positive sign. At

[10] Incident and scattered fields are measured looking into the incident beam, while the reflected fields are measured in a different coordinate system looking into the reflected beam. Even though reflection is just scattering, this convention assigns the opposite handedness to scattered and reflected fields. Therefore the direct reflection and direct scattering levels are $R_{-+} = S_{++}$, $R_{+-} = S_{--}$.

normal incidence - when the experimental arrangement is not chiral - circular dichroism and circular birefringence are absent both in transmission and reflection. When the metamaterial is tilted around its symmetry axis, it becomes optically active at a small but non-zero angle of incidence. In transmission a narrow band of exceptionally large circular birefringence and circular dichroism appears, which weakens and broadens at larger angles of incidence. At $\theta = 10^\circ$ the transmitted wave is rotated by an impressive -81° (in absence of linear birefringence / dichroism and circular dichroism) and the contrast between direct transmission for RCP and LCP reaches 26 dB (at a different frequency). On the other hand, reflection optical activity is weak at small angles of incidence and becomes more pronounced as θ increases. For $\theta = 30^\circ$, the reflected polarization state rotates by up to 24° (17° in absence of linear birefringence / dichroism and circular dichroism) and reflection circular dichroism reaches 11 dB.

Large circular dichroism on a background of small linear birefringence / dichroism is achieved simultaneously in transmission and reflection between 9 and 9.4 GHz. For $\theta > 0$ direct transmission is high for left-handed circularly polarized radiation while direct reflection is high for incident right-handed waves, which become left-handed upon direct reflection. Thus a novel type of beam splitter or circular polarizer has been realized[11], which splits any incident wave into two left-handed circularly polarized beams. While $\theta > 0$ corresponds to a left-handed beam splitter, a right-handed beam splitter is simply achieved for the enantiomeric arrangement of incident beam and metamaterial, $\theta < 0$.

Importantly, the maximum of transmission rotation coincides with absence of both linear birefringence / dichroism and circular dichroism in transmission and reflection. In this narrow frequency band, the metamaterial acts as an ideal polarization rotator both for the transmitted and reflected beams. Notably, transmitted and reflected (scattered) waves are rotated in opposite directions and they have approximately orthogonal polarizations. For example for $\theta = +10^\circ$ the transmitted polarization is rotated by -81°, while the reflected polarization is rotated by $+7^\circ$. Thus a polarization rotating beam splitter (polarization rotator) has been realized, which splits any

[11] This is a proof of concept. Practical applications will require an optimized structure showing a larger contrast between the wanted direct transmission/reflection and the unwanted terms (circular polarization conversion and the unwanted direct transmission/reflection). Here this contrast is limited to 7 dB.

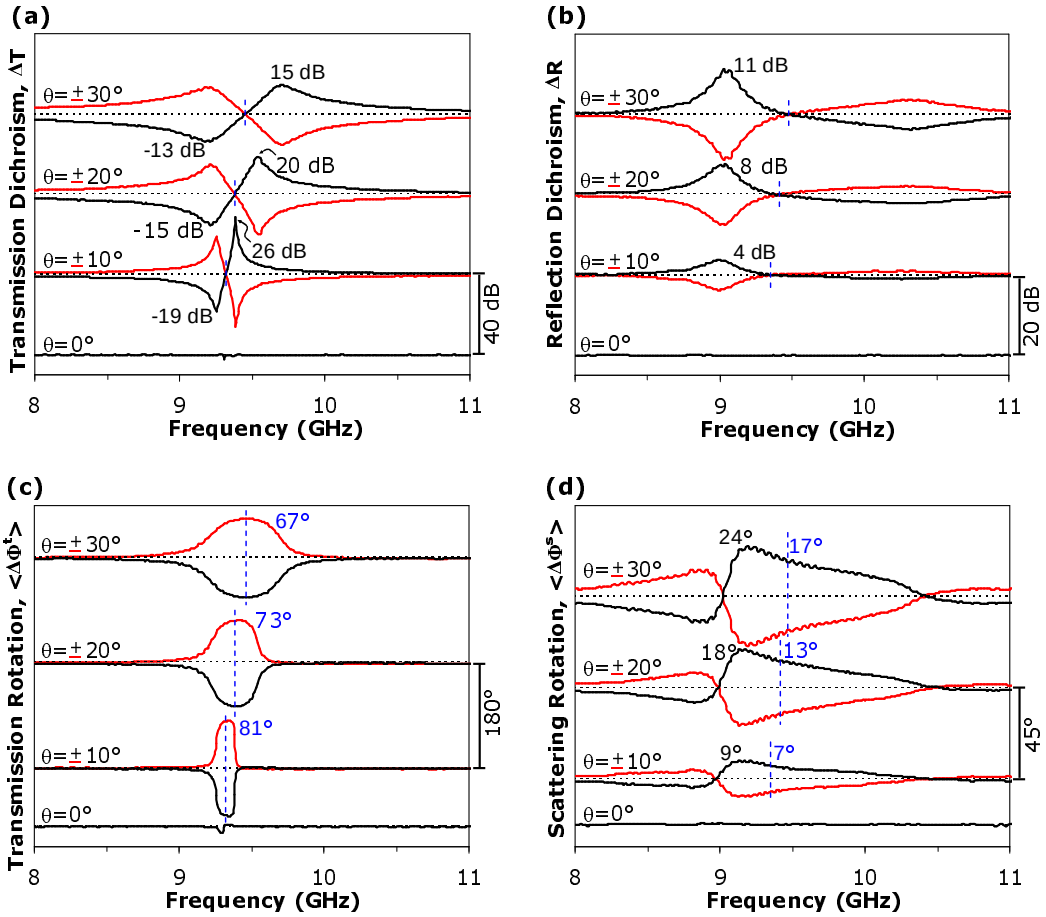

Figure 4.8: ***Transmission and reflection optical activity for a lossless planar metamaterial as a function of the angle of incidence*** θ. *The metamaterial's line of mirror symmetry is normal to the plane of incidence in all cases,* $\tilde{\varphi} = 90°$. *(a) Transmission circular dichroism, (b) reflection circular dichroism, (c) transmission polarization rotation and (d) scattering polarization rotation. Frequencies of zero circular dichroism and zero linear birefringence / dichroism are indicated by vertical dashed lines. The respective zero level is indicated by a horizontal dashed line.*

incident linearly polarized wave into two rotated orthogonally polarized beams. Both the polarization azimuth rotation and the relative power of these beams are controlled by the angle of incidence θ and the beam splitter's in-plane orientation $\tilde{\varphi}$. It should be noted that the metamaterial's performance as a polarization rotator is remarkably close to the theoretical limits derived for planar metamaterials in section 2.7.4. This is illustrated by Fig. 2.17 and details are given in the figure caption.

Fig. 4.9 illustrates the dependence of circular birefringence and circular dichroism on the metamaterial's in-plane orientation $\tilde{\varphi}$ for a fixed angle of incidence of $\theta = 30°$. For achiral configurations, $\tilde{\varphi} = 0, 180°$, when the metamaterial's line of mirror symmetry

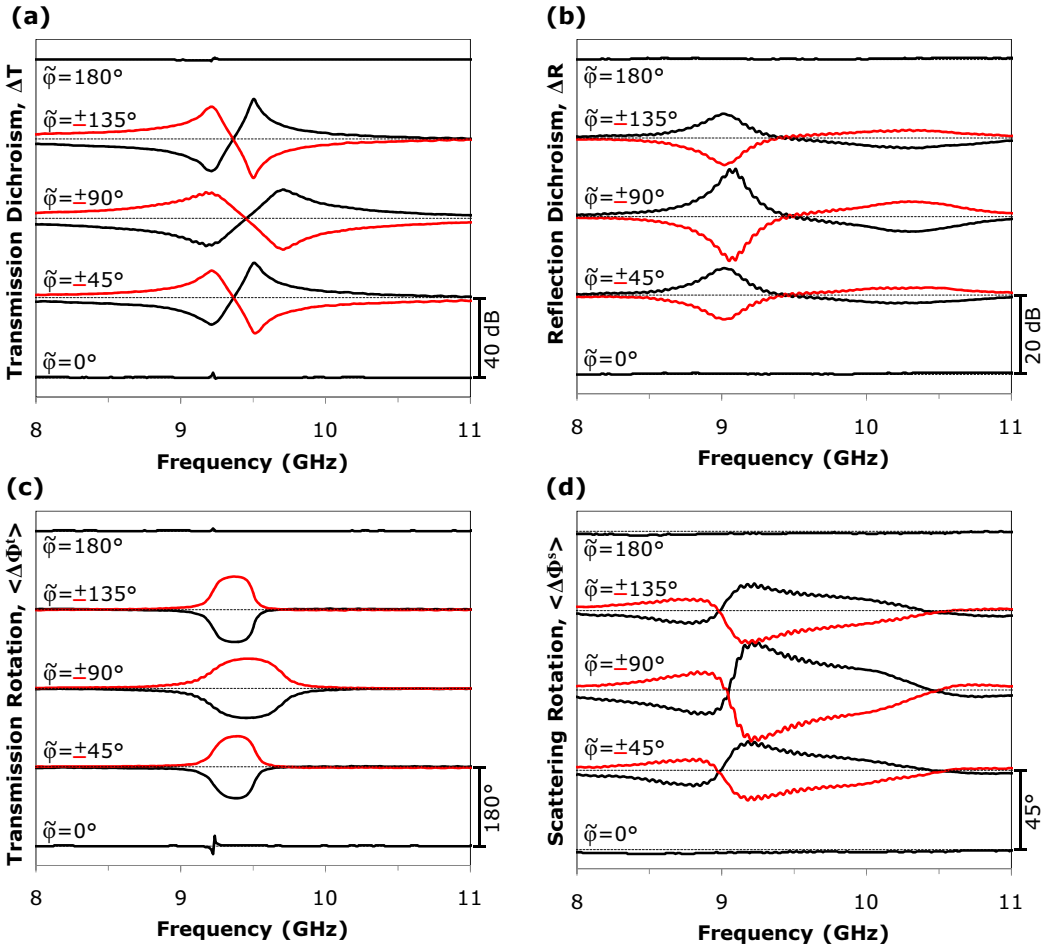

Figure 4.9: ***Transmission and reflection optical activity for a lossless planar metamaterial as a function of the metamaterial orientation*** $\tilde{\varphi}$. *The angle of incidence is* $\theta = 30°$ *in all cases. The respective zero level is indicated by a horizontal dashed line. (a) Transmission circular dichroism, (b) reflection circular dichroism, (c) transmission polarization rotation and (d) scattering polarization rotation.*

coincides with the plane of incidence, no optically active response can be observed. For any other in-plane orientation of the metamaterial, circular birefringence and circular dichroism are present both in transmission and reflection. As predicted in section 2.4.1 opposite orientations $\pm\tilde{\varphi}$ and $\tilde{\varphi}, \tilde{\varphi} + 180°$ as well as opposite angles of incidence $\pm\theta$ (see Fig. 4.8) result in optically active responses of opposite sign.

Following section 2.2.1 lossless Babinet complementary planar metamaterials should exhibit interchanged direct transmission and scattering properties for circularly polarized waves and their circular polarization conversion characteristics in transmission and reflection should be identical. Even though the split ring aperture array discussed here and the wire split ring array (which is supported by a lossy dielectric substrate) studied

in section 4.2 are not exactly Babinet complementary structures, this can be clearly seen. The extrinsically 3D-chiral aperture array's reflection spectrum [Fig. 4.7 (b)] strongly resembles the transmission spectrum measured for the same orientation of the wire array (Fig. 4.3). Similarly, reflection dichroism and transmission dichroism [compare Figs. 4.8 (b) and 4.4 (a)] as well as scattering rotation and transmission rotation [compare Figs. 4.8 (d) and 4.4 (b)] for aperture and wire arrays strongly resemble each other respectively, as predicted in section 2.4.1.

In summary, exceptionally large circular birefringence and circular dichroism have been demonstrated in transmission and reflection for a lossless planar metamaterial. The angular dependence of the phenomenon was shown to follow the predictions made in section 2.4.1 and its performance as a polarization rotator was found to be close to the limits identified in section 2.7.4. The effect can be exploited for the realization of various polarization transforming mirrors or beam splitters including circular polarizers of reversible handedness and tunable polarization rotators operating in transmission and/or reflection. In particular, novel types of beam splitters have been identified, which can split any incident beam into either two circularly polarized waves of the same handedness or two beams with rotated polarization states of orthogonal azimuth. Further potential applications include modulators and tilt/orientation sensors.

4.5 Dipole Model of Optical Activity in Planar Split Ring Arrays

I have developed the model presented in this section jointly with Vassili Fedotov and Nikolay Zheludev. Most of the arguments presented here have also been published in [55, 56, 99].

Consistently with the predictions of section 2.4.1, the following key features of the optically active response of planar non-chiral metamaterials have been identified in sections 4.2 - 4.4:

- No effect can be observed at normal incidence, $\theta = 0$, or when the plane of incidence contains the structure's line of mirror symmetry, $\tilde{\varphi} = 0, 180°$.
- The magnitude of polarization rotation and circular dichroism is controlled by

the angle of incidence θ and the metamaterial's in-plane orientation $\tilde{\varphi}$.

- Opposite angles of incidence $\pm\theta$ yield circular dichroism and polarization rotation of opposite sign.

As with conventional optical activity exhibited by 3D-chiral molecules, optical activity in planar metamaterials must result from the simultaneous presence of electric and magnetic responses of the structure. Here, it will be explained how this can happen for arrays of asymmetrically split wire rings, like those discussed in sections 4.2 and 4.3. It follows from section 2.2.1 that analogous arguments should apply to the Babinet complementary structure: an array of asymmetrically split ring apertures, see section 4.4. The above properties follow from the model presented below.

The asymmetry of the split rings plays a key role. For example, as illustrated in Fig. 4.10 (a), a wave polarized along the split induces unequal currents oscillating in the upper and lower arches of the ring. Such a current configuration may be represented as a sum of (b) symmetric and (c) antisymmetric[12] currents corresponding to an electric dipole **d** induced in the plane of the ring and a magnetic dipole **m** oscillating perpendicular to the plane, respectively. Here blue, green and red arrows represent the wave vector **k** and induced electric **d** and magnetic **m** dipoles of the metamaterial's unit cell, while dashed arrows show projections of the corresponding dipole moments onto the plane perpendicular to the wave vector.

For oblique incidence, $\theta \neq 0$, the metamaterial shows optical activity if the structure's line of symmetry does not coincide with the plane of incidence, $\tilde{\varphi} \neq 0, 180°$, while the maximum effect is observed when the split ring's mirror line is perpendicular to the plane of incidence, $\tilde{\varphi} = \pm 90°$ [see Figs. 4.10 (d) and (e)]. Indeed, in this case the wave vector **k**, **d** and **m** are co-planar, and similarly to how it happens in conventional 3D-chiral media, the electric and magnetic dipole components perpendicular to **k** create scattered electromagnetic waves with orthogonal polarization in the direction of wave propagation, so that the polarization of the transmitted (and reflected) wave rotates. The mutual phase difference between the electric and magnetic responses and thus the signs of circular birefringence and circular dichroism depend on the sign of the angle of incidence θ [compare projections of **d** and **m** in Figs. 4.10 (d) and (e)].

[12] The excitation such anti-symmetric currents / trapped modes / magnetic dipoles in asymmetrically split rings has been confirmed by [57].

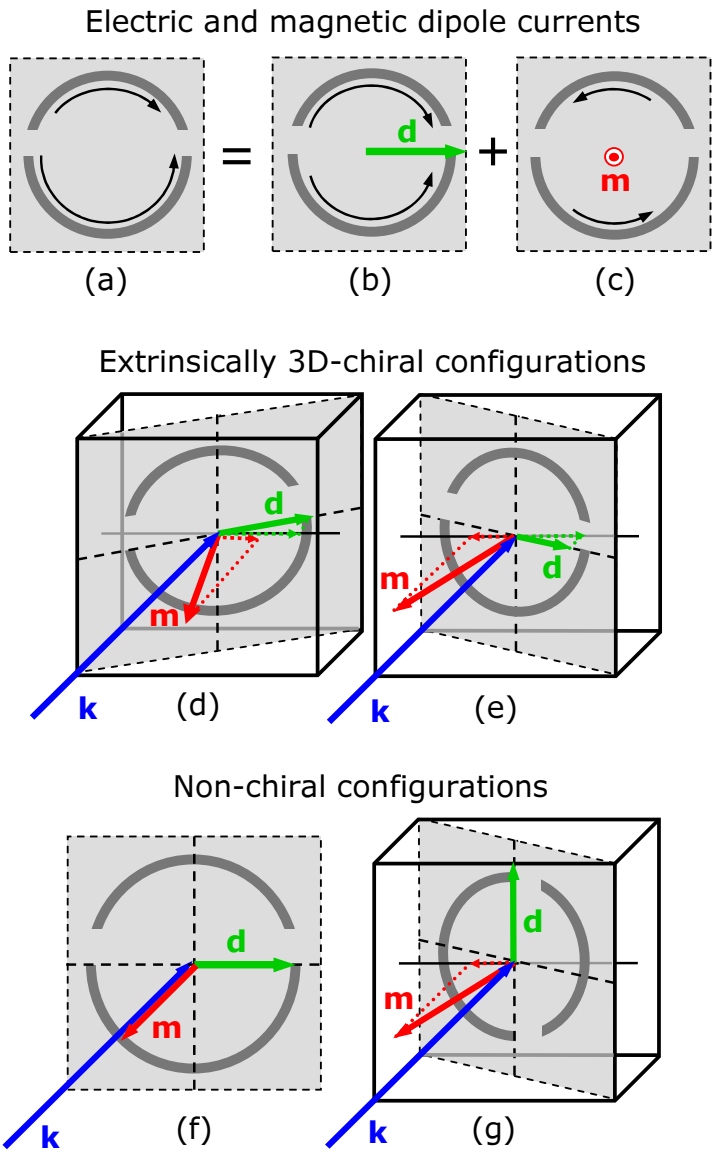

Figure 4.10: ***The mechanism of optical activity due to extrinsic 3D chirality*** *is linked to electric and magnetic responses of the metamaterial. (a) Oscillating currents in an asymmetrically split ring can be represented as a sum of (b) symmetric and (c) anti-symmetric currents, corresponding to an electric dipole* $\mathbf{d}$ *(green arrow) and a magnetic dipole* $\mathbf{m}$ *(red arrow). Optical activity is controlled by the projections of* $\mathbf{d}$ *and* $\mathbf{m}$ *onto the plane perpendicular to the incident wave vector* $\mathbf{k}$ *(green and red dashed arrows correspondingly): the strongest optical activity, of opposite sign, occurs if these projections are either (d) parallel or (e) anti-parallel; while the effect is absent either when (f) one of the projections is zero (normal incidence) or if (g) the projections are orthogonal.*

On the contrary, if the structure's line of mirror symmetry coincides with the plane of incidence, $\tilde{\varphi} = 0, 180°$, $\mathbf{d}$ and $\mathbf{m}$, as well as their projections, are orthogonal [see Fig. 4.10 (g)]. In this case the oscillating magnetic and electric dipoles emit electromagnetic waves of the same polarization and the structure does not show any optical

activity. At normal incidence, $\theta = 0$, optical activity cannot be observed as the projection of **m** on the plane normal to the **k**-vector is zero [see Fig. 4.10 (f)]. In these non-chiral cases the metamaterial response is limited to simple linear birefringence / dichroism along the preferred directions of the split ring.

In chapter 2, it has been derived from symmetry considerations that extrinsic 3D chirality and optical activity cannot occur for planar metamaterials with 2-fold rotational symmetry. The above model of optical activity offers an alternative explanation: For patterns with 2-fold rotational symmetry, local magnetic dipoles excited in different parts of the structure have opposite signs and will compensate each other. Therefore no net magnetic dipole moment that could contribute to optical activity can be excited in patterns with 2-fold rotational symmetry.

4.6 Summary

In this chapter, circular birefringence and circular dichroism have been observed for the first time in non-chiral metamaterials. In contrast to conventional optically active materials, the planar metamaterials studied here are not (and cannot be) intrinsically 3D-chiral. Nevertheless, exceptionally large optical activity has been observed both in transmission and reflection. This becomes possible through the presence of extrinsic 3D chirality, i.e. 3D chirality of the experimental arrangement consisting of the metamaterial and the direction of incidence. **Extrinsic 3D chirality** as a source of optical activity has several advantages over traditional intrinsic 3D chirality:

- It is **inherently tunable**, in particular circular birefringence and circular dichroism can be reversed (opposite angles of incidence) and switched off (normal incidence).
- It leads to **large optical activity at ultra-thin interfaces**[13].
- It causes **large reflection circular birefringence and circular dichroism**, while for intrinsically 3D-chiral structures these effects are usually tiny and of no practical importance.

[13] A single functional layer that is very thin compared to the wavelength is sufficient.

- It leads to large optical activity at **simple, easy-to-manufacture interfaces** compatible with established planar technologies like photo- and electron beam lithography as well as focussed ion beam milling.

In general, extrinsic 3D chirality should be expected to lead to optical activity for oblique incidence onto any structured interface without 2-fold rotational symmetry[14], provided that the interface has no line of (glide) mirror symmetry in the plane of incidence. In particular, it has been shown that extrinsic 3D chirality is a highly significant source of circular birefringence and circular dichroism in metamaterials. The metamaterials studied here are planar arrays of asymmetrically split rings, for which optical activity and its angular dependence have been explained microscopically through the excitation of electric and magnetic dipole modes and their simultaneous scattering contributions.

Large 3D-chiral polarization effects have been observed for planar metamaterials in the microwave and optical parts of the spectrum. The results indicate a wide range of potential polarization control and sensing applications from microwaves to optics, including modulators and tilt/orientation sensors as well as devices resembling standard optical components: Tunable polarization rotators and circular polarizers of reversible handedness operating in transmission and/or reflection have been demonstrated here. Even beam splitters that create two circularly polarized beams of the same handedness from any incident non-circular polarization state have been shown to be possible. Furthermore a tunable polarization rotating beam splitter can be realized which divides any incident wave into two beams with rotated polarization states of orthogonal azimuth.

[14] Wallpaper symmetry groups without 2-fold rotational symmetry: $p1$, pm, pg, cm, $p3$, $p3m1$, $p31m$.

Chapter 5

Optical Activity in 3D-Chiral Stereometamaterials

5.1 Introduction

Optical activity corresponds to different direct transmission (reflection) properties for right-handed (RCP, +) and left-handed (LCP, -) circularly polarized waves, which manifest themselves as circular birefringence and circular dichroism. As introduced in section 1.4.1, circular birefringence is the ability to rotate the polarization state of electromagnetic waves. The average polarization rotation[1] $< \Delta\Phi^t >$ for a wave transmitted by an optically active medium is given by the phase difference between its direct transmission coefficients for RCP and LCP,

$$< \Delta\Phi^t > \;=\; -\tfrac{1}{2}\left[\arg(t_{++}) - \arg(t_{--})\right]. \tag{5.1}$$

On the other hand, circular dichroism corresponds to different direct transmission (and reflection) levels for RCP and LCP,

$$\Delta T \;=\; T_{++} - T_{--}, \tag{5.2}$$

where $T_{ij} = |t_{ij}|^2$. Both manifestations of optical activity are identical for opposite directions of wave propagation as illustrated by Fig. 1.7.

[1] Polarization rotation averaged for all possible incident polarizations, see derivation in section 2.4.1.

As detailed in section 1.4.1, optical activity has been linked to intrinsically 3D-chiral materials through the pioneering works of François J. D. Arago [72], Louis Pasteur [73], and Jagadis C. Bose [14] during the 19$^{\text{th}}$ century. As discussed in chapter 4, it has since been shown that also extrinsic 3D chirality of the experimental arrangement is an important source of optical activity. Nevertheless, all current applications of optical activity are linked to intrinsic 3D chirality. Intrinsically 3D-chiral structures cannot be superimposed with their mirror image and include helices, sugar molecules and the crystal lattice of quartz, further examples are shown in Figs. 1.6 (a)-(c) and 1.8 (a)-(b).

In contrast to extrinsic 3D chirality, intrinsic 3D chirality is only possible for structures of non-zero thickness and any electromagnetic manifestations of intrinsic 3D chirality require interaction of wave and material over some distance. Therefore, circular birefringence and circular dichroism in intrinsically 3D chiral materials are propagation effects, accumulating along the direction of wave propagation and linked to different refractive indices $n_{\pm}$ for RCP and LCP.

$$n_{\pm} \quad = \quad \sqrt{\varepsilon\mu} \pm \kappa \tag{5.3}$$

Here ε and μ correspond to the relative permittivity and relative permeability respectively. The chirality parameter κ is a direct measure of the strength of the medium's 3D-chiral response, its real part is proportional to the structure's polarization rotary power while its imaginary part is proportional to transmission circular dichroism (when measured in dB).

Optical activity exhibited by natural materials like quartz is quite weak and limited to the optical spectral range. Consequently artificial optically active structures are of interest for polarization control applications in microwave and optoelectronic devices [87, 143, 144]. In particular, various artificial optically active media based on helices have been studied, including composites of metal helices [30, 74, 75], sculptured thin films consisting of helical pillars [76, 145] and helical photonic crystals [77, 78] and metamaterials [79]. Also metamaterials that derive intrinsic 3D chirality from stacking 2D-chiral patterns [81] or placing 2D-chiral patterns on a substrate have been investigated [80], see also section 1.4.1.

Since B. Bokut' et al. [82], J. Pendry [83] and S. Tretyakov et al. [84, 85] predicted

that sufficiently large circular birefringence would drive the refractive index negative for one circular polarization, artificial intrinsically 3D-chiral materials have attracted a lot of attention as potential candidates for achieving negative refraction [86,146–148]. With respect to the realization of negative refraction due to circular birefringence, however, little progress was made until very strong optical activity at microwave frequencies was reported for a single pair of mutually twisted metal patterns in parallel planes [71].

In this chapter, the first metamaterials based on mutually twisted planar metal patterns in parallel planes will be studied. In section 5.2, such a microwave metamaterial is shown to exhibit a negative index of refraction due to circular birefringence [51]. Additionally the structure shows giant polarization rotation and circular dichroism as well as negative electric and magnetic responses. In section 5.3 it will be demonstrated that mutually twisted metal patterns in parallel planes also lead to exceptionally large polarization rotation in the optical part of the spectrum [50].

It should be noted that a negative refractive index due to circular birefringence has also been demonstrated for a 3D-chiral terahertz metamaterial [52] and later for microwave metamaterials based on mutually twisted pairs of wire crosses [89] and split rings [149]. Furthermore, the study of mutually twisted metal patterns in parallel planes has expanded into the new field of stereometamaterials [150], which investigates how the properties of a metamaterial depend on the spacial arrangement of the "meta-atoms" forming its meta-molecules.

5.2 Giant Optical Activity and Negative Refraction at Microwave Frequencies

The work presented here is the result of a collaboration between Iowa State University and University of Southampton. Simulations and effective parameter retrieval were conducted by Jiangfeng Zhou, Jianfeng Dong and Thomas Koschny from Costas M. Soukoulis' group at Iowa State University in the US. I have designed the metamaterials and carried out the experiments. Furthermore, I have been involved in the interpretation of both experimental and numerical results. Most of the following work has also been published as [51].

Here it is demonstrated experimentally and numerically that metamaterials based

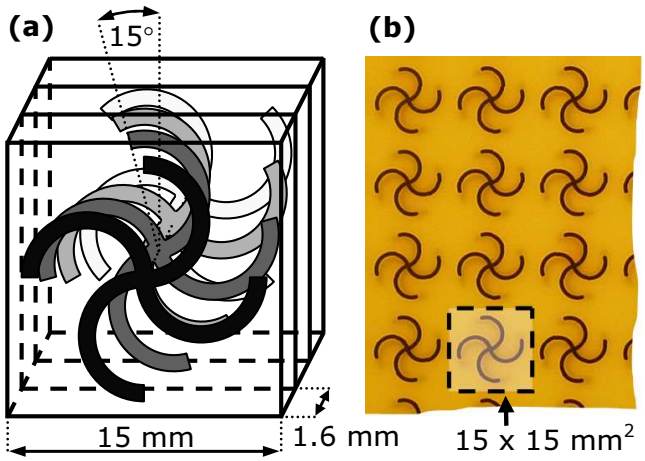

Figure 5.1: ***Intrinsically 3D-chiral layered metamaterial.*** *(a) Schematics of the 4-layered metamaterial's unit cell. The gammadions in neighboring layers have a relative twist of* 15°*. The structure of metamaterials with a different number of layers is analogous. (b) Photograph of part of a bilayered metamaterial sheet. The twisted gammadions of the* 2^{nd} *layer can be seen as a shaded area thanks to partial transparency of the substrate. A unit cell has been marked.*

on multiple layers of mutually twisted planar metal patterns in parallel planes (Fig. 5.1) support a wealth of useful electromagnetic properties including giant circular birefringence and circular dichroism, strong negative electric and magnetic responses and negative refraction. Also mirror-like reflectivity and invisibility have been observed.

The metamaterial is double-periodic with a square unit cell of 15×15 mm^2, which ensures that the structure does not diffract below 20 GHz. The overall size of the samples is approximately 220×220 mm^2. The metamaterial's unit cell contains stacked planar copper rosettes of 4-fold rotational symmetry in parallel planes, which are separated by thin (1.6 mm) dielectric layers. The rosettes themselves consist of four copper semicircles of radius 2.9 mm, line width 0.8 mm and thickness 35 μm. Here results are presented for four different forms of the metamaterial, corresponding to unit cells containing 1, 2, 3 and 4 coaxial rosettes. A mutual anti-clockwise twist[2] of 15° introduced between adjacent rosettes makes the unit cells containing more than one rosette intrinsically 3D-chiral. The metamaterial has been manufactured by lithography using standard FR4 circuit board substrates with a dielectric constant of $\varepsilon \approx 4.5 - 0.15i$. All transmission and reflection measurements were performed at normal incidence using the experimental and data processing techniques described in appendix A.1. The

[2] A mutual twist of 15° was chosen as it led to the largest optical activity for single meta-molecules consisting of two metal rosettes in parallel planes [71].

bilayered form of the metamaterial was also modeled with Comsol Multiphysics and CST Microwave Studio.

Due to the 4-fold rotationally symmetric design, circular polarization conversion is absent in all forms of the intrinsically 3D-chiral metamaterial and the structures have circularly polarized eigenstates. As shown in section 2.8.2 for isotropic (3-fold or higher rotational symmetry) planar metamaterials, the 2D-chiral nature of the rosettes does not (cannot) lead to any chiral polarization effect at normal incidence. Importantly, it is shown for a bilayered metamaterial consisting of pairs of mutually twisted rosettes, that its negative refractive index arises from the structure's 3D-chiral symmetry. In contrast to conventional negative index materials, like split ring wire media [35], fishnet structures [42] and double crosses [122], the negative index is not caused by simultaneous negative electric and magnetic responses. Two layers of mutually twisted metal rosettes show strong polarization rotary power and circular dichroism. For this case it is studied by modeling how the polarization state changes as the wave propagates through the metamaterial. Finally it is demonstrated that multi-layered versions of the metamaterial, consisting of four or more layers of rosettes, exhibit exceptionally strong transmission circular birefringence and circular dichroism combined with reduced insertion losses, making such structures practical thin polarization rotators or circular polarizers.

5.2.1 Giant Polarization Rotation and Circular Dichroism

Figs. 5.2 (a)-(b) show transmission properties of the bilayered form of the metamaterial. The structure shows exceptionally large optical activity in transmission. However, in contrast to the extrinsically 3D-chiral planar metamaterials discussed in chapter 4, reflection optical activity could not be detected in the intrinsically 3D-chiral metamaterials studied here, see Fig. 5.2 (c). This implies that the observed transmission optical activity is not an interface effect, but that it is linked to different refractive indices $n_{\pm}$ seen by RCP and LCP propagating through the metamaterial. In particular, the bilayered structure's huge transmission circular dichroism of up to 20 dB must be fully accounted for by different absorption losses for circularly polarized waves of opposite handedness. For linear polarization, azimuth rotation of up to 25° is achieved, however, in this case the transmitted polarization state becomes elliptical. Pure circular

birefringence, i.e. polarization azimuth rotation without any change of ellipticity, is achieved between resonances **A** and **B**, where the absolute rotation is about 7°. Even though larger pure circular birefringence can be achieved in extrinsically 3D-chiral planar metamaterials, see chapter 4, these values are substantial for an intrinsically 3D-chiral structure considering the material's thickness of only 1/30 wavelength λ at 6 GHz where the strongest effects occur. In terms of rotation per material thickness of one wavelength the structure's peak rotary power and pure circular birefringence are $780°/\lambda$ and $250°/\lambda$ respectively. This is gigantic compared to naturally circularly birefringent crystals like quartz ($0.02°/\lambda$ at 400 nm) in the visible part of the spectrum. The metamaterial also rotates several times stronger than helix-based artificial structures for microwaves ($156°/\lambda$ [75]). The metamaterial's exceptionally strong optical activity is confirmed by numerical results (faint lines, Fig. 5.2), which are in excellent agreement with the experiments (dark lines). The simulations also reveal the nature of the resonances **A**-**D**. The highly optically active resonances **A** and **B**, which will be discussed in detail in the following section, correspond to $\lambda/2$ current modes, while the weaker high frequency resonances **C** and **D** have $3\lambda/2$ current modes.

It is interesting to note that the structure also exhibits invisibility and mirror-like behavior. At resonance **B** the metamaterial does not transmit and it reflects electromagnetic waves like a metal mirror (amplitude and phase). On the other hand the structure is almost perfectly invisible around 8 GHz, here the transmitted wave is not affected by the presence of the metamaterial (amplitude and phase) and the structure does not reflect, see Fig. 5.2. Effective parameter retrieval, see next section, shows that the metamaterial's refractive index, relative permittivity and relative permeability are all approximately 1 (like air or vacuum) in its invisible frequency range.

5.2.2 Negative Refraction due to 3D Chirality

So far, negative refraction has been achieved in a variety of structures, from split ring wire media [35] to fishnet designs [42] and double crosses [122]. All of these structures were designed to superimpose electric and magnetic resonances, which separately drove the relative permittivity ε and relative permeability μ negative in the same frequency range. While these achiral negative index materials have attracted a lot of attention, chiral negative index media have not been studied experimentally prior to the work

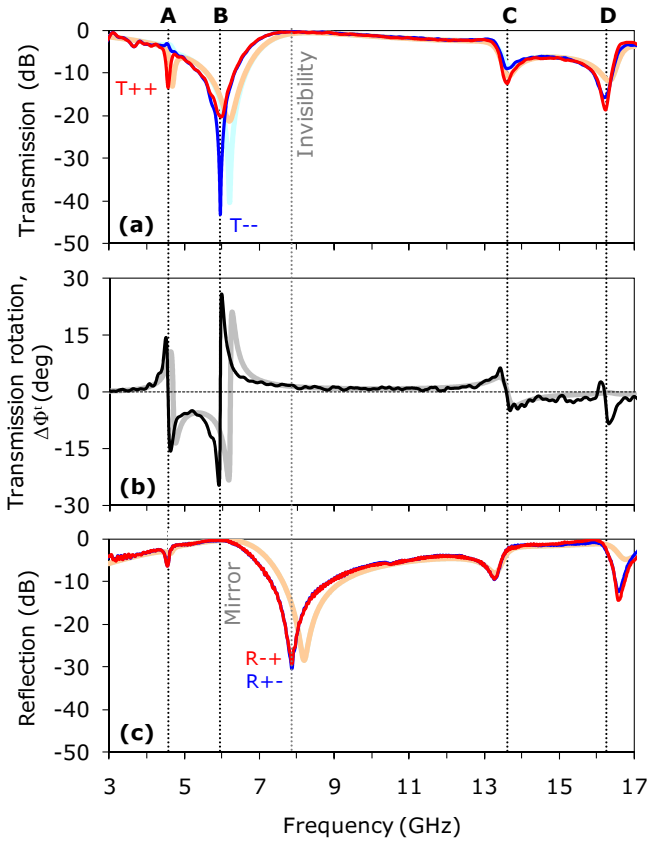

Figure 5.2: ***Optical activity of the bilayered metamaterial.*** *Measurements (dark lines) and numerical simulations (faint lines) are shown. (a) Direct transmission levels for right-handed (RCP, T_{++}, red) and left-handed (LCP, T_{--}, blue) circularly polarized waves. (b) Azimuth rotation in transmission for incident linearly polarized waves. (c) Direct reflection levels for RCP (R_{-+}, red) and LCP (R_{+-}, blue).*

presented here[3]. This is surprising, since Pendry and Tretyakov predicted that negative refraction could be easier to achieve in 3D-chiral media [83, 84]. Importantly, for 3D-chiral media the refractive index is $n_{\pm} = \sqrt{\varepsilon\mu} \pm \kappa$, where '+' and '-' refer to the right-handed (RCP) and left-handed (LCP) circularly polarized eigenstates and κ is the chirality parameter. This implies that in principle strong enough circular birefringence is sufficient to achieve negative refraction for one circular polarization. The difficulty here is, that if $\sqrt{\varepsilon\mu}$ is not very close to zero, then very strong circular birefringence is required indeed. The bilayered metamaterial shows exceptionally large optical activity and thus it is an ideal candidate for negative refraction due to 3D chirality.

Based on transmission and reflection the refractive index $n_{\pm}$, chirality parameter

[3]Further 3D-chiral negative index media have since been studied at terahertz [52] and microwave [89, 149] frequencies.

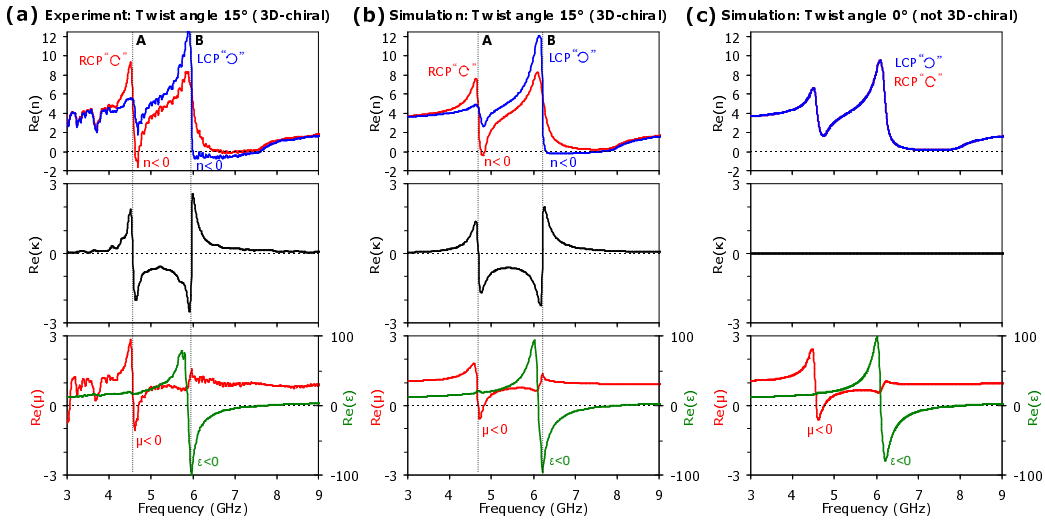

Figure 5.3: ***Effective medium parameters of the bilayered metamaterial.*** *Experimental (a) and numerical (b) results for refractive index n (top), chirality parameter κ (middle) and relative permeability μ and relative permittivity ε (bottom) are shown for the 3D-chiral bilayered metamaterial. (c) Effective parameters derived from numerical simulations for a bilayered metamaterial with no relative twist between layers of rosettes. Note that ε and μ are almost identical for both cases. Negative n in the 3D-chiral case arises from the contribution of the large chirality parameter κ and vanishes when 3D chirality is removed.*

κ, relative permeability μ and relative permittivity ε were calculated[4] for the bilayered 3D-chiral metamaterial and a reference structure in which 3D chirality was removed by reducing the relative twist between paired rosettes to zero. The results, which are shown in Fig. 5.3, reveal that both chiral and achiral forms of the metamaterial have remarkably similar electric and magnetic responses. Particularly in both cases

[4]Relative impedance $z = \sqrt{\mu/\varepsilon}$ and refractive indices $n_\pm$ were determined from the transmission and reflection data as explained in [151]. Using (5.3) it can be easily shown that the remaining parameters are given by $\kappa = (n_+ - n_-)/2$, $\mu = z(n_+ + n_-)/2$ and $\varepsilon = (n_+ + n_-)/2z$.

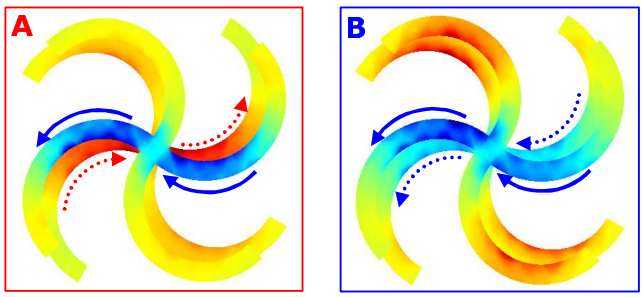

Figure 5.4: ***Current modes leading to a negative refractive index.*** *The anti-symmetric current mode (**A**) is excited by RCP at 4.7 GHz and the symmetric currentmode (**B**) is excited by LCP at 6.2 GHz. The horizontal component of the excited currents is shown, where blue and red correspond to currents in opposite directions.*

resonance **A** leads to negative permeability while resonance **B** corresponds to negative permittivity. The negative magnetic behavior for **A** results from anti-symmetric current oscillations in top and bottom rosettes, each pair of rosettes effectively forms a current loop, and thus a magnetic dipole (see Fig. 5.4 **A**). On the contrary the electric response for **B** results from in-phase current oscillations in pairs of rosettes, i.e. here pairs of rosettes act like a single electric dipole (see Fig. 5.4 **B**). The origin of the negative electric and magnetic responses of the bilayered structure is of the same nature as for fishnet structures [42] and double crosses [122].

In contrast to conventional negative index media, however, permeability and permittivity become negative in separate bands and $\sqrt{\varepsilon\mu}$ is always positive for both structures. Nevertheless the 3D-chiral metamaterial has a negative refractive index just above resonances **A** (for RCP) and **B** (for LCP). Remarkably it is the large contribution from the chirality parameter that drives the refractive index $n_{\pm} = \sqrt{\varepsilon\mu} \pm \kappa$ negative. This is further illustrated by the fact, that the negative index disappears if 3D chirality is removed from the structure.

Above resonance **A** a negative index is achieved due to the material's exceptionally large optical activity, while above resonance **B** a wide band of negative refraction can be achieved by moderate circular birefringence as $\mathrm{Re}\sqrt{\varepsilon\mu}$ is close to zero. The experimentally observed negative index reaches -1.7 with a figure of merit of $-\mathrm{Re}(n)/\mathrm{Im}(n) = 0.5$. The imaginary part of the negative index here is due to losses in the substrate and can be reduced substantially by using specialized microwave materials.

Also multi-layered forms of the metamaterial show clear signs of negative refraction. However, as these thicker structures cannot be assumed to be thin compared to the effective wavelength within the medium, effective parameter retrieval for multiple layers proves more difficult[5].

5.2.3 Polarization State Evolution within an Optically Active Metamaterial

As shown above, the bilayered intrinsically 3D-chiral metamaterial shows exceptionally large circular dichroism and polarization rotary power sufficient to lead to a negative

[5]The absolute phase delay of transmitted waves can only be measured up to multiples of 2π. This ambiguity is difficult to resolve in thicker structures, leading to multiple possible solutions for the refractive index.

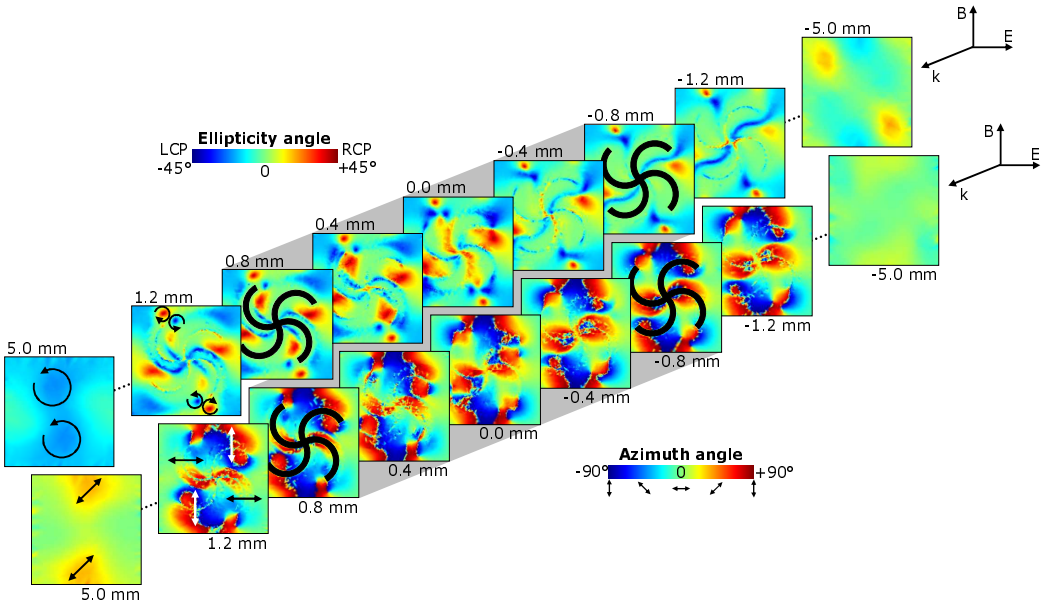

Figure 5.5: ***Polarization state evolution*** *for the total field as a linearly polarized wave propagates through the bilayered metamaterial at 4.6 GHz. The top sequence shows the ellipticity angle of the total local field, while the bottom sequence shows the polarization azimuth.*

refractive index. The structure's highly optically active response is a consequence of strong electromagnetic interaction between the mutually twisted wire patterns through the local field. The color-coded field maps shown in Fig. 5.5 present the evolution of the local field in terms of ellipticity (top) and azimuth (bottom) for the case of a linearly polarized wave propagating through the structure. The data corresponds to the frequency of 4.6 GHz, where the metamaterial rotates the transmitted wave by 11° and induces an ellipticity angle of 13° (circular dichroism 4 dB), while transmission is still reasonably large. Simulations show that the incident linearly polarized plane wave is significantly perturbed by the metamaterial's structure within about 4 mm ($\lambda/16$) of the material's surface. However, changes of the field's effective polarization state occur only within the rosette structure [6]. Close to and within the metamaterial the local field is weak at the center of the rosette pattern, most of the field's energy is found in the vicinity of the outer parts of the rosette arms and in the unstructured dielectric areas at the edge of the unit cell. The field itself develops a complex structure, which can be understood in terms of two regimes. In the ultimate vicinity of each rosette the local

[6] The effective polarization state is the polarization of the average field in the plane perpendicular to the propagation direction.

field is dominated by the presence of the nearby metal structure, which leads to a local electric field linearly polarized perpendicular to the metal wire. Due to each rosette's 4-fold rotational symmetry, however, this alone cannot affect the far-field polarization state. It is the coupling between both mutually twisted metal patterns, that makes the metamaterial polarization sensitive and allows it to rotate the far-field polarization state. Locally this can be seen from the complex field structure in regions that experience substantial field contributions from both rosettes. Here, depending on the phase delays and magnitudes of excited currents, left-handed and right-handed local fields with rotated azimuth are excited. Notably, despite the complex structure of the local fields, azimuth and ellipticity of the effective field typically change continuously along the propagation direction. For the transmitted wave, the complicated substructure of the local field interferes away within about the first 4 mm of the metamaterial's surface, leaving a rotated elliptical plane wave which propagates to the far-field.

5.2.4 Multi-layered Metamaterials: Thin Rotators and Circular Polarizers.

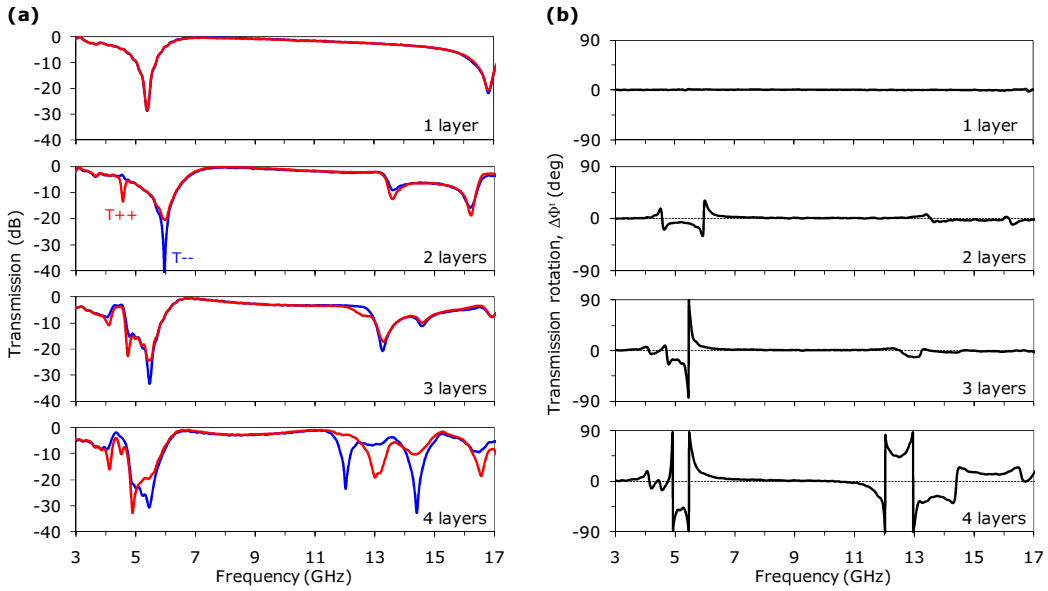

Figure 5.6: ***Development of the metamaterials' transmission characteristics when increasing the number of layers from 1 to 4.*** *(a) Transmission spectra measured for the metamaterials' circular eigenpolarizations LCP (blue, -) and RCP (red, +). (b) Polarization azimuth rotation measured for linear polarization.*

Exceptionally large rotary power and circular dichroism for the bilayered structure

suggest that multi-layered forms of the metamaterial may have very promising optically active properties. Fig. 5.6 shows the evolution of the transmission properties with increasing number of layers of mutually twisted planar metal rosettes. Transmission levels are presented for both circular polarizations and polarization azimuth rotation is shown for linear polarization. Similarly to the bilayered structure, the reflection levels for RCP and LCP were found to be the same within experimental accuracy in all cases. Therefore, any transmission circular dichroism must be fully accounted for by different absorption levels for circularly polarized waves of opposite handedness.

It is evident that a single layer of metal rosettes on a dielectric substrate (top graphs) does not lead to any significant optical activity, even though the metamaterial has intrinsic 3D chirality, as the 2D-chiral rosettes are placed on only one side of the substrate [80]. A minimum of 2 layers of rosettes is required to achieve strong optical activity (see detailed discussion above). In the mono-layered case two isolated resonances corresponding to $\lambda/2$ and $3\lambda/2$ electric dipole excitations ($\uparrow$) can be observed. No significant magnetic mode can be excited and therefore optical activity is negligible. The introduction of a second layer changes this situation dramatically, by allowing the resonances to hybridize into symmetric ($\uparrow\uparrow$, electric) and anti-symmetric ($\uparrow\downarrow$, magnetic) current modes excited in pairs of rosettes. In analogy with orbital hybridization in chemistry, the anti-symmetric mode corresponds to a lower energy bonding state, while the symmetric mode corresponds to a higher energy anti-bonding state [150]. The structure's strong optical activity results from the simultaneous scattering contributions of electric and magnetic modes excited in the intrinsically 3D-chiral structure.

The response of a 3-layered version of the metamaterial is quite similar to the bilayered case, especially in terms of the magnitude of its optical activity. However, the resonances split 3-fold compared to 2-fold for the bilayered metamaterial, which can be explained by the fact that there are now three possible modes that can be excited in the structure: $\uparrow\downarrow\uparrow$, $\uparrow\uparrow\downarrow$, $\uparrow\uparrow\uparrow$.

For 1 to 3 layers, RCP and LCP couple similarly to the same resonant modes. Importantly, this is not true for more complex structures with 4 or more layers, where different higher-frequency resonances are excited by RCP and LCP. This allows the 4-layered metamaterial to be almost transparent for one circular polarization while being opaque for the other, making it an efficient circular polarizer. For example at

12 GHz transmission losses are only 3 dB for RCP but substantial 23 dB for LCP, leading to a contrast of 20 dB. Between resonances, where transmission levels are equal for both circular polarizations, losses are relatively low while the material's rotary power can be very large. Here the metamaterial shows pure circular birefringence, as it will only rotate the azimuth of the polarization state, without changing its ellipticity. Particularly at 12.5 GHz large absolute rotation of 45° is achieved with relatively low losses of less than 6 dB and without changing the polarization state's ellipticity. It must be noted that these functionalities are achieved by a metamaterial that is only $\lambda/5$ (at 12 GHz) in thickness, whereas conventionally rotators and circular polarizers are large components many wavelengths in thickness. The combination of small size, large optical activity and relatively low losses makes multi-layered forms of the metamaterial suitable for practical use as thin rotator and circular polarizer.

5.2.5 Summary

In summary a class of intrinsically 3D-chiral metamaterials has been realized, which has very versatile properties including a negative index of refraction due to circular birefringence, negative permeability, negative permittivity, invisibility, mirror-like reflectivity and for transmitted waves giant polarization rotary power and very large circular dichroism. In contrast to the extrinsically 3D-chiral planar metamaterials discussed in chapter 4, no reflection optical activity has been detected. Evidence has been given that for a bilayered metamaterial, which is based on mutually twisted planar metal rosettes in parallel planes, the negative refractive index does indeed result from the 3D-chiral nature of the metamaterial and not from driving permeability and permittivity negative in the same frequency range as for conventional negative index media. It has been illustrated in terms of local fields how the highly optically active structure interacts with electromagnetic waves. And finally it has been shown that multi-layered versions of the metamaterial show enhanced performance, not only in terms of larger circular dichroism and polarization rotation, but also in terms of reduced insertion losses, making them suitable for use as thin circular polarizers and polarization rotators in practical applications.

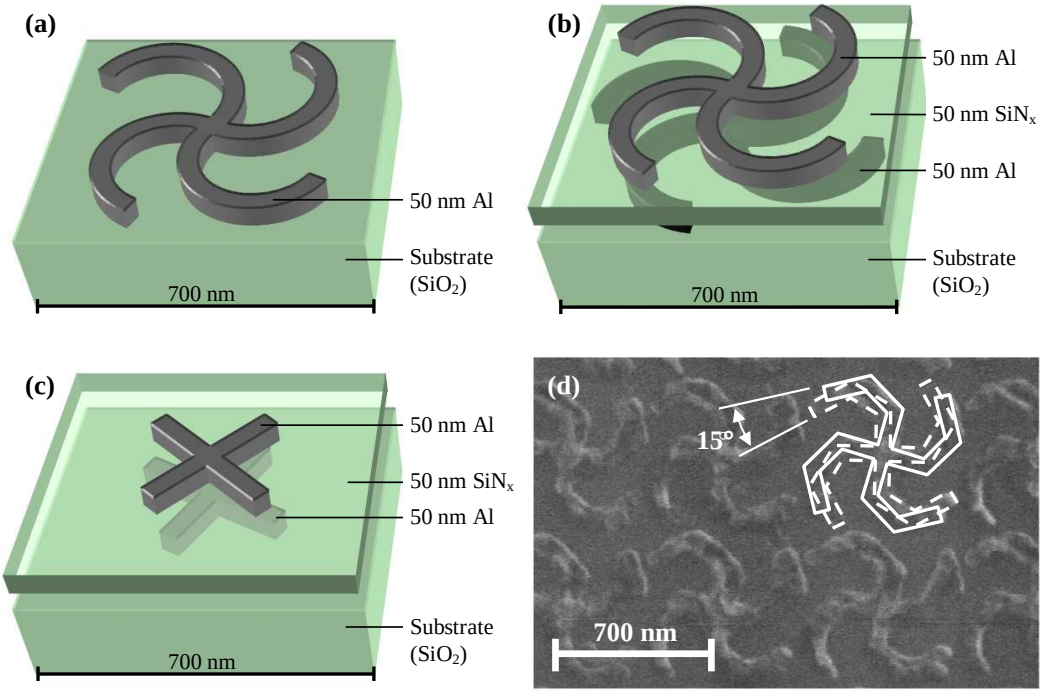

Figure 5.7: ***Structure of the intrinsically 3D-chiral photonic metamaterials.*** *Meta-molecules: (a) "single rosettes", (b) "twisted rosettes" and (c) "twisted crosses". (d) Scanning electron microscope image of the "twisted rosettes" metamaterial.*

5.3 Circular Birefringence in Layered Photonic Nanostructures

The work presented here is the result of a collaboration. The samples were designed by Alexander S. Schwanecke from University of Southampton and manufactured by Yifang Chen from Rutherford Appleton Laboratory. I characterized the metamaterial samples experimentally with some assistance of Alexander S. Schwanecke and Vassili A. Fedotov and I interpreted the results. Parts of the work presented here have also been published as [50].

Here it is demonstrated that mutually twisted metal patterns in parallel planes also lead to exceptionally large circular birefringence in the optical part of the spectrum. Being compatible with established planar manufacturing techniques such structures are easier to mass-produce than helical nanostructures.

In order to investigate the response of mutually twisted pairs of metal nanopatterns in parallel planes, three photonic metamaterials were manufactured by electron beam lithography. The metamaterial samples are 250 $\times$ 250 μm^2 in size, each consisting

of a two-dimensional array of more than 10^5 meta-molecules on a 500 μm thick silica substrate. Here the metamaterials will be referred to according to the shape of their meta-molecules as "single rosettes" [Fig. 5.7 (a)], "twisted rosettes" [Fig. 5.7 (b)] and "twisted crosses" [Fig. 5.7 (c)]. The meta-molecules, which are 700 $\times$ 700 nm^2 in size, contain cross/rosette elements made from aluminum nanowires with a cross-section of 50 $\times$ 50 nm^2. The rosette pattern consists of four semicircles with a radius of 190 nm and the crosses are composed of two perpendicular bars which are 390 nm in length. In case of pairs of crosses or rosettes the metal patterns are mutually twisted by 15° and separated by a 50 nm thick dielectric spacer layer made from silicon nitride. It should be noted that these latter structures, which derive their electromagnetic properties from the mutual orientation of identical "meta-atoms" (rosettes or crosses), constitute the first examples of stereometamaterials [150].

All meta-molecule designs have 4-fold rotational symmetry making them isotropic for electromagnetic waves at normal incidence, however, manufacturing of these structures is by no means an easy process. Astigmatism of the electron beam would cause anisotropy leading to linear birefringence and linear dichroism in crosses and rosettes. For the bilayered twisted samples precise alignment between the two layers is crucial, therefore special gold alignment marks were used during manufacturing to ensure good alignment of the centers of crosses/rosettes in different layers. Small miss-alignments would cause some residual anisotropy of the structures.

The sample quality was checked in several experiments. Given their periodicity of 700 nm the structures should not diffract at wavelengths longer than 700 nm, however, in the visible part of the spectrum they should act as diffraction gratings. The sample periodicity was confirmed by measuring the angular position of the transmitted first order diffraction maxima for a 532 nm green laser at normal incidence. As expected, all three metamaterial structures were found to have 2-fold 700 nm periodicity within experimental accuracy. In order to check the sample surfaces for any obvious damage and to assess the sample isotropy, the metamaterials were rotated between crossed polarizers under a microscope. Cross-polarization microscopy was done for both transmitted and reflected light, however, as the observations were very similar, only transmission will be discussed here. Fig. 5.8 shows transmission photographs of the structures between

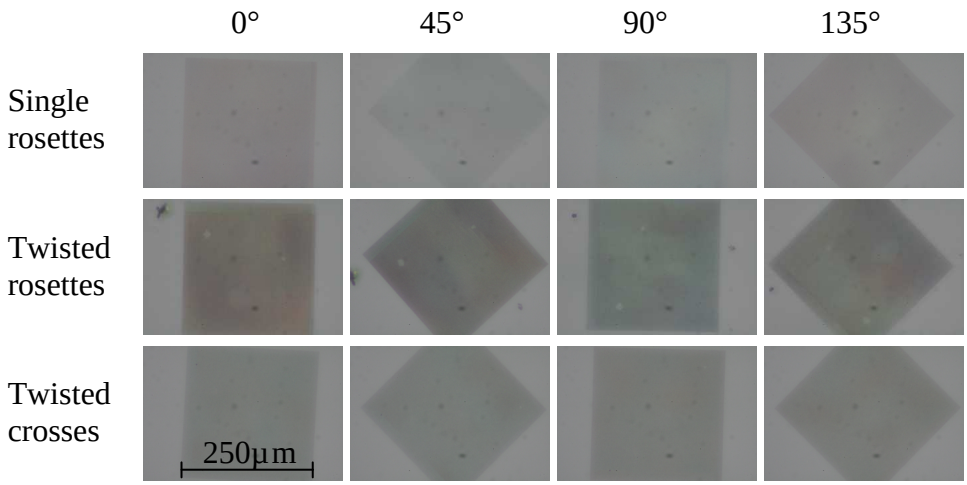

Figure 5.8: ***Transmission photographs of the nanostructures*** *between (almost) crossed polarizers observed through an optical microscope. The structures were rotated in steps of 45°. Some residual anisotropy of the metamaterials can be seen as color shifts between red and green for different rotation angles. A frame-like pattern towards the edge of the samples indicates small additional manufacturing inaccuracies.*

almost[7] crossed polarizers. The metamaterials do not show any indications of significant damage, but some residual anisotropy resulting from limitations in manufacturing was observed. Rotation of the samples by 90° between crossed polarizers leads to color shifts between red and green indicating the presence of anisotropy. The anisotropy of the structures also changes with position, in particular a frame-like structure can be seen close to the sample edges. Anisotropy in general and varying anisotropy with position both are strongest for the "twisted rosettes" structure but they do occur for all samples. The anisotropy has been taken into account when studying the metamaterials' transmission optical activity as discussed later.

In order to identify interesting frequency regions where the metamaterials would be likely to show strong polarization effects, the normal incidence transmission and reflection spectra[8] of the structures were measured using a linearly polarized supercontinuum laser source and two optical spectrum analyzers. One optical spectrum analyzer was used to monitor spectral intensity fluctuations of the laser source while the other one measured the spectrum after transmission through a metamaterial sample. The reflection spectra were calibrated relative to the reflectivity of the plain glass substrate and a

[7] Perfectly crossed polarizers yield the same qualitative results, but are much more difficult to photograph.

[8] These transmission and reflection spectra were measured by Alexander S. Schwanecke and myself jointly.

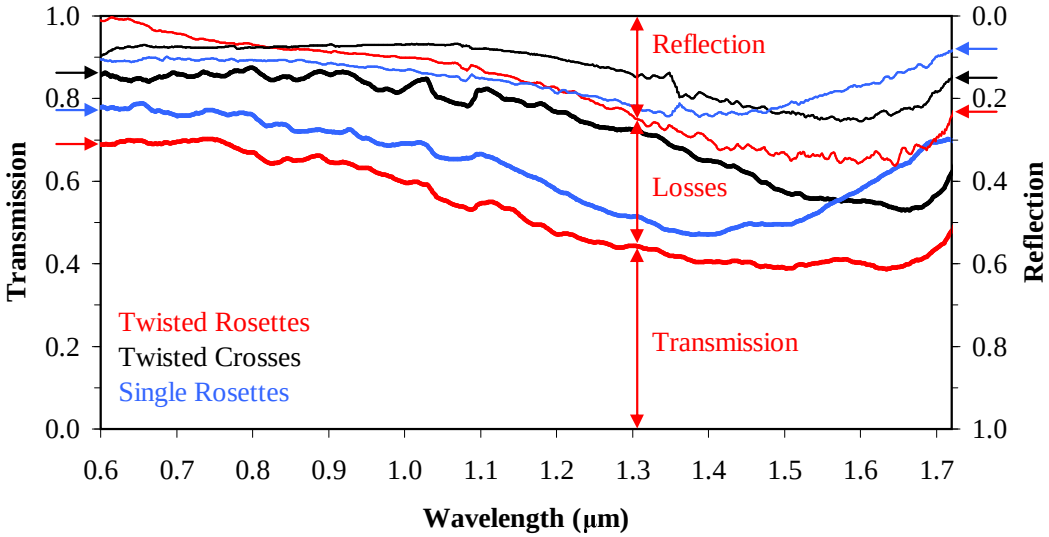

Figure 5.9: ***Spectral dependence of transmission*** *(thick lines),* ***reflection*** *(thin lines)* ***and losses*** *at normal incidence for the photonic metamaterials: "twisted rosettes" (red), "twisted crosses" (black) and "single rosettes" (blue). Transmission, reflection and losses are indicated explicitly for the "twisted rosettes" nanostructure at 1310 nm, where the strongest circular birefringence was measured.*

sample-sized aluminum mirror taking the reflectivity of glass and a reflectivity spectrum of aluminum from the literature into account. Transmission spectra were measured relative to the glass substrate, then the reflectivity of glass was taken into account to calculate the absolute transmission levels. The final calibrated transmission and reflection spectra are shown in Fig. 5.9. All structures show a broad resonance in the near infrared. In transmission it is strongest for "single rosettes" around $1.3 - 1.4$ μm, for "twisted rosettes" around $1.3 - 1.6$ μm and for "twisted crosses" around $1.5 - 1.7$ μm.

Using normally incident linearly polarized electromagnetic waves, the transmission optical activity of the metamaterials was measured at three characteristic wavelengths: before the resonances at 660 nm, at the beginning of the resonances at 980 nm and at 1310 nm which is at the resonance of the rosette-based structures. In order to be able to separate the effects of 3D chirality and anisotropy, it was necessary to measure any changes of polarization azimuth or ellipticity as a function of input polarization azimuth. Such measurements of polarization azimuth rotation were performed at 660 nm using two crossed linear polarizers[9]. The polarization plane rotation and ellipticity change at 980 nm and 1310 nm were measured using an infrared polarimeter.

As shown in section 2.4.1, anisotropy causes a modulation of azimuth rotation $\Delta\Phi^t$

[9]Polarization azimuth rotation at 660 nm was measured by Vassili A. Fedotov.

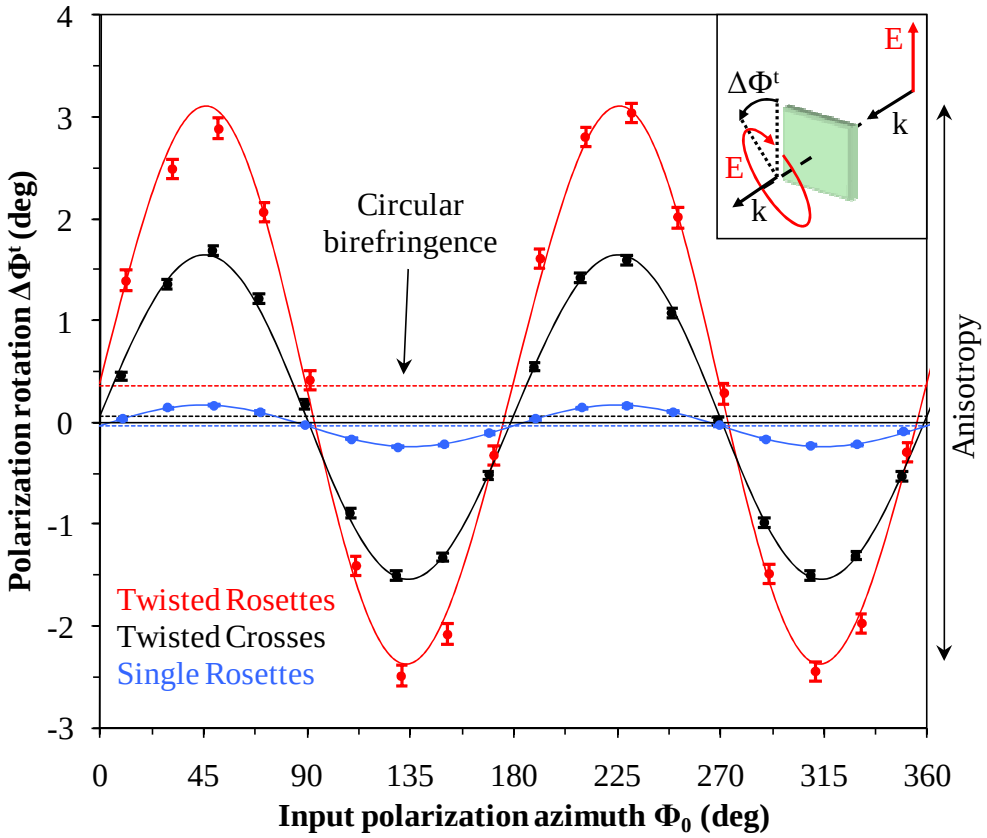

Figure 5.10: ***Polarization plane rotation as a function of initial polarization azimuth*** *for transmission through the photonic metamaterials at 1310 nm: "twisted rosettes" (red), "twisted crosses" (black) and "single rosettes" (blue). Solid lines are numerical fits and the dashed lines indicate the true levels of circular birefringence.*

that depends on the azimuth Φ_0 of the incident wave's polarization state, but it has no impact on the average polarization rotation $< \Delta\Phi^t >$. Thus, a metamaterial's true circular birefringence is given by the polarization rotation averaged over all possible incident (linear) polarizations. Here, as only a finite number of incident polarizations could be measured, the circular birefringence has been determined by fitting the experimental data with equation (2.41), which quantitatively describes the impact of anisotropy (linear birefringence / dichroism) on the rotation of the transmitted polarization state. Similarly, the ellipticity of the transmitted wave was measured in order to determine the circular dichroism of the metamaterials. Measurements of ellipticity change as a function of initial polarization azimuth did show some anisotropy, but the effective ellipticity change was too small to be measured reliably in all cases. However, a recent follow-up study of a photonic stereometamaterial based on pairs of mutually twisted gold crosses suggests that larger circular dichroism should have been observable

Table 5.1: *Average polarization rotation* $< \Delta\Phi^t >$

Structure	660 nm	980 nm	1310 nm
Single rosettes	$< 0.01°$	$< 0.01°$	$\simeq -0.03°$
Twisted rosettes	$0.09°$	$0.09°$	$0.37°$
	$(600°/\text{mm})$	$(600°/\text{mm})$	$(2500°/\text{mm})$
Twisted crosses	$0.05°$	$0.05°$	$0.04°$
	$(330°/\text{mm})$	$(330°/\text{mm})$	$(270°/\text{mm})$

further into the infrared [88]. Fig. 5.10 shows the measured polarization rotation and the numerical fits at 1310 nm for all three photonic metamaterials. The anisotropic oscillations of azimuth rotation are well described by the fits and the average polarization rotation $< \Delta\Phi^t >$ - indicated by dashed lines - corresponds to the true circular birefringence without linear birefringence / dichroism.

The average polarization plane rotation exhibited by the different materials is listed in table 5.1. The effective rotation is small for the "single rosettes" metamaterial. In fact it is only measurable at 1310 nm close to the structure's resonance. Adding a layer of twisted rosettes results in a large increase of rotary power. The "twisted rosettes" material has strong polarization rotary power of about $600°/\text{mm}$ below 1000 nm which increases to $2500°/\text{mm}$ at 1310 nm near the material's resonance. For the "twisted crosses" material the rotary power seems to be about constant around $300°/\text{mm}$ over the measured range, however, it might increase further into the infrared where the material resonance is strongest.

The rotary power of the "twisted rosettes" material at 1310 nm is remarkably high. In units of polarization rotation per material thickness of one wavelength it reaches $3.2°/\lambda$ which is more than two orders of magnitude stronger than quartz in the visible part of the spectrum ($0.02°/\lambda$ at 400 nm). It also rotates stronger than helical sculptured thin films ($2.4°/\lambda$ at 400 nm, [76]).

For each metamaterial the average polarization plane rotation for waves normally incident on front or back of the structure was found to be the same within experimental accuracy, as should be expected for a 3D-chiral phenomenon. This even applies to the "single rosettes" structure which becomes 3D-chiral only due to the presence of the substrate. However, the signs of polarization rotation for "single rosettes" and "twisted rosettes" are opposite and the latter material rotates at least one order of magnitude stronger. Therefore the response of the twisted structures cannot be understood as the

added effect of two monolayered materials, but their response must be caused by the electromagnetic interaction between the twisted rosettes/crosses in different layers, see also section 5.2.

In summary a new type of layered photonic metamaterial with remarkably strong circular birefringence in the near infrared has been demonstrated. The structure is based on pairs of mutually twisted planar metal elements in parallel planes.

5.4 Summary

In this chapter, the first stereometamaterials have been studied experimentally. These metamaterials, which are based on intrinsically 3D-chiral pairs of mutually twisted metal patterns in parallel planes[10] have been found to form a very versatile class of novel artificial structures. The following properties have been observed in the microwave part of the spectrum:

- exceptionally large transmission circular birefringence and circular dichroism,
- negative refractive index due to circular birefringence for one circular polarization (first experimental demonstration),
- negative permittivity and negative permeability (in separate bands),
- invisibility and mirror-like reflectivity.

Furthermore remarkably large polarization rotary power has also been observed in the optical part of the spectrum for a nanoscale metamaterial of this type.

In contrast to more conventional helical structures, the metamaterials studied here are based on planar elements, making them suitable for mass-production using established planar manufacturing technologies like lithography. Such stereometamaterials have a large range of potential applications from circular polarizers and polarization rotators of sub-wavelength thickness to negative index applications like superlensing.

[10] Single meta-molecules of this type were previously studied by [71].

Chapter 6

Conclusions

6.1 Summary

This thesis represents a study of many aspects of chirality in metamaterials. Both the 2D-chiral phenomenon of circular conversion dichroism and 3D-chiral optical activity have been investigated in detail.

Prior to the work presented here, circular conversion dichroism was known to lead to directionally asymmetric total transmission of circularly polarized waves in lossy, anisotropic, intrinsically 2D-chiral metamaterials. This transmission phenomenon had been observed in the microwave and optical spectral ranges. In this thesis, a number of theoretical and experimental advances have been made.

- It has been derived for planar metamaterials that circular conversion dichroism necessarily leads to enantiomerically sensitive and directional **asymmetries in total transmission and reflection**. These asymmetries have the same magnitude, **cannot exceed** 25 % of the incident power each and are accounted for by a corresponding **absorption asymmetry**. Directional transmission asymmetries of more than $\frac{4}{5}$ of the theoretical limit have been observed and the reflection and absorption asymmetries have been experimentally studied for the first time.

- Circular conversion dichroism has been linked to the excitation of **enantiomerically sensitive current modes**. It has been shown that the largest effect results from excitation of electric dipole currents and non-scattering (anti-symmetric) currents respectively by counterpropagating circularly polarized waves of the same

handedness.

- Circular conversion dichroism has been observed for the first time in the **terahertz spectral range**.
- A superior metamaterial design based on **intrinsically 2D-chiral split rings** has been introduced, which exhibits 60% larger circular conversion dichroism than previously studied structures.
- Circular conversion dichroism caused by a **2D-chiral periodic arrangement of non-chiral elements** (structural 2D chirality) has been observed for the first time.
- **Circular conversion dichroism in non-chiral structures** has been first observed. The phenomenon requires absorption losses and is caused by **extrinsic 2D chirality**, which is present at oblique incidence when a structured interface combined with the preferred direction associated with the plane of incidence is 2D-chiral. Extrinsic 2D chirality is inherently tunable and can be realized for any periodically structured interface.

Insights have also been gained about 3D-chiral optical activity (circular birefringence and circular dichroism). The effect had been largely regarded a transmission phenomenon, as reflection optical activity had been found to be too weak to be of practical importance. It had been predicted that circular birefringence could cause a negative index of refraction. Several advances have been made in this thesis.

- Based on a previous study of a single meta-molecule consisting of mutually twisted metal patterns in parallel planes [71], in this thesis the **first stereometamaterials** have been realized, yielding
  - the first material with **negative refractive index due to circular birefringence**, and
  - the first experimental demonstration of **giant optical activity** in intrinsically 3D-chiral stereometamaterials.

- **Optical activity in non-chiral metamaterials** has been observed for the first time. The effect is due to **extrinsic 3D chirality**, which is present when the material combined with the direction of incidence forms a 3D-chiral experimental arrangement. Extrinsic 3D chirality is inherently tunable, can be realized for any structure without 2-fold rotational symmetry[1] and has been found to lead to exceptionally large, tunable circular birefringence and circular dichroism in transmission and reflection.

Furthermore, polarization effects in planar metamaterials - which can have 2D chirality and extrinsic 3D chirality - have been characterized theoretically, identifying fundamental limits for potential applications as polarization transformers. Transmission and reflection planar metamaterial polarization rotators, for example, would face a trade-off between rotary power and insertion loss, which makes 90° rotators impossible. A similar trade-off between phase delay and insertion loss of transmission and reflection wave plates makes planar half wave plates impossible. Nevertheless, due to their tunability (rotators) and vanishing thickness planar metamaterials have great potential as polarization transformers in miniaturized photonic circuits.

6.2 Outlook

This thesis contains a number of "proof of concept" demonstrations of polarization transformers, e.g. polarization rotators and circular polarizers based on stereometamaterials or planar metamaterials. In particular such planar metamaterial devices have interesting properties like tunability, vanishing thickness and functionality in transmission and reflection. Such devices could be optimized and possibly commercialized.

In this thesis, the effects of extrinsic 2D and 3D chirality on the electromagnetic properties of planar metamaterials have been studied. It could be very promising to extend this work to multi-layered structures. This may be of particular interest for applications, as the fundamental trade-offs faced by some planar metamaterial devices, e.g. rotary power versus insertion loss for polarization rotators, may not apply to multi-layered structures.

The work presented here was limited to linear effects. However, energy concentrates

[1] Wallpaper symmetry groups without 2-fold rotational symmetry: $p1$, pm, pg, cm, $p3$, $p3m1$, $p31m$.

in resonant metamaterials and therefore such structures are a promising platform for nonlinear effects. It may be interesting to explore the interplay of intrinsic and extrinsic 2D and 3D chirality with non-linear phenomena like second harmonic generation.

Like all approaches to negative refraction, also the chirality-induced negative index studied here battles with losses. Loss-compensation in chiral metamaterials is therefore a possible avenue to negative index materials for practical applications. In the optical part of the spectrum, metamaterials combined with quantum dots, dye molecules or rare-earth-doped glasses and an external pump are a promising direction.

Also switchable intrinsically or extrinsically chiral materials could be investigated. For example, by combining a metamaterial pattern with a phase change substrate or superstrate, e.g. a chalcogenide glass, optical activity and circular conversion dichroism could be switched between different frequency bands.

Appendix A

Characterization of Microwave Metamaterials

A.1 Experimental Technique and Data Processing

All microwave metamaterials were characterized in an anechoic chamber using two linearly polarized horn antennas (Schwarzbeck BBHA 9120D) and a vector network analyzer (Agilent E8364B) allowing simultaneous measurements of amplitude and phase of microwaves in the 1-18 GHz frequency range. The divergent emission of the antennas was collimated using microwave lenses which are described in section A.2.

In transmission experiments, the antennas were spaced about 2 m apart to ensure that plane waves were incident on the metamaterial, which was placed in the middle between the antennas. A reflecting screen was used to shield the receiver from microwaves propagating around the metamaterial and any anisotropy arising from the shape of the samples was eliminated using an aluminum sample holder with a circular aperture, see Fig. A.1 (a)-(b). Details regarding sample holder and screen are given in section A.2. Measurements of phase and amplitude were calibrated relative to data recorded in the same transmission setup without the metamaterial.

In reflection experiments, both antennas were placed next to each other facing the metamaterial, see Fig. A.1 (c). For (quasi) normal incidence reflection measurements an angle of incidence of 3.5° was achieved by placing the antennas about 40 cm apart and about 3 m from the metamaterial. Amplitude and phase were calibrated relative to

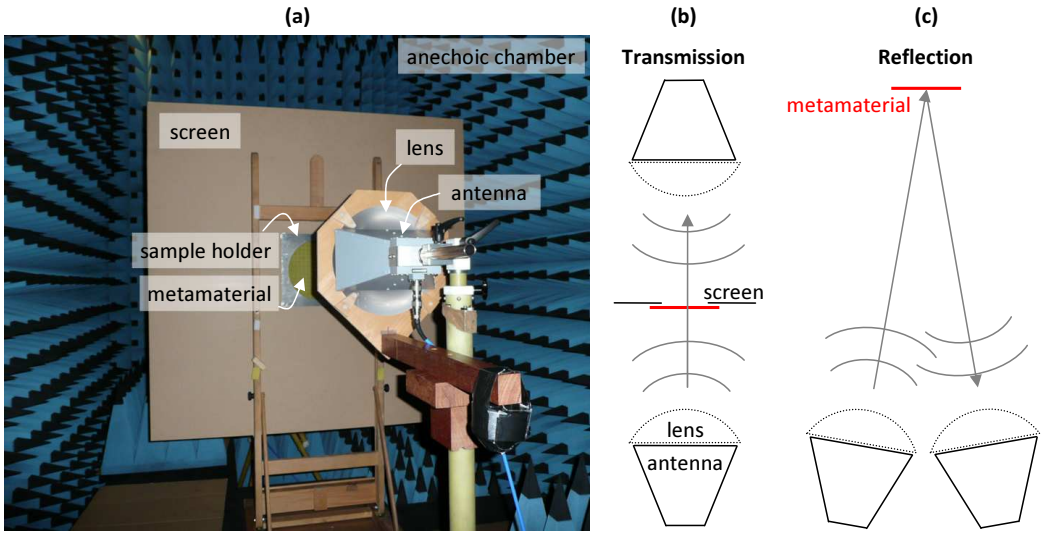

Figure A.1: ***Microwave experimental setups.*** *(a) Photograph of the transmission setup. The screen acts as a microwave mirror, as it is covered with aluminum foil on the other side, see Fig. A.2. All experiments were carried out in an anechoic chamber with microwave absorbing walls. (b) and (c) show schematics of the transmission and reflection setups respectively.*

reference measurements from the same reflection setup with the metamaterial replaced by an aluminum plate (microwave mirror) of the same size as the metamaterial.

In order to fully characterize the transmission (reflection) properties of a metamaterial, measurements were taken for all four possible combinations of horizontally and vertically polarized emitter and receiver and for wave propagation in both directions. This way the metamaterial's linear transmission (reflection) matrix was measured for both directions of propagation. It describes a linear material's transmission (reflection[1]) properties for linearly polarized waves and it is defined by $E_i^{out} = \tilde{t}_{ij} E_j^0$ where E^{out} is the transmitted (reflected) and E^0 the incoming electric field. The indices i, j correspond to the plane of polarization x or y.

For the study of chiral metamaterials the circular transmission (reflection) matrix $E_i^{out} = t_{ij} E_j^0$, describing the transmission (reflection) properties for circularly polarized waves is of particular interest. Here i, j correspond to left-handed (LCP, -) or right-handed (RCP, +) circularly polarized waves, with the handedness defined as the electric field vector's direction of rotation at a fixed point in space, seen by an observer looking into the beam. The circular transmission (reflection) matrix t can be calculated from the linear transmission (reflection) matrix $\tilde{t}$ using the following basis transformation.

[1]The following equations apply to reflection, when the matrix is renamed from t to r.

$$t = \begin{pmatrix} t_{++} & t_{+-} \\ t_{-+} & t_{--} \end{pmatrix} = \frac{1}{2} \begin{pmatrix} \tilde{t}_{xx} + \tilde{t}_{yy} + i(\tilde{t}_{xy} - \tilde{t}_{yx}) & \tilde{t}_{xx} - \tilde{t}_{yy} - i(\tilde{t}_{xy} + \tilde{t}_{yx}) \\ \tilde{t}_{xx} - \tilde{t}_{yy} + i(\tilde{t}_{xy} + \tilde{t}_{yx}) & \tilde{t}_{xx} + \tilde{t}_{yy} - i(\tilde{t}_{xy} - \tilde{t}_{yx}) \end{pmatrix} \quad \text{(A.1)}$$

Optical activity corresponds to unequal direct transmission (direct reflection[2]) terms of the circular transmission (reflection) matrix, i.e. $t_{++} \neq t_{--}$ and $r_{-+} \neq r_{+-}$. Transmission and reflection/scattering circular dichroism are defined as

$$\Delta T = |t_{++}|^2 - |t_{--}|^2, \quad \text{(A.2)}$$

$$\Delta S = \Delta R = |r_{-+}|^2 - |r_{+-}|^2, \quad \text{(A.3)}$$

while the average polarization plane rotation (circular birefringence) in transmission and reflection/scattering corresponds to

$$\Delta\Phi^t = -\tfrac{1}{2}[\arg(t_{++}) - \arg(t_{--})], \quad \text{(A.4)}$$

$$\Delta\Phi^s = -\Delta\Phi^r = -\tfrac{1}{2}[\arg(r_{-+}) - \arg(r_{+-})]. \quad \text{(A.5)}$$

Circular conversion dichroism corresponds to unequal magnitudes of the conversion terms of the circular transmission (reflection) matrix, $|t_{-+}| \neq |t_{+-}|$ and $|r_{++}| \neq |r_{--}|$. The phenomenon can be measured as the conversion difference for either counterpropagating circularly polarized waves of the same handedness or copropagating waves of opposite handedness, i.e.

$$\begin{aligned} \overrightarrow{T_+} - \overleftarrow{T_+} &= |\overrightarrow{t_{-+}}|^2 - |\overleftarrow{t_{-+}}|^2 \\ &= |\overrightarrow{t_{-+}}|^2 - |\overrightarrow{t_{+-}}|^2. \end{aligned} \quad \text{(A.6)}$$

A.2 Improvements to the Microwave Experimental Setup

In order to reliably measure the transmission characteristics of a metamaterial the following conditions need to be met.

- All microwaves that reach the receiver should have propagated through the sam-

[2]The handedness of a circularly polarized wave is reversed upon direct reflection (e.g. metal mirror), therefore the indices are different for reflection.

ple, not around it.

- The sample holder and the sample shape must not introduce any chirality or anisotropy into the setup that might affect the transmitted polarization state.

As the samples are 227×272 mm^2 in size, i.e. rectangular and much smaller than the microwave beam, both conditions are not met when a metamaterial sample is simply placed in between the horn antennas. In this case most of the antennas' divergent microwave emission propagates around the metamaterial, which also causes a weak signal level in reflection measurements. In order to make the reliable characterization of microwave metamaterials possible, these issues had to be addressed.

A.2.1 Sample Holder

The potential influence of the rectangular sample shape was eliminated by building a sample holder that makes the effective sample area circular, thus removing any preferred direction due to the shape of the sample. The sample holder consists of two square aluminum sheets 272×272 mm in size with a 222 mm circular aperture. Samples are placed between these aluminum sheets which are held together by plastic screws. The use of screws of appropriate length allows stacking of up to about 8 metamaterial sheets permitting the the study complex multi-layered structures.

A.2.2 Microwave Screen

In order to prevent microwaves from reaching the receiver without propagating through the metamaterial, a large reflective screen was manufactured. The screen, which is shown in Fig. A.2 consists of a 1222×1222 mm^2 medium density fiber board covered by aluminum foil. It has a 222 mm centered circular aperture and a pair of holes allowing the sample holder to be attached to the screen using two of its plastic screws. The hole positions ensure that the 222 mm apertures of the holder and the screen automatically line up. This screen reflects microwaves that are not incident on the sample against the absorbing walls of the anechoic chamber. However, as it is more desirable to absorb these microwave directly, a 600×600 mm^2 piece of microwave-absorbing foam was added to the central area of one side of the screen. The foam has a tapered aperture with an inner diameter of 156 mm at its center.

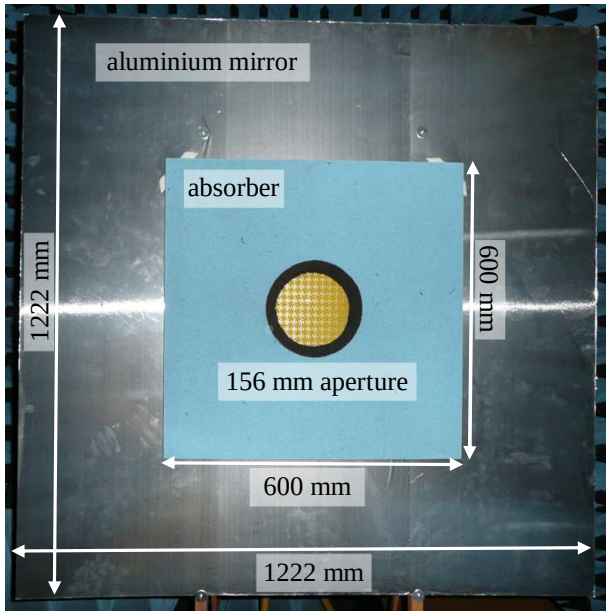

Figure A.2: ***Screen for microwave experiments.*** *The screen has a circular aperture. It is completely covered by aluminum foil acting as a microwave mirror and its central area is additionally covered by microwave-absorbing foam. The sample holder is attached to the screen on the other side, see Fig. A.1 (a).*

A.2.3 Microwave Lenses

If the microwave antennas' highly divergent emission is not focussed, only a small fraction of the emitted power is incident on the metamaterial sample. In order to address this issue, microwave lenses were designed that turn the highly divergent microwave emission of the horn antennas into a more collimated beam. Clear acrylic was chosen as the lens material as it is easily available and as it has a fairly constant refractive index of about 1.6 at GHz frequencies. Thus reflectivity is still low ($\sim 5\%$) while refraction is already strong enough to construct a lens. To keep the cost of manufacturing reasonable a planoconvex spherical lens shape was chosen. As the lenses had to be large enough to cover the opening of the horn antennas (almost) completely, a diameter of 260 mm was chosen for the flat side, leaving only one free parameter in the lens design: the thickness (or the radius of curvature). In order to decide on the thickness of the lens the wave propagation through horn antenna and lens was simulated for different lens thicknesses using COMSOL Multiphysics [Fig. A.3 (a)]. The best beam collimation was achieved for a lens thickness around 80 mm [Fig. A.3 (b)]. Two 80 mm thick lenses, weighing 2.7 kg each, were manufactured using a CNC lathe by the workshop of University of

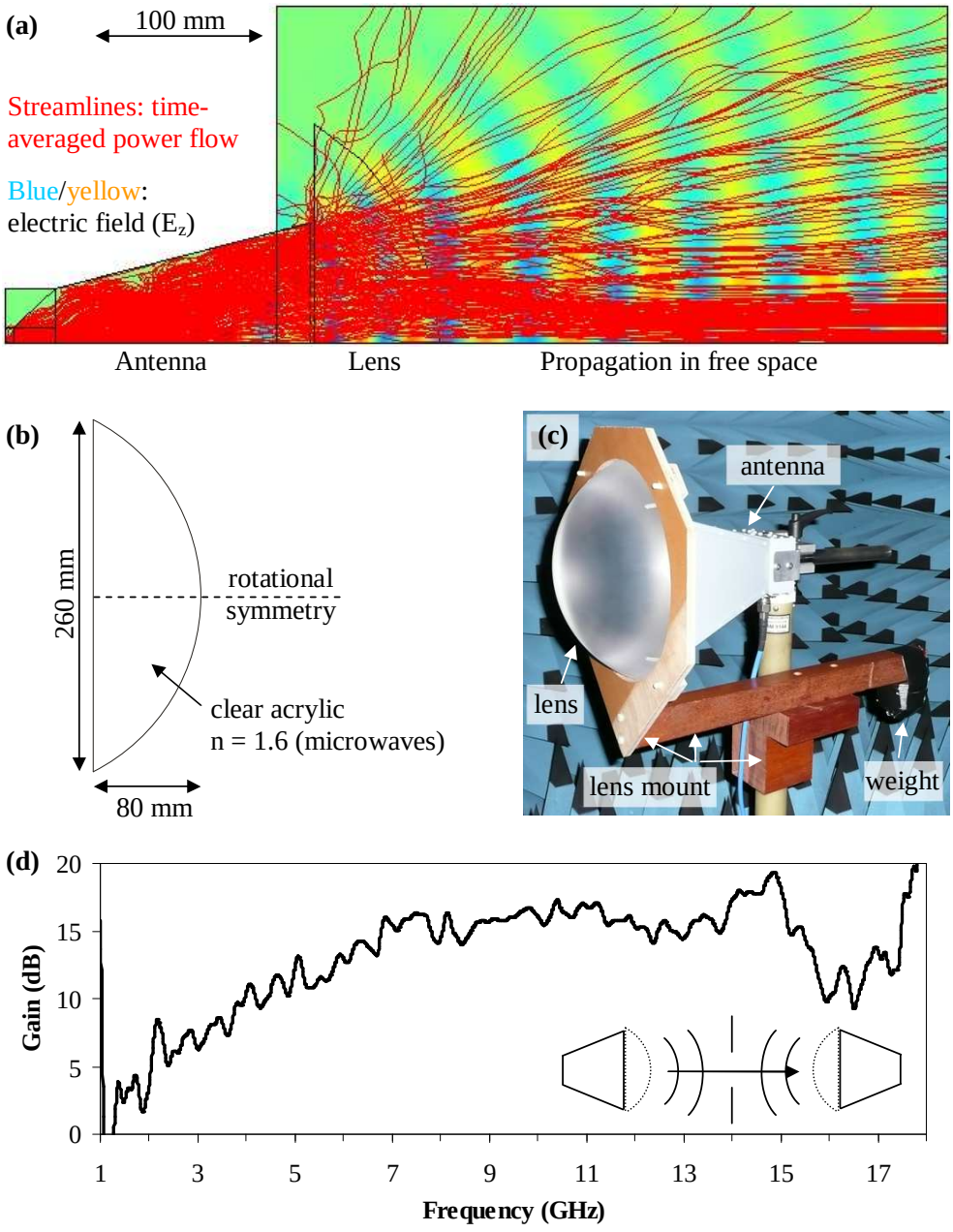

Figure A.3: ***Microwave lens.*** *(a) Simulation of microwave emission by the horn antenna at 6 GHz and wave propagation through a microwave lens with refractive index 1.6 (acrylic), thickness 75 mm and diameter 260 mm. (b) The final lens design: A lens made from clear acrylic with diameter 260 mm and thickness 80 mm. (c) Photo of one of the lenses mounted in front of a microwave horn antenna. (d) Gain achieved by the lenses for wave propagation through a circular aperture 222 mm in diameter. Here the distance between aperture and antennas is 800 mm.*

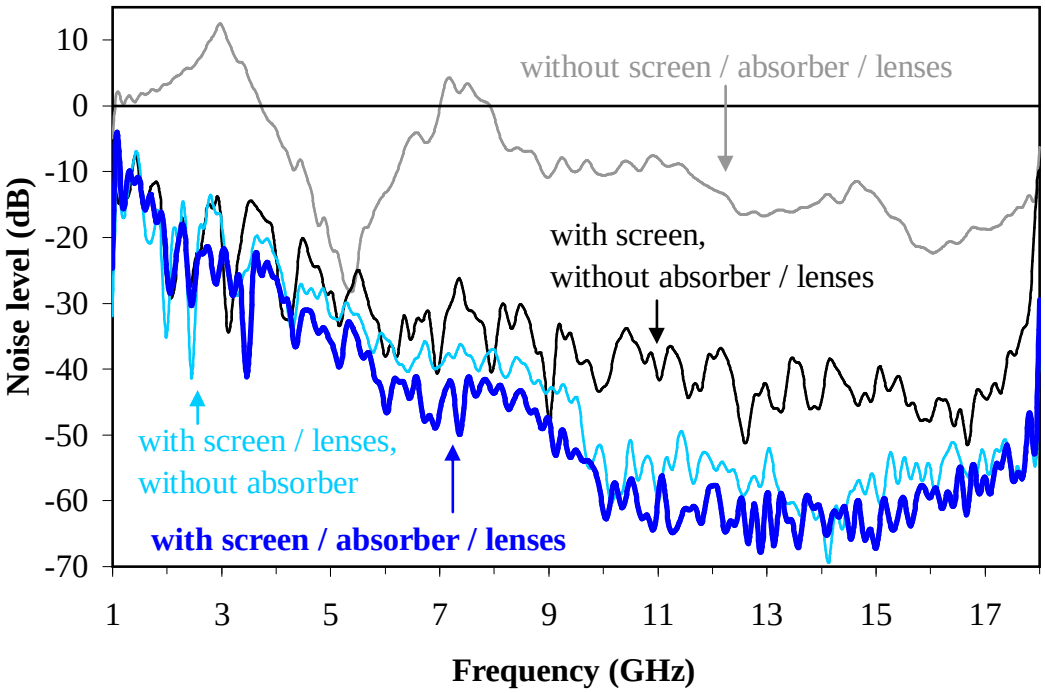

Figure A.4: ***Improvements of the noise level in microwave transmission measurements*** *achieved by introducing microwave screen (initially without absorbing foam), microwave lenses and absorbing foam. Here the noise level corresponds to transmission from one antenna to the other when a reflective metal plate is inserted in the sample holder. 0 dB corresponds to transmission through the sample holder when it is empty.*

Southampton's School of Physics and Astronomy. Furthermore, lens holders that position these lenses in front of the horn antennas were designed and manufactured. The final design, which attaches the lenses to the antenna posts, is shown in Fig. A.3 (c). It allows the lenses to be rotated away from the horn antennas and back into place easily. In order to reduce unwanted reflections the lens holders were made from wood and plastic screws (dielectrics), apart from a few metal screws far away from the beam near the antenna posts. Measurements of the power transmitted through the aperture of the screen indicate that the focusing effect of the lenses results in a typical gain of 10-15 dB, confirming that the microwave beam becomes much more collimated.

Ideally the transmitted power should be high when the sample holder's aperture is empty and it should be negligibly small when this aperture is blocked by a microwave mirror (aluminum plate). The contrast between these two cases is a measure of the noise level of the transmission setup. Fig. A.4 shows how the different improvements of the microwave setup reduced this noise level. Without the screen apparently more microwave energy went around the sample holder than through it, making the paradox

situation possible that at some frequencies more energy reached the receiver when the aperture was blocked by the aluminum plate. Introducing the reflective screen reduced the noise level to around -35 dB. Adding the microwave lenses reduced the noise level further, especially at frequencies above 9 GHz. Here the lenses resulted in an improvement of about 15 dB more. Adding the absorber to the reflective screen pushed the noise level down by an additional $\sim$ 5 dB. These improvements made the reliable characterization of microwave metamaterials possible.

Appendix B

Wallpaper Symmetry Groups

Like all planar periodic structures, planar metamaterials can be classified according to their wallpaper symmetry group [93, 108, 109]. Fig. B.1 shows the symmetries of the unit cell for each of the seventeen wallpaper symmetry groups, using the short form of the crystallographic notation [110].

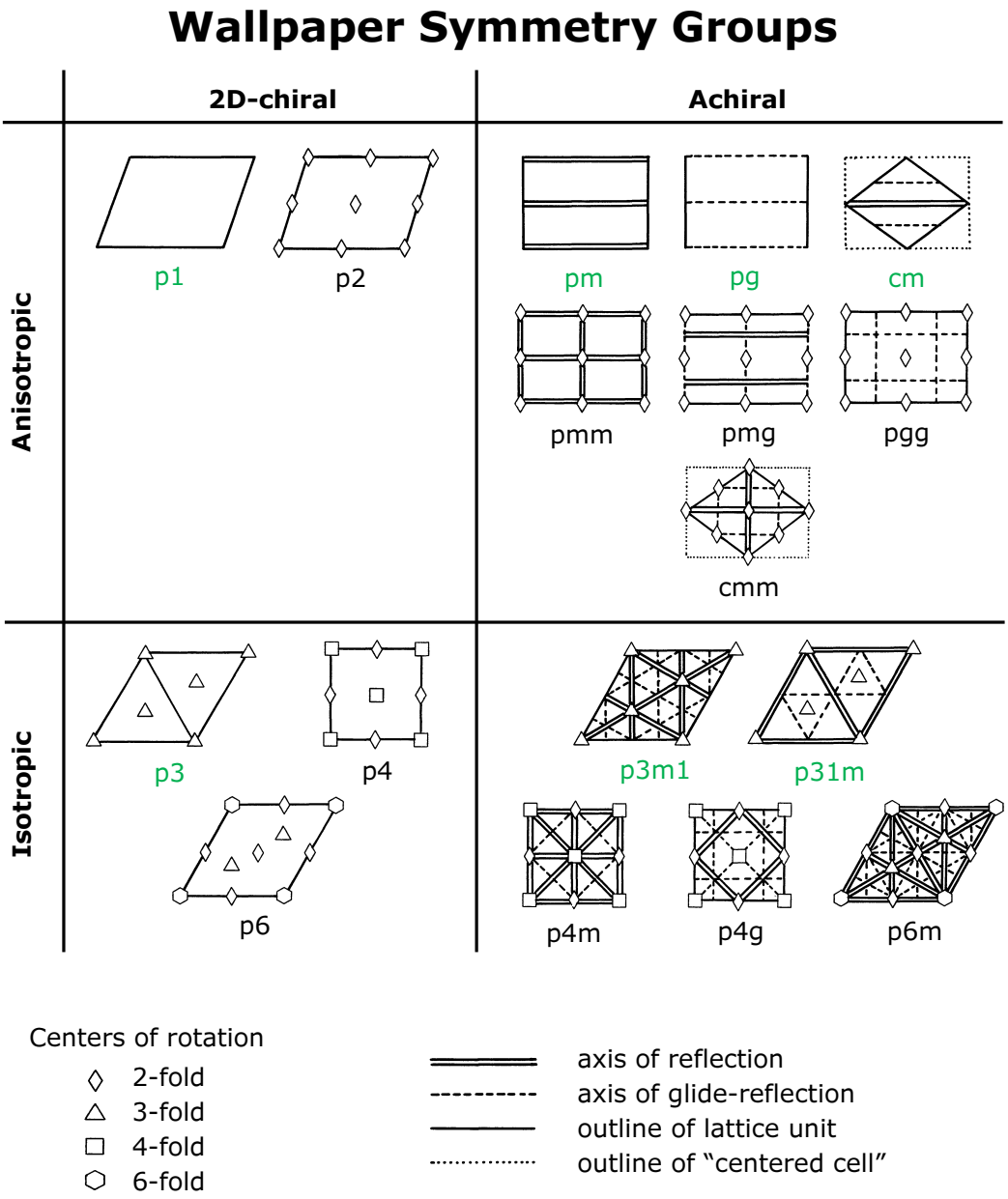

Figure B.1: ***Wallpaper symmetry groups.*** *The unit cells or meta-molecules with symmetries are shown for all seventeen wallpaper symmetry groups. Circular conversion dichroism at normal incidence is exhibited only by lossy patterns that are simultaneously anisotropic and intrinsically 2D-chiral (symmetry groups p1 and p2). Extrinsic 3D-chirality, which leads to optical activity, is possible for oblique incidence on patterns without 2-fold rotational symmetry, which are marked by green labels (symmetry groups p1, pm, pg, cm, p3, p3m1, p31m). This figure has been adapted from chart 2 in [110].*

Appendix C

Resonant Modes in Split Ring Aperture Arrays

As discussed in chapter 2, the scattering properties of planar metamaterials result from the excitation of currents in the conductive parts of such structures. This is true for wire patterns as well as aperture arrays in conductive interfaces.

In case of wire patterns, where the flow of currents is confined to the wires, the possible modes of excitation are relatively easy to predict. In the structures studied in this thesis, the fundamental resonant modes typically correspond to geometrical resonances where half of the effective wavelength matches the length of a resonant wire. Following [57], Fig. C.1 illustrates these resonant modes for asymmetrically split wire rings consisting of two wires of different lengths. In this case the lowest frequency resonances, which are excited by an incident wave polarized parallel to the wires, correspond to (I) an electric dipole excitation of the longer wire, (II) anti-symmetric currents in both wires (giving rise to an effective magnetic dipole) and (III) an electric dipole excitation of the shorter wire.

For aperture arrays the resonant current modes are less obvious. Using COMSOL simulations, here we study the resonances of the Babinet complementary structure (see section 2.2.1) of the asymmetrically split wire ring array: an array of asymmetrically split ring apertures. The simulated structure corresponds to the metamaterial discussed in section 4.4, i.e. a 1 mm thick metal sheet perforated with 1 mm wide apertures corresponding to 160° and 140° arcs of 6 mm radius. These apertures were arranged in

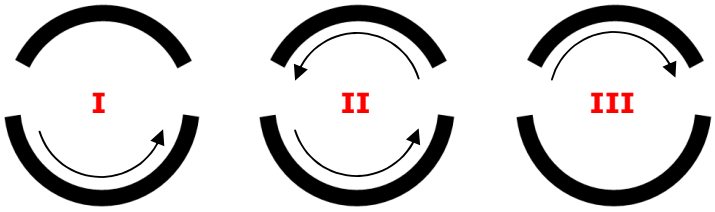

Figure C.1: ***Resonant current modes of asymmetrically split wire rings.*** *These current modes, indicated by arrows, are excited by the polarization parallel to the wires when the effective wavelength is twice as long as the length of the resonant wire(s). The resonance frequency increases form mode (I) to (III), where modes (I) and (III) correspond to high reflectivity and mode (II) corresponds to high transmission. For a detailed analysis refer to [57].*

a square lattice with a period of 15 mm. The metal structure was treated as a perfect electric conductor and the simulations were carried out in the frequency domain for normal incidence onto a single unit cell with periodic boundary conditions.

As illustrated by Fig. C.2 (a), and consistently with experiments, the metamaterial shows strongly resonant behavior around 9 GHz for the **y** polarization (perpendicular to the slits). In this region, the metamaterial properties rapidly change from (I) perfectly transparent to (II) highly reflective and then again to (III) perfectly transparent. Consistently with Babinet's principle this behavior is just opposite to that of the complementary wire structure: The responses for **x** and **y** polarizations as well as the transmission and reflection properties are interchanged. This remarkable behavior is linked to currents excited around the rim of the apertures. For symmetry reasons the currents excited by **y**-polarization must be symmetric with respect to the split ring's mirror line. Thus no current can flow around the center of the apertures. So current oscillations are limited to half the rim of the apertures and similarly to wire split rings, this length corresponds to about half the wavelength at the resonances. Also similarly to wire split rings, the fundamental modes of excitation of the aperture array are linked to (I) the long arc, (II) both arcs and (III) the short arc, see Fig. C.2 (b).

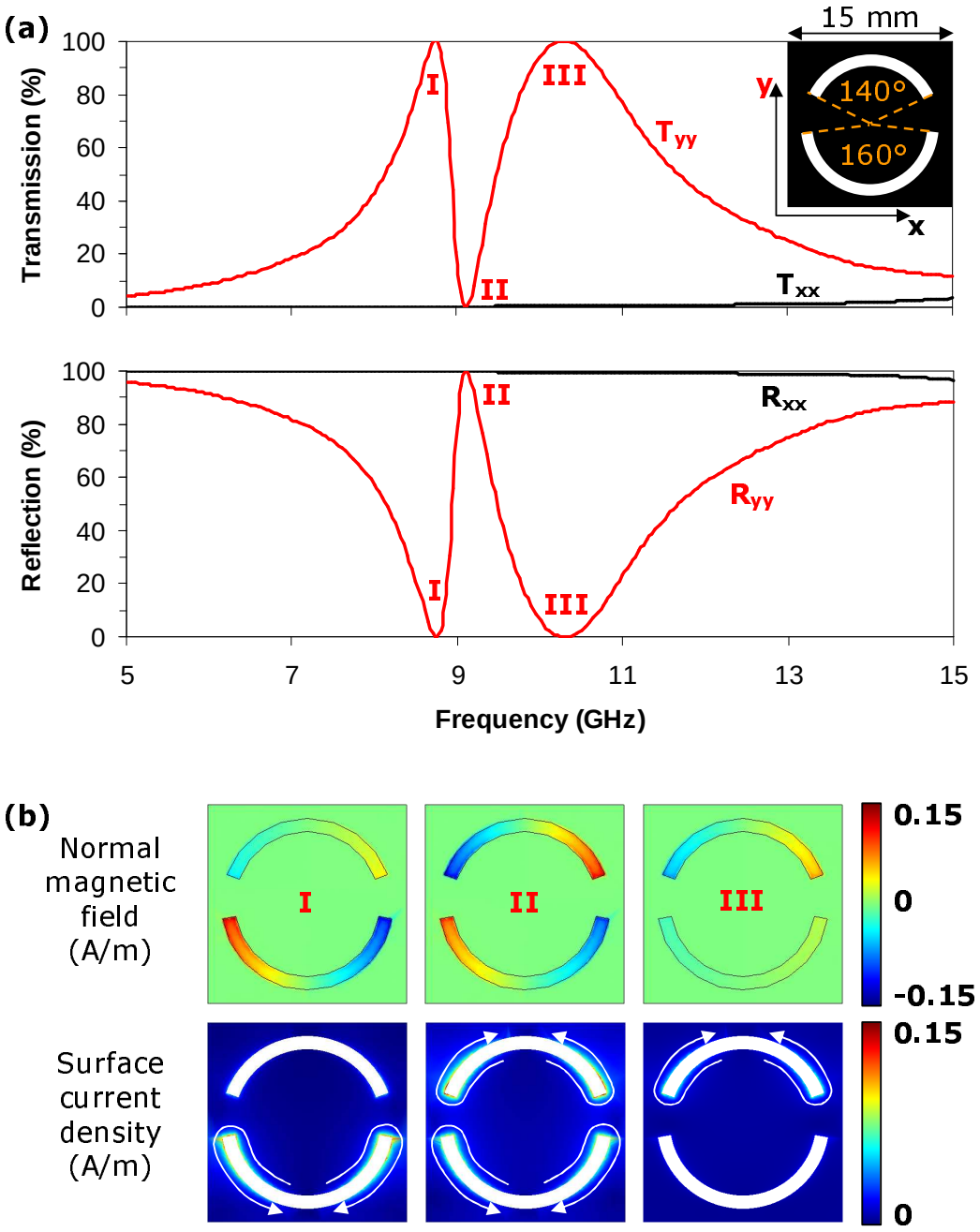

Figure C.2: ***Resonant modes of asymmetrically split ring apertures.*** *(a) Simulated transmission and reflection spectra for normal incidence. (b) Modes of excitation caused by* **y***-polarized incident waves with an electric field strength of 1 V/m. The resonant modes are shown in terms of the normal magnetic field and the magnitude of the surface current density, where the instantaneous direction of the surface currents is indicated by arrows.*

Appendix D

Publications

D.1 Journal Publications

- R. Singh, E. Plum, C. Menzel, C. Rockstuhl, A. K. Azad, R. A. Cheville, F. Lederer, W. Zhang, and N. I. Zheludev. "Terahertz metamaterial with asymmetric transmission". *Phys. Rev. B*, 80:153104, 2009.

- E. Plum, V. A. Fedotov, and N. I. Zheludev. "Extrinsic electromagnetic chirality in metamaterials". *J. Opt. A: Pure Appl. Opt.*, 11:074009, 2009.

- E. Plum, V. A. Fedotov, P. Kuo, D. P. Tsai, and N. I. Zheludev. "Towards the lasing spaser: controlling metamaterial optical response with semiconductor quantum dots". *Opt. Express*, 17(10):8548, 2009.

- E. Plum, V. A. Fedotov, and N. I. Zheludev. "Planar metamaterial with transmission and reflection that depend on the direction of incidence". *Appl. Phys. Lett.*, 94:131901, 2009.

- E. Plum, X.-X. Liu, V. A. Fedotov, Y. Chen, D. P. Tsai, and N. I. Zheludev. "Metamaterials: optical activity without chirality". *Phys. Rev. Lett.*, 102:113902, 2009.

- E. Plum, J. Zhou, J. Dong, V. A. Fedotov, T. Koschny, C. M. Soukoulis, and N. I. Zheludev. "Metamaterial with negative index due to chirality". *Phys. Rev. B*, 79:035407, 2009.

- E. Plum, V. A. Fedotov, and N. I. Zheludev. "Optical activity in extrinsically chiral metamaterial". *Appl. Phys. Lett.*, 93:191911, 2008.

- E. Plum, V. A. Fedotov, A. S. Schwanecke, N. I. Zheludev, and Y. Chen. "Giant optical gyrotropy due to electromagnetic coupling". *Appl. Phys. Lett.*, 90:223113, 2007. Also selected for *Virtual Journal of Nanoscale Science & Technology*, 15(23), 2007.

D.2 Submitted

- E. Plum and N. I. Zheludev. *Structured Surfaces as Optical Metamaterials*, chapter Chirality and Anisotropy of Planar Metamaterials. Cambridge University Press, submitted.

- E. Plum, V. A. Fedotov, and N. I. Zheludev. "Asymmetric transmission: a generic property of two-dimensional periodic patterns". *Phys. Rev. E*, submitted.

- V. A. Fedotov, N. Papasimakis, E. Plum, A. Bitzer, M. Walther, P. Kuo, D. P. Tsai, and N. I. Zheludev. "Spectral collapse in ensembles of meta-molecules". *Phys. Rev. Lett.*, submitted.

D.3 Conference Contributions

- (invited) E. Plum, V. A. Fedotov, and N. I. Zheludev. "Intrinsic and extrinsic 2D chirality in metamaterials: an easy route to asymmetric transmission". *Metamaterials: Fundamentals and Applications III*, San Diego, CA, USA, 01 - 05 Aug 2010

- (keynote) N. I. Zheludev, A. Nikolaenko, K. F. MacDonald, V. A. Fedotov, D. Hewak, G. Adamo, Z. Smson, E. Plum, D. P. Tsai, E. Difabrizio, and F. De Angelis. "Nonlinear and switchable plasmonic metamaterials". *Progress in Electromagnetics Research Symposium (PIERS 2010)*, Xi'an, China, 22 - 26 Mar 2010

- (invited) N. I. Zheludev, V. A. Fedotov, N. Papasimakis, E. Plum, and J. Shi. "Metamaterials - from modeling and fabrication to application". *2009 MRS Fall Meeting*, Boston, Massachusetts, USA, 30 Nov - 4 Dec 2009

- (invited) E. Plum. "Metamaterials: the next photonic revolution". *Marconi Society Annual Symposium*, Bologna, Italy, 8 - 10 Oct 2009

- (keynote) N. I. Zheludev, V. A. Fedotov, E. Plum, and N. Papasimakis. "Coherent metamaterials". *Metamaterials 2009 Congress*, London, UK, 30 Aug - 4 Sep 2009

- (invited) E. Plum, V. A. Fedotov, X.-X. Liu, and N. I. Zheludev; [presenter: K. F. MacDonald]. "Tunable chirality in photonic metamaterials". *Metamaterials: Fundamentals and Applications II*, San Diego, California, USA, 2 - 6 Aug 2009

- (invited) N. Papasimakis, E. Plum, V. A. Fedotov, and N. I. Zheludev. "Mimicking EIT, BEC, ferromagnetism, the Mössbauer and the Bunn effects in photonic metamaterials". *ICMAT 2009*, Singapore, 28 Jun - 3 Jul 2009

- (oral) E. Plum, X.-X. Liu, V. A. Fedotov, Y. Chen, D. P. Tsai, N. I. Zheludev. "Tuning chirality in photonic metamaterials with semiconductor quantum dots". *CLEO/Europe-EQEC*, Munich, Germany, 14 - 19 Jun 2009

- (invited) E. Plum, V. A. Fedotov, and N. I. Zheludev. "Twisting the double-helix of light with metamaterials". *Electrical, Transport and Optical Properties of Inhomogeneous Media (ETOPIM) 8*, Rethymnon, Crete, Greece, 7-12 Jun 2009

- (oral) E. Plum, X.-X. Liu, V. A. Fedotov, Y. Chen, D. P. Tsai, and N. I. Zheludev. "Optical activity in achiral metamaterials". *IQEC 09*, Baltimore, Maryland, USA, 31 May - 5 Jun 2009

- (poster) J. Zhou, B. Wang, E. Plum, T. Koschny, V. A. Fedotov, H.-T. Chen, A. J. Taylor, J. O'Hara, N. I. Zheludev and C. Soukoulis. "Chiral metamaterials with negative refractive index". *International Workshop on Electromagnetic Metamaterials III*, Los Alamos, New Mexico, USA, 18 - 19 May 2009

- (oral) E. Plum, X.-X. Liu, V. A. Fedotov, Y. Chen, D. P. Tsai and N. I. Zheludev. "Gyrotropy in photonic metamaterials due to extrinsic chirality". *NANOMETA 2009*, Seefeld, Austria, 5 - 8 Jan 2009

- (oral) E. Plum, V. A. Fedotov, and N. I. Zheludev. "Optical activity without chirality: a new way to negative index metamaterials". *Plasmonics and Metamaterials (META)*, Rochester, New York, USA, 20 - 23 Oct 2008

- (poster) E. Plum, J. Zhou, J. Dong, V. A. Fedotov, T. Koschny, C. M. Soukoulis, and N. I. Zheludev. "Negative refraction in 3-d-chiral metamaterial". *Plasmonics and Metamaterials (META)*, Rochester, New York, USA, 20 - 23 Oct 2008

- (invited) V. A. Fedotov, N. Papasimakis, E. Plum, S. L. Prosvirnin, and N. I. Zheludev. "Metamaterials enter the physics playground: from EIT to lasing spaser". *Metamaterials 2008*, Pamplona, Spain, 23 - 26 Sep 2008

- (oral) E. Plum, A. S. Schwanecke, V. A. Fedotov, N. I. Zheludev, Y. Chen, V. V. Khardikov and S. L. Prosvirnin. "Asymmetric transmission through planar chiral photonic nanostructures". *IoP Quantum Electronics and Photonics Conference (QEP-18)*, Edinburgh, UK, 26 - 29 Aug 2008

- (oral) V. A. Fedotov, E. Plum, C. Soukoulis, and N. I. Zheludev. "Optical magnetism in chiral metamaterials". *META'08 NATO Advanced Research Workshop on Metamaterials for Secure Information and Communication Technologies*, Marrakesh, Morocco, 7 - 10 May 2008

- (oral) E. Plum, V. A. Fedotov, and N. I. Zheludev. "Asymmetric transmission through chiral symmetry breaking in planar metamaterials". *QELS 2008*, San Jose, CA, USA, 4 - 9 May 2008.

- (oral) E. Plum, J. Dong, J. Zhou, V. A. Fedotov, T. Koschny, C. Soukoulis, and N. I. Zheludev. "3D-chiral metamaterial with artificial magnetic response". *QELS 2008*, San Jose, CA, USA, 4 - 9 May 2008.

- (invited) N. I. Zheludev, V. A. Fedotov, N. Papasimakis, E. Plum, and S. L. Prosvirnin. "Close-mode resonances in metamaterials and lasing spaser". *Photonics Europe (SPIE Europe)*, Strasbourg, France, 7 - 11 Apr 2008.

- (invited) V. A. Fedotov, E. Plum, A. S. Schwanecke, Y. Chen, V. V. Khardikov, S. L. Prosvirnin, and N. I. Zheludev. "Planar and layered chiral meta-surfaces".

Metamaterials 2007: First International Congress on Advanced Electromagnetic Materials in Microwaves and Optics, Rome, Italy, 22 - 26 Oct 2007.

- (invited) N. I. Zheludev, V. A. Fedotov, A. S. Schwanecke, E. Plum, N. Papasimakis, and K. Marinov. "Plasmon resonances in photonic chiral metamaterials". *Frontiers in Optics 2007*, San Jose, CA, USA, 16 - 20 Sep 2007.

- (oral) V. A. Fedotov, E. Plum, A. S. Schwanecke, Y. Chen, and N. I. Zheludev. "Metamaterials with giant optical activity". *CLEO/Europe-IQEC2007*, Munich, Germany, 17 - 22 Jun 2007.

- (oral) V. A. Fedotov, A. S. Schwanecke, E. Plum, N. I. Zheludev, V. V. Khardikov, and S. L. Prosvirnin. "Enantiomerically sensitive plasmons". *Surface Plasmon Photonics SPP-3*, Dijon, France, 17 - 22 Jun 2007.

- (oral) V. A. Fedotov, E. Plum, A. S. Schwanecke, Y. Chen, V. V. Khardikov, S. L. Prosvirnin, and N. I. Zheludev. "Photonic chiral metamaterials". *Photonic Metamaterials: From Random to Periodic*, Jackson Hole, Wyoming, USA, 4 - 7 Jun 2007.

- (oral) V. A. Fedotov, E. Plum, Y. Chen, A. S. Schwanecke, and N. I. Zheludev. "Chiral photonic metamaterial". *QELS (CLEO/QELS 2007)*, Baltimore, MD, USA, 6 - 11 May 2007.

- (poster) V. A. Fedotov, E. Plum, Y. Chen, A. S. Schwanecke, and N. I. Zheludev. "Giant microwave and optical gyrotropy in bilayered chiral metamaterials". *NANOMETA 2007*, Seefeld, Austria, 9 - 11 Jan 2007.

References

[1] S. Kinoshita. *Structural colors in the realm of nature*. World Scientific Publishing, 2008.

[2] P. Vukusic and J. R. Sambles. "Photonic structures in biology". *Nature*, 424:852, 2003.

[3] D. G. Stavenga, S. Foletti, G. Palasantzas, and K. Arikawa. "Light on the moth-eye corneal nipple array of butterflies". *Proceedings of the Royal Society B*, 273:661, 2006.

[4] V. Sharma, M. Crne, J. O. Park, and M. Srinivasarao. "Structural origin of circularly polarized iridescence in jeweled beetles". *Science*, 325:449, 2009.

[5] "Mineral Spectroscopy Server, Caltech". `minerals.caltech.edu/Silica_Polymorphs/`, 13 Nov 2009.

[6] U. Leonhardt. "Invisibility cup". *Nature Photonics*, 1:207, 2007.

[7] "The Lycurgus Cup". The British Museum website, `www.britishmuseum.org`, 14 Nov 2009.

[8] P. Preuss. "Making the buckyballs ring". *The Berkeley Lab View*, April 1st, 2005.

[9] J. Fraunhofer. "Kurzer Bericht von den Resultaten neuerer Versuche ber die Gesetze des Lichtes, und die Theorie derselben". *Annalen der Physik*, 74(8):337, 1823.

[10] J. C. Maxwell. "A dynamical theory of the electromagnetic field". *Philosophical Transactions of the Royal Society of London*, 155:459, 1865.

[11] J. W. S. Rayleigh. "On the maintenance of vibrations by forces of double frequency, and on the propagation of waves through a medium endowed with a periodic structure". *Phil. Mag.*, 24:145, 1887.

[12] J. W. S. Rayleigh. "On the remarkable phenomenon of crystalline reflexion described by Prof. Stokes". *Phil. Mag.*, 26:256, 1888.

[13] J. C. Bose. "On the selective conductivity exhibited by some polarising substances". *Roy. Proc. Soc.*, 60:433, 1896.

[14] J. C. Bose. "On the rotation of plane of polarization of electric waves by a twisted structure". *Proceedings of the Royal Society of London*, 63:146–152, 1898.

[15] D. T. Emerson. "The works of Jagadis Chandra Bose: 100 years of mm-wave research". *IEEE Transactions on Microwave Theory and Techniques*, 45:2267, 1997.

[16] R. Ott, R. Kouyoumjian, and L. Peters, Jr. "Scattering by a twodimensional periodic array of narrow plates". *Radio Sci.*, 2:1347, 1967.

[17] C. Chen. "Scattering by a two-dimensional periodic array of conducting plates". *IEEE Trans. Antennas Propagat.*, AP-18:660, 1970.

[18] B. Munk, R. Kouyoumjian, and L. Peters Jr. "Reflection properties of periodic surfaces of loaded dipoles". *IEEE Trans. Antennas Propagat.*, AP-19:612, 1971.

[19] Ben A. Munk. *Frequency Selective Surfaces: Theory and Design.* Wiley-Interscience, 1st edition, 2000.

[20] J. Huang, T. K. Wu, and S. W. Lee. "Tri-band frequency-selective surface with circular ring elements". *IEEE T. Antenn. Propag.*, 42(2):166, 1994.

[21] R. Ulrich. "Far infrared properties of metallic mesh and its complementary structure". *Infrared Phys.*, 7(1):37, 1967.

[22] V. P. Tomaselli, D. C. Edewaard, P. Gillan, and K. D. Möller. "Far infrared bandpass filters from cross shaped grids". *Appl. Opt.*, 20:1361, 1981.

[23] J. A. Bossard, D. H. Werner, T. S. Mayer, J. A. Smith, Y. U. Tang, R. P. Drupp, and L. Li. "The design and fabrication of planar multiband metallodielectric frequency selective surfaces for infrared applications". *IEEE Transactions on Antennas and Propagation*, 54(4):1265, 2006.

[24] P. Russell. "Photonic crystal fibers". *Science*, 299:358, 2003.

[25] O. L. J. Pursiainen, J. J. Baumberg, H. Winkler, B. Viel, P. Spahn, and T. Ruhl. "Nanoparticle-tuned structural color from polymer opals". *Opt. Exp.*, 15:9553, 2007.

[26] E. Yablonovitch. "Inhibited Spontaneous Emission in Solid-State Physics and Electronics". *Physical Review Letters*, 58(20):2059, 1987.

[27] S. John. "Strong localization of photons in certain disordered dielectric superlattices". *Physical Review Letters*, 58(23):2486, 1987.

[28] J. J. Wierer, M. R. Krames, J. E. Epler, N. F. Gardner, M. G. Craford, J. R. Wendt, J. A. Simmons, and M. M. Sigalas. "InGaN/GaN quantum-well heterostructure light-emitting diodes employing photonic crystal structures". *Appl. Phys. Lett.*, 84:3885, 2004.

[29] A. Sihvola. "Metamaterials in electromagnetics". *Metamaterials*, 1:2, 2007.

[30] Karl F. Lindman. "Über eine durch ein isotropes System von spiralförmigen Resonatoren erzeugte Rotationspolarisation der elektromagnetischen Wellen". *Ann. Phys.*, 368(23):621, 1920.

[31] J. Brown. "Artificial dielectrics having refractive indices less than unity". *Proc. IEE*, 100(62R):51, 1953.

[32] W. Rotman. "Plasma simulation by artificial dielectric and parallel-plate media". *IRE Transactions on Antennas and Propagation*, 10:82, 1962.

[33] D. J. Robbins J. B. Pendry, A. J. Holden and W. J. Stewart. "Magnetism from conductors and enhanced nonlinear phenomena". *IEEE Trans. Microwave Theory Tech.*, 47(11):2075, 1999.

[34] W. N. Hardy and L. A. Whitehead. "Split-ring resonator for use in magnetic resonance from 200-2000 MHz". *Rev. Sci. Instrum.*, 52(2):213, 1981.

[35] D. R. Smith, W. J. Padilla, D. C. Vier, S. C. Nemat-Nasser, and S. Schultz. "Composite Medium with Simultaneously Negative Permeability and Permittivity". *Phys. Rev. Lett.*, 84:4184, 2000.

[36] V. G. Veselago. "The Electrodynamics of Substances with Simultaneously Negative Values of ε and μ". *Sov. Phys. Uspekhi*, 10:509, 1968.

[37] J. B. Pendry. "Negative Refraction Makes a Perfect Lens". *Phys. Rev. Lett.*, 85:3966, 2000.

[38] R. A. Shelby, D. R. Smith, and S. Schultz. "Experimental Verification of a Negative Index of Refraction". *Science*, 292:77, 2001.

[39] A. Grbic and G. V. Eleftheriades. "Overcoming the diffraction limit with a planar left-handed transmission-line lens". *Phys. Rev. Lett.*, 92:117403, 2004.

[40] J. Zhou, T. Koschny, M. Kafesaki, E. N. Economou, J. B. Pendry, and C. M. Soukoulis. "Saturation of the magnetic response of split-ring resonators at optical frequencies". *Physical Review Letters*, 95:223902, 2005.

[41] V. M. Shalaev, W. Cai, U. K. Chettiar, H.-K. Yuan, A. K. Sarychev, V. P. Drachev, and A. V. Kildishev. "Negative index of refraction in optical metamaterials". *Opt. Lett.*, 30:3356, 2005.

[42] Gunnar Dolling, Christian Enkrich, Martin Wegener, C. M. Soukoulis, and Stefan Linden. "Simultaneous Negative Phase and Group Velocity of Light in a Metamaterial". *Science*, 312:892, 2006.

[43] G. Dolling, M. Wegener, C. M. Soukoulis, and S. Linden. "Negative-index metamaterial at 780 nm wavelength". *Opt. Lett.*, 32:53, 2007.

[44] C. M. Soukoulis. "Negative index materials". CLEO/Europe, Munich, Germany, 2007. abstract no. CK1-1-MON.

[45] J. B. Pendry, D. Schurig, and D. R. Smith. "Controlling electromagnetic fields". *Science*, 312:1780, 2006.

[46] U. Leonhardt. "Optical conformal mapping". *Science*, 312:1777, 2006.

[47] W. Cai, U. K. Chettiar, A. V. Kildishev, and V. M. Shalaev. "Optical cloaking with metamaterials". *Nature Photonics*, 1:224, 2007.

[48] D. Schurig, J. J. Mock, B. J. Justice, S. A. Cummer, J. B. Pendry, A. F. Starr, and D. R. Smith. "Metamaterial electromagnetic cloak at microwave frequencies". *Science*, 314:977, 2006.

[49] J. Valentine, J. Li, T. Zentgraf, G. Bartal, and X. Zhang. "An optical cloak made of dielectrics". *Nature Materials*, 8:568, 2009.

[50] E. Plum, V. A. Fedotov, A. S. Schwanecke, N. I. Zheludev, and Y. Chen. "Giant optical gyrotropy due to electromagnetic coupling". *Appl. Phys. Lett.*, 90:223113, 2007.

[51] E. Plum, J. Zhou, J. Dong, V. A. Fedotov, T. Koschny, C. M. Soukoulis, and N. I. Zheludev. "Metamaterial with negative index due to chirality". *Phys. Rev. B*, 79:035407, 2009.

[52] S. Zhang, Y.-S. Park, J. Li, X. Lu, W. Zhang, and X. Zhang. "Negative refractive index in chiral metamaterials". *Phys. Rev. Lett.*, 102:023901, 2009.

[53] V. A. Fedotov, P. L. Mladyonov, S. L. Prosvirnin, and N. I. Zheludev. "Planar electromagnetic metamaterial with a fish scale structure". *Phys. Rev. E*, 72(5):056613, 2005.

[54] X. G. Peralta, E. I. Smirnova, A. K. Azad, H.-T. Chen, A. J. Taylor, I. Brener, and J. F. O'Hara. "Metamaterials for THz polarimetric devices". *Opt. Express*, 17(2):773, 2009.

[55] E. Plum, V. A. Fedotov, and N. I. Zheludev. "Optical activity in extrinsically chiral metamaterial". *Appl. Phys. Lett.*, 93:191911, 2008.

[56] E. Plum, X.-X. Liu, V. A. Fedotov, Y. Chen, D. P. Tsai, and N. I. Zheludev. "Metamaterials: optical activity without chirality". *Phys. Rev. Lett.*, 102:113902, 2009.

[57] V. A. Fedotov, M. Rose, S. L. Prosvirnin, N. Papasimakis, and N. I. Zheludev. "Sharp Trapped-Mode Resonances in Planar Metamaterials with a Broken Structural Symmetry". *Phys. Rev. Lett.*, 99:147401, 2007.

[58] N. Papasimakis, V. A. Fedotov, S. L. Prosvirnin, and N. I. Zheludev. "Metamaterial analog of electromagnetically induced transparency". *Physical Review Letters*, 101:253903, 2008.

[59] S. Zhang, D. A. Genov, Y. Wang, M. Liu, and X. Zhang. "Plasmon-induced transparency in metamaterials". *Physical Review Letters*, 101:047401, 2008.

[60] N. Liu, T. Weiss, M. Mesch, L. Langguth, U. Eigenthaler, M. Hirscher, C. Sönnichsen, and H. Giessen. "Planar Metamaterial Analogue of Electromagnetically Induced Transparency for Plasmonic Sensing". *Nano Lett.*, advance online publication, 2009.

[61] P. Tassin, L. Zhang, T. Koschny, E. N. Economou, and C. M. Soukoulis. "Low-Loss Metamaterials Based on Classical Electromagnetically Induced Transparency". *Phys. Rev. Lett.*, 102:053901, 2009.

[62] N. I. Zheludev, S. L. Prosvirnin, N. Papasimakis, and V. A. Fedotov. "Lasing spaser". *Nature Photonics*, 2:351, 2008.

[63] E. Plum, V. A. Fedotov, P. Kuo, D. P. Tsai, and N. I. Zheludev. "Towards the lasing spaser: controlling metamaterial optical response with semiconductor quantum dots". *Opt. Express*, 17(10):8548, 2009.

[64] V. A. Fedotov, P. L. Mladyonov, S. L. Prosvirnin, A.V. Rogacheva, Y. Chen, and N. I. Zheludev. "Asymmetric Propagation of Electromagnetic Waves through a Planar Chiral Structure". *Phys. Rev. Lett.*, 97:167401, 2006.

[65] Lord Kelvin. *Baltimore Lectures on Molecular Dynamics and the Wave Theory of Light*, page 619. C.J. Clay and Sons, Cambridge University Press Warehouse, London, 1904.

[66] `www.nanotubes.com.cn`, 6 Oct 2008.

[67] Wikipedia Commons, `en.wikipedia.org/wiki/File:DNA_Overview.png`, 6 Oct 2008.

[68] Wikimedia Commons, `commons.wikimedia.org/wiki/Image:Turitellidae.jpg`, 6 Oct 2008.

[69] R. Raval. "Chemistry: Mirrors in Flatland". *Nature*, 425:463, 2003.

[70] R. L. Fullman and D. L. Wood. "Origin of spiral eutectic structures". *Acta Metallurgica*, 2:188, 1954.

[71] A. V. Rogacheva, V. A. Fedotov, A. S. Schwanecke, and N. I. Zheludev. "Giant Gyrotropy due to Electromagnetic-Field Coupling in a Bilayered Chiral Structure". *Phys. Rev. Lett.*, 97:177401, 2006.

[72] F. J. D. Arago. "Mémoire sur une modification remarquable qu'éprouvent les rayons lumineux dans leur passage à travers certains corps diaphanes et sur quelques autres nouveaux phénomènes d'optique". *Mémoires de la classe des sciences math. et phys. de l'Institut Impérial de France*, 1:93, 1811.

[73] L. Pasteur. "Mémoire sur la relation qui peut exister entre la forme cristalline et la composition chimique, et sur la cause de la polarization rotatoire". *C. R. Acad. Sci. Paris*, 26:535, 1848.

[74] I. Tinoco and M. P. Freeman. "The Optical Activity of Oriented Copper Helices. I. Experimental". *J. Phys. Chem.*, 61:1196, 1957.

[75] R. D. Hollinger, V. V. Varadan, D. K. Ghodgaonkar, and V. K. Varadan. "Experimental characterization of isotropic chiral composites in circular waveguides". *Radio Sci.*, 27:161, 1992.

[76] I. Hodgkinson, Q. H. Wu, B. Knight, A. Lakhtakia, and K. Robbie. "Vacuum deposition of chiral sculptured thin films with high optical activity". *Appl. Opt.*, 39:642, 2000.

[77] M. Thiel, M. Decker, M. Deubel, M. Wegener, S. Linden, and G. v. Freymann. "Polarization Stop Bands in Chiral Polymeric Three-Dimensional Photonic Crystals". *Adv. Mater.*, 19:207, 2007.

[78] M. Thiel, M. S. Rill, G. von Freymann, and M. Wegener. "Three-dimensional bi-chiral photonic crystals". *Adv. Mater.*, 21:4680, 2009.

[79] J. K. Gansel, M. Thiel, M. S. Rill, M. Decker, K. Bade, V. Saile, G. von Freymann, S. Linden, and M. Wegener. "Gold helix photonic metamaterial as broadband circular polarizer". *Science*, 325:1513, 2009.

[80] M. Kuwata-Gonokami, N. Saito, Y. Ino, M. Kauranen, K. Jefimovs, T. Vallius, J. Turunen, and Y. Svirko. "Giant Optical Activity in Quasi-Two-Dimensional Planar Nanostructures". *Phys. Rev. Lett.*, 95:227401, 2005.

[81] M. Decker, M. W. Klein, M. Wegener, and S. Linden. "Circular dichroism of planar chiral magnetic metamaterials". *Opt. Lett.*, 32:856, 2007.

[82] B. V. Bokut', V. V. Gvozdev, and A. N. Serdyukov. "Peculiar waves in naturally gyrotropic media". *J. Appl. Spectrosc.*, 34(4):460, 1981.

[83] J. B. Pendry. "A Chiral Route to Negative Refraction". *Science*, 306:1353, 2004.

[84] S. Tretyakov, I. Nefedov, A. Sihvola, S. Maslovski, and C. Simovski. "Waves and Energy in Chiral Nihility". *J. Electromagn. Waves Appl.*, 17:695, 2003.

[85] S. Tretyakov, A. Sihvola, and L. Jylhä. "Backward-wave regime and negative refraction in chiral composites". *Photonics Nanostruct. Fundam. Appl.*, 3:107, 2005.

[86] C. Monzon and D. W. Forester. "Negative Refraction and Focusing of Circularly Polarized Waves in Optically Active Media". *Phys. Rev. Lett.*, 95:123904, 2005.

[87] Y. Svirko, N. Zheludev, and M. Osipov. "Layered chiral metallic microstructures with inductive coupling". *Appl. Phys. Lett.*, 78:498, 2001.

[88] M. Decker, M. Ruther, C. E. Kriegler, J. Zhou, C. M. Soukoulis, S. Linden, and M. Wegener. "Strong optical activity from twisted-cross photonic metamaterials". *Opt. Lett.*, 34:2501, 2009.

[89] J. Zhou, J. Dong, B. Wang, T. Koschny, M. Kafesaki, and C. M. Soukoulis. "Negative refractive index due to chirality". *Phys. Rev. B*, 79:121104(R), 2009.

[90] A. S. Schwanecke, V. A. Fedotov, V. V. Khardikov, S. L. Prosvirnin, Y. Chen, and N. I. Zheludev. "Nanostructured metal film with asymmetric optical transmission". *Nano Lett.*, 8:2940, 2008.

[91] L. Hecht and L. D. Barron. "Rayleigh and Raman optical activity from chiral surfaces". *Chem. Phys. Lett.*, 225:525, 1994.

[92] L. R. Arnaut and L. E. Davis. "Dispersion charcteristics of planar chiral structures". In *Proceedings of the International Conference on Electromagnetics in Advnaced Applications*, pages 381–388, Swanley, UK, 1995. Nexus Media.

[93] A. Papakostas, A. Potts, D.M. Bagnall, S. L. Prosvirnin, H. J. Coles, and N. I. Zheludev. "Optical Manifestations of Planar Chirality". *Phys. Rev. Lett.*, 90:107404, 2003.

[94] S. L. Prosvirnin and N. I. Zheludev. "Polarization effects in the diffraction of light by a planar chiral structure". *Phys. Rev. E*, 71:037603, 2005.

[95] R. Singh, E. Plum, C. Menzel, C. Rockstuhl, A. K. Azad, R. A. Cheville, F. Lederer, W. Zhang, and N. I. Zheludev. "Terahertz metamaterial with asymmetric transmission". *Phys. Rev. B*, 80:153104, 2009.

[96] Aurlien Drezet, Cyriaque Genet, Jean-Yves Laluet, and Thomas W. Ebbesen. "Optical chirality without optical activity: How surface plasmons give a twist to light". *Opt. Exp.*, 16:12559, 2008.

[97] V. A. Fedotov, A. S. Schwanecke, N. I. Zheludev, V. V. Khardikov, and S. L. Prosvirnin. "Asymmetric transmission of light and enantiomerically sensitive plasmon resonance in planar chiral nanostructures". *Nano Lett.*, 7:1996–1999, 2007.

[98] E. Plum, V. A. Fedotov, and N. I. Zheludev. "Planar metamaterial with transmission and reflection that depend on the direction of incidence". *Appl. Phys. Lett.*, 94:131901, 2009.

[99] E. Plum, V. A. Fedotov, and N. I. Zheludev. "Extrinsic electromagnetic chirality in metamaterials". *J. Opt. A: Pure Appl. Opt.*, 11:074009, 2009.

[100] H. Tamada, T. Doumuki, T. Yamaguchi, and S. Matsumoto. "Al wire-grid polarizer using the s-polarization resonance effect at the 0.8-mu m-wavelength band". *Opt. Lett.*, 22(6):419, 1997.

[101] S. W. Ahn, K. D. Lee, J. S. Kim, S. H. Kim, J. D. Park JD, S. H. Lee, and P. W. Yoon. "Fabrication of a 50 nm half-pitch wire grid polarizer using nanoimprint lithography". *Nanotechnology*, 16(9):1874, 2005.

[102] N. Papasimakis and N. I. Zheludev. "Metamaterial-induced transparency". *Optics & Photonics News*, 20:22, 2009.

[103] A. N. Serdyukov, I. V. Semchenko, S. A. Tretyakov, and A. Sihvola. *Electromagnetics of bi-anisotropic materials: Theory and applications*. Gordon and Breach Science Publishers, 2001.

[104] T. G. Mackay and A. Lakhtakia. *Electromagnetic Anisotropy and Bianisotropy*. World Scientific Publishing, 2010.

[105] J. A. Kong. *Electromagnetic Wave Theory*. EMW Publishing, Cambridge, MA, 2005.

[106] J. D. Jackson. *Classical Electrodynamics*. Wiley, New York, 3rd edition, 1999.

[107] F. Falcone, T. Lopetegi, M. A. G. Laso, J. D. Baena, J. Bonache, M. Beruete, R. Marqués, F. Martín, and M. Sorolla. "Babinet Principle Applied to the Design of Metasurfaces and Metamaterials". *Phys. Rev. Lett.*, 93(19):197401, 2004.

[108] W. J. Padilla. "Group theoretical description of artificial electromagnetic metamaterials". *Opt. Express*, 15:1639, 2007.

[109] C. M. Bingham, H. Tao, X. Liu, R. D. Averitt, X. Zhang, and W. J. Padilla. "Planar wallpaper group metamaterials for novel terahertz applications". *Opt. Express*, 16:18565, 2008.

[110] D. Schattschneider. "The Plane Symmetry Groups: Their Recognition and Notation". *The American Mathematical Monthly*, 85(6):439, 1978.

[111] C. W. Bunn. *Chemical Crystallography*, page 88. Oxford University Press, New York, 1945.

[112] R. Williams. "Optical Rotatory Effect in the Nematic Liquid Phase of p-Azoxyanisole". *Phys. Rev. Lett.*, 21:342–344, 1968.

[113] R. Williams. "Optical-rotary power and linear electro-optic effect in nematic liquid crystals of p-azoxyanisole". *J. Chem. Phys.*, 50:1324, 1969.

[114] S. V. Zhukovsky, A. V. Novitsky, and V. M. Galynsky. "Elliptical dichroism: operating principle of planar chiral metamaterials". *Opt. Lett.*, 34(13):1988, 2009.

[115] E. Plum, V. A. Fedotov, and N. I. Zheludev. "Asymmetric transmission: a generic property of two-dimensional periodic patterns". *Phys. Rev. E*, submitted.

[116] B. Ferguson and X.-C. Zhang. "Materials for terahertz science and technology". *Nat. Mater.*, 1:26, 2002.

[117] T. J. Yen, W. J. Padilla, N. Fang, D. C. Vier, D. R. Smith, J. B. Pendry, D. N. Basov, and X. Zhang. "Terahertz Magnetic Response from Artificial Materials". *Science*, 303:1494, 2004.

[118] S. Linden, C. Enkrich, M. Wegener, J. Zhou, T. Koschny, and C. M. Soukolis. "Magnetic response of metamaterials at 100 Terahertz". *Science*, 306:1351, 2004.

[119] H. O. Moser, B. D. F. Casse, O. Wilhelmi, and B. T. Saw. "Terahertz Response of a Microfabricated RodSplit-Ring-Resonator Electromagnetic Metamaterial". *Phys. Rev. Lett.*, 94:063901, 2005.

[120] A. K. Azad, J. Dai, and W. Zhang. "Transmission properties of terahertz pulses through subwavelength double split-ring resonators". *Opt. Lett.*, 31:634, 2006.

[121] H. T. Chen, W. J. Padilla, J. M. O. Zide, A. C. Gossard, A. J. Taylor, and R. D. Averitt. "Active terahertz metamaterial devices". *Nature*, 444:597, 2006.

[122] O. Paul, C. Imhof, B. Reinhard, R. Zengerle, and R. Beigang. "Negative index bulk metamaterial at terahertz frequencies". *Opt. Express*, 16:6736, 2008.

[123] J. F. O'Hara, R. Singh, I. Brener, E. Smirnova, J. Han, A. J. Taylor, and W. Zhang. "Thin-film sensing with planar terahertz metamaterials: sensitivity and limitations". *Opt. Express*, 16:1786, 2008.

[124] N. Liu, S. Kaiser, and H. Giessen. "Magnetoinductive and Electroinductive Coupling in Plasmonic Metamaterial Molecules". *Adv. Mater.*, 20:4521, 2008.

[125] R. Singh, C. Rockstuhl, F. Lederer, and W. Zhang. "Coupling between a dark and a bright eigenmode in a terahertz metamaterial". *Phys. Rev. B.*, 79:085111, 2009.

[126] D. Grischkowsky, S. Keiding, M. van Exter, and Ch. Fattinger. "Far-infrared time-domain spectroscopy with terahertz beams of dielectrics and semiconductors". *J. Opt. Soc. Am. B*, 7:2006, 1990.

[127] M. He, A. K. Azad, S. He, and W. Zhang. "Far-infrared signature of animal tissues characterized by terahertz time-domain spectroscopy". *Opt. Commun.*, 259:389, 2006.

[128] L. Li. "New formulation of the Fourier modal method for crossed surface-relief gratings". *J. Opt. Soc. Am. A*, 14:2758, 1997.

[129] A. Potts, D. M. Bagnall, and N. I. Zheludev. "A new model of geometric chirality for two-dimensional continuous media and planar meta-materials". *J. Opt. A*, 6:193, 2004.

[130] N. Papasimakis, V. A. Fedotov, Y. H. Fu, D. P. Tsai, and N. I. Zheludev. "Coherent and incoherent metamaterials and order-disorder transitions". *Phys. Rev. B*, 80:041102(R), 2009.

[131] N. Papasimakis, Y. H. Fu, V. A. Fedotov, S. L. Prosvirnin, D. P. Tsai, and N. I. Zheludev. "Metamaterial with polarization and direction insensitive resonant transmission response mimicking electromagnetically induced transparency". *Appl. Phys. Lett.*, 94:211902, 2009.

[132] B. Bai, Y. Svirko, J. Turunen, and T. Vallius. "Optical activity in planar chiral metamaterials: Theoretical study". *Phys. Rev. A*, 76:023811, 2007.

[133] K. Konishi, B. Bai, X. Meng, P. Karvinen, J. Turunen, Y. P. Svirko, and M. Kuwata-Gonokami. "Observation of extraordinary optical activity in planar chiral photonic crystals". *Opt. Express*, 16(10):7189, 2008.

[134] M. P. Silverman, W. Strange, J. Badoz, and I. A. Vitkin. "Enhanced optical rotation and diminished depolarization in diffusive scattering from a chiral liquid". *Opt. Commun.*, 132(5-6):410, 1996.

[135] M. Silverman, N. Ritchie, G. Cushman, and B. Fisher. "Experimental configurations using optical phase modulation to measure chiral asymmetries in light specularly reflected from a naturally gyrotropic medium". *J. Opt. Soc. Am. A*, 5:1852, 1988.

[136] M. P. Silverman and J. Badoz. "Light reflection from a naturally optically active birefringent medium". *J. Opt. Soc. Am. A*, 7(7):1163, 1990.

[137] A. R. Bungay, Y. P. Svirko, and N. I. Zheludev. "Experimental observation of specular optical activity". *Phys. Rev. Lett.*, 70(20):3039, 1993.

[138] A. R. Bungay, N. Kugler, and N. I. Zheludev. "Specular optical activity in GaAs". *Phys. Lett. A*, 174(4):335, 1993.

[139] M. P. Silverman, J. Badoz, and B. Briat. "Chiral reflection from a naturally optically active medium". *Opt. Lett.*, 17(12):886, 1992.

[140] H. H. J. de Jongh and M. B. J. Meinders. "Proteins at air-water interfaces studied using external reflection circular dichroism". *Spectrochim. Acta A*, 58(14):3197, 2002.

[141] G. Lakhwani, S. C. J. Meskers, and R. A. J. Janssen. "Circular differential scattering of light in films of chiral polyfluorene". *J. Phys. Chem. B*, 111(19):5124, 2007.

[142] E. Plum, V. A. Fedotov, and N. I. Zheludev. "Tunable reflection optical activity due to extrinsic chirality". to be submitted.

[143] D. L. Jaggard and N. Engheta. "Chirosorb as an invisible medium". *Electron. Lett.*, 25:173, 1989.

[144] G. Shvets. "Optical polarizer/isolator based on a rectangular waveguide with helical grooves". *Appl. Phys. Lett.*, 89:141127, 2006.

[145] A. Lakhtakia and R. Messier. *Sculptured Thin Films: Nanoengineered Morphology and Optics*. SPIE Press, 2005.

[146] Y. Jin and S. He. "Focusing by a slab of chiral medium". *Opt. Express*, 13:4974, 2005.

[147] Q. Cheng and T. J. Cui. "Negative refractions in uniaxially anisotropic chiral media". *Phys. Rev. B*, 73:113104, 2006.

[148] V. M. Agranovich and Yu N. Gartstein. "Spatial dispersion and negative refraction of light". *Physics-Uspekhi*, 49(10):1029, 2006.

[149] B. Wang, J. Zhou, T. Koschny, and C. M. Soukoulis. "Nonplanar chiral metamaterials with negative index". *Appl. Phys. Lett.*, 94:151112, 2009.

[150] N. Liu, H. Liu, S. Zhu, and H. Giessen. "Stereometamaterials". *Nature Photonics*, 3:157, 2009.

[151] B. Wang, J. Zhou, T. Koschny, M. Kafesaki, and C. M. Soukoulis. "Chiral metamaterials: simulations and experiments". *J. Opt. A: Pure Appl. Opt.*, 11:114003, 2009.

[152] E. Plum and N. I. Zheludev. *Structured Surfaces as Optical Metamaterials*, chapter Chirality and Anisotropy of Planar Metamaterials. Cambridge University Press, submitted.

[153] V. A. Fedotov, N. Papasimakis, E. Plum, A. Bitzer, M. Walther, P. Kuo, D. P. Tsai, and N. I. Zheludev. "Spectral collapse in ensembles of meta-molecules". *Phys. Rev. Lett.*, submitted.

Index